

Ph.D. Thesis

***MICROSTRUCTURAL EVOLUTION AND
MECHANICAL PROPERTIES IN STEELS
TREATED BY QUENCHING & PARTITIONING
WITH THE PARTITIONING STAGE IN THE
INTERCRITICAL RANGE***

Author:

Eider Del Molino Duran

Bilbao, May 2022

Advisors:

Javier Jesús González Martínez

Maribel Arribas Tellería

Ph.D. Thesis

***MICROSTRUCTURAL EVOLUTION AND
MECHANICAL PROPERTIES IN STEELS
TREATED BY QUENCHING & PARTITIONING
WITH THE PARTITIONING STAGE IN THE
INTERCRITICAL RANGE***

Author:

Eider Del Molino Duran

Bilbao, May 2022

Advisors:

Javier Jesús González Martínez

Maribel Arribas Tellería

tecnal:a

MEMBER OF BASQUE RESEARCH
& TECHNOLOGY ALLIANCE

*Science makes people reach selflessly
for truth and objectivity;
it teaches people to accept reality,
with wonder and admiration,
not to mention the deep awe and joy
that the natural order of things
brings to the true scientist.*

Lise Meitner

ACKNOWLEDGMENTS

Tesia idazten hasi nintzen momentuan ez nuen inondik inora espero atalik zailenetakoa (zailena ez bada) hau izango zenik. Asko izan baitzarete bide luze honetan, animoak eman eta nigan sinistu izan duzuenok eta ez nuke inor bidean utzi nahi.

En primer lugar, quiero agradecer a TecNALIA el haberme dado la oportunidad de realizar la tesis. En especial, a mi directora de tesis de TecNALIA, Maribel Arribas, por haber puesto todo tu empeño en hacer que este viaje me fuera lo más sencillo y enriquecedor posible. Soy incapaz de imaginarme una persona más idónea para realizar ese desempeño. Por supuesto, gracias a el resto de los compañeros y compañeras de trabajo, comidas, cafés, etc., por haberme acogido desde el primer día como una más y haber hecho que estos años se pasen volando. Se me hace imposible mencionarlos a todos y todas individualmente, pero sí que me gustaría darles las gracias en particular a Iñaki e Igor, por todo el tiempo dedicado a apoyarme en el desarrollo de gran parte experimental de la tesis.

También quiero agradecer a la UPV/EHU la oportunidad de realizar esta tesis. A mi director, el profesor Javier Jesús González, por tu asesoramiento en todos los momentos en los que lo he necesitado y por haberme aportado tanta experiencia. Tampoco me gustaría dejar de lado al profesor José Tomás San José, por haberme ofrecido tu ayuda de una forma totalmente desinteresada desde que comencé mis estudios de Máster y hasta el día de hoy. ¡Muchas gracias a los dos!

I would like to extend my gratitude to the Advanced Steel Processing and Products Research Center (ASPPRC) at Colorado School of Mines. Thanks to Casey Gilliams for the time sacrificed, without which part of this thesis would not have been possible. Thanks also to Prof. John G. Speer and Prof. Emmanuel De Moor because, although the pandemic situation has not allowed me to meet you in person, it has been a true honor to discuss the results of my thesis with experts like you.

I would also like to thank Dr. Artem Arlazarov, from ArcelorMittal Maizières, for the supply of the medium Mn steels employed in this thesis and for sharing your knowledge with me.

Por otro lado, ya que esta tesis se ha desarrollado en el marco de varios proyectos de investigación, quería alargar mis agradecimientos a la financiación recibida en el programa RFCS, de la Comisión Europea, para la ejecución del proyecto HIGHQP (grant number:

709855) y el programa HAZITEK, del Gobierno Vasco, para la ejecución del proyecto CHALET (expediente: ZL-2020/00434).

Eskerrik asko nire kuadrilako lagunei, nigmatik arduratzeagatik eta nire ausentzia (batez ere azkenengo hilabete hauetakoa) ulertzeagatik. Zuek gabe bide hau ez litzateke berdina izango. Mila esker unibertsitateko lagunei ere, zeren, nahiz eta sakrifikatutako denborak zuekin are gutxiago egoteko aukera eman didan, frogatu didazuenez, urte gutxi batzuetan eraikitako adiskidetasuna denboran mugarik gabe luzatu daitekeelako (txip-txip).

Muchas gracias a mi familia. A mi amama, porque aunque no la llamo, ni visito tanto como debería (casi) siempre tiene buenas palabras para mí. A mi aita, por esa manera tan peculiar que ha tenido siempre de motivarme, que con los años he ido “entendiendo”, aunque más de una vez me haya sacado de quicio. A mi ama, por ser un pilar fundamental en mi vida y un espejo de superación en el que mirarme.

Azkenengo hitzak, urte hauetan zehar gehien aguantatu nauen pertsonarentzat. Jon Ander, eskerrik asko nire oreka puntua izateagatik. Momentu onetan eta, batez ere, txarretan, irribarre bat ateratzen jakiteagatik. Indarrak transmititzeagatik. Bizi izandako une guztiengatik eta biziko ditugunengatik.

Guztiei, eskerrik asko bihotz bihotzez. Muchas gracias. Thank you.

LABURPENA

Erresistentzia handiagoko altzairuak sortzeko eskariak, beste propietate batzuk mantentzen diren bitartean, hala nola konformagarritasun plastikoa edo soldagarritasuna, Erresistentzia Handiko Altzairu Aurreratuak garatzea eskatu du (AHHS, ingeleseko sigletan). Tesi honetan ikertutako Q&P (Quenching and Partitioning) altzairuak AHSSen hirugarren belaunaldiaren barruan daude. Altzairu horien ezaugarri nagusia austenita atxikitu balio altu samarrak eta matrize martensitikoa dituztela da. Horrek erresistentzia eta konformagarritasun handia ematen die eta, beraz, oso interesgarriak dira automobilak fabrikatzeko.

Q&P altzairuen prozesatzea bi etapako tratamendu termiko baten datza. Lehenengoan, altzairua M_s - M_f (hau da, martensita hasierako tenperatura - martensita amaierako tenperatura) tarteko tenperatura lehenetsi batera hozten da, mikroegitura partzialki martensitikoa eta austenitikoa sortzeko. Bigarrenak, partizio etapa izenekoak (altzairu martensitikoaren iraoketa klasikoa gogorarazten duena), austenitaren karbono edukia aberastea du helburu, martensitaren karbono edukia (partzialki) murriztuz. Horrela, karbonoz egonkortutako austenita mikroegituran atxikitzea lortzen da, giro tenperaturara hoztu ondoren.

Tesi honetan, Q&P tratamendua Mn edukia duten altzairuetan aplikatu da, eta berritasuna partizio etapa tarte interkritikoari dagokion tenperatura batean egin dela da, martensitatik austenitarako transformazioaren fenomeno eraginez. Horrela, atxikitako austenita eduki handiagoak lortu nahi izan dira eta, horretaz gain, austenita karbonoak ez ezik, manganesoak ere egonkortu du. Altzairuaren konposizio kimikoak (manganeso eta nikel eduki desberdineko altzairutzat ikertuta) eta tratamendu termikoak (tenplaketa tenperatura eta partizio denbora) bilakaera mikroegituralean, fase austenitikoaren egonkortzean eta trakzioarekiko propietateetan duten eragina ikertu da.

Tratatutako altzairuen mikroegituraren karakterizazioari esker, manganeso gehien duten altzairuetan, atxikitutako austenita eduki handiak baieztatu ahal izan dira, baita fase austenitikoko manganeso aberastea ere. Gainera, partizio etaparen aurreko mikroegiturak (tenplaketa tenperaturak zehaztua) eragin handia duela ikusi da, eta baldintzetako batzuetan mikroegitura finagoa, austenita eduki handiagoak eta aparteko trakzioarekiko propietateak lortu izan dira, trakzioarekiko erresistentziaren eta elongazio totalaren arteko produktuan 30 GPa% gaituz. Nikela gehitzea onuragarria izan da austenita atxikitu gehiago eta produktu horren balio handiagoak lortzeko. Trakzioarekiko emaitzak martensita

sekundarioaren presentziarekin eta deformazioak eragindako austenitatik martensitarako transformazioaren fenomenoarekin erlazionatu dira batez ere.

Bestalde, duela gutxi higadurarekiko erresistentziak zeregin garrantzitsua duen beste eremu batzuetan ere, Q&P altzairuak erabiltzeko aukera ikertu da; hala nola, meatzaritzan, ebaketa erremintetan eta abarretan. Karga mekaniko baten pean, atxikitako austenita kantitate handiago batek geruza gogortu lodiagoa lortzen lagun dezake, martensitarako transformazioaren ondorioz. Horrela, higadura eta marruskadura murrizten dira ukipeneko gainazalean. Horregatik, Q&P bidez tratatutako altzairuak garatzearen bideragarritasunari buruzko azterlan bat ere egin nahi izan da, tenple eta iraoketa konbentzionalarekin tratatutakoekin alderatuta (Q&T, ingeleseko siglengatik) higadurarekiko-propietate hobetuak dituztenak sortzeko. Beraz, tesi honetan, karbono eduki ertain eta handiko altzairuak Q&P bidez tratatu dira eta, ondoren, mikroegiturari, nahiz higadurari eta zailtasunari dagokionez karakterizatu dira. Oro har, higadurarekiko erresistentzia antzekoa izan da Q&T eta Q&P bidez tratatutako altzairuetan. Azkenik, ondorioztatu da austenitaren egonkortasun mekanikoa altuegia izan dela, eta gainazala ez dela behar adina gogortu martensitarako transformazioagatik; beraz, azterketa sakonagoa egin behar da prozesua optimizatu ahal izateko.

RESUMEN

La demanda para crear aceros con mayor resistencia mientras se mantienen otras propiedades, como la conformabilidad plástica o la soldabilidad, ha requerido del desarrollo de Aceros Avanzados de Alta Resistencia (AHSS, por sus siglas en inglés). Los aceros Q&P (Quenching and Partitioning) investigados en esta tesis se encuentran dentro de la tercera generación de AHSS. Estos aceros se caracterizan por poseer valores de austenita retenida relativamente altos y una matriz martensítica, lo que les confiere una elevada resistencia y conformabilidad, por lo que resultan muy interesantes para la fabricación de automóviles.

El procesado de los aceros Q&P consiste en un tratamiento térmico de dos etapas, donde el acero se enfría hasta una temperatura predeterminada (quenching temperature, QT) en el rango M_s - M_f (es decir, temperatura de inicio de transformación martensítica - temperatura de final de transformación martensítica) para producir una microestructura parcialmente martensítica y austenítica. La segunda, denominada etapa de partición (que recuerda el revenido clásico de los aceros martensíticos), tiene como objetivo el enriquecimiento en carbono de la austenita por la reducción (parcial) de carbono de la martensita. De esta forma, la austenita estabilizada con carbono se retiene en la microestructura después del enfriamiento final a temperatura ambiente.

En esta tesis, el tratamiento Q&P ha sido aplicado en aceros de contenido medio en Mn, con la novedad de que la etapa de partición se ha realizado a una temperatura correspondiente al rango intercrítico, dando lugar al fenómeno de reversión de la fase austenítica. De esta forma se ha perseguido obtener mayores niveles de austenita retenida, siendo ésta estabilizada no solo por carbono, sino también por elementos sustitucionales, como el manganeso. Se ha investigado la influencia de la composición química del acero (considerándose aceros con distinto contenido de manganeso y níquel) y las condiciones del tratamiento térmico (temperatura de temple y tiempo de partición), en la evolución microestructural, estabilización de la fase austenítica y propiedades a tracción.

La caracterización microestructural de los aceros tratados ha permitido confirmar altos valores de austenita retenida en los aceros con mayor contenido en manganeso y el enriquecimiento en manganeso de la fase austenítica. Además, se ha observado una gran influencia de la microestructura previa a la etapa de partición (determinada por la temperatura de temple), resultando en algunas de las condiciones en una microestructura más fina, mayor contenido de austenita retenida y valores excepcionales a tracción,

superando los 30 GPa% en el producto de la resistencia y el alargamiento total. La adición de níquel ha sido beneficiosa para alcanzar un mayor contenido de austenita retenida y valores superiores de dicho producto. Los resultados a tracción se han relacionado principalmente con la presencia de martensita secundaria y el fenómeno de transformación de austenita en martensita inducida por deformación.

Por otro lado, recientemente también se ha investigado la posibilidad de emplear aceros Q&P en otros campos en los que la resistencia al desgaste juega un papel importante, tales como minería, herramientas de corte, etc. Bajo una carga mecánica, una mayor cantidad de austenita retenida puede ayudar a obtener una capa endurecida más gruesa debido a la transformación en martensita, reduciendo el desgaste y la fricción en superficies en contacto. Es por ello, que también se ha querido realizar un estudio sobre la viabilidad de desarrollar aceros tratados mediante Q&P con propiedades a desgaste mejoradas respecto a los tratados con el convencional temple y revenido (Q&T, por sus siglas en inglés). Por lo tanto, en esta tesis, aceros de medio y alto contenido en carbono han sido tratados mediante Q&P y posteriormente caracterizados tanto microestructuralmente como a desgaste y tenacidad. En general, la resistencia al desgaste ha sido similar en los aceros tratados mediante Q&T y Q&P. Finalmente, se ha concluido que la estabilidad mecánica de la austenita ha sido demasiado alta, no produciéndose el suficiente endurecimiento por transformación en martensita, por lo que se requiere de un estudio más en profundidad para poder optimizar el proceso.

ABSTRACT

The demand to create steels with higher strength while maintaining other properties, such as plastic formability or weldability, required the development of Advanced High Strength Steels (AHSS). The Q&P (Quenching and Partitioning) steels investigated in this thesis are within the third generation of AHSS. These steels are characterized by containing relatively high retained austenite values and a martensitic matrix, which brings them high strength and formability, making them quite interesting for automobile manufacturing.

The processing of Q&P steels consists of a two-stage heat treatment, where the steel is quenched to a predetermined quenching temperature (QT) in the M_s - M_f range (i.e., martensite transformation start temperature - end of martensite transformation temperature) to produce a partially martensitic and austenitic microstructure. The second, called the partitioning stage (which recalls the classical tempering of martensitic steels), is designed to enrich the remaining austenite with carbon by the (partial) carbon reduction in the martensite. Thus, the carbon-stabilized austenite is retained in the microstructure after final cooling to room temperature.

In this thesis, the Q&P treatment was applied to medium Mn steels, with the innovation that the partitioning stage was carried out in the intercritical range, giving rise to Austenite Reverse Transformation (ART) phenomenon. Thereby, the aim was to obtain higher levels of retained austenite, stabilized not only by carbon, but also by substitutional elements, such as manganese. The influence of the steel chemical composition (manganese and nickel content) and the heat treatment conditions (quenching temperature and partitioning time) on microstructure evolution, austenite stabilization and tensile properties, was investigated.

The microstructural characterization of the treated steels confirmed high values of retained austenite in the steels with highest content of manganese and the enrichment in manganese of the austenite phase. In addition, a great influence of the microstructure prior to partitioning stage (fixed by the quenching temperature) was observed, resulting in some of the conditions in a finer microstructure, higher content of retained austenite and exceptional tensile properties, exceeding 30 GPa% in the product of strength and total elongation. The addition of nickel was beneficial for retaining more austenite in the final microstructure and improving tensile properties. Tensile properties were related mainly to the presence of secondary martensite and strain induced transformation of austenite into martensite.

On the other hand, the possibility of employing Q&P steels in other fields in which wear resistance plays an important role, such as mining, cutting tools, etc., has recently been investigated. Under mechanical loading, a higher amount of retained austenite may aid to obtain a thicker hardened layer due to transformation into martensite, reducing wear and friction on surfaces in contact. Hence, it was considered to carry out a study on the feasibility of developing Q&P treated steels with improved wear properties compared to those treated with a conventional quenching and tempering (Q&T). Therefore, in this thesis, medium and high carbon steels were treated by Q&P and afterward characterized both microstructurally and in terms of wear and toughness. In general, the wear resistance was similar in steels treated by Q&T and Q&P. Finally, it was concluded that the mechanical stability of austenite was too high to take advantage of transformation hardening, so a more in-depth study is required to optimize the process.

Table of Contents

Chapter 1 Introduction	3
1.1 Advanced High Strength Steels (AHHS)	3
1.2 Quenching and partitioning (Q&P) steels	5
1.2.1 Fundamentals of the Q&P process	5
1.2.2 Carbon partitioning	6
1.2.3 Competing reactions during Q&P heat treatment	7
1.2.4 Alloying elements employed in Q&P steels.....	9
1.2.5 Q&P cycle parameters.....	15
1.2.6 Microstructural evolution during Q&P process	19
1.2.7 Variations from the original Q&P cycle.....	21
1.3 Retained austenite and its role	21
1.3.1 Thermal stability of the austenite.....	21
1.3.2 Mechanical stability of the austenite.....	22
1.4 Relationship between microstructure and mechanical properties	24
1.5 Medium Mn steels (MMnS)	25
1.6 Q&P treatment for automotive industry.....	26
1.6.1 Commercialized Q&P steels.....	26
1.6.2 Weldability of Q&P steels	27
1.7 Q&P treatment for applications requiring wear resistance	28
1.7.1 Toughness in Q&P steels for wear applications	30
Chapter 2 Motivation and objectives	33
2.1 Motivation	33
2.2 Objectives of the thesis	34
Chapter 3 Materials and experimental procedures	39

3.1	Materials and processing	39
3.1.1	Materials	39
3.1.2	Design of the Q&P cycles based on dilatometry	43
3.1.3	Application of the Q&P heat treatments: Furnaces and salt baths	51
3.2	Microstructural characterization	53
3.2.1	X-ray diffraction (XRD)	53
3.2.2	Scanning Electron Microscope (SEM and FE-SEM).....	54
3.2.3	Electron Backscatter Diffraction (EBSD).....	55
3.2.4	Transmission Electron Microscopy (TEM)	56
3.3	Mechanical behavior	59
3.3.1	Tensile test	59
3.3.2	Interrupted tensile test.....	60
3.3.3	Hardness	60
3.3.4	Tribology: pin-on-disk (PoD).....	61
3.3.5	Toughness	63
Chapter 4 Results and discussion		67
4.1	Q&P applied to medium Mn and Ni steels	67
4.1.1	Dilatometry curves of the Q&P heat treatments.....	67
4.1.2	Microstructure after the Q&P heat treatments.....	70
4.1.3	Tensile properties	77
4.1.4	Interrupted tensile test results	81
4.1.5	Analysis of the influence of the heat treatment parameters on microstructure and austenite stabilization.....	82
4.1.6	Analysis of the influence of Ni on microstructure and austenite stabilization	86
4.1.7	Theoretical analysis of austenite stabilization using DICTRA.....	87
4.1.8	Relationship between microstructure and tensile properties	92
4.2	Q&P applied to medium and high C steels	96

4.2.1	Dilatometry study to select the steels and Q&P cycle to further study	96
4.2.2	Dilatometry curves of the Q&P cycle applied in furnaces and salt baths	97
4.2.3	Microstructure after Q&P treatment.....	99
4.2.4	Hardness	102
4.2.5	Wear behavior	103
4.2.6	Retained austenite stability	105
4.2.7	Toughness	106
Chapter 5 Conclusions		111
5.1	Q&P applied to medium Mn and Ni steels	111
5.2	Q&P applied to medium and high C steels	112
Chapter 6 Future work		117
6.1	Q&P applied to medium Mn and Ni steels	117
6.2	Q&P applied to medium and high C steels	118
Chapter 7 Bibliography		121
Publications related to the doctoral thesis		137
Appendix A: Dilatometry		139
Appendix B: Route followed in the furnaces and salt baths		151
Appendix C: Tensile test specimens.....		152
Appendix D: Hardness measurements		155
Appendix E: Charpy specimens		156

List of Figures

Figure 1. Global Formability Diagram (2021) comparing strength and elongation of current and emerging steel grades. Courtesy of WorldAutoSteel [2].	4
Figure 2. Schematic of a typical Q&P cycle representing the different microstructures and C content of each phase within the cycle, where α' is martensite, α'_{sec} is secondary martensite and γ is austenite.	6
Figure 3. Total elongation versus tensile strength diagrams after the application of Q&P heat treatments showing the effect of C and Mn additions [49].	11
Figure 4. Total elongation versus ultimate tensile strength for Q&P treated 0.3C-Mn-1.6Si steels containing various levels of manganese [86].	13
Figure 5. Volume fraction of retained austenite and corresponding carbon content after full austenization, quenching to different temperatures and partitioning at 400 °C for 100 s [108].	16
Figure 6. Volume fraction of retained austenite after Q&P treatment at different partitioning temperatures and times [8].	19
Figure 7. Microstructural evolution that undergoes during Q&P cycles showing the different phases and carbon contents of each phase expected at austenization, quenching temperature, at the end of partitioning, and final microstructure. In this figure, it is assumed that neither austenite decomposition nor carbide precipitation occurred.	20
Figure 8. SEM micrographs of a typical Q&P microstructure containing retained austenite (RA), tempered martensite (M1), secondary martensite (α'_{sec}), and martensite-austenite islands (MA). Adapted from [117].	20
Figure 9. Schematic of the typical processing route of medium-Mn steels, where α' is martensite, α is ferrite and γ is austenite.	25
Figure 10. Comparison of Charpy impact energies at different temperatures of Q&T and Q&P treated specimens [194].	30
Figure 11. Light optical metallography (LOM) images and hardness of the hot rolled microstructures. The 2Mn (a), 4Mn (b), 6Mn (c) and 6Mn2Ni (d) steels after hot rolling, and the 4Mn (e), 6Mn (f) and 6Mn2Ni (g) steels after soft annealing.	41

Figure 12. Theoretical CCT curves of 1.2990 (a), 1.2344 (b), and 300M (c) steels obtained with JMatPro.....	42
Figure 13. Global view on L78 RITA dilatometer.....	43
Figure 14. Dilatometry curves representing the determination of A_{c1} and A_{c3} temperatures of the 2Mn (a) and 1.2344 (b) steels. In (a) A_{c1} was determined as the temperature with maximum change in length just before transformation started and A_{c3} was determined by the tangent method; in (b) both temperatures were obtained by the tangent method.	44
Figure 15. Dilatometry curve of the 2Mn steel for the determination of M_s , M_f and martensite transformation curve (a) and the corresponding martensitic transformation curve showing the determination of the temperature corresponding to a transformation of 75% martensite (b).	46
Figure 16. Dilatometry curve showing the obtention of T_{ART} of the 6Mn2Ni steel reheating from QT25.....	48
Figure 17. Schematic of the Q&P cycles carried out in this work for medium Mn steels. ...	49
Figure 18. Schematic of the Q&P cycles carried out in this work for medium and high C steels.	50
Figure 19. Sheet of the 2Mn steel prepared to carry out Q&P thermal treatment in furnaces and salt baths with one thermocouple welded in the center and other in the edge. The dimensions of the showed sheet were 250 mm length, 50 mm wide, and 1.5 mm thick. ...	51
Figure 20. Cylinder of the 300M steel employed to carry out the Q&P thermal treatment in furnaces and salt baths representing the position of the thermocouples.	52
Figure 21. Schematic representation of the route followed to carried out Q&P thermal cycles in the furnaces and salt baths. Blue and red labels and arrows represents cooling and heating stages, respectively.....	52
Figure 22. Schematic representation of Bragg diffraction of crystallographic planes.	53
Figure 23. Funnel where samples were glued to be polished.	57
Figure 24. Hand drill employed to take out 3 mm diameter discs from the samples thinned down to 100 μm	57
Figure 25. Sample holder for the electrolytic bath and electropolishing equipment.	58
Figure 26. Intensity-Voltage curve.	58

Figure 27. Dimensions of the tensile specimens. All measurements are expressed in mm.	59
Figure 28. Samples cut for XRD measurements from tensile specimens after the application of different strains.....	60
Figure 29. Vickers hardness test principle.	61
Figure 30. Pin-on-disk system.....	61
Figure 31. Cross-sectional areas of the wear track employed for the measurement of wear rate.....	62
Figure 32. Standard subsize specimen dimensions (ASTM A370).	63
Figure 33. Dilatometry curves of the applied Q&P cycles: 2Mn steel (a), 4Mn steel (b), 6Mn steel (c), and 6Mn2Ni steel (d).	68
Figure 34. Relative change in length measured during the partitioning stage for the ref cycle.	69
Figure 35. Relative change in length measured during the partitioning stage for the QT10- Pt1000 and the QT25-Pt1000 cycles: 6Mn (a) and 6Mn2Ni (b) steels. Evolution of the austenite formed during the partitioning (reverted γ) in the QT10-Pt1000 and the QT25- Pt1000 cycles in the 6Mn (c) and 6Mn2Ni (d) steels.	69
Figure 36. Retained austenite contents as a function of partitioning time measured after the application of all Q&P cycles.....	71
Figure 37. FE-SEM micrographs corresponding to the QT25-Pt1000 cycle for the 6Mn (a), and 6Mn2Ni (b) steels; the QT10-Pt1000 cycle for the 6Mn (c), and 6Mn2Ni (d) steels; and the QT10-Pt3600 cycle for the 6Mn2Ni steel (e).....	73
Figure 38. EBSD scans corresponding to the QT25-Pt1000 cycle for the 6Mn (a), and 6Mn2Ni (b) steels; and the QT10-Pt1000 cycle for the 6Mn (c), and 6Mn2Ni (d) steels.	74
Figure 39. TEM analysis of 6Mn2Ni steel: Micrographs and SAD patterns for the QT25 (a) and the QT10 (b) conditions; EDS analysis representing the distribution of Mn concentration for the QT25 (c) and QT10 (d) conditions, and Ni concentration for the QT25 (e) and QT10 (f) conditions; concentration profiles of Mn and Ni line scans performed within the areas marked in (a) and (b) for the QT10 (g) and QT25 (h) conditions.	76

Figure 40. TEM micrographs of the 6Mn steel (a) and the 6Mn2Ni steel (c) after QT10-Pt1000 cycle, TEM-EDS spectrum of a globular carbide marked in (a) (b), and compositional mapping of the (c) micrograph (d). In the micrograph (c), acicular and globular carbides are visible; in the compositional map (d) a higher concentration of Mn is visible in the globular and acicular carbides.....	77
Figure 41. Engineering stress-strain curves obtained after Q&P treatments for the 2Mn steel.	78
Figure 42. Engineering stress-strain curves obtained after Q&P treatments for the 4Mn steel.	78
Figure 43. Engineering stress-strain curves obtained after Q&P treatments for the 6Mn steel.	78
Figure 44. Engineering stress-strain curves obtained after Q&P treatments for the 6Mn2Ni steel.	79
Figure 45. Relationship between total elongation (%) and tensile strength (MPa) obtained after Q&P cycles in 2Mn, 4Mn, 6Mn and 6Mn2Ni steels.	81
Figure 46. Engineering stress-strain curves obtained for the QT10-Pt1000 condition and RA measured at different strains for the 6Mn (a) and 6Mn2Ni (b) steels.	82
Figure 47. TEM micrograph of the 6Mn2Ni steel after the QT10-Pt1000 condition (a); and line scans of Mn and Ni weight concentration (b), corresponding to the line shown in (a).	87
Figure 48. DICTRA simulations for 6Mn2Ni steel at 640 °C: schematic of the initial conditions of the simulations for set up (1) (a); results for set up (1), showing a comparison between the growth of austenite in QT10 and QT25 with Pt1000 and diffusion of Mn (b) and Ni (d) (the initial interface was set in the same position for QT10 and QT25), and showing the comparison between the growth of austenite with Pt300, Pt1000, and Pt3600 in QT10 and diffusion of Mn (c) and Ni (e).	89
Figure 49. DICTRA simulations for 6Mn2Ni steel at 640 °C: schematic of the initial conditions of the simulations for set up (2) (a), and results for set up (2) configuration, where austenite nucleated at θ/α interface (b).	91
Figure 50. Tensile properties of the Q&P treated samples: yield strength (a); tensile strength (b); total elongation (c); and TEL x TS product (d).....	93

Figure 51. Graphical representation of the relationship between the product of tensile strength and total elongation and RA for each Q&P cycle of the 6Mn and 6Mn2Ni steels.	93
Figure 52. Volume percent of each phase in the 6Mn and 6Mn2Ni steels after the application of Q&P cycles calculated based on dilatometry curves and RA measured by XRD.	94
Figure 53. Evolution of normalized RA during tensile tests stopped at different strains for 6Mn and 6Mn2Ni steels after QT10-Pt1000 cycle.	95
Figure 54. Dilatometry curves, hardness and RA content for the 1.2990 steel after the PT300 (a) PT400 (b) cycles; for the 1.2344 steel after the PT300 (c) and PT400 (d) cycles; and for the 300M steel after the PT300 (e) and PT400 (f) cycles.	97
Figure 55. Dilatometry curves of the thermal Q&P cycle applied in the furnaces and salt baths for the 1.2990 and 300M steels.	98
Figure 56. Relative change in length measured during the partitioning stage for the Q&P cycle applied to the 1.2990 and 300M steels.	99
Figure 57. SEM micrograph of the 300M steel after the Q&P treatment.	99
Figure 58. SEM micrographs (a) and (b), and EDS analysis of the matrix (c), globular carbide (d), and coarse carbides (e) and (f) of the 1.2990 steel after the Q&P treatment.	100
Figure 59. Phase fraction as a function of temperature of (a) 1.2990 and (b) 300M steels, and composition of 1.2990 steel (c) M7C3 and (d) M23C6 phases obtained by Thermo-Calc calculations.	101
Figure 60. Hardness values measured in the 1.2990 and 300M steels after the application of Q&T or Q&P heat treatments.	103
Figure 61. Wear rate ($\text{mm}^3/\text{N.m}$) calculated from the PoD tests. Comparison between Q&P and Q&T treated 1.2990 (a) and 300M (b) steels; and comparison between Q&P treated 1.2990 and 300M steels tested with the same linear velocity (c).	104
Figure 62. RA measured in the surface and wear tracks formed during PoD characterization of the 1.2990 and 300M steels.	105

List of Tables

Table 1. Short review of typical steels with Fe-C-Mn-Si/Al compositions employed in Q&P process.	9
Table 2. Short review of steels with Fe-C-Mn-Si compositions and Ni and/or Cr additions employed in Q&P process.	10
Table 3. Short review of compositions employed in Q&P steels with Mo and/or V additions.	10
Table 4. Tensile properties and volume % of retained austenite obtained by Q&P.	24
Table 5. Typical mechanical property ranges for industrially produced QP980 and QP1180. Adapted from [151].	27
Table 6. Replacing DP590 with QP980 allows for downgauging. Adapted from [157].	27
Table 7. Composition (wt.%) of the medium Mn steels employed in this work.	40
Table 8. Composition (wt.%) of the medium and high C steels employed in this work.	43
Table 9. Phase transformation temperatures (A_{c1} , A_{c3} , M_s and M_f), critical cooling rates (CCR) and the austenite measured in the quenching state of all the steels employed in this work.	45
Table 10. QT25, QT10 and T_{ART} values employed in the Q&P cycles corresponding for each steel.	48
Table 11. Selection of the QT, PT and Pt parameters employed in each Q&P cycle.	49
Table 12. Summary of conditions carried out in each steel.	49
Table 13. Q&P cycle parameters (QT, PT and Pt) employed in each condition and steel.	51
Table 14. Parameters used for the pin-on-disk tests.	62
Table 15. Comparison between retained austenite content (RA %) measured by XRD and EBSD. Average austenite grain size (RA nm) measured by EBSD.	74
Table 16. Summary of tensile properties for the 2Mn, 4Mn, 6Mn and 6Mn2Ni steels after each Q&P treatment.	79
Table 17. Summary of the austenite and secondary martensite values estimated and measured at the end of the partitioning and in the final microstructure.	84

Table 18. Toughness values (J/cm^2) obtained in Charpy V-notch impact test of the Q&P and Q&T treated 1.2990 steel.	107
--	-----

Chapter 1

Introduction

Chapter 1

Introduction

Probably, the importance of the materials in our culture is greater than is usually believed. Nearly every segment of our daily lives is influenced, to a greater or lesser extent, by materials, such as transport, housing, and communication. Historically, the development and evolution of the societies has been tightly linked to the capacity of its members to produce and shape the necessary materials to satisfy their needs. Over time, human beings discovered techniques to produce materials with properties superior to those of natural ones. Furthermore, it was discovered that the properties of a material could be modified by heat treatments or by the addition of other substances.

Years after Iron Age II, blacksmiths realized that by using semi-furnaces with charcoal for a longer time to heat the iron that they later forged, a stronger final element was achieved. Thus, steel was discovered, but it was not until the middle of the 19th century that the appearance of the Bessemer converter revolutionized the manufacture of this material.

Countless steel grades have been developed and this material has been greatly exploited, becoming the world's most important industrial material. Specifically, in 2021 more than 1.9 billion tons were produced. Furthermore, incessant demand for new steels with better properties than conventional ones, specific for each use, is required, and that means that research in this field remains very active at global level.

1.1 Advanced High Strength Steels (AHSS)

In order to meet the demand for higher strength steels while maintaining other properties as plastic formability or weldability, Advanced High Strength Steels (AHSS) were developed in the mid-1990s. Early efforts to achieve lighter weight and enhanced crash performance in vehicles were aimed at the development of higher strength and formability parameters with a low content of alloying elements. These requirements were summarized by the term AHSS,

which is the name of the new generation of structural steel, revolutionizing the automotive industry.

Based on the different development stages and microstructures/properties, AHSSs are generally divided into three generations [1]. Figure 1 shows the locations of conventional steels and the three generations of AHSS grades in an elongation versus tensile strength diagram [2].

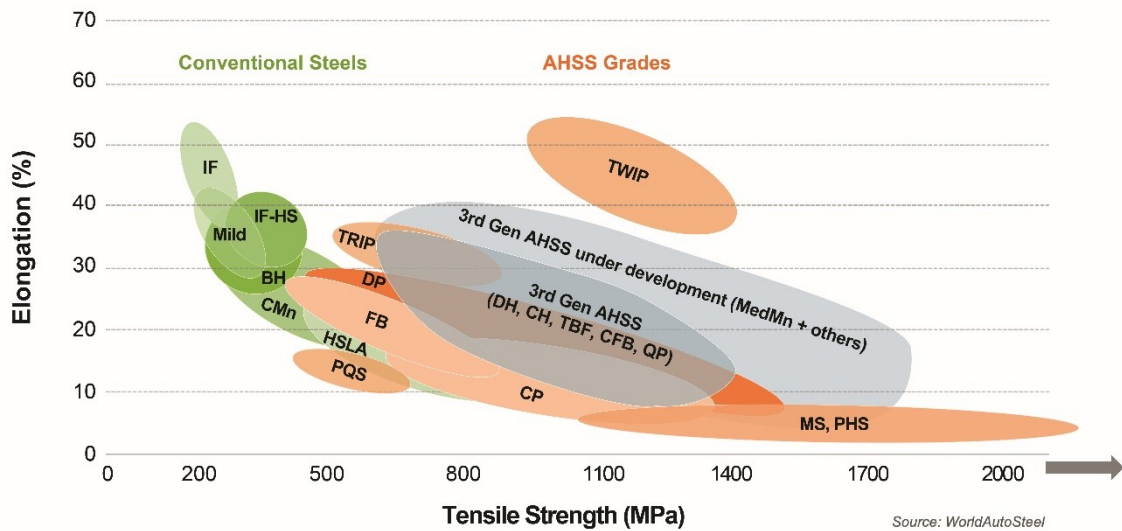


Figure 1. Global Formability Diagram (2021) comparing strength and elongation of current and emerging steel grades. Courtesy of WorldAutoSteel [2].

The first generation of AHSS include dual phase (DP), transformation induced plasticity (TRIP), complex-phase (CP), martensitic (MS) and press hardened (PHS) steels. The general characteristics of these steels are a higher strength than conventional high strength steels with little reduction in ductility, without a considerable increase in cost. These steels are typically low alloyed and have ferrite based multiphase microstructures [3]. The demand for steels with significantly better combination of strength and ductility led to the development of the second generation AHSS which consist of highly alloyed austenitic steels, such as the austenitic twinning induced plasticity (TWIP) steels. These steels exhibit extremely good mechanical properties, with an excellent strength and an enhanced formability compared to first generation steels, but these AHSS grades face some difficulties of manufacturing and are highly alloyed with high cost alloying elements, resulting in significant production cost increase, so its general use is hampered [4]. For this reason, it is not surprising the increasing interest in developing third generation AHSS during the last two decades. The enhanced formability, measured in different tests as tensile, sheared edge, or bending, of these steels is due to their multi-phase microstructure. In these steels, specific proportions and

distributions of the phases are searched; typically, bainite or martensite matrix with relatively high amounts of retained austenite (RA) and, occasionally, some amounts of ferrite and/or precipitates. Generally, the high retained austenite amounts contained in the third generation AHSS is the responsible of their high elongation, and also partly the strength, due to the transformation induced plasticity (TRIP) effect, derived from the deformation-induced transformation to martensite. The most promising families are quenching and partitioning (Q&P), medium manganese (MMnS), and TRIP aided bainitic-ferrite (TBF) steels [5]. The third-generation grades are currently under research and development and it was not until around 2020 that its global commercialization started [2].

1.2 Quenching and partitioning (Q&P) steels

1.2.1 Fundamentals of the Q&P process

Quenching & Partitioning was first proposed in 2003 by Speer *et al.* [6] to produce third generation AHSS with controlled fractions and stabilities of retained austenite. The process is based on the stabilization of austenite by means of carbon diffusion from martensite. Figure 2 shows the schematic representation of a typical Q&P heat treatment. As seen in the figure the steel is first fully austenitized at a temperature above A_{c3} followed by a quenching to a temperature between the martensite start (M_s) and martensite finish (M_f) transformation temperatures, to obtain a partially martensitic and partially austenitic microstructure. Then, a partitioning treatment (which recalls the classical tempering of martensitic steels) designed to enrich the remaining untransformed austenite with carbon that escapes from the martensite phase is carried out. Thereby, carbon-stabilized austenite is retained in the microstructure after final quenching to room temperature [6], while carbon content available to cementite and transition carbides precipitation is minimized by proper addition of Si and/or Al [7]. Through this process, a martensitic microstructure with significant content of retained austenite (RA), typically in the range of 5–20% [8], can be obtained.

The final microstructure of Q&P steels is expected to exhibit desirable combinations of strength, ductility, and toughness, which permit their use in a new generation of AHSSs for automobiles. However, during the final cooling to room temperature part of the austenite, not enough stabilized, may transform into secondary martensite, which is a hard and relatively brittle phase that may deteriorate the total ductility. Therefore, the selection of suitable processing parameters, such as quenching temperature (QT), partitioning temperature (PT) and partitioning time (Pt), is vital.

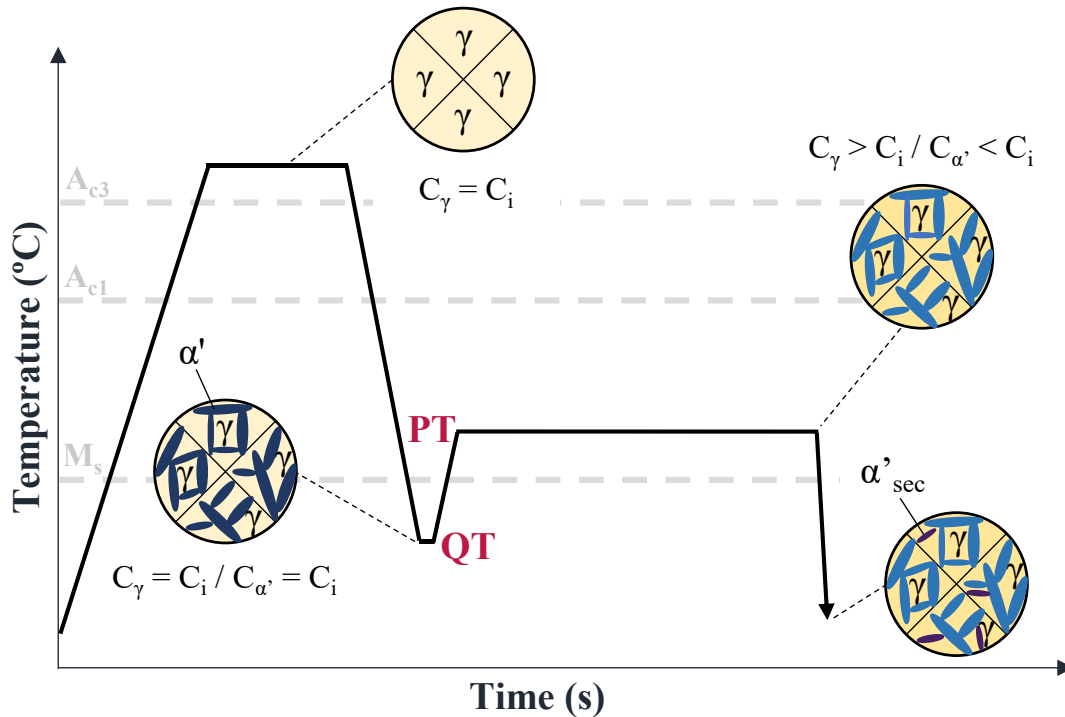


Figure 2. Schematic of a typical Q&P cycle representing the different microstructures and C content of each phase within the cycle, where α' is martensite, α'_{sec} is secondary martensite and γ is austenite.

Development of Q&P treatment has so far been focused to sheet processing directed to automotive industry. However, development of Q&P type microstructures in thicker sections is of interest to heavy industry, including mining and mineral processing. For such applications, the thicknesses of the steel sheets are too low and therefore steel plates are required. In that aspect, only a few studies considered the possibility of applying Q&P in steel plates [9–11].

1.2.2 Carbon partitioning

Carbon supersaturation in martensite is ordinarily eliminated by mechanisms like carbide precipitation during tempering [12,13]. In addition, the temperature which is used normally in steel treatment processes is too low for substantial amounts of carbon diffusion to occur [12]. Consequently, although carbon-enriched retained austenite in martensitic steels was not unknown [14], the thermodynamics of carbon partitioning between martensite and retained austenite has been scarcely considered.

Recently, a model has been developed in order to address carbon partitioning from as-quenched martensite into austenite. This model predicts the endpoint of partitioning when martensite is in metastable equilibrium with austenite. It assumes that the diffusion of

substitutional atoms is restricted, the martensite/austenite interface is immobile, and carbide formation and carbon segregation to dislocations in martensite are assumed to be suppressed [6]. In particular, it has been recently suggested that the carbon partitioning from martensite into austenite is controlled by the constrained carbon equilibrium (CCE) criterion [12,13,15]. According to this, to reach the metastable martensite/austenite equilibrium by the completion of carbon partitioning, both equal chemical potential of carbon in martensite and austenite and conservation of all substitutional atoms in each phase are required.

The results of the CCE model served to successfully propose the novel Q&P process. However, the grain size of the austenite and its mechanical stability due to the appearance of dislocations during cooling can affect both the M_s temperature [16] and the predictions of the phase fractions [17]. The morphology of the austenite and the characteristics of the martensite, such as carbon supersaturation and dislocation density [18,19], can also influence carbon diffusion, along with the coupling of austenite with neighboring phases.

A later analysis [20] about the character of the interface in the partitioning stage included the possibility of a mobile interface based on experimental evidence of interface migration. In recent studies [21,22], it was found out that the interface migrates during the partitioning step. This migration was evident since they measured a significant increase in austenite fraction after partitioning as compared to the as-quenched condition. Zhong *et al.* [23] found that in Q&P steels with high amount of C the interface probably migrates to increase the austenite fraction, whereas in low C Q&P steels it probably migrates to reduce it.

1.2.3 Competing reactions during Q&P heat treatment

In addition to carbon partitioning into austenite, other processes could occur during the partitioning step. Including decomposition of austenite to other phases, such as bainite, formation of cementite and/or transitional carbides, and carbon trapping in martensite interfaces and dislocations.

1.2.3.1 Carbides precipitation

Controlling the precipitation of carbides is of vital importance to obtain the desired microstructures in a Q&P process [12]. Since the stabilization of the austenite is based on its carbon-enrichment, it is crucial that carbon is not lost in competitive reactions. Thus, it is necessary to understand and control any carbide precipitation that might occur during the Q&P cycle. The untransformed austenitic region during the first quench can vary depending on its morphology, which can be interlath-lamellar or blocky, or the composition of the steel

[13]. Furthermore, the exact distribution of the austenitic regions at quenching temperature is not known. Therefore, it can be concluded that the carbon escape route may vary for each case.

In the martensite, fine transition carbides generally are not considered detrimental, whereas cementite can be more concerning. Therefore, the greatest effort has been made to understand when transition carbides are replaced by cementite [24,25], rather than the initiation of transition carbides precipitation itself. However, any transition carbide precipitation decreases austenite carbon-enrichment potential in Q&P processing and, hence, it is necessary to develop a better understanding of the initiation of transition carbide formation, including composition and processing effects [26,27].

Carbon chemical potential is quite higher in as-quenched martensite than in retained austenite, so the carbide nucleation is more likely to occur in BCC ferrite than in austenite [27,28]. The α/γ interface is also a propitious site for carbide formation [28]. Carbon trapping at crystallographic defects, and austenite decomposition to ferrite and cementite as a result of martensite tempering during Q&P is consistent with the lower experimental austenite fractions often achieved compared with predictions [18,19,29–31].

1.2.3.2 Other phase transformations

Apart from carbide precipitation, austenite decomposition can also take place during the partitioning. The normally employed range of partitioning temperatures (350 °C – 450 °C) enables the bainite-ferrite formation from austenite [32]. Some authors demonstrated that bainitic transformation in austenite–martensite mixture is faster than that starting from single-phase austenite [33,34]. The authors suggested that the boundary between martensite and austenite serves as a nucleation site for bainitic ferrite. Bainite formation decreases the amount of austenite available for carbon enrichment and therefore is often undesirable [35]. Some researchers assume that small amounts of bainite are formed mostly in the beginning of partitioning [36]. Further enrichment of remaining austenite with carbon lowers the B_s temperature which should significantly suppress the bainitic reaction so that eventually B_s can drop below the partitioning temperature and bainitic reaction can stop completely.

In some recent studies [37–39], in which the employed partitioning temperature was higher than usual, decomposition of untransformed austenite into perlite was observed. The rapid carbon enrichment of austenite and the higher partitioning temperature promote pearlite formation at prior austenite grain boundaries and cementite precipitation within austenite

films [38]. This transformation is obviously undesired, as consumes carbon for austenite enrichment and decreases the retained austenite content.

The last competing reaction is the formation of secondary martensite during the final cooling. If competitive reactions occurred during the partitioning stage, part of the austenite might not be sufficiently carbon-enriched to be stable at room temperature and, consequently, it might transform into secondary martensite at the last cooling [13,38,40,41], which was considered as detrimental for ductility [40,42].

1.2.4 Alloying elements employed in Q&P steels

In this section the influence of different alloying elements on Q&P process and resultant properties is analyzed. The role of alloying elements in Q&P steels could be described in this way:

- Prevent any competing reaction such as carbide precipitation or decomposition of austenite into ferrite, bainite or pearlite during partitioning [6,13,43]; the addition of silicon as alloying element is the key to obtain the desired results.
- Improve the hardenability and final mechanical properties of the steel [43,44]; the addition of manganese is the simplest key in this question, existing other possibilities.

Alloying elements also influence on phase transformation temperatures (A_{c1} , A_{c3} , M_s , and M_f), which are important to design Q&P cycles. From the industrial point of view, the lower these temperatures, the more reduction in the energy consumption and costs. In Table 1, Table 2 and Table 3 a short review of typical compositions containing the elements discussed in the next sections is shown. The typical Q&P steels contain Fe, C, Mn and Si, while other elements could be also added depending on the purpose.

Table 1. Short review of typical steels with Fe-C-Mn-Si/Al compositions employed in Q&P process.

Studies with Fe-C-Mn-Si/Al compositions				
Ref.	C	Mn	Si	Al
[45]	0.25	3.00	1.50	-
[46]	0.29	3.00	1.40	-
[47]	0.25	3.00	1.50	0.02
[48]	0.20	3.50	1.54	-
	0.20	3.50	0.45	0.22
[49]	0.2	3.00	1.60	0.06
	0.29	2.95	1.59	0.06
	0.28	4.95	1.64	0.06
[50]	0.29	1.49	1.47	0.26
[51]	0.19	1.61	0.35	1.10

Table 2. Short review of steels with Fe-C-Mn-Si compositions and Ni and/or Cr additions employed in Q&P process.

Studies with Fe-C-Mn-Si compositions and Ni and/or Cr additions					
Ref.	C	Mn	Si	Ni	Cr
[52]	0.19	6.00	-	-	-
	0.19	5.80	1.40	-	-
	0.19	6.00	-	2.10	-
	0.19	5.70	1.40	1.60	-
[53]	0.24	1.38	1.39	0.03	-
	0.21	1.44	1.44	1.01	-
	0.28	1.41	1.46	1.99	-
[54]	0.2	1.54	1.30	0.07	1.48
	0.19	1.52	1.32	1.53	0.01
[55]	0.21	4.00	1.60	-	1.00
[56]	0.22	1.30	0.25	-	0.20
	0.27	1.50	1.61	-	-
	0.28	1.46	1.58	-	0.97
[57]	0.12	0.87	0.26	-	12.00

Table 3. Short review of compositions employed in Q&P steels with Mo and/or V additions.

Studies with Mo and/or V additions							
Ref.	C	Mn	Si	Ni	Cr	Mo	V
[58]	0.43	0.59	2.03	0.07	1.33	0.03	-
	0.43	0.59	2.03	0.07		0.03	-
[59]	0.37	2.27	2.45	1.47	0.80	0.58	-
	0.22	2.42	2.49	1.39	0.72	0.49	-
	0.39	2.39	2.64	4.83	0.78	0.50	-
	0.28	2.37	3.00	5.30	0.71	0.60	-
[60]	0.20	1.50	1.50	-	-	0.13	-
[61]	0.21	1.65	1.67	-	0.03	-	0.20
	0.22	1.89	0.52	-	0.03	-	-
[62]	0.24	1.90	1.50	-	-	-	-
	0.24	1.88	1.47	-	-	-	0.03
	0.24	1.83	1.52	-	-	-	0.16
[9]	0.10	1.51	1.48	-	-	0.30	0.04

1.2.4.1 Carbon

C is important in Q&P steels because it helps retaining austenite and significantly increases the strength of the martensite [63]. C also decreases M_s temperature and therefore, if sufficient austenite carbon-enrichment occurs, austenite retention at room temperature is enhanced. Morito *et al.* [64] reported that, increasing C content up to 0.6 wt.%, also increased dislocation densities of as-quenched martensitic microstructures. These results suggest that the strengthening from increasing C content may be strongly correlated with the resulting

dislocation density. However, the C content is generally kept at levels in which the carbon equivalent remains in the range of weldable steels.

The effect of increasing C content from 0.2 wt.% to 0.3 wt.% on tensile properties of Q&P steels has been studied in [49] for a steel containing 3 wt.% Mn and 1.6 wt.% Si. In the fully austenitized condition, the 0.2 wt.% C steel exhibited ultimate strength levels of 1200-1450 MPa and total elongations of 9–15% and increasing it to 0.3 wt.% increased the ultimate tensile strength levels into a range of 1400–1700 MPa and also total elongation levels to 11–17%. The results obtained in the study are represented in Figure 3.

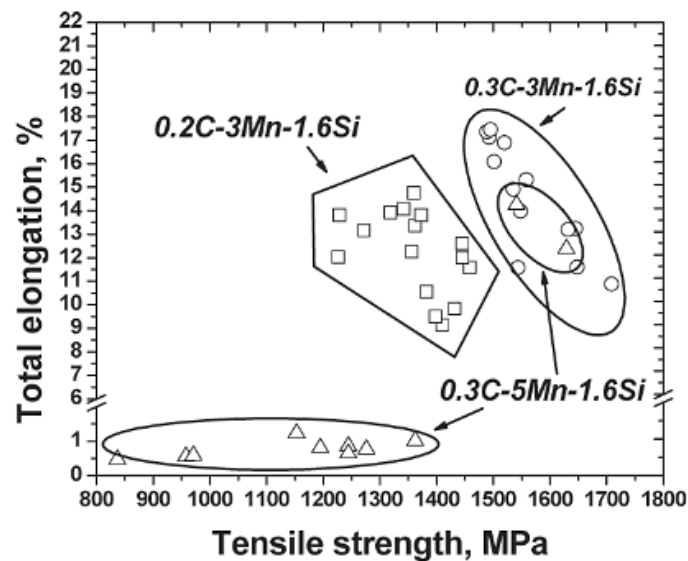


Figure 3. Total elongation versus tensile strength diagrams after the application of Q&P heat treatments showing the effect of C and Mn additions [49].

1.2.4.2 Silicon and Aluminum

It is known that the formation of undesirable cementite can be inhibited by adding Si, Al, or their combination. Most of the Q&P studies employ Si-bearing grades with 1–2.5 wt.% Si (typically around 1.5 wt.% Si is added) [56,65]. Si plays an important role in carbon precipitation suppression during Q&P process [62,66]. Since the solubility of Si in cementite is negligible, for cementite precipitation to occur during tempering, Si must diffuse into the matrix from the carbide-matrix interface. Simultaneously, carbon needs to diffuse in the opposite direction. At low Si levels, this process is controlled by carbon diffusion, while at higher Si levels, Si diffusion begins to control cementite precipitation.

Furthermore, Owen [67] reported that higher tempering temperatures are required for the decomposition of austenite with higher Si contents. Earlier researchers showed that Si retards or even eliminates bainite formation in the partitioning step due to the near-to-zero

solubility of Si in the cementite phase [68]. These studies suggest that between 1.25 and 2 wt.% Si is required to suppress bainite formation during reheating [69–72].

Si content may affect the final mechanical properties. However, increasing the Si amount to 1.5–2 wt.% does not seem to considerably affect hardness values. By contrast, other investigations reported a slight enhancement of hardness [69,73].

The problem associated with high Si contents is the formation of Si superficial oxide, together with the iron oxide, during the hot rolling. These oxides are difficult to remove by pickling and cause surface finish problems by reducing hot dip galvanizability [74,75]. A possible alternative is the use of Al which, like Si, is not soluble in cementite and hence prevents carbide formation without deterioration of galvanizability [35]. Aluminum alloying has been shown to result in significant retained austenite fractions, and to increase austenite carbon content in TRIP steels [35,76,77]. However, utilization of aluminum in steels for Q&P processing is limited because it has such a strong effect on the A_{c3} temperature that only the intercritical initial heating is possible.

The response of both Si and Al in Q&P steels has been investigated in multiple studies [48,50,51,78–80], as displayed in Table 1. In [80] the results show that increasing Al contents leads to a decrease in retained austenite fraction, strength and elongation levels, comparing with Si alloyed steel. Santofimia *et al.* [48] studied two Q&P steels with different Si and Al contents and they found that the partial substitution of Si by Al lead to lower retained austenite and higher cementite fractions. Furthermore, they reported a decrease in the strength levels. Ande and Sluiter [81] conducted a density functional theory (DFT) calculation and they showed that Si is almost twice more effective than Al suppressing carbides. Al has also been reported to delay strain-induced martensite transformation, enhancing TRIP effect [76,82,83].

1.2.4.3 Manganese

Austenite stabilization is mainly controlled by C enrichment although other austenite stabilizing elements, such as Mn, can be effective as well [66]. Mn is a common alloying element in this type of Q&P steels since it has effective austenite stabilization capacity, it increases hardenability by retarding austenite to ferrite, perlite or bainite transformation during initial fast cooling, it helps lowering phase transformation temperatures (strongly decreases the M_s temperature), and contribute to the overall strength of the steel by solid solution strengthening [84]. Mn contents added to Q&P steels are typically in the order of 1.5 wt.%, with the aim of avoiding diffusional transformations during the quenching step.

Furthermore, since Mn retards bainitic reaction can be intentionally added to avoid competing reactions also in the partitioning. Higher contents of Mn are considered to enhance austenite retention, employing the austenite stabilizing effects of Mn to adjust the relative amounts of martensite and austenite [85].

In recent Q&P studies [37,45–49,55], interesting tensile properties were obtained with steels containing increased Mn contents. For example, the use of Mn additions of 3 wt.% and 5 wt.% in Q&P steels has been successful in developing very high strength cold-formable sheet steels with tensile strengths exceeding 1500 MPa, in combination with total elongations above 20% (Figure 4) [86]. However, an earlier study of the same authors showed that, after a partitioning stage at 400 °C, the 5 wt.% Mn containing steel showed a microstructure with untempered martensite, leading to very low ductility with most samples failing at strains lower than 2% [85].

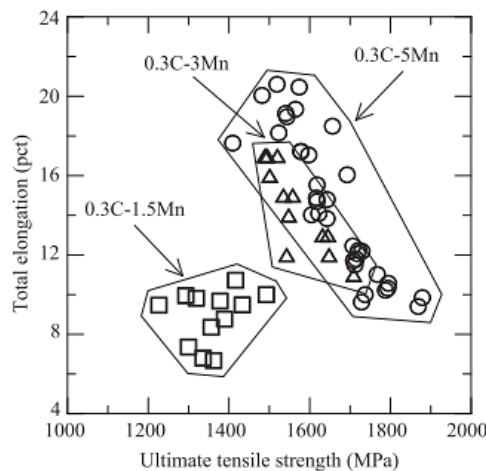


Figure 4. Total elongation versus ultimate tensile strength for Q&P treated 0.3C-Mn-1.6Si steels containing various levels of manganese [86].

High Mn contents lead to the development of strong band structure, which might reduce TRIP effect and, consequently, the ductility of the steel [84]. As a medium carbide-forming element, Mn will decrease the diffusivity of C in austenite and thus, slow down the growth kinetics of bainitic ferrite [87].

1.2.4.4 Chromium and Nickel

Additions of Ni and Cr have both been reported to increase retained austenite amounts after Q&P [56,58]. Pierce *et al.* [54] also observed that a comparable fraction of austenite was stabilized in the alloy with Cr with respect to the alloy with Ni, being Cr rather cheaper.

Cr additions up to ~7 wt.% are reported to be austenite stabilizers in Fe-Cr binary steels, while higher amounts starts to stabilize ferrite rather than austenite [90]. The reasons why Cr

is a good austenite stabilizer is because it lowers M_s temperature and considerably reduces the C diffusivity in austenite, increasing the resistance of martensite to tempering [88], slowing austenite decomposition kinetics [89] and, consequently, delaying bainite transformation [56]. E. J. Seo *et al.* [56] analyzed the role of Q&P treatment on a Si (1.6 wt.%) and Cr (1 wt.%) added medium Mn steel. They observed that the addition of Cr resulted in an increase in the retained austenite amount and, consequently, significantly improved plasticity without decreasing of the strength.

On the other hand, Ni also reduces the M_s temperature but is a significantly stronger austenite stabilizer than Cr and enhances the kinetics of C diffusion in austenite [88]. Additionally, it can assist in controlling major competing reactions, such as precipitation of carbides inside austenite and pearlite formation, and in increasing thermal stability of austenite [52]. Increasing wt.% Ni also lead to grain refinement and increases the retained austenite fraction in volume. However, due to the higher cost, Ni content should be kept to a minimum [91].

Rizzo *et al.* [59] observed that a high Ni content steel, apparently having larger amounts of retained austenite relative to the other experimental alloys, had less desirable strength/ductility combinations. On the contrary, other researchers reported that lower additions offer better mechanical properties because of a large fraction of retained austenite in volume [56,92,93]. Finally, Kikum *et al.* [53] observed that increasing Ni content the amount and stability of retained austenite increased. The Ni addition also led to grain refinement. The strain-induced transformation kinetics were retarded and they also reported solid-solution strengthening effect. Consequently, an improvement in tensile strength and elongation, and hardness was achieved.

1.2.4.5 Molybdenum and Vanadium

Normally, the composition of the Q&P steel does not contain any carbide forming elements, such as Nb, V, Ti, Mo, etc. This means that the Q&P steel excludes the advantage of precipitation strengthening of carbides and fine-grain strengthening [94]. However, there are several studies which investigate the influence of these elements in Q&P process [65,86–95].

The addition of Mo and/or V to the compositions of Q&P steels pursues the strengthening produced by carbide precipitation. Some studies carried out an additional tempering after the quenching and partitioning process to further promote this [10,98,99]. Mo is also reported to improve the hardenability of the steel [9]. Another property of both Mo and V is that they act as austenite grain refinement [9,60,97,98]. Regarding mechanical properties V addition

improves strength and work hardening [60] and also wear resistance [95] of the Q&P treated steels. Zhang *et al.* [60] also reported that V addition improved the ductility by refining the grain size and enhancing the austenite stability.

1.2.5 Q&P cycle parameters

The original Q&P process (Figure 2) can be summarized in four main steps:

- Austenization: In this step the steel is fully austenitized (or, sometimes, partially, in order to introduce ferrite into the microstructure with the aim of decreasing yield strength and raising elongation [100]). The initial microstructure [101,102], soaking temperature (ST) [103,104] and soaking time (St) [103] influence on the characteristics of the austenite formed in this step.
- Quenching: The steel is quenched from the ST to a temperature between M_s and M_f , called quenching temperature (QT), with the aim of obtaining a partially martensitic and partially austenitic microstructure (and partially ferritic in the case of the partially austenitized steels). The rate of cooling during quenching is important because it is necessary to prevent the formation of lower bainite in case of cooling after full austenization.
- Partitioning: During this step the carbon migrates from martensite into austenite. In one-step Q&P cycles the partitioning temperature (PT) is the same than QT, whereas in two-step Q&P cycles it is higher, and usually above M_s . In the time that steel remains in PT, called partitioning time (Pt), competitive reaction such as carbide precipitation or austenite decomposition might occur.
- Final cooling: The steel is cooled to room temperature. If austenite is sufficiently carbon-enriched, secondary martensite formation is supposed to be avoided.

The control of processing parameters such as quenching temperature, partitioning temperature and partitioning time is crucial to obtain the desired microstructures, and therefore mechanical properties. Hence, numerous studies have been carried out to investigate the influence of these parameters.

1.2.5.1 Quenching temperature (QT)

Quenching temperature determines the austenite and martensite fractions for the following partitioning step. If QT is too low, near to M_f , a small amount of austenite will be available for carbon-enrichment and final retention. On the contrary, a high QT, slightly below M_s , left little martensite to provide carbon to the austenite and, consequently, austenite is unlikely to be

stabilized and retained at room temperature. Thus, a determination of the optimal QT to reach the maximum austenite volume fraction is needed.

Initially, Speer *et al.* [6] proposed a calculation of the optimum QT based on the prediction of the maximum retained austenite fraction at room temperature. This model is based on constrained carbon equilibrium (CCE) and assumes that there is full carbon partitioning from martensite into austenite at the end of the partitioning, that diffusion of substitutional atoms is restricted and that austenite fraction remains the same (i.e., there are no competitive reactions and martensite/austenite interface is fixed). Even with a good approximation of the calculated optimal QT, the carbon quantity that really migrates from martensite into austenite, depends on the carbon partitioning kinetics. As a result, the retained austenite volume fraction predicted as a function of QT is much less sensitive to QT than it would be expected based on the full carbon migration theory. Later, Santofimia *et al.* [105] proposed a model for carbon diffusion during partitioning step assuming migration of the martensite/austenite interface.

Experimental results on various studies [106–108] suggest that exists a wide processing window to obtain the desired retained austenite content, as it is shown in Figure 5.

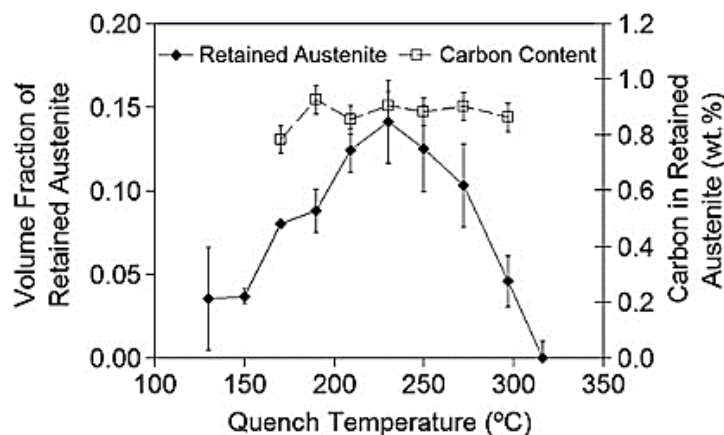


Figure 5. Volume fraction of retained austenite and corresponding carbon content after full austenization, quenching to different temperatures and partitioning at 400 °C for 100 s [108].

1.2.5.2 Partitioning temperature (PT)

Partitioning temperature could be the same as QT (one-step partitioning) or higher than QT (two-step partitioning). In the last, temperatures typically range between 350 °C and 450 °C. The increase of PT increases carbon partitioning from martensite, leading to the formation of tempered martensite with less stored energy and hardness [109]. However, the risk of carbide precipitation and the formation of other phases, such as bainite, is increased at

higher temperatures [110]. The amount of retained austenite and its carbon concentration increases with temperature and then decreases probably due to carbides' formation. Santofimia *et al.* [43,48] studied the influence of partitioning temperature in austenite stabilization employing different partitioning times in a high alloyed steel. They observed that at very short partitioning times higher partitioning temperatures led to higher retained austenite amounts, whereas at longer times the tendency was the opposite (Figure 6).

Regarding mechanical properties, tensile strength decreased with increasing partitioning temperature due to softening of martensite. Finally, elongation increased with partitioning temperature despite of slight decrease in retained austenite fraction for temperatures above 420 °C, probably due to dominant role of material softening [8].

Although in the early days of Q&P only carbon diffusion was considered to occur during the partitioning, in last years the diffusion of substitutional elements, such as Mn or Si, at relatively high partitioning temperature (450 °C) has been proved [111]. This implies a mobile martensite/austenite interface, highlighting the importance of interface migration to adjust the retained austenite fraction and, correspondingly, the austenite carbon content and mechanical stability [20]. However, in these studies partitioning temperature was limited to 450 °C and the partitioning of substitutional alloying elements only occurred a few nanometres away from the interface.

Ayenampudi *et al.* [39] applied high partitioning temperature treatments, in the 400 °C – 600 °C range, to a medium Mn steel. They observed strong competitive reactions, such as cementite precipitation in austenite films and pearlite formation from blocky austenite. However, at the highest temperature of 600 °C, high austenite volume fractions were obtained in the final microstructure, as a result of austenite reversion and effective austenite stabilization. This result was in line with the work published in [37], where it was also observed that the high austenite volume fraction did not result in a significant improvement of mechanical properties, which was potentially due to the formation of secondary martensite after partitioning and poor mechanical stability of austenite.

Ding *et al.* [112] conducted a study where, as usual in Q&P cycles, the first quenching was interrupted in a temperature between M_s and M_f , but then the partitioning stage was carried out in the intercritical range. Thus, they observed the formation of new austenite by reheating the initial primary martensite + pre-existing austenite microstructure in a Fe-0.2C-8Mn-2Al steel. The new austenite formed during the partitioning stage was enriched with Mn and, hence, was stable during final quenching. The pre-existing austenite grew during partitioning

but only the newly formed austenite region was enriched in Mn and, therefore, the initial region transformed into secondary martensite due to the low chemical stability. They also analysed the influence of pre-existing austenite fraction on mechanical properties, observing that an excessive content (30%) resulted in coarse secondary martensite which made the material less ductile. Furthermore, the study concluded that a small fraction of pre-existing austenite could apparently accelerate the austenite reversion kinetics.

The research work described in the previous two paragraphs [37,39,112] are the only known studies that consider a partitioning temperature in the intercritical range. These studies showed that it can be a promising strategy to retain a high amount of austenite in the final microstructure. However, further research is needed to determine the influence of alloying elements and process parameters (QT, PT, Pt) on microstructure and mechanical properties.

1.2.5.3 Partitioning time (Pt)

In the study made by Santofimia *et al.* [43] it is shown that the time to attain the maximum retained austenite fraction can be predicted by the calculations of martensite formation and kinetics of carbon partitioning in a binary Fe–0.2C system. The calculations confirm the existence of two peaks, which were previously experimentally observed by Matlock *et al.* [113]. The first peak indicates the stabilization of austenite due to rapid kinetics of carbon partitioning from martensite into austenite, whereas the second was explained by redissolution of transitional carbides formed at lower temperatures provided that cementite formation is suppressed after longer partitioning times. However, optimal partitioning time depends on the austenite fraction at QT, PT and steel composition [107]. It should be also pointed out that sufficient partitioning time is necessary to homogenize partitioned carbon content within the austenite grains. However, too long partition times can lead to the formation of transitional carbides, thus deteriorating the mechanical properties. Figure 6 shows an example of the influence of the partitioning time at different partitioning temperatures for a high alloyed steel.

Regarding mechanical properties, the longer partitioning time, the higher softening of martensite, tending to reduce tensile strength of the steel. Contrarily, depending on the partitioning temperature, the increase in the partitioning time, up to 30-100 s, lead to an increase in the yield strength. Generally, with the increase in the partitioning time, the amount of retained austenite initially decreases and then remains almost constant or increased. Regarding C concentration in austenite, it rapidly grows at the beginning of the partitioning, but then significantly slows down at longer partitioning times [8].

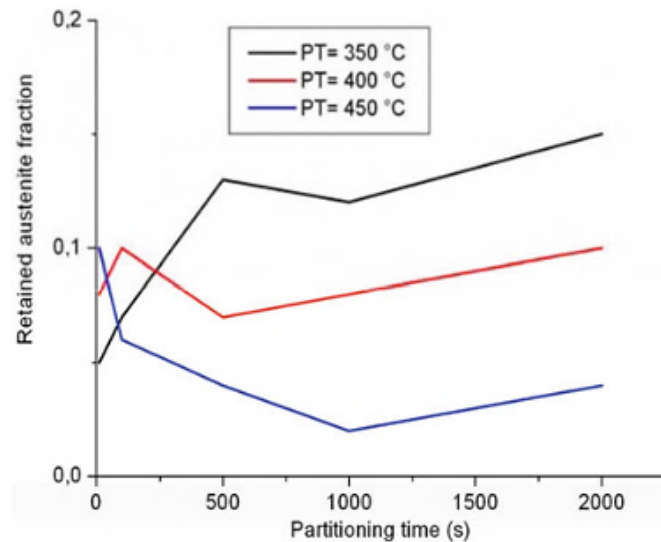


Figure 6. Volume fraction of retained austenite after Q&P treatment at different partitioning temperatures and times [8].

1.2.6 Microstructural evolution during Q&P process

Q&P process aims at obtaining a final microstructure that consists of martensite and retained austenite. However, typically, the final microstructure of Q&P steel, is the mixture of tempered martensite, retained austenite, secondary martensite and possibly lower bainite. Assuming that austenite decomposition during the partitioning and carbide precipitation are avoided, the microstructural evolution during the Q&P cycle would evolve as shown in Figure 7, resulting in a final microstructure formed by:

- Carbon-depleted martensite laths, or tempered martensite (α'), formed during the quenching to QT and subsequent partitioning stages, which provides carbon to the austenite. In some cases, carbide precipitation can be observed in this phase due to the auto-tempering of the martensite.
- Carbon-enriched retained austenite (RA).
- Secondary martensite (α'_{sec}) formed during the final cooling from austenite which was not enough carbon-enriched. Since this martensite is formed from somewhat carbon-enriched austenite, it usually has higher carbon content than the tempered one.

Due to the short partitioning time and/or coarse austenite, the carbon content in austenite grains can be highly nonhomogeneous causing significant variability in stability of these grains. Thus, it is common that secondary martensite starts transforming from the interior of blocky austenite due to gradients in the carbon content, originating martensite-austenite (MA) islands with RA across the grain boundary [112,114].

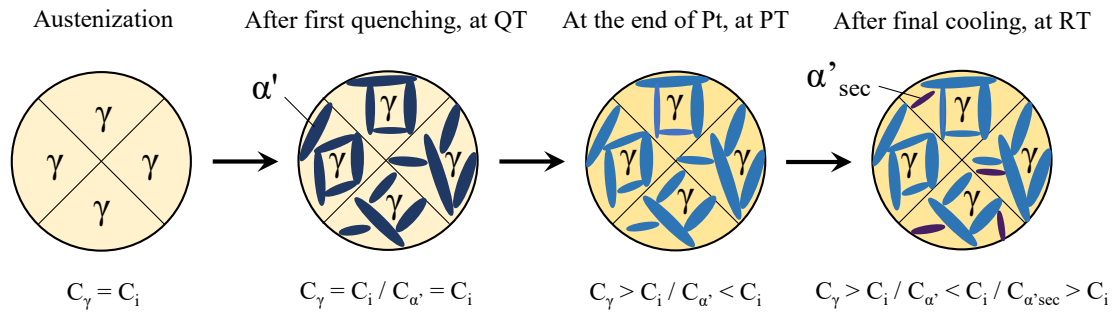


Figure 7. Microstructural evolution that undergoes during Q&P cycles showing the different phases and carbon contents of each phase expected at austenization, quenching temperature, at the end of partitioning, and final microstructure. In this figure, it is assumed that neither austenite decomposition nor carbide precipitation occurred.

The final martensite and austenite contents will depend on the employed QT, as it determines the volume fraction of each phase and hence the grain size prior to partitioning stage. On the other hand, the carbon content and gradient in each of the phases, determining the thermal stability of the austenite, will depend on the partitioning stage parameters [43,115].

The different Q&P heat treatments routes would lead to different microstructures with a combination of RA, α' , α'_{sec} , MA islands and in some cases even ferrite, bainite, pearlite and/or carbides, and each microstructure would lead to a different mechanical behavior. An accurate description of the microstructure is essential for better understanding of the microstructure formation and better control of the final properties of the material [110]. However, the combination of different phases makes complex the understanding of the microstructures obtained by Q&P process. Figure 8 shows an example of a typical Q&P microstructure. Dilatometry can support the understanding of the features of the final microstructure, and specially, can help understanding microstructure evolution during Q&P processing, which cannot be described by metallography [38,39,106,116].

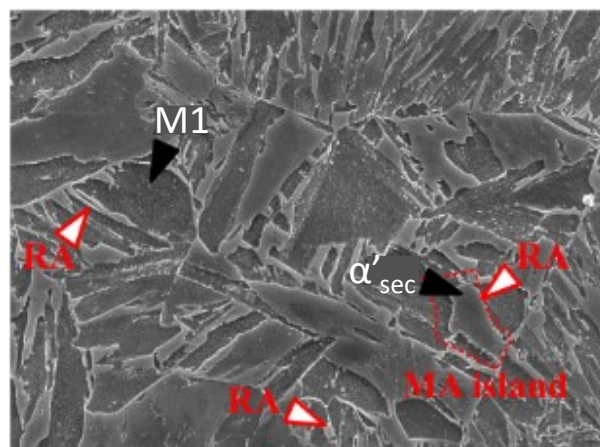


Figure 8. SEM micrographs of a typical Q&P microstructure containing retained austenite (RA), tempered martensite (M1), secondary martensite (α'_{sec}), and martensite-austenite islands (MA). Adapted from [117].

1.2.7 Variations from the original Q&P cycle

Several variants of the original Q&P process have been proposed and explored recently:

- Stepping-quenching and partitioning (S-Q&P): The objective is to divide blocky austenite into film-like austenite to obtain a finer microstructure by the repetition of several thermal cycles [118].
- Quenching and partitioning-tempering (Q&P-T): In this process the matrix strength is enhanced via nano-carbides precipitation (e.g. NbC or VC) in the tempered matrix [119]. The method certainly works but requires an even tighter control of the partitioning temperature and time [98].
- Quenching-tempering and partitioning (Q-T&P): Here the initial quenching temperature is fixed at room temperature [79,120]. In order to ensure the room temperature is located between M_s temperature and M_f temperature, the alloying composition must be tailored carefully. The main advantage is that sophisticated cooling equipment to control the QT are not needed.
- Quenching and flash-partitioning (Q&FP): In this process Q&P is integrated in the cooling stage of the press-hardening process. Dynamic carbon partitioning from martensite into austenite is allowed as martensite formation proceeds during the press-hardening process [121]. To ensure carbon flash-partitioning occurs during the continuous cooling, a considerable amount of Si must be added to retard cementite precipitation, whereas amount of Mn must be kept to the minimum to have higher M_s temperatures.

1.3 Retained austenite and its role

Austenite amount and stability are important for mechanical properties. RA stability can be analyzed from two different perspectives: Thermal stability achieved during the heat treatment to retain the highest amount of RA in the final microstructure and mechanical stability during deformation.

1.3.1 Thermal stability of the austenite

Thermal stability of austenite directly determines whether austenite will be retained at room temperature or not. The stability during heat treatment is often thought to depend on the chemical composition. Elements such as Mn or C, which are austenite stabilizers, lower the M_s temperature and, also, the eutectoid, widening the temperature range in which austenite

is stable. On the other hand, Si helps to stabilize austenite by suppressing cementite precipitation, thus leaving more C available to enrich the austenite [122]. Therefore, increasing the addition of austenite stabilizer elements can lead to a higher retained austenite amount.

Carbon content in austenite depends on partitioning parameters and, typically, was found to reach ~1 wt.%. However, as mentioned above, C gradients may appear within either bulk of steel or across a single austenite grain and consequently the less carbon-enriched areas may transform into secondary martensite during final cooling.

Stabilization of austenite during partitioning step compromised two important stages: carbon diffusion from martensite into austenite, which in general is a quick stage (it can take place in less than 1 s), and homogenization of carbon within the austenite, which was found to need much longer time [123]. DICTRA simulation can be of great help when studying these two stages [38,124]. Hidalgo *et al.* [38] simulated carbon partitioning at the partitioning stage in a 0.3C-4.5Mn-1.5Si steel and they found that, at 400 °C, less than 1 s was needed for carbon partitioning to occur. However, 50 s were necessary for its distribution to become homogenized in a 100 nm thickness austenite lath.

In addition, some recent studies reported that the stability of retained austenite also depends on its morphology and therefore on the locations where it was formed during microstructure evolution. Numerous studies proved the coexistence of blocky and film-like retained austenite morphologies, being reported the film-like austenite as the most stable. Sun *et al.* found three types of retained austenite in 0.2C-1.5Si-1.9Mn steel, including austenite films located between the martensite laths with a width of about 100 nm, blocky austenite incorporated into ferritic matrix, and ultrafine austenite films, of about 20-30 nm thick, between the plates of ferritic bainite [106]. On the other hand, Arlazarov *et al.* [125] investigated the role the grain size plays in thermal stability of austenite in a Medium-Mn steel and they found that a grain size smaller than 0.5 μm clearly lowered the M_s , increasing austenite stability.

1.3.2 Mechanical stability of the austenite

The mechanical stability of retained austenite is the stability against the formation of martensite under the influence of deformation or transformation-induced plasticity (TRIP) effect. The TRIP effect increases the work hardening rate and delays necking, thereby improving uniform elongation (UE). The studies performed with Q&P steels often indicate no direct correlation between volume fraction of retained austenite and ductility of steel, which

means that the role of stability of the austenite looks more important than that of its volume fraction. If the austenite into martensite phase transformation occurs at small strains it is unable to retard the necking of the material. On the contrary, if it is too stable (i.e., no phase transformations at large strains) then it will not contribute to the TRIP-effect [126,127].

The stability of RA in steels that exhibit the TRIP effect is affected by chemical composition [126] (mainly C content), grain size [128], morphology [129], and surrounding microstructure [130]. Therefore, a better understanding of RA stability can aid in designing a microstructure that will provide the desired combination of strength and formability.

Jacques *et al.* [126] performed experiments on steels with low and high silicon contents and similar amounts of RA. The difference between the RA in the two steels consisted in the C content and the amount of the surrounding phases, being the grain sizes similar in both steels. The high silicon steel's austenite had the higher C content, due to the carbide precipitation occurred in the low Si steel, and the studies demonstrated that higher C content decreased the austenite transformation rate during straining. Therefore, they concluded that the high silicon steels had a slower RA transformation rate during straining due to the more carbon-enriched RA required a higher amount of strain to transform into martensite.

Xiong's *et al.* [129] researches revealed that although blocky austenite had higher carbon content (1.14 wt.%) compared to that in film-like austenite (0.64 wt.%) located between martensite laths, "high C" blocky RA appeared to be less resistant to martensite transformation. The blocky austenite began to transform into martensite at tensile strain of 2% and by 12% strain all blocky austenite had transformed. Nevertheless, numerous film-like austenite grains were still present at that strain, indicating that carbon content is not always a dominating factor. This could be explained by the differences in yield strength of the surrounding phases. In the work [129] the Q&P cycle was started with a partial austenization in the intercritical range, and blocky austenite was surrounded by ferrite, while film-like austenite was surrounded by higher yield strength martensite laths and the martensite transformation requiring volume expansion could be suppressed.

The other factor is grain size effect. Generally, it was reported that coarse austenite grains are less stable than the finer ones. In [83] it was studied the influence of grain size on austenite stability of Q&P steels and they concluded that the optimal austenite grain size was between 0.01 and 1 μm . RA grain sizes above 1 μm transformed into austenite at quite low strains, whereas a size below 0.01 μm led to a too stable austenite that did not transform even at high strain levels.

Finally, De Knijf *et al.* [131] reported that austenite stability was negatively affected by the appearance of secondary martensite. As secondary martensite is formed, the distribution of strains in the microstructure can be significantly affected, since the amount of strain that can be accommodated in tempered martensite is drastically reduced. Consequently, the transformation stability of austenite decreases.

1.4 Relationship between microstructure and mechanical properties

Q&P steels are of significant interest to generate desirable combinations of strength and formability. The key of these properties is the microstructure combining a martensitic matrix with significant fractions of carbon-enriched retained austenite [17]. However, the correlation between mechanical properties with the parameters of microstructure and its constituents is still a subject of study. Table 4 shows some examples of the tensile properties obtained in Q&P treated steels and the retained austenite measured after the treatment.

Table 4. Tensile properties and volume % of retained austenite obtained by Q&P.

Steel	UTS (MPa)	TEL (%)	RA (%)	Ref.
0.2C1.96Mn1.49Si0.25Mo	1280-1510	4-15	11-16	[80]
0.3C3Mn1.6Si	1500	17	1-15	[49]
0.2C3.5Mn1.5Si	1415-1630	15-23	8-19	[48]
0.2C1.57Mn1.55Si	1220-1340	12-16	6-14	[132]
0.5C2.01Mn1.03Si1.58Cr0.34Mo0.11Ti	1741-1931	2-12	12-28	[133]
0.28C4.08Mn1.42Si	1399-1548	13-16	12-19	[134]

Several studies on Q&P steels reported the trend that the increase in RA is accompanied by increasing total elongation (TEL) but not so much by uniform elongation (UE), which reflects the contribution of TRIP effect. As mentioned in the previous section, it is the stability of the retained austenite, rather than its amount, which determines the final mechanical properties. Seo *et al.* [135] concluded that, in Q&P processed medium Mn steels, the key factors determining the mechanical properties were the kinetics of the mechanically-induced austenite to martensite transformation and the amount of secondary martensite. One characteristic of Q&P steels is the elevated YS/TS ratio due to a considerable amount of tempered martensite and, therefore, the strain hardening rate of these steels is relatively low. This results favorable for hole expansion, but the presence of secondary martensite significantly reduce YS and, consequently, the YS/TS ratio [8].

1.5 Medium Mn steels (MMnS)

Medium manganese steels (MMnS), with Mn contents between 4 wt.% and 10 wt.% [52], are considered another promising third generation AHSS due to their combinations of properties. These steels are based on a concept proposed by Miller [136] in 1972. In this case, cold rolled martensitic microstructures are intercritically annealed forming austenite by the so-called Austenite Reverse Transformation (ART) phenomenon [137]. Austenite stabilization can be achieved through diffusion of substitutional elements, such as Mn, (and also C) into austenite during high temperature processing [138,139], resulting in rather high contents of retained austenite (20–40%) [140–142]. A schematic of this process is shown in Figure 9. The stability of retained austenite and ultra-fine microstructure in MMnS, seem to play a key role in the impressive strength/ductility balance of these steels [143–145].

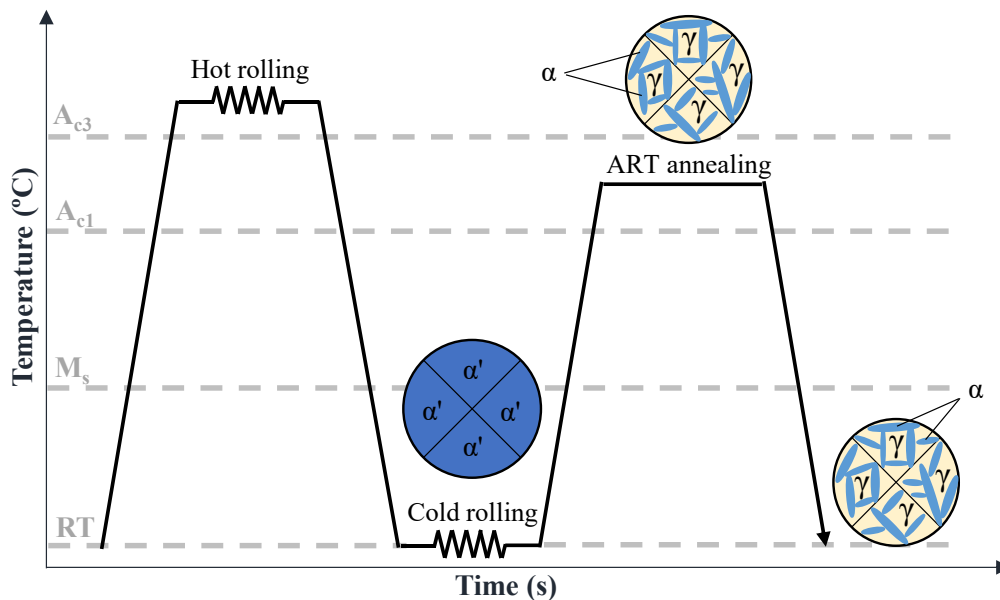


Figure 9. Schematic of the typical processing route of medium-Mn steels, where α' is martensite, α is ferrite and γ is austenite.

Intercritical annealing stage carried out in MMnS implies much longer times (typically hours) than the partitioning stage in Q&P process (typically ranging from a few seconds to few minutes). On the other hand, having both a tempered martensite matrix, the ultrafine-grained ferrite in medium Mn steels is softer. Therefore, the strength of Q&P steels is generally higher than that of medium Mn steels, but Q&P steels have a much lower elongation due to a lower RA fraction [146].

Although last years advanced, the understanding of medium manganese steels is still under development. The microstructure evolution, microstructure-properties relationship, the effect of alloying elements and contents, effects of processing and post-manufacturing, etc. are

some of the aspects which need to be approached. Moreover, although it is easier than for second-generation advanced high strength steels, such as TWIP steels, processing of MMnS in industrial environments is still challenging due to their relatively high alloy contents [147].

Even though the phase transformation behavior given in medium Mn steels during its processing is relatively understood, the precipitation and dissolution of the carbides and how does it affect austenite reversion required further study. Specifically, the understanding of how the heating rate and austenite reversion temperature affects the evolution of carbides would offer new awareness for the novel microstructure designs in MMnS [146].

1.6 Q&P treatment for automotive industry

The requirements of the automotive industry for weight reduction, improved fuel efficiency, and CO₂ mitigation along with crash safety standards imposed by governments make the development of third generation AHSS a priority to the steel industry, as they provide an opportunity for the development of cost-effective and light-weight parts with improved safety and optimized environmental performance [148–150].

The ultra-high strength and excellent ductility, or formability, of Q&P steels make them well suited for weight reduction in car bodies, while increasing occupant safety. Q&P steels have a higher stretch-forming capability than conventional high strength steels (HSS) due to the significantly higher rate of work hardening. Furthermore, compared to most HSS with the similar tensile strength, Q&P steels have substantially higher formability; therefore, they are especially suitable for structural and safety parts of automobiles, such as cross members, longitudinal beams, B-pillar reinforcements, sills, and bumper reinforcements, which are difficult to cold form with conventional HSS with the same strength [151]. Q&P steels are still at an early stage of industrial implementation and might be developed for both high-strength components in automotive and other applications.

1.6.1 Commercialized Q&P steels

To date, two levels of Q&P steels are in global production, with 980 MPa and 1180 MPa in tensile strength. The enhanced properties of Q&P steels offer benefits over similar strength steels of other microstructures. For example, compared against Dual Phase steel with similar yield and tensile strength, Baosteel produce a Q&P steel which shows higher uniform elongation, total elongation, work hardening index, and higher lowest point on the forming

limit curve (FLC_0) [152]. ArcelorMittal reports similar strength and elongation properties of the QP980 steel, with a targeted 23% hole expansion ratio [153].



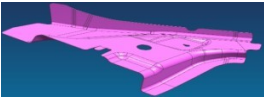



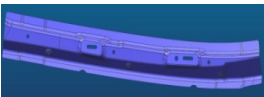

QP980 is undergoing increasing use in automotive production. In 2016 General Motors presented the first application in the Chevrolet Sail from SAIC-GM [154]. Later, the 2021 Ford Bronco used hot dip galvanized QP980 in five components of the front and rear floor assemblies [155]. 60% of the body structure of the 2021 Jeep Grand Cherokee L is made from AHSS, with some parts stamped from 3rd generation AHSS [156]. Table 5 contains typical mechanical property ranges for industrially produced QP980 and QP1180 [151].

Table 5. Typical mechanical property ranges for industrially produced QP980 and QP1180. Adapted from [151].

Material	Yield strength (MPa)	Tensile strength (MPa)	Total elongation (%)
QP980	650-800	980-1050	17-22
QP1180	950-1150	1180-1300	8-14

A recent conference highlighted several applications (Table 6) where thinner gauge QP980 replaced DP590 in General Motors vehicles [157]. The same presentation showed the example of QP980 replacing press hardening steels in B-pillar reinforcements and door anti-intrusion beams in a First Auto Works vehicle.

Table 6. Replacing DP590 with QP980 allows for downgauging. Adapted from [157].

Part	Material	Part model	Part prototype
Kick Down Lower	DP590 1.8 → QP980 1.6 Weight saving: 0.38 kg		
A Pillar Inner Lower	DP590 1.2 → QP980 1.0 Weight saving: 0.20 kg		
Hinge Pillar Inner	DP590 1.2 → QP980 1.0 Weight saving: 0.58 kg		
A Pillar Inner upper	DP590 1.2 → QP980 1.0 Weight saving: 0.30 kg		

1.6.2 Weldability of Q&P steels

In addition to low weight and good mechanical behavior, high levels of weldability are important to have a competitive material to the automotive industry since high-quality welded joints are required to ensure the vehicle body's safety [158,159]. However, numerous studies

demonstrated that, due to the thermal effect of welding, apparent material softening can occur during different types of welding methods, such as laser welding (LW) [160–162], resistance spot welding (RSW) [163–165], gas metal arc welding (GMAW) [160,166] or friction stir welding (FSW) [167–170], in AHSSs like DP steel [160,165–168], TRIP steel [161,169,171], and martensitic steel [162,166,171]. Usually, property losses are related with the tempering of the material, which produces heterogeneities in the microstructure of the heat-affected zone where local stress or strain concentration is preferentially developed during deformation.

In Q&P steels the martensite is tempered during partitioning, while the austenite is stabilized. Therefore, the internal structures of Q&P steels are more stable. Recent studies verified the extraordinary welding performance of QP980 steel during LW [172–174] and FSW [175,176], and equal strength joints to the steel were successfully fabricated with negligible heat-affected zone softening. Wang *et al.* [177] demonstrated the viability of achieving high strength joints in the QP1180 steel, while in TRIP [169] and DP [170] steels with similar strength levels are difficult to achieve such joint strength levels.

The performance of the joint is determined by the welding method since, under various heat source energies, welding speeds, and cooling rates, the dimension and degree of softening of the heat-affected zone can vary considerably [160,178,179]. Although several works showed that Q&P steels have high welding performance [172,173,175,177,180], further research is required to determine the influence on the microstructure and mechanical properties, especially in ultrahigh strength steels (>1 GPa).

1.7 Q&P treatment for applications requiring wear resistance

It is complex to estimate the wear resistance of a material, as it is defined by the conjunction of many properties of the material and varies with the wear condition, environment, and mechanism. Typically, wear resistance is directly related with hardness, although many other factors must be considered. Increased hardness is generally obtained by increasing the carbon content of the steel. However, the higher carbon content typically leads to a decrease in other properties of interest, such as toughness, bendability, and weldability [181]. Therefore, other methods are being investigated to increase the wear resistance of steel without drastic loss of other important properties.

Although quenched and tempered (Q&T) steels show good abrasive wear performance, some studies demonstrated that microstructures containing RA, despite having lower hardness, presented better wear resistance. The benefits of RA were observed in block on ring testing of austempered ductile iron [182], pin on-disk testing of both mottled cast iron [183] and a D-2 tool steel [184] and a non-standard impact-abrasion test of a 13.8 wt.% Cr, 2.7 wt.% Mn containing steel [185].

More recently, Q&P steels have been studied in a wear context and have shown to be of interest for wear applications. All the Q&P studies related to wear are very recent and most of them correspond to the mining industry. In general, it is concluded that the retained austenite is very beneficial for the tribological behavior (wear and friction). Under mechanical loading, a higher amount of retained austenite helps to obtain a thicker hardened layer due to transformation into martensite. In Q&P steels, apart from the direct relationship between hardness and wear resistance, the latter also depends on the microstructure and, therefore, on the Q&P process conditions (QT, PT, Pt) [186]. Generally, higher austenite content translates into better abrasive wear performance. A clear example of this phenomenon is shown in the work of Wasiak *et al.* [187], who observed that wear is reduced by practically 50% in the case of Q&P compared to Q&T in a 35CrSiMn5-5-4 steel, so that the improvement obtained is substantial. The employed Q&P cycle consisted of a full austenization followed by an oil quenching to 235 °C and a partitioning at 260 °C, obtaining 20% of RA.

P. Wolfram *et al.* [188] calculated the volume loss of Q&P treated 9260 steel with normalized samples with respect to the performance of AR400F samples during dry sand and rubber wheel (DSRW) wear tests, and here also a beneficial effect of austenite was confirmed. In a subsequent study, the material was examined in a simulated wear track after controlled scratch tests for different microstructural conditions: after fast quenching and after quenching and tempering (Q&T) and quenching and partitioning (Q&P). The rapidly cooled material fractured out of the wear track in response to the indentation force. In Q&T, the wear track edges showed a chipping mechanism, while much less fragmentation was observed with the austenite-containing Q&P condition, which helps explaining the improved wear resistance of the Q&P microstructures. The same team also confirmed that the high Si Q&P processed steel exhibited a better combination of hardness and wear resistance than the same Q&T processed steel.

Another recent study [189] studied the wear resistance of direct quenched and partitioned (DQ&P) steels subjected to impeller-tumbler impact-abrasive wear testing [189]. This study

found that wear performance depended solely on hardness, regardless of microstructure, and did not see improvements with increasing RA. However, it must be considered that the wear resistance measured at laboratory level depends on the tests carried out, and these are very sensitive to the test parameters.

Generally, wear applications require thicker materials than those used in the automotive industry. Therefore, there is a need to understand the thermal gradients that can arise when applying Q&P to thicker samples. Stewart *et al.* [190] carried out some simulations to reproduce the thermal history that would occur in a 300M plate steel of 18 mm thick at different thicknesses, observing different quenching temperatures and non-isothermal partitioning depending on the thickness. Then, they evaluated the microstructures arising from each thermal cycle, discovering that the retained austenite varied between 5% and 27% between the surface and the center of the sample. As appreciable amounts of austenite were retained through the simulated plate thickness regardless of initial quench, they concluded that the insensitivity to quenching conditions might suggest behavior that would be considered beneficial in the framework of robust industrial implementation.

1.7.1 Toughness in Q&P steels for wear applications

In Q&P steels for wear applications, toughness is usually a desired property. Reported literature show that generally this parameter is improved in Q&P steels with respect to those treated by a conventional Q&T treatment [191–193]. This improvement is likely due to the lower hardness values measured in Q&P steels. Figure 10 shows a comparison between the Charpy impact energies obtained for a Fe-0.19C-1.5Si-1.46Mn steel treated by two different Q&P and Q&T cycles [194]. As it can be seen, the improvement achieved by the Q&P treatment is substantial, specially at high temperatures.

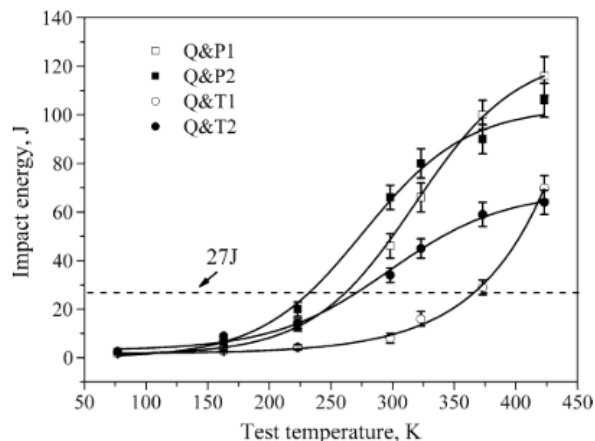


Figure 10. Comparison of Charpy impact energies at different temperatures of Q&T and Q&P treated specimens [194].

Chapter 2

Motivation and objectives

Chapter 2

Motivation and objectives

2.1 Motivation

The need to simultaneously reduce the weight of automobiles by manufacturing thinner parts and ensuring high passenger safety has led recent research in this field to focus on so-called third generation advanced high-strength steels (AHSS). Since in 2003 Speer *et al.* [6] published the first paper on it, one of the most promising approaches to produce such steels is the heat treatment known as “Quenching and Partitioning” (Q&P). The high retained austenite fractions present in Q&P steels are believed to result in a better balance between strength and ductility. In fact, documented tensile tests for these steels have shown outstanding combinations between these two parameters, indicating that Q&P steels are promising candidates to meet the demanding goals that car manufacturers must achieve.

The research carried out in Q&P field has generally considered partitioning temperatures in 350 °C–450 °C range. In this way, the austenite stabilization is mainly laid on C diffusion from martensite into austenite. Employing higher partitioning temperatures, corresponding to the intercritical range, the diffusion of substitutional elements, such as Mn and Ni, is also expected. Furthermore, due to the austenite reverse transformation phenomenon, higher levels of retained austenite are expected in the final microstructure, which may result in a further enhancement of the mechanical properties. Therefore, the motivation of this thesis is to investigate high partitioning temperature cycles as a new concept for stabilizing austenite in a Q&P style route and a new route for further improving mechanical properties for the automotive sector.

This thesis is also motivated by recent research in the field of Q&P which has found that this thermal treatment can be very interesting for other applications in which wear resistance plays an important role, such as mining, cutting tools, etc. Under mechanical loading, a higher amount of retained austenite helps to obtain a thicker hardened layer due to transformation into martensite, which can be beneficial for wear resistance.

2.2 Objectives of the thesis

The scope of this thesis can be divided into two sections depending on the final application of the Q&P treated steel. On the one hand, new Q&P cycles are designed in which the partitioning stage is carried out in the intercritical range with the aim of creating steels with improved properties for the automotive sector. The high partitioning temperature cycles are applied to medium Mn and Ni steels. On the other hand, an initial study is carried out on the applicability of the Q&P treatment for developing steels with good wear resistance. In this case, medium and high carbon steels are considered.

Q&P applied to medium Mn and Ni steels:

The major objective is to investigate the microstructure evolution and mechanical properties during a high partitioning temperature Q&P thermal treatment through experimental and modelling techniques. The high partitioning temperature corresponds to the intercritical range which results in the formation of reverted austenite accompanied by the diffusion of substitutional alloying elements such as Mn and Ni. The specific objectives are the following:

- To develop new third generation advanced high strength steels for the automotive sector with **enhanced tensile properties**, based on the application of a new high temperature Q&P route in which the stabilization of austenite is achieved not only by C diffusion, but also by the diffusion of substitutional alloying elements such as Mn and Ni.
- To investigate different Q&P parameters and different content of alloying elements to achieve **the most effective stabilization of austenite**, contributing to the optimization of process conditions and control of the alloying elements. In particular, to study austenite reverse transformation phenomenon and austenite stabilization **considering different austenite/martensite prior microstructures**.
- To understand the **partitioning behavior of substitutional alloying elements** (Mn and Ni) and their role in stabilizing austenite.
- To understand the influence of austenite content and its mechanical stability, along with tempered martensite, on the tensile properties. In particular, to **determine the TRIP (transformation induced plasticity) effect** that this austenite stabilized through mainly substitutional elements gives rise.

Q&P applied to medium and high C steels:

The specific objectives of this part of the thesis are:

- To investigate the **stabilization of austenite in medium and high C steels** heat treated by Q&P.
- To understand the influence of retained austenite content and mechanical stability on the wear and toughness properties. In particular, to perform a study of the **austenite transformation into martensite during the wear test**.
- To assess the opportunity to **improve wear resistance** of steel treated by a conventional quenching and tempering (Q&T) heat treatment replacing it by a Q&P heat treatment.
- To compare the **impact resistance** between a steel treated by Q&P and Q&T.

Chapter 3

Materials and experimental procedures

Chapter 3

Materials and experimental procedures

In this chapter the materials and techniques employed in this work are described. The reasons for selecting the chemical compositions, as well as the procedures employed to carry out the Q&P cycles are presented. Finally, the methods and experimental techniques employed to perform both microstructural and mechanical characterization are also described.

3.1 Materials and processing

3.1.1 Materials

The materials employed in this work were divided in two groups:

- Low C medium Mn steels with different Mn and Ni additions to be treated by high partitioning temperature Q&P treatments and study of their microstructure and strength-ductility behavior. These materials were produced in the laboratory in the form of cold rolled sheets and were studied as potential candidates for the automotive sector.
- Medium and high C steels employed to investigate the benefits of Q&P heat treatment in relation with wear applications. Several commercial grades were Q&P treated and characterized in terms of microstructure and hardness, wear resistance and toughness properties. In this case, classical Q&P cycles were applied, and the application of high partitioning temperatures was planned as part of a future work.

3.1.1.1 Medium Mn steels

Four steels, referred to as 2Mn, 4Mn, 6Mn and 6Mn2Ni, and which composition is shown in Table 7, were studied. The 2Mn steel, which has a typical composition of a Q&P steel, was established as the reference steel. The other steels were medium Mn steels and 6Mn2Ni

steel also contained Ni. Alloying elements and their amounts were selected in order to study the influence of Mn additions (the 4Mn and 6Mn steels with respect to the 2Mn steel), and Ni additions (the 6Mn2Ni steel with respect to the 6Mn steel). The addition of both Mn and Ni was made to promote the partitioning of these elements in order to increase the stability of the austenite. The addition of Ni was also motivated by its lower segregation in comparison with Mn. Silicon was added to suppress carbides formation.

Table 7. Composition (wt.%) of the medium Mn steels employed in this work.

Steel ref.	C	Mn	Ni	Si	P	S	N
2Mn	0.2	2.0	-	1.5	0.013	0.0015	0.0031
4Mn	0.19	3.8	-	1.4	0.012	0.0017	0.0035
6Mn	0.19	5.8	-	1.4	0.011	0.0013	0.003
6Mn2Ni	0.19	5.7	1.6	1.4	0.014	0.0019	0.0041

Ingots of four steel grades were produced in the laboratory (ArcelorMittal, France, in the frame of the HIGHQP project, grant No 709855) using a vacuum induction melting furnace. The ingots were reheated to ~1250 °C and a roughing stage was performed to decrease the thickness from 60 mm to 30 mm. The obtained slabs were then cut into five small ingots which were hot rolled after being reheated to ~1250 °C. The hot rolling consisted of five hot rolling passes (T_{end} of rolling approximately above 900 °C) and coiling at 500 °C. The hot rolled sheets of about 4 mm thickness were ground on both surfaces to decrease the thickness to 2.8 mm. A softening anneal was applied before cold rolling which consisted of holding at 600 °C for 1 h followed by water quench. Then, the sheets were cold rolled with approximately 50% reduction to obtain a final thickness of 1.5 mm.

Hot rolled materials were characterized before and after softening annealing by microstructure observation with a light optical microscope (LOM) after polishing down to 1 μm and etching with sodium metabisulfite (ArcelorMittal, France, in the frame of the HIGHQP project, grant No 709855). Vickers microhardness tests with 9.8 N load were also performed with the hot rolled samples. The results of the hardness measurements of hot rolled materials at different steps, together with some examples of the observed microstructures, are presented in Figure 11. The hardness of the 2Mn steel was 224 HV, which was acceptable for further cold rolling and therefore was not heat treated. In contrast, the obtained hardness of other steels was quite high (420 HV–490 HV). This means that direct cold rolling of these hot rolled sheets was difficult, and therefore specific softening treatments were applied as explained in the previous paragraph. After the softening treatments, the obtained hardness was in range of 280 HV–320 HV, which allows for laboratory cold rolling procedures.

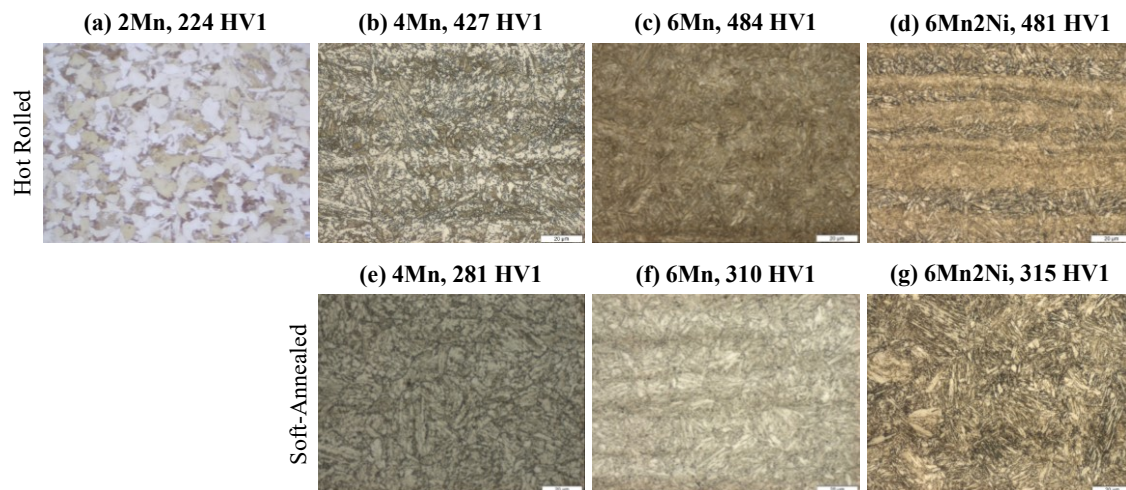


Figure 11. Light optical metallography (LOM) images and hardness of the hot rolled microstructures. The 2Mn (a), 4Mn (b), 6Mn (c) and 6Mn2Ni (d) steels after hot rolling, and the 4Mn (e), 6Mn (f) and 6Mn2Ni (g) steels after soft annealing.

As can be seen in the micrographs of Figure 11, the 2Mn steel mainly presented a ferrite-pearlite structure with some minor fractions of bainite and martensite. The microstructure in the remaining steels consisted of a mixture of bainite–martensite. In the case of the 4Mn steel, the major phase seemed to be bainite and in the 6Mn and 6Mn2Ni steels, it was martensite. These microstructure observations were in agreement with the measured microhardness levels of the different hot rolled sheets. The presence of hard phases such as bainite and martensite was a consequence of the higher Mn and Ni contents added to the steels. Softening annealing performed on the 4Mn, 6Mn, and 6Mn2Ni steels resulted in the recovery of the structure (decrease of dislocation density), which was helpful in the reduction of steel hardness and, in some cases, led to the precipitation of carbides.

3.1.1.2 Medium and high C steels

For this part of the work, three commercial medium and high C steels were selected (Table 8). The carbon content of the selected steels was high enough to guarantee a minimum hardness, allowing to achieve wear resistance values similar to those currently achieved in fields where wear resistance is required. In addition, it was ensured that the steels to be studied contained a significant amount of silicon in their chemical composition in order to avoid the formation of cementite in the partitioning stage of the Q&P treatment. On the other hand, it must be considered that Q&P treatment has been typically studied in low thickness products (such as cold rolled sheets). However, the products employed in wear applications may show higher thickness. As hardenability is a constraint if Q&P is applied in high thickness products, the steels were intended to contain a series of chemical elements that ensure

hardenability, as Mn, Cr, etc. At the same time, these elements were intended to retard the formation of bainite in the partitioning stage and harden the martensitic matrix.

The selection of the 3 commercial steel grades was done supported by JMatPro (v10.2) thermodynamic software. Using this software critical cooling rates to avoid diffusion-based phase transformations (CCR) and hardness in the as-quenched state were calculated for several commercial steel grades. Based on these results, 1.2990, 1.2344, and 300M steels were selected (Table 8) with the criteria that critical cooling rates were minimized, and the hardness values were maximized, ensuring a suitable content of Si. The continuous cooling transformation (CCT) diagrams calculated by JMatPro employed for the predictions of CCR and hardness for the selected steels are shown in Figure 12. The first two steel (1.2990 and 1.2344) are tool steels which are typically heat treated by quenching and tempering. These steels contain high amounts of carbides forming elements (Cr, Mo, V), which give rise to the secondary hardening phenomenon in the tempering. The main difference among both steels is the C content. The third steel, 300M, was selected mainly due to the high Si content.

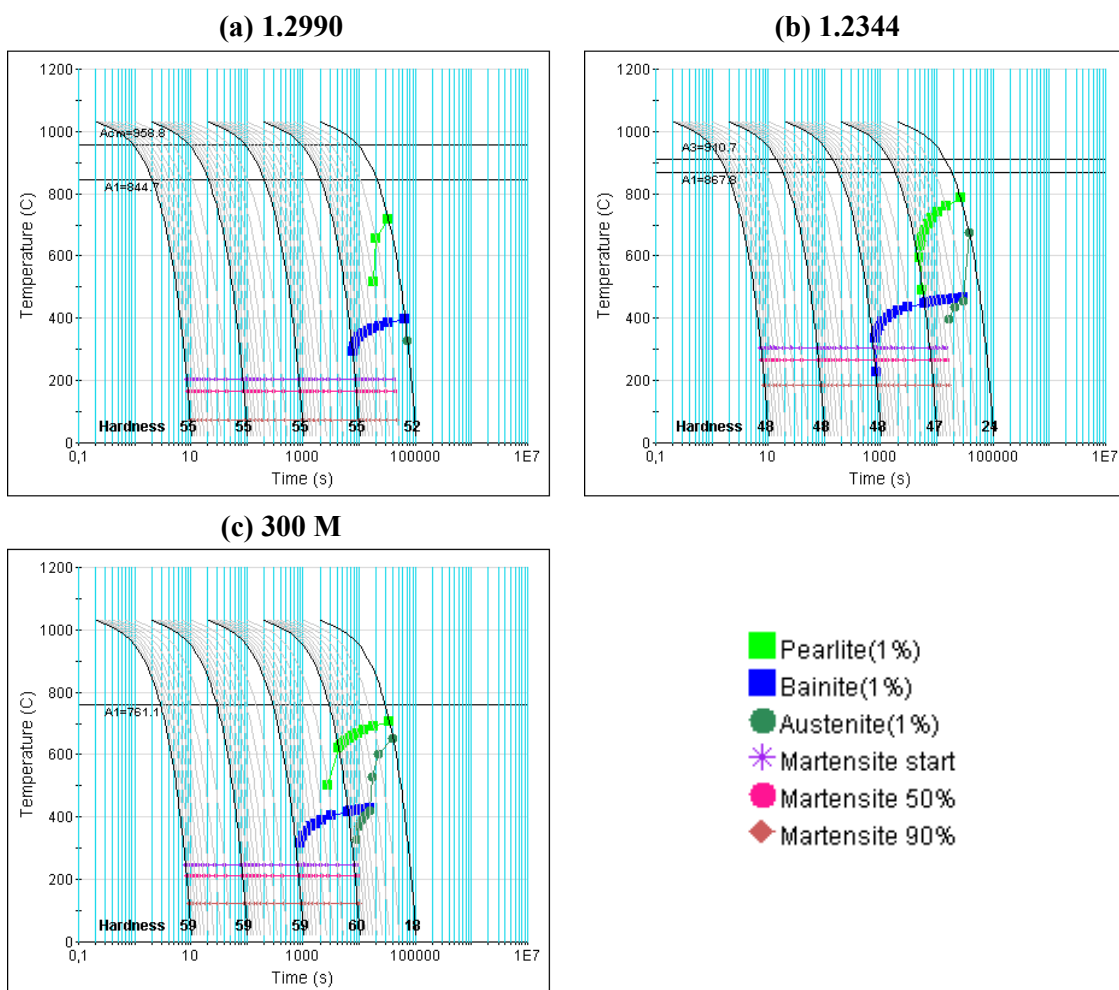


Figure 12. Theoretical CCT curves of 1.2990 (a), 1.2344 (b), and 300M (c) steels obtained with JMatPro.

Table 8. Composition (wt.%) of the medium and high C steels employed in this work.

Steel ref.	C	Si	Mn	Cr	Mo	Ni	V
1.2990	0.92	0.96	0.36	7.9	1.0	-	1.5
1.2344	0.39	0.97	0.37	5.1	1.2	-	0.92
300M	0.41	1.6	0.83	0.78	0.38	1.8	0.06

3.1.2 Design of the Q&P cycles based on dilatometry

A LINSEIS L78 RITA dilatometer (Tecnalia, Spain) was used to obtain the phase transformation temperatures, critical cooling rates, Q&P cycle parameters, and then physically simulate the whole Q&P cycles to understand microstructure evolution by the analysis of the expansion/contraction behavior. A picture of L78 RITA dilatometer is presented in Figure 13. The dilatometer follows the length variations of the sample occurring during the imposed heat treatment. The samples were heated and maintained at temperature by induction heating. Temperature control was done by Type K thermocouples. The samples were maintained by vertical hollow quartz rods, being the upper rod mobile. Hence, when length variations occurred, one rod moved, and the linear displacement was captured by an LVDT (Linear Variable Differential Transducer) sensor.



Figure 13. Global view on L78 RITA dilatometer.

In the present work, cylindrical samples, of 3 mm diameter and 10 mm length, were used. After machining, the samples were cleaned by immersion in ethanol within an ultrasound bath (to remove dirt and oils from machining) and just before the test, they were cleaned again with ethanol. Type K thermocouple was welded in the middle of the clean surface of the sample. To avoid oxidation during treatment vacuum was done in the experimental chamber, then, a small amount of helium (He) was injected.

3.1.2.1 Obtention of phase transformation temperatures and critical cooling rates

First, A_{c1} and A_{c3} phase transformation temperatures were determined by dilatometry. For that, samples were heated up to 1000 °C (in the case of Medium Mn steels) and 1100 °C (in the case of medium and high C steels) at 5 °C/s (medium Mn steels) and 10 °C/s (medium and high C steels) and then, after 120 s of maintenance, cooled down to room temperature. Two tests were carried out for each medium Mn steel, whereas only one test was carried out for each medium and high C steel. Once the dilatometry curve was obtained, A_{c1} and A_{c3} temperatures were determined by the application of the tangent method. As in medium Mn steels a deviation was observed just before austenite transformation curve, A_{c1} was considered the temperature with maximum relative change in length just before transformation started. As reference of each A_{c1} obtention methods, in Figure 14 the curves of the 2Mn and 1.2344 steels showing A_{c1} and A_{c3} temperatures are presented. The dilatometry curves for all steels are shown in Appendix A. The results for all steels are shown in Table 9. It can be seen that, in medium Mn steels, Mn additions led to lower austenization temperatures and Ni addition resulted in a further decrease. Since the medium and high C steels have different amounts of different alloying elements it is not possible to establish a direct correlation between the austenization temperatures.

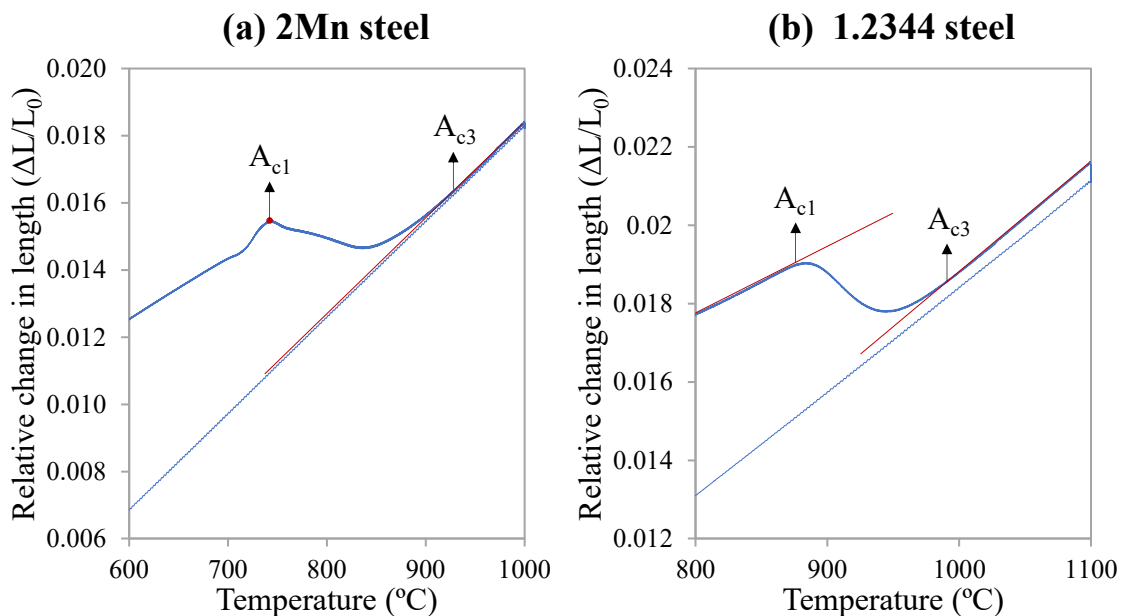


Figure 14. Dilatometry curves representing the determination of A_{c1} and A_{c3} temperatures of the 2Mn (a) and 1.2344 (b) steels. In (a) A_{c1} was determined as the temperature with maximum change in length just before transformation started and A_{c3} was determined by the tangent method; in (b) both temperatures were obtained by the tangent method.

Once A_{c3} temperatures were determined, critical cooling rates to avoid any undesirable transformation during quenching were experimentally determined by dilatometry. The

procedure to obtain these values was as follows: first, samples were heated up to a soaking temperature 50 °C above A_{c3} and after a soaking time of 120 s were cooled down to room temperature employing different cooling rates. The first cooling rate selected for each steel was based on theoretical results obtained by a thermodynamic software. If that cooling rate resulted in any further transformation apart from martensitic a higher one was tested. The dilatometry curves for all steels are shown in Appendix A and all CCR are presented in Table 9. It can be seen that increasing Mn in medium Mn steels led to a considerable decrease of this parameter and the alloying contents of the medium and high C steels were also sufficient to achieve low CCRs.

Table 9. Phase transformation temperatures (A_{c1} , A_{c3} , M_s and M_f), critical cooling rates (CCR) and the austenite measured in the quenching state of all the steels employed in this work.

Steel ref.	A_{c1} (°C)	A_{c3} (°C)	M_s (°C)	M_f (°C)	CCR (°C/s)	As-quenched RA (%)
Medium Mn steels						
2Mn	760	920	363	215	60	1
4Mn	730	873	313	101	0.5 – 2	3
6Mn	695	841	252	<RT	<0.1	7
6Mn2Ni	690	793	219	<RT	<0.1	7
Medium and high C steels						
1.2990	881	987	342	<RT	0.5 – 1	<5
1.2344	866	993	317	~RT	<1	-
300M	758	875	270	~RT	<2	-

3.1.2.2 Obtention of martensitic transformation curve

There are different ways to obtain the martensitic transformation curve. The first method, purely theoretical, consists in calculating the M_s temperature by means of the Andrews equation (1) [195] and, then, calculate the austenite fraction corresponding to each temperature by means of the Koistinen-Marburger equation (2) [196]:

$$M_s = 539 - 423C - 30.4Mn - 17.7Ni - 11.0Si - 12.1Cr - 7.5Mo \quad (1)$$

where the alloying elements are expressed in weight percent.

$$f_\gamma = \exp(-\alpha_m \times (M_s - T)) \quad (2)$$

where f_γ is austenite volume fraction; T is current temperature, °C; and α_m is a constant coefficient with a value equal to 0.011 K⁻¹.

Other method, the one employed in this work, is to obtain the transformation curve experimentally by dilatometry. Thus, the samples were heated up to $A_{c3} + 50$ °C at 5 °C/s

(medium Mn steels) and 10 °C/s (medium and high C steels) and, after 120 s, were cooled down to room temperature. The applied cooling rate was 100 °C/s in the 2Mn steel, 20 °C/s in the medium Mn steels, and 45 °C/s in the medium and high C steels. Then, the samples were reheated up to 500 °C at 5 °C/s. Applying the lever rule between the expansion of the untransformed austenite curve and that from the reheating, martensite transformation curves were calculated. The final change in length was associated with the amount of martensite in the as-quenched state, which was obtained from the following dilatometry: a sample was quenched to room temperature from $A_{c3} + 50$ °C after austenitizing it for 120 s, considering the same cooling rate as before. Then, austenite content of the sample was measured by magnetization in medium Mn steels (TU Delft, the Netherlands, in the frame of the HIGHQP project, grant No 709855), and X-ray diffraction in medium and high C steels (SGIker, UPV/EHU, Spain). The measured values are collected in the last column of Table 9. From the martensitic transformation curve, M_s and M_f temperatures were obtained as the temperatures in which 5% and 95% of the martensite transformation occurred, respectively. As an example, in Figure 15a the dilatometry curve of the 2Mn steel is shown and the M_s and M_f temperatures for all the steels are presented in Table 9. The dilatometry curves for all steels used to obtain the martensitic curve are shown in Appendix A. The QTs selected for each Q&P cycle were obtained from the corresponding martensitic transformation curve and are detailed in the next section. In Figure 15b the procedure to obtain a QT corresponding to 25% of untransformed austenite (QT25) is represented by red arrows.

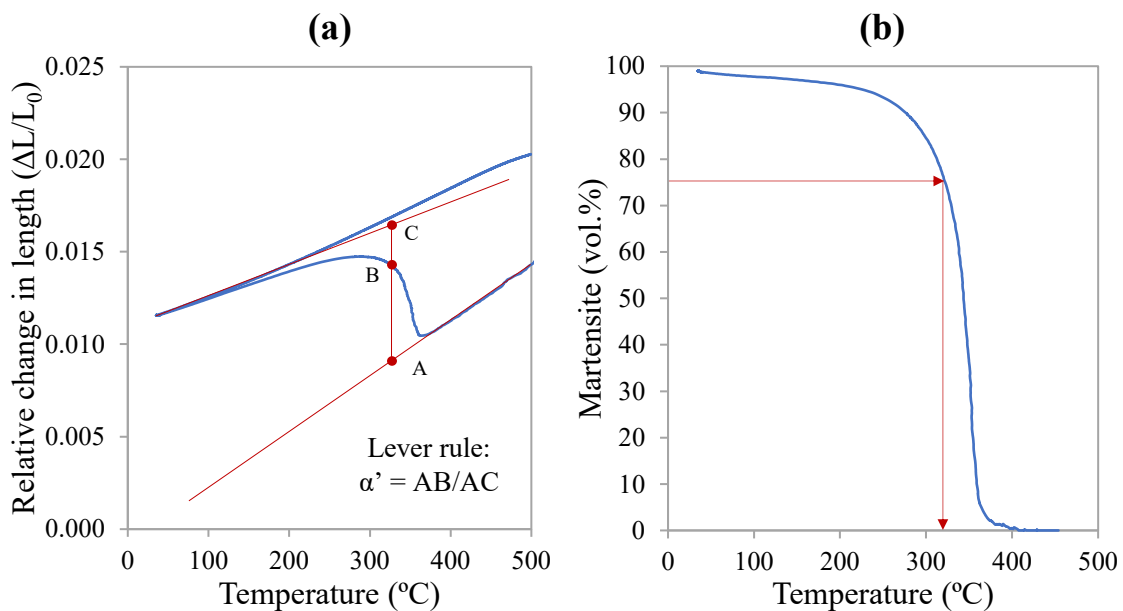


Figure 15. Dilatometry curve of the 2Mn steel for the determination of M_s , M_f and martensite transformation curve (a) and the corresponding martensitic transformation curve showing the determination of the temperature corresponding to a transformation of 75% martensite (b).

3.1.2.3 Design of the heat treatments (QT, PT and Pt)

The selection of the thermal cycle parameters followed a different strategy depending on the required final properties. Therefore, a series of treatments was designed to medium Mn steels and another to medium and high C steels.

Design of cycle parameters in medium Mn steels:

In all cases, full austenization was performed by heating at $A_{c3} + 50$ °C. Then, after 120 s of soaking, samples were cooled down to the selected QTs at a cooling rate above CCR. After 5 s at the QT, samples were heated up to the established PT. Finally, once the partitioning time was completed, samples were cooled down to room temperature.

In a first stage, three Q&P cycles were designed: A reference cycle with a typical partitioning temperature of 400 °C and a quenching temperature corresponding to 25% of untransformed austenite (QT25), and two high partitioning temperature cycles with different quenching temperatures, one of which coincided with that used in the reference cycle and other corresponding to 10% of untransformed austenite (QT10). In this way, both the influence of PT and QT on the microstructure could be investigated.

High partitioning temperature was selected as the temperature in which austenite reverse transformation starts (T_{ART}). The selection of T_{ART} as partitioning temperature was motivated from previous work, in which it was observed that temperatures beyond the intercritical range lead to undesirable decomposition of austenite into pearlite [39]. Higher partitioning temperatures might also lead to excessive austenite which would be difficult to stabilize. Nevertheless, the investigation of the effect of partitioning temperatures around T_{ART} would be interesting as part of a future work.

The consideration of two QT conditions (QT10 and QT25) followed by a partitioning stage at T_{ART} , aimed at investigating the influence of different contents of pre-existing austenite on the formation of reverted austenite. The pre-existing austenite contents were defined based on a previous work [112] where it was reported that ductility strongly decreased when pre-existing austenite was higher than 30% due to the presence of secondary martensite. The formation of secondary martensite was reported to be the consequence of insufficient austenite stabilization during the partitioning stage. Therefore, in this thesis, pre-existing austenite contents were kept below 30%.

The temperature for the start of austenite reverse transformation (T_{ART}) upon heating from the QT, was determined by dilatometry for each steel. For this, samples were heated to

$A_{c3} + 50$ °C, held for 120 s, cooled down at 100 °C/s (2Mn steel) and 20 °C/s (rest of steels) to QT25 and QT10, and re-heated again up to $A_{c3} + 50$ °C. It was shown that T_{ART} was very similar between reheating from QT25 and QT10. As an example, the dilatometry curve for the obtention of T_{ART} , reheating from QT25, in 6Mn2Ni steel is shown in Figure 16. The red portion of the curve corresponds to the reheating starting from QT and the final cooling to room temperature. The dilatometry curves for all medium Mn steels are shown in Appendix A.

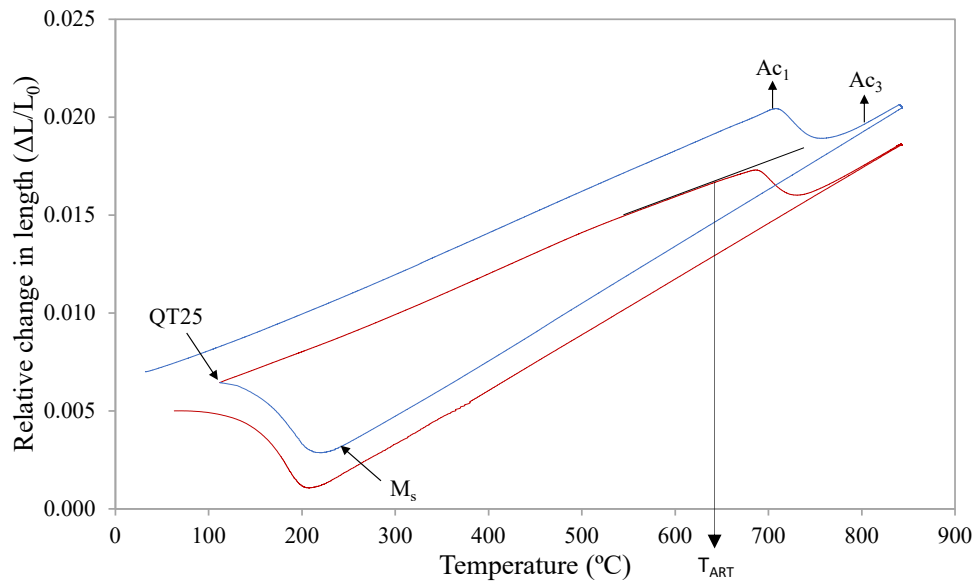


Figure 16. Dilatometry curve showing the obtention of T_{ART} of the 6Mn2Ni steel reheating from QT25.

The selected QT25 and QT10 conditions were obtained for each steel from the martensitic transformation curves. Thus, the needed temperature parameters (QT and PT) were obtained by dilatometry and Table 10 collects the corresponding values for each parameter and steel. The addition of both Mn and Ni resulted in a significant decrease in QT25 and QT10 and also decreased T_{ART} .

Table 10. QT25, QT10 and T_{ART} values employed in the Q&P cycles corresponding for each steel.

Steel ref.	QT25 (°C)	QT10 (°C)	T_{ART} (°C)
2Mn	320	272	708
4Mn	237	164	680
6Mn	148	60	660
6Mn2Ni	114	44	640

Partitioning times were different depending on the PT condition. In the low PT condition (PT = 400 °C), 300 s were considered, whereas in the high PT condition (PT = T_{ART}) samples were held at this temperature during 1000 s. The longer time at T_{ART} was defined to increase the diffusion of substitutional alloying elements into austenite.

After the application of the defined Q&P cycles and subsequent characterization, it was found that the most promising retained austenite values were obtained in the 6Mn and 6Mn2Ni steels after the high partitioning temperature and QT10 cycle. Thus, two more cycles were added in this condition in order to study the influence of partitioning time. The selected parameters (QT, PT and Pt) for each condition are collected in Table 11. Furthermore, Table 12 collects which cycle was applied to each steel and Figure 17 shows the schematic of all Q&P cycles carried out.

Table 11. Selection of the QT, PT and Pt parameters employed in each Q&P cycle.

Param.	Condition 1 ref	Condition 2 QT25-Pt1000	Condition 3 QT10-Pt300	Condition 4 QT10-Pt1000	Condition 5 QT10-Pt3600
QT ($\gamma\%$)	25	25	10	10	10
PT ($^{\circ}\text{C}$)	400	T_{ART}	T_{ART}	T_{ART}	T_{ART}
Pt (s)	300	1000	1000	300	3600

Table 12. Summary of conditions carried out in each steel.

Steel ref.	Condition 1	Condition 2	Condition 3	Condition 4	Condition 5
2Mn	✓	✓	✓	✗	✗
4Mn	✓	✓	✓	✗	✗
6Mn	✓	✓	✓	✓	✓
6Mn2Ni	✓	✓	✓	✓	✓

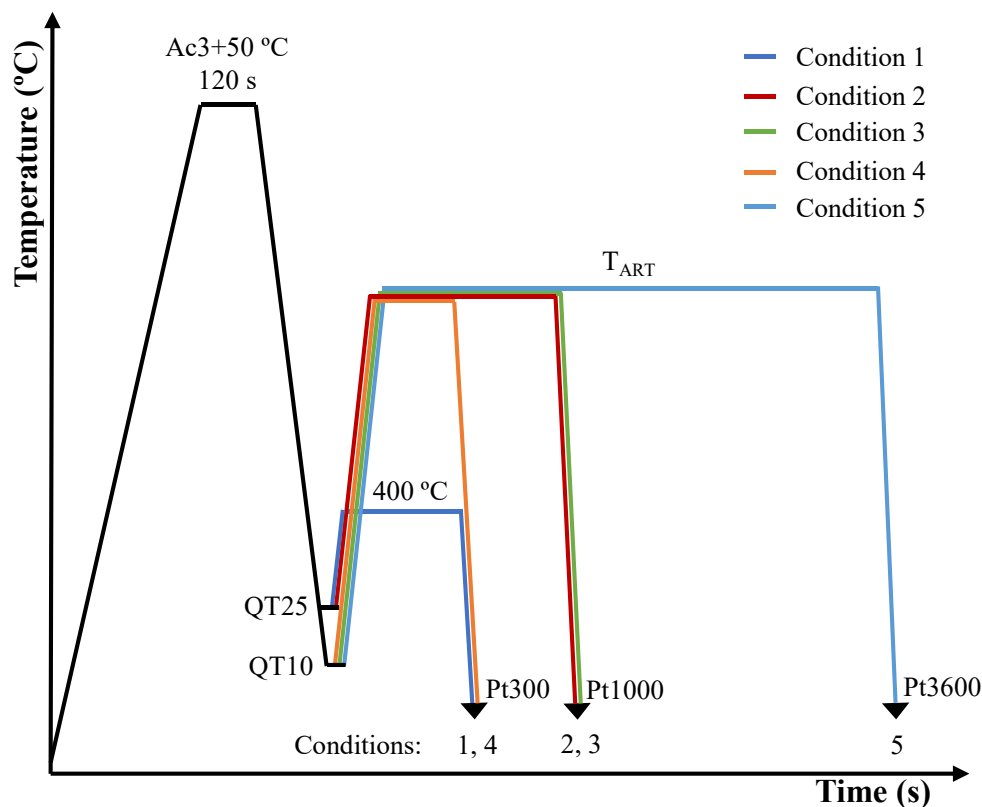


Figure 17. Schematic of the Q&P cycles carried out in this work for medium Mn steels.

Design of cycle parameters in medium and high C steels:

Medium and high C steel samples were also fully austenitized by heating at $A_{c3} + 50$ °C and holding during 120 s. Then, samples were cooled down to the selected QT and after 5 s were heated up to the established PT. Finally, once the partitioning time was completed, samples were cooled down to room temperature. In this case, the definition of the thermal treatments followed the classical design of Q&P cycles, employing conventional PTs and Pts. The application of high partitioning temperatures was planned as part of a future work, where it will be interesting to study the formation of Cr, Mo and/or V carbides as competitive reactions. The selected QT was the temperature corresponding to 20% of untransformed austenite (QT20) for each steel, which was obtained from the martensitic transformation curve. Regarding the partitioning step, two different PT were chosen, specifically 400 °C and 300 °C, and the Pts were 120 s and 300 s, respectively. The two Q&P cycle parameters are collected in Table 13 and the thermal routes are schematically represented in Figure 18.

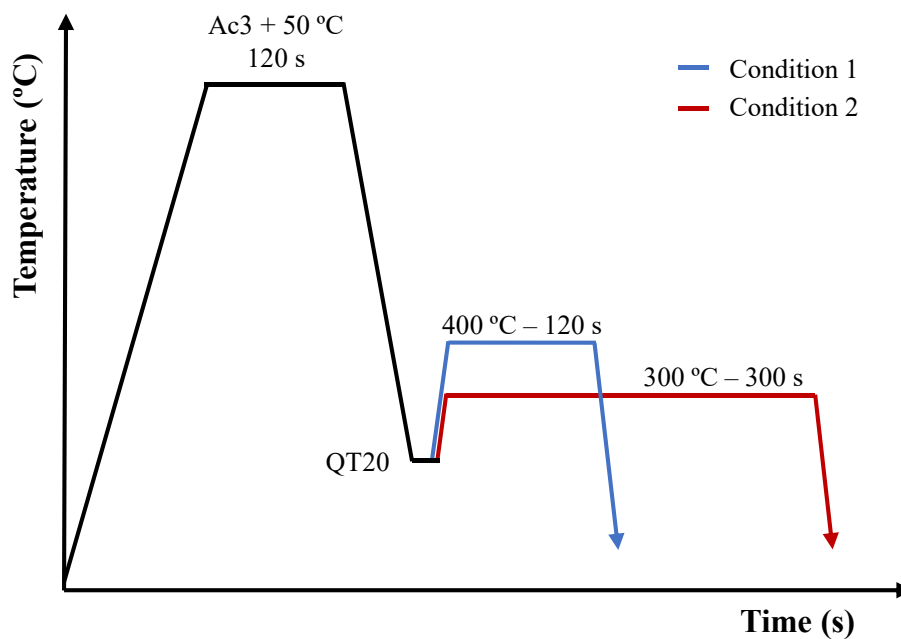


Figure 18. Schematic of the Q&P cycles carried out in this work for medium and high C steels.

First, the Q&P cycles shown in Table 13 were applied in the dilatometer considering 1.2990, 1.2344 and 300M steels. The heating and cooling rates values for the dilatometry cycles were selected according to what was expected to be obtained later in the furnaces and salt baths, considering previous experience. Thus, the thermal route fixed at the dilatometer was as follows: First, samples were heated up to $A_{c3} + 50$ °C at 10 °C/s. Then, after 120 s of soaking were cooled down to QT20 at 45 °C/s. After 5 s at QT20, samples were heated up to the established PT at 20 °C/s. Finally, once the partitioning time was completed, samples

were cooled down to room temperature at 50 °C/s. Afterward, based on the measured hardness and RA results, the most interesting steels and Q&P cycles were selected and applied employing salt baths.

Table 13. Q&P cycle parameters (QT, PT and Pt) employed in each condition and steel.

	Steel ref.	QT20 (°C)	PT (°C)	Pt (s)
Condition 1	1.2990	180		
	1.2344	187	400	120
	300M	175		
Condition 2	1.2990	180		
	1.2344	187	300	300
	300M	175		

3.1.3 Application of the Q&P heat treatments: Furnaces and salt baths

The Q&P cycles were reproduced employing laboratory furnaces and salt baths. The temperature during thermal cycles was monitored employing thermocouples and a datalogger. In the case of medium Mn steels, cold rolled sheets were heat treated. In the first trials, two thermocouples were welded in the surface, one in the center of the sheet and other in the middle of one of the edges (Figure 19). Later, it was found that there were not temperature gradients between both thermocouples during the heat treatment, so from then only the exterior one was used.



Figure 19. Sheet of the 2Mn steel prepared to carry out Q&P thermal treatment in furnaces and salt baths with one thermocouple welded in the center and other in the edge. The dimensions of the showed sheet were 250 mm length, 50 mm wide, and 1.5 mm thick.

Regarding medium and high C steels, the dimensions of the samples were designed for subsequent pin-on-disk analysis. Thus, disks with 6 mm height were machined. As described before, first, the designed Q&P cycles were applied in the dilatometer and afterward the most interesting steels (1.2990 and 300M) and conditions (PT400 cycle) were considered in the salt baths. Because of material limitation, the diameter of the disks were 100 mm and 35 mm for the 1.2990 and 300M steels, respectively. Due to samples thickness, thermal gradients between the center and the surface were expected, hence two thermocouple were used to

monitor the temperature, one welded in the center of the disk (drilling 3 mm from the center of the surface to insert the thermocouple) and other in the surface (Figure 20).

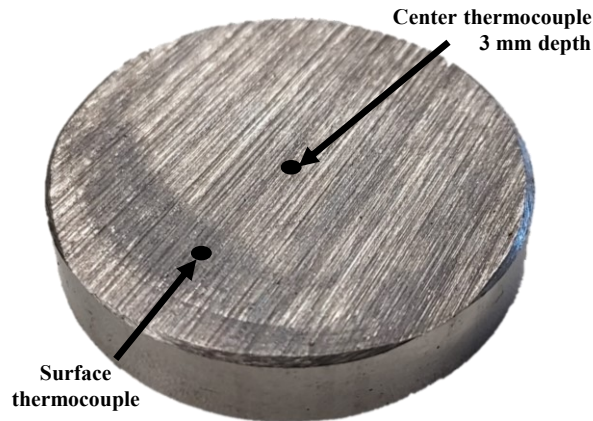


Figure 20. Cylinder of the 300M steel employed to carry out the Q&P thermal treatment in furnaces and salt baths representing the position of the thermocouples.

The installations for the heat treatments (Tecnalia, Spain) consisted of one resistance furnace that allows heating the sample in an inert atmosphere, two salt baths (mixture of alkaline nitrites and nitrates), and another resistance furnace. Depending on the steel and the Q&P route to follow, the equipment and the order in which they were used was different. In general, the order outlined in Figure 21 was followed. The specific route followed for each steel and condition is detailed in Appendix B.

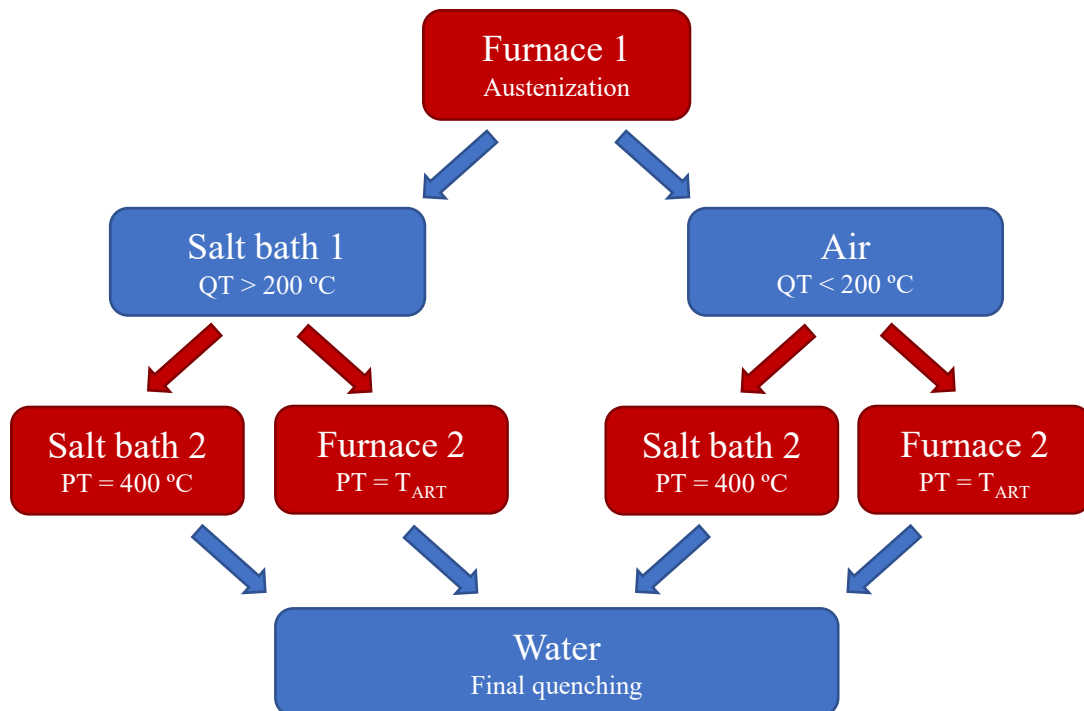


Figure 21. Schematic representation of the route followed to carried out Q&P thermal cycles in the furnaces and salt baths. Blue and red labels and arrows represents cooling and heating stages, respectively.

The main reason for using one piece of equipment or another was the temperature limitation of the salt baths. It is not recommended to use the salts neither at a temperature below 200 °C, nor above 450 °C. Thus, cooling to QT in steels with a QT above 200 °C was done employing the first salt bath, whereas cooling was done in air when QT was somewhat below this temperature. In the latter, it was shown that the cooling rate achieved was more than sufficient to avoid any unwanted transformation during this step. On the other hand, in the cycles with a low PT the second salt bath was used to apply the partitioning, whereas the high partitioning temperature stages were applied employing the second furnace.

In medium and high C steels, the wear resistance obtained after Q&P treatments was compared with that obtained after a Quenching & Tempering (Q&T) treatment. In the case of the 1.2990 steel, industrially Q&T treated material was available at Tecnalía. The 300M steel, however, was not available after Q&T treatment, therefore, apart from the Q&P treatment, a Q&T treatment was also applied in the laboratory following the specifications of the steel given by the supplier.

3.2 Microstructural characterization

3.2.1 X-ray diffraction (XRD)

X-Ray Diffraction (XRD) is a technique employed in the study of the fine structure of matter [197]. Its main uses are the determination of crystalline structures, volumetric fractions of the different phases, chemical analysis, and stress measurement.

Depending on the planes of atoms within a material, X-ray beams will diffract at specific angles, and these diffracted beams are usually used in the characterization of various properties of materials. There are two properties linked with the diffracted beams that are used: the angle between the incident and diffracted beams (2θ) and the intensity of the diffracted beam (I) (Figure 22).

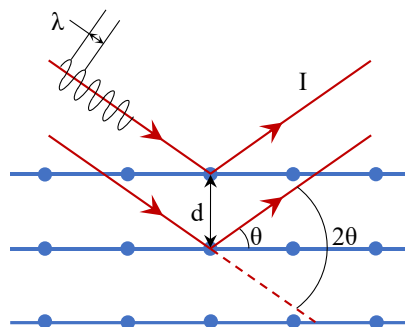


Figure 22. Schematic representation of Bragg diffraction of crystallographic planes.

Bragg's law relates the angle θ , the wavelength of the beam (λ) and the spacing between the planes of atoms in the material (d), and n is an integer representing the order of the diffraction peak:

$$n\lambda = 2d \sin \theta \quad (3)$$

Additionally, the volume of material that has planes with the same space and orientation to the diffraction and the intensity of a diffracted beam in a particular direction are proportional. Thus, from the relative intensities of the diffracted beams, the relative volume of a polycrystalline material phases can be estimated [197].

The samples studied in this work are assumed to be consisted of ferrite (which represent martensite) and austenite. According to ASTM E975-13, the volume fraction of austenite (V_γ) can be calculated as follows:

$$V_\gamma = \frac{I_\gamma/R_\gamma}{I_\alpha/R_\alpha + I_\gamma/R_\gamma} \quad (4)$$

where I_γ and I_α are the measured intensities of a particular (hkl) peak above the background of austenite and ferrite, respectively; and R_γ and R_α are the calculated intensities of a particular (hkl) austenite and ferrite peak (standard value), respectively. In this work, the employed (hkl) peak for both austenite and ferrite was (200), being the corresponding R values 34.78 and 20.73, respectively.

Thus, in this work, for the measurement of RA in the Q&P samples, X-ray powder diffraction patterns were collected by using a Bruker D8 Discover diffractometer (SGIker, UPV/EHU, Spain) equipped with a Cr Twist tube, V filter ($\lambda = 2.291 \text{ \AA}$), PolyCap™ (1 μ single crystal cylinders) system for parallel beam generation (divergence of 0.25°), and a 1-D LynxEye detector (active length in 2θ 2.7°). The samples were mounted on a Eulerian Cradle with automatic controlled X-Y-Z stage. Data were collected from 50 to 120° 2θ (step size = 0.04 and time per step = 1 s). Peak area intensity was evaluated using the peak-fit option of the WinPLOTR software.

3.2.2 Scanning Electron Microscope (SEM and FE-SEM)

Scanning electron microscopy (SEM) is a microstructural characterization technique in which a high-energy electron beam is focused onto a fine probe that scatters inelastically when it strikes the surface of a solid sample. The electrons are inelastically scattered, thus generating various signals from the sample that are collected and amplified. Scanning the

probe beam across the sample surface forms a digitized image displaying one or more of the collected signals on a monitor that has the same time base as the probe scan. Various signals are generated as a result of the impact of the incident electrons, being the secondary electrons the most commonly used, although characteristic X-rays, high energy backscattered electrons, visible cathodoluminescence and the net specimen current have all been used to acquire microstructural information from samples examined in the scanning electron microscope [198]. In this work a field emission source for the electron beam was used in some of the medium Mn steel samples to improve the performance of SEM (FE-SEM).

Samples selected for FE-SEM (JEOL® JSM7000F) (Colorado School of Mines, EEUU) were prepared by conventional polishing to 1 μm , followed by a final polishing with colloidal silica. Then, there were etched with 2% Nital for 30 s. Characterization conditions were a beam voltage of 15 KV, a medium probe current, and a working distance of 10 mm.

SEM (QUANTA 200 FEI) (Tecnalia, Spain) characterization was performed to the Q&P samples of the 1.2990 and 300M steels. In this case, samples were prepared by conventional polishing to 1 μm and etched with 2% Nital for 1 min. A beam voltage of 25 KV, and a working distance of 10 mm were employed. In addition, energy-dispersive X-ray spectroscopy (EDS) analysis was carried out in order to identify the composition of some of the phases presented in the 1.2990 steel.

3.2.3 Electron Backscatter Diffraction (EBSD)

Electron backscatter diffraction (EBSD) is a scanning electron microscope (SEM) based technique. It allows the measurement of microtexture (texture on the scale of the microstructure) [199], microstructure quantification [200], grain and phase boundary characterization [201,202], phase identification [203] and strain determination [204] in crystalline multiphase materials of any crystal structure.

By focusing an electron beam on a crystalline sample, diffracted patterns are obtained, which are subsequently evaluated and indexed. Generally, this is done automatically, and the data is output graphically and statistically. The most versatile and illuminating results are the OIM maps, which are a quantitative representation of an area of the analyzed microstructure in terms of its crystallographic constituents [205]. One such map is image quality (IQ), which is a metric that describes the quality of a diffracted pattern. An IQ map is constructed by mapping the measured IQ value for each diffraction pattern obtained during an OIM scan to

a gray or color scale. Both the "perfection" of the crystal lattice and the atoms present within the diffraction volume affect the IQ [206,207].

In this work, scans were performed on a field emission scanning electron microscope (FE-SEM, JEOL® JSM7000F) (Colorado School of Mines, EEUU) with a beam voltage of 20 KV and a medium probe current. The acquisition of EBSD scans was done using a step size of 0.06 μm . Selected samples were prepared by conventional polishing to 1 μm , followed by a final polishing with colloidal silica. The obtained results consisted on IQ maps and identification of average grain size of the retained austenite.

3.2.4 Transmission Electron Microscopy (TEM)

The transmission electron microscope (TEM) can be comprehended as a tool engineered specifically for the analysis and visualization of samples at micrometric and nanometric scale. This kind of electron microscope has capability of reveal highly complex levels of detail which are inaccessible by a conventional light microscope.

In the TEM high energy electrons are elastically scattered as they penetrate a thin specimen. The transmitted electrons are then focused by electromagnetic lenses to form a well-resolved image that can be viewed on a fluorescent screen or a charge-coupled device [208].

In this work microstructure characterization of some of the Q&P treated medium Mn steel samples was done by means of a TEM (Talos F200i field emission gun instrument equipped with a Brüker X-Flash100 XEDS spectrometer) (SGIker, UPV/EHU, Spain). Elemental maps were obtained by XEDS in the STEM mode under a high annular dark field (HAADF) detector for Z contrast imaging in STEM conditions (camera length of 160 mm) using a pixel size of 2 nm, a dwell time of 900 s and an image size of 512 x 512 pixels.

Thin-foil specimens were prepared for the observation in the transmission electron microscope. A thin-foil is a 3 mm diameter disk with a central hole around which the TEM observation was performed. The thin-foil specimens must be less than 100 nm in thickness to minimize inelastic scattering of the transmitted beam as it passes through the specimen. Good specimen preparation is critical. The procedure employed in this work for the preparation of the foils was as follow:

- First, sheets of Q&P treated material were cut into pieces of about 10 mm x 10 mm.
- Once the sample was cut, it was glued to a resin block or a metallic funnel (Figure 23) with Loctite. 250 μm thick copper tape was glued to each side of the sample and the sample was sanded down to that thickness.

- Having thinned the sample to 250 μm , being the last pass with 1200 grit sandpaper, the sample was peel off and stick it back to polish the other side. This time, 100 μm tapes were placed and sample was thinned down to that thickness, finishing the polished with 1 μm cloth.



Figure 23. Funnel where samples were glued to be polished.

- In this way samples had approximately 100 μm thickness, and 3 mm diameter disks could be obtained. This is done lowering the red lever of the "hand drill" shown in Figure 24. As many disks as possible were obtained from each sample.

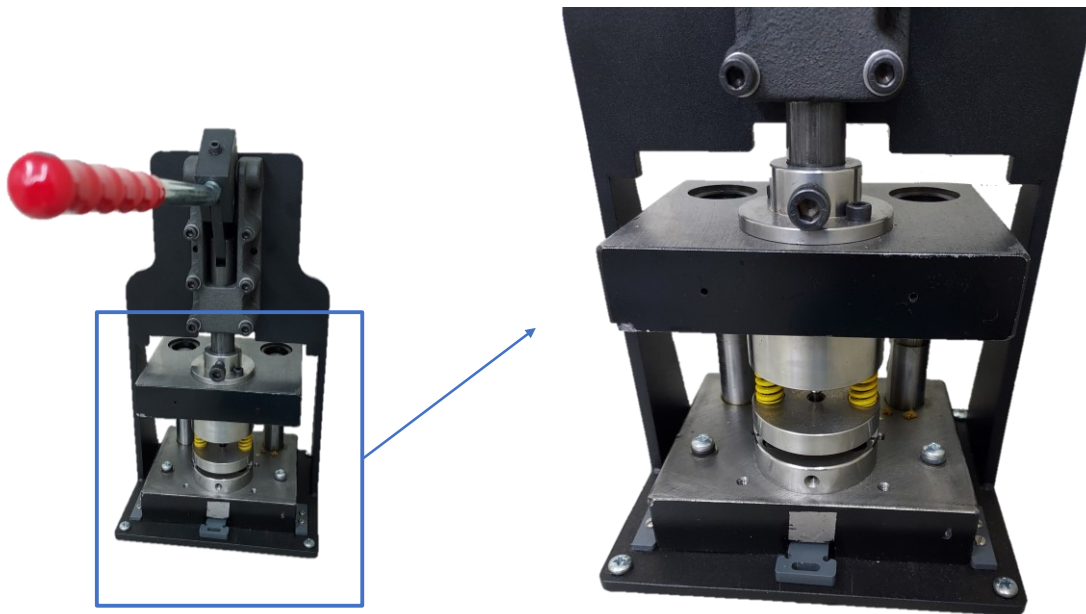


Figure 24. Hand drill employed to take out 3 mm diameter discs from the samples thinned down to 100 μm .

- Next, the side of the disk that was polished only down to 1200 grit sandpaper, was finished by polishing down to 1 μm cloth.

- Thus, disks were completely mirror polished on both sides. To make the central hole, around which the TEM observation was to be carried out, an electropolishing bath was used. The employed electrolyte was a mixture of 5% perchloric acid and 95% ethanol (absolute). The equipment has a sample holder to place the discs (Figure 25).

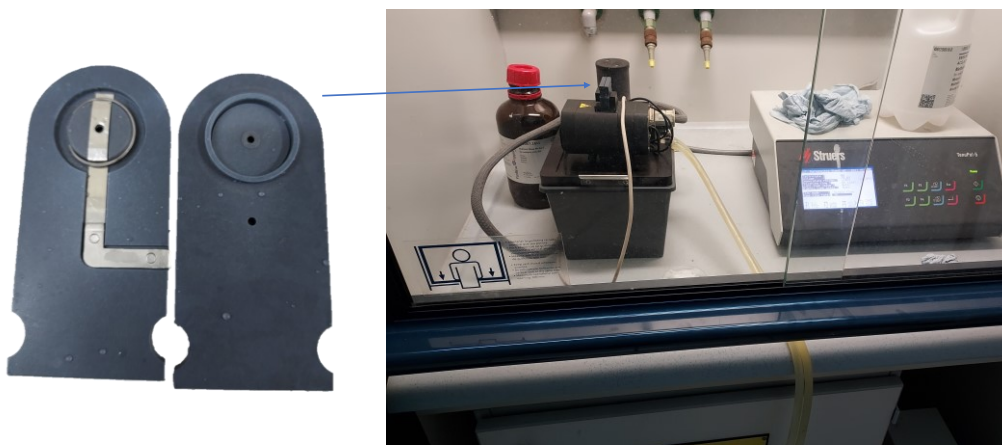


Figure 25. Sample holder for the electrolytic bath and electropolishing equipment.

- Once the first disc was placed, a scan was carried out at different temperatures to find the appropriate voltage and temperature to make the hole by electropolishing. Through these scans, the intensity-voltage curve was represented at the temperature of the bath. The curve must consist of 3 parts (Figure 26), a first ascending part in which the sample would be attacked, a second in which a plateau is found, where the sample would be polished, and a third, also ascending, in which the sample would be spoiled by chopping. Testing with temperatures of $-10\text{ }^{\circ}\text{C}$ and $-15\text{ }^{\circ}\text{C}$ was impossible to distinguish the plateau. At room temperature it was clearly seen that the plateau was at 29 V.

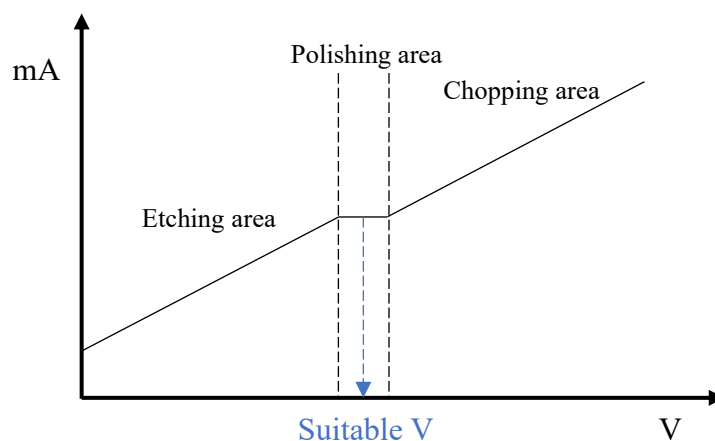


Figure 26. Intensity-Voltage curve.

- Once the voltage and temperature to be used were established, it was advisable to carry out the electropolishing with a new disk, since when performing the scanner in a wide voltage range, the sample likely was already etched, polished and even chopped.
- The equipment was therefore programmed to operate at 29 V. A sensitivity of 10% was set (this is measured by detecting the light that passes through the sample so that the test ends as soon as the hole has been made, around of 1 minute with these samples).
- Once electropolished, the disk was quickly immersed in ethanol to remove any traces of acid and was passed from one ethanol bath to another by immersing the sample up to three different baths.
- Finally, the disk was left to dry, and it was observed if the holes were performed by an optical microscope.

3.3 Mechanical behavior

3.3.1 Tensile test

Tensile Testing is a form of tension testing whereby controlled tension is applied to a sample until it fully fails. This is one of the most common mechanical testing techniques. It is used to find out how strong a material is and how much it can be strained before it breaks. In this work, this test method was used to determine yield strength, tensile strength, and ductility of all the medium Mn steels Q&P treated in the furnaces and salt baths. Two tests were performed for each steel/Q&P condition. Tensile specimens were water cut from the treated sheets. The dimensions of the specimens corresponded to a standard geometry of 50 mm gauge length and are specified in Figure 27.

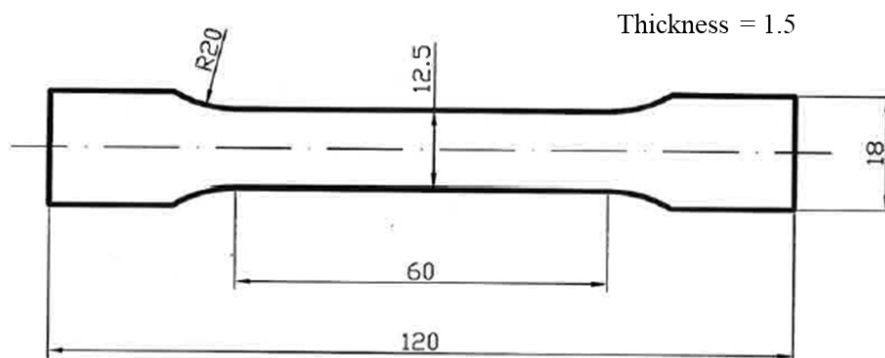


Figure 27. Dimensions of the tensile specimens. All measurements are expressed in mm.

Tests were performed in a universal INSTRON tensile testing machine (Tecnalia, Spain), with a strain rate of 0.001 s^{-1} and a contact extensometer following the UNE-EN ISO 6892-1:2019.

3.3.2 Interrupted tensile test

Interrupted tensile tests were performed to the selected steels and Q&P conditions in order to assess the evolution of the RA under mechanical loading. For that, once the total elongation was known for a given steel/Q&P condition, different strain levels were selected to stop the tensile tests. Then, the RA fraction was measured by X-ray diffraction in the way aforementioned in the section 3.2.1. In the tensile specimens with low strains the center section of the specimen was selected for the measurement of RA, whereas in specimens with higher strains the thinner area of the tensile specimen was selected. RA was measured in broken specimens as well. In Figure 28 the different sections employed for RA measurements are shown.

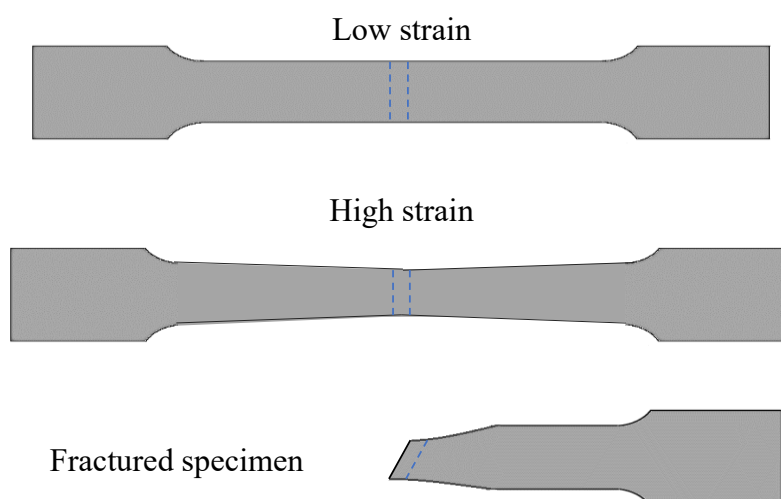


Figure 28. Samples cut for XRD measurements from tensile specimens after the application of different strains.

3.3.3 Hardness

Materials with wear resistance requirements must have a relatively high hardness. Thus, in medium and high C steels studied in this work hardness was an important parameter. Hardness measurements were carried out in a Vickers Hardness Tester FV-700 model (FUTURE-TECH) (Tecnalia, Spain) using a 10 kg load, applied for 10 s according to the ISO 6507-1. To minimize errors, 5 indentations per sample were performed.

The Vickers test consists of an indenter in the form of a straight pyramid with a square base and with a specific angle between opposite faces at the vertex (α), which is introduced with

a certain force (F) on the surface of the specimen of the material to be tested. Subsequently, the diagonals of the imprint (d_1 and d_2) remaining on the surface are measured and, finally hardness value is obtained by means of (5), where “ d ” is the average value between d_1 and d_2 . The Vickers hardness test principle is depicted in Figure 29.

$$HV = \frac{0.189 \times F}{d^2} \quad (5)$$

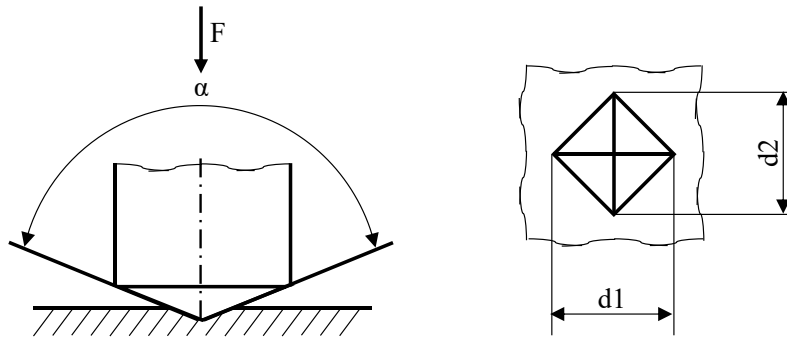


Figure 29. Vickers hardness test principle.

3.3.4 Tribology: pin-on-disk (PoD)

To characterize the wear resistance of medium and high C steels, pin-on-disk (PoD) tests were carried out in a MICROTTEST tribometer (Tecnalia, Spain) to the Q&P and Q&T treated samples of 1.2990 and 300M steels. The PoD consists in placing two materials in contact, keeping one of them in motion and both subjected to constant pressure for a determined time or distance. As shown in Figure 30, this test reproduces the unidirectional sliding process between two different materials under certain conditions.

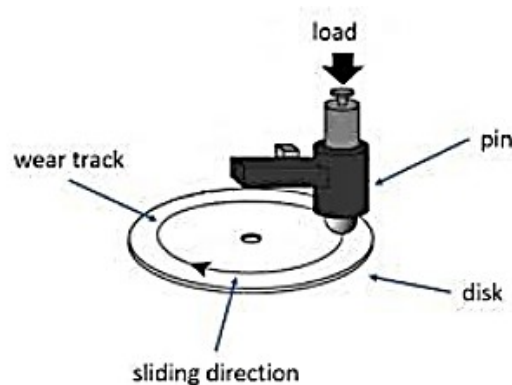


Figure 30. Pin-on-disk system.

In these tests, the disks (materials investigated in this work) are the ones in motion. The pin can be a cylinder with a flat surface, spherical or a ball. In this case, the pin was a 6 mm diameter ball. The dimension of the disk for the application of PoD were 4 mm thickness

disks, with a diameter of 100 mm and 35 mm in the 1.2990 and 300M steels, respectively, and an inner hole of 5.5 mm diameter. The test parameters are summarized in Table 14. Two tests were performed for each steel/Q&P condition.

Table 14. Parameters used for the pin-on-disk tests.

Steel ref.	1.2990	300M
Test radius (mm)	15 and 45	15
Lineal velocity (cm/s)	78.3 and 208.3	78.3
Load (N)	20	20
Temperature (°C)	RT	RT
Relative humidity (%)	50	50
Pin material	Al ₂ O ₃	Al ₂ O ₃
Pin dimensions (mm)	Ø6	Ø6
Distance (m)	15000	5638

After carrying out the test, the worn volume was evaluated on the disk, measuring a series of wear profiles. The evaluation consists of making 4 profiles on the track left in the test, thus obtaining 4 cross-sectional areas (Figure 31). This operation was carried out using a Dektak 150 Contact Profilometer. Then, the wear volume was calculated by the following geometrical relation:

$$V = 2\pi r \cdot A \quad (6)$$

where r is the test radius in mm, and A is the average wear area obtained by profilometer, expressed in mm².

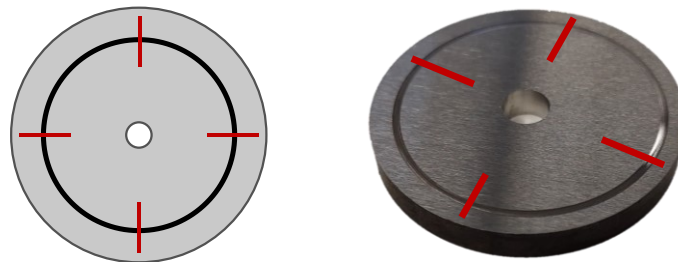


Figure 31. Cross-sectional areas of the wear track employed for the measurement of wear rate.

Finally, the specific wear rates (K) in mm³/N·m of the investigated materials were obtained. This rate is defined as the volume worn divided by the normal load and the test distance using the following equation:

$$K = \frac{V}{L \cdot d} \quad (7)$$

Being V the volume of wear (mm³), L the normal load (N) and d the total distance of the test (m).

3.3.5 Toughness

Toughness is the ability of a material to absorb energy and plastically deform without fracturing. The toughness of a material can be measured using a small specimen of that material. A typical testing machine is a Charpy V-notch impact test. This is a dynamic test in which a notched specimen is struck and broken by a single blow in a specially designed testing machine.

In this work, a preliminary toughness study was realized with the 1.2990 steel to compare the energy absorption capacity of Q&P and Q&T treated steels. Due to material limitation, standard subsize specimens were used. Three test per heat treatment were performed. Figure 32 shows the dimensions of the standard subsize specimens according to ASTM A370.

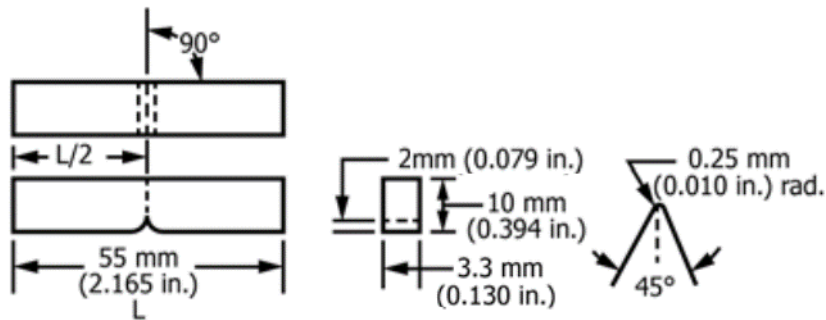


Figure 32. Standard subsize specimen dimensions (ASTM A370).

The equipment used to carry out the impact tests was an AMSLER RKP 300 model pendulum from ROELL + KORTHAUS (University of Cantabria, Spain), with a capacity of 300 J and a hammer weight of 20.4 kg (200 N), with a travel angle of up to 150 ° and maximum impact speed of 5.42 m/s.

Chapter 4

Results and discussion

Chapter 4

Results and discussion

In this chapter, the main results in terms of microstructure and mechanical properties obtained after the application of the Q&P heat treatments are presented and discussed. The influence of both cycle parameters and composition of the steel on the microstructure are investigated. In addition, the influence of the characteristics of the microstructure on the different mechanical properties is also studied. In a first section, the results and discussion for medium Mn and Ni steels are presented and, in a second section, for medium and high C steels.

4.1 Q&P applied to medium Mn and Ni steels

4.1.1 Dilatometry curves of the Q&P heat treatments

The Q&P cycles carried out in the furnaces and salt baths were simulated in the dilatometer. As mentioned in the previous chapter, three thermal cycle were applied to the four medium Mn and Ni steels: *ref*, which is the reference cycle with a partitioning temperature of 400 °C, and QT25-Pt1000 and QT10-Pt1000, which are high partitioning temperature cycles. In addition, with the aim of studying the influence of the partitioning time, two additional cycle (QT10-Pt300 and QT10-Pt3600) were applied to the 6Mn and 6Mn2Ni steels. The obtained dilatometry curves of the complete Q&P cycle are represented in Figure 33 for each thermal cycle applied to each steel.

In the *ref* cycle, with a partitioning temperature of 400 °C, expansion was observed during partitioning in the four steel. This expansion was related with bainite formation or, to a lesser extent, with carbon partitioning [108,209]. The more intense expansion in 2Mn and 4Mn alloys revealed the effect of alloying elements; it is to say, the more Mn content was in the alloy, the less expansion occurred, while the effect of Ni was less noticeable (Figure 34). Regarding high partitioning temperature cycles, contraction was observed during partitioning in the four steels, which was related with austenite reverse transformation. The relative change in length measured during the partitioning stage is presented for the 6Mn and 6Mn2Ni

steels in Figure 35a and Figure 35b, respectively, considering Pt1000 cycles for both QT conditions. In the latter figures, a continuous contraction of the samples during partitioning was observed in all cases. These curves reveal that equilibrium conditions were not reached in the austenite formation reaction in any of the conditions, since contraction had not yet reached a plateau. Moreover, in the QT10 condition the contraction was greater than in the QT25 condition, particularly in the 6Mn steel. The reverted austenite formed during partitioning was calculated using the lever-rule and it is shown in Figure 35c-d. It can be observed that the QT10 condition resulted in a greater increase in the austenite fraction during partitioning, and thus faster austenite formation kinetics.

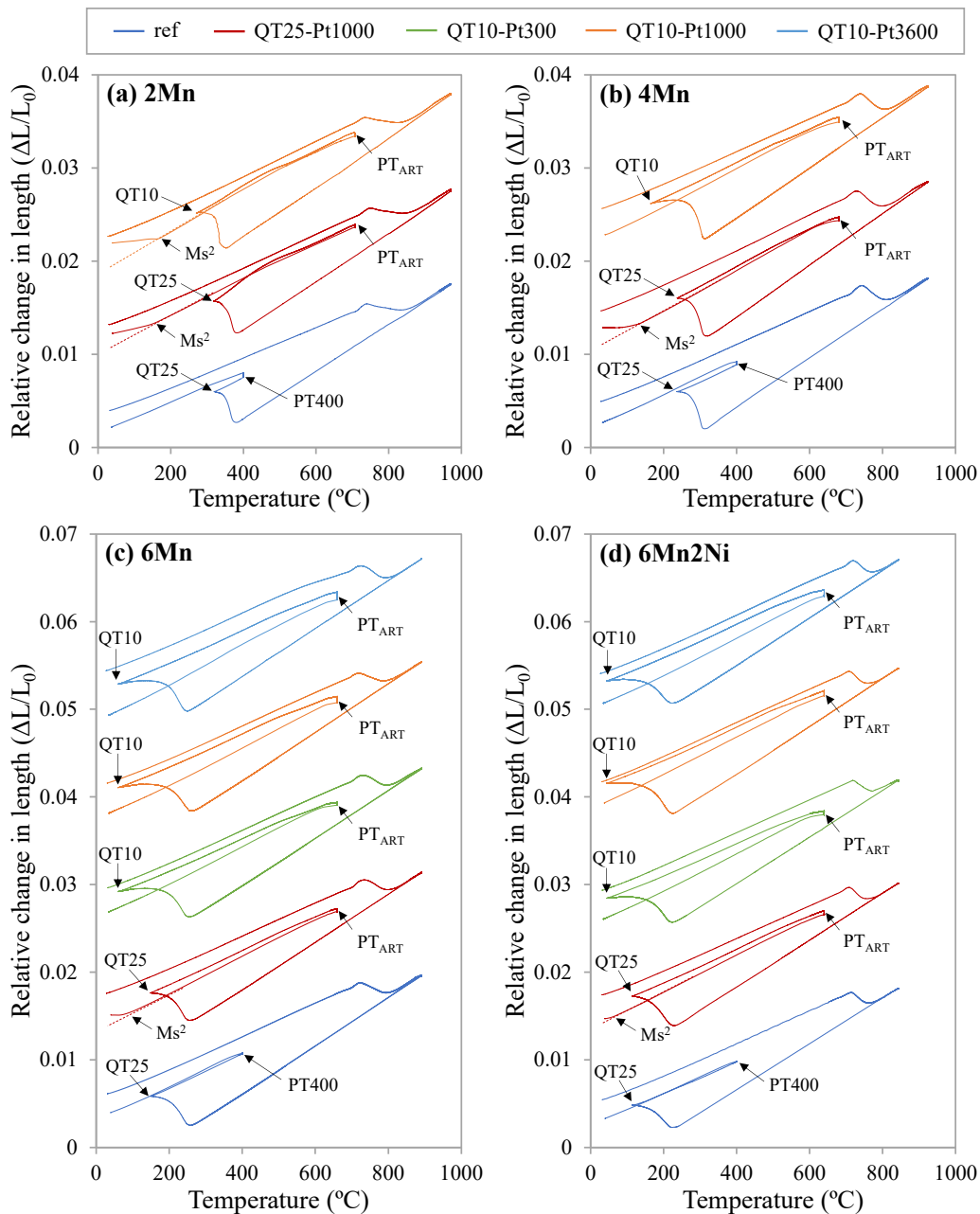


Figure 33. Dilatometry curves of the applied Q&P cycles: 2Mn steel (a), 4Mn steel (b), 6Mn steel (c), and 6Mn2Ni steel (d).

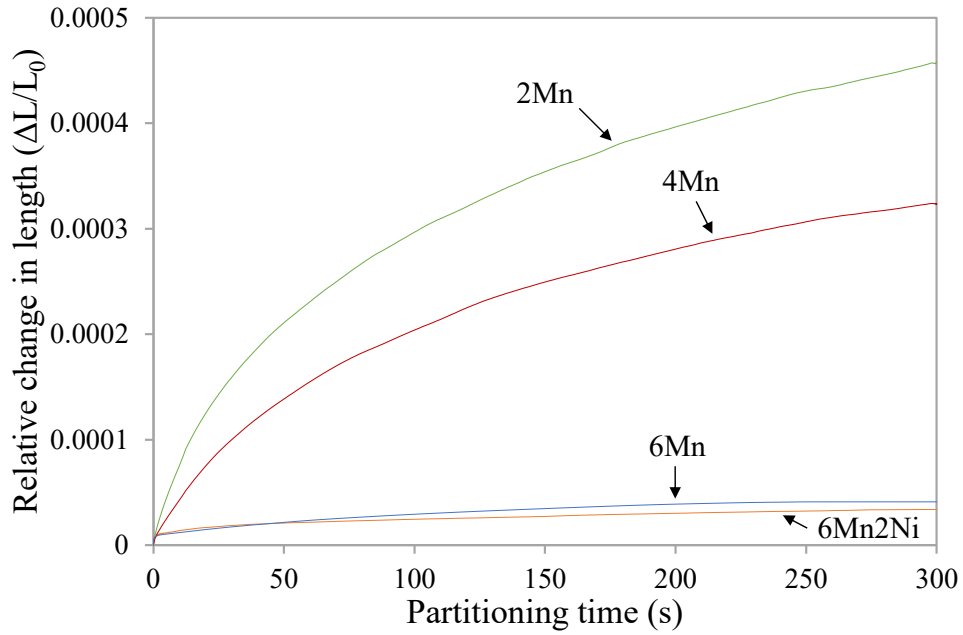


Figure 34. Relative change in length measured during the partitioning stage for the ref cycle.

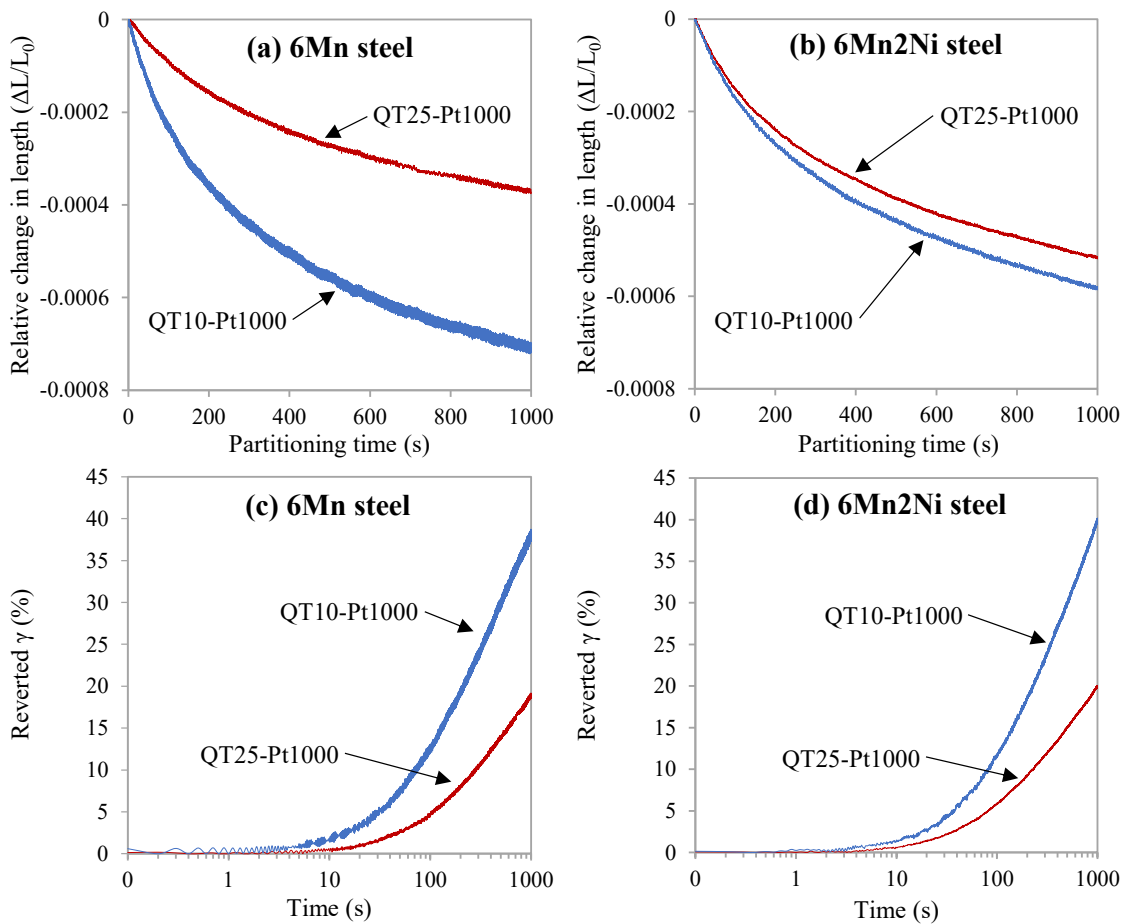


Figure 35. Relative change in length measured during the partitioning stage for the QT10-Pt1000 and the QT25-Pt1000 cycles: 6Mn (a) and 6Mn2Ni (b) steels. Evolution of the austenite formed during the partitioning (reverted γ) in the QT10-Pt1000 and the QT25-Pt1000 cycles in the 6Mn (c) and 6Mn2Ni (d) steels.

The dilatometry curves during final cooling to room temperature were analyzed to study the possible formation of secondary martensite (Figure 33). The curve was linear in all the QT10 conditions except for the 2Mn steel, which showed a secondary martensite transformation temperature (M_s^2) of 167 °C. This means that the formation of secondary martensite was not significant in the steels with at least 4 wt.% of Mn and, therefore, most of the austenite available at the end of partitioning was retained in the final microstructure. In this sense, the QT10 condition seemed to be beneficial for the stabilization of austenite. In contrast, for the QT25 condition, the dilation curves deviated from linear contraction, which denoted secondary martensite transformation during final cooling. The secondary M_s^2 were determined to be 157 °C, 133 °C, 103 °C and 57 °C in the 2Mn, 4Mn, 6Mn and 6Mn2Ni steels, respectively. The lower M_s^2 temperature observed with the increase of the alloying content in the steels indicated that austenite stabilization was enhanced, which was likely due to the known stabilization capacity of Mn [66] and Ni [37,52,53,210].

4.1.2 Microstructure after the Q&P heat treatments

The retained austenite contents were measured by XRD for all Q&P conditions and steels. Then, the most interesting conditions were selected for being analysed by means of FE-SEM, EBSD and TEM.

The retained austenite contents measured by XRD are shown in Figure 36 as a function of partitioning time for all Q&P cycles and steels. Regarding ref cycle, the alloying content greatly influenced on the stabilization of austenite. In the 2Mn steel only 7% of the 25% austenite available at the QT was stabilized. As mentioned in the previous section, greater expansion was observed during partitioning in this steel which was related to bainite formation, thus, it is likely that a considerable amount of austenite transformed into bainite during partitioning resulting in a lower content of final austenite. With higher alloying contents the austenite was effectively retained at room temperature, achieving to stabilize all of it in the 6Mn2Ni steel.

After the high partitioning temperature cycles with a partitioning time of 1000 s, almost no retained austenite was detected in the 2Mn steel regardless of the QT condition, showing that 2 wt.% Mn was not enough to stabilize austenite. In the rest of the steels, all the cycles resulted in a final retained austenite content greater than the austenite content existing at the QT with the exception of the QT25-Pt1000 cycle in the 4Mn steel, likely due to the secondary martensite transformation observed in the dilatometry curve (Figure 33b). In the case of the

QT25-Pt1000 cycle applied to the 6Mn steel, the increase in austenite content was small, but in the 6Mn2Ni steel was considerable. This is in good agreement with the M_s^2 measured in the dilatometry curves (Figure 33), where this temperature decreased with the alloying content of the steel. In all QT10 conditions, a very substantial increase was observed. The maximum content of RA was 47%, which was obtained after the application of the QT10-Pt1000 cycle in the 6Mn2Ni steel.

The Ni addition clearly resulted in a significant increase in RA content, regardless of the thermal treatment conditions. Furthermore, comparing the QT25-Pt1000 and the QT10-Pt1000 conditions, it can be seen that a lower austenite content at the QT clearly resulted in an increased content of austenite in the final microstructure of the 6Mn and 6Mn2Ni steels.

As to the influence of partitioning time in the QT10 condition, increasing partitioning time from 300 to 1000 s also increased RA content. However, a further increase to 3600 s resulted in a slight decrease in RA content. The influence of partitioning time on RA content was very similar for the 6Mn and 6Mn2Ni steels.

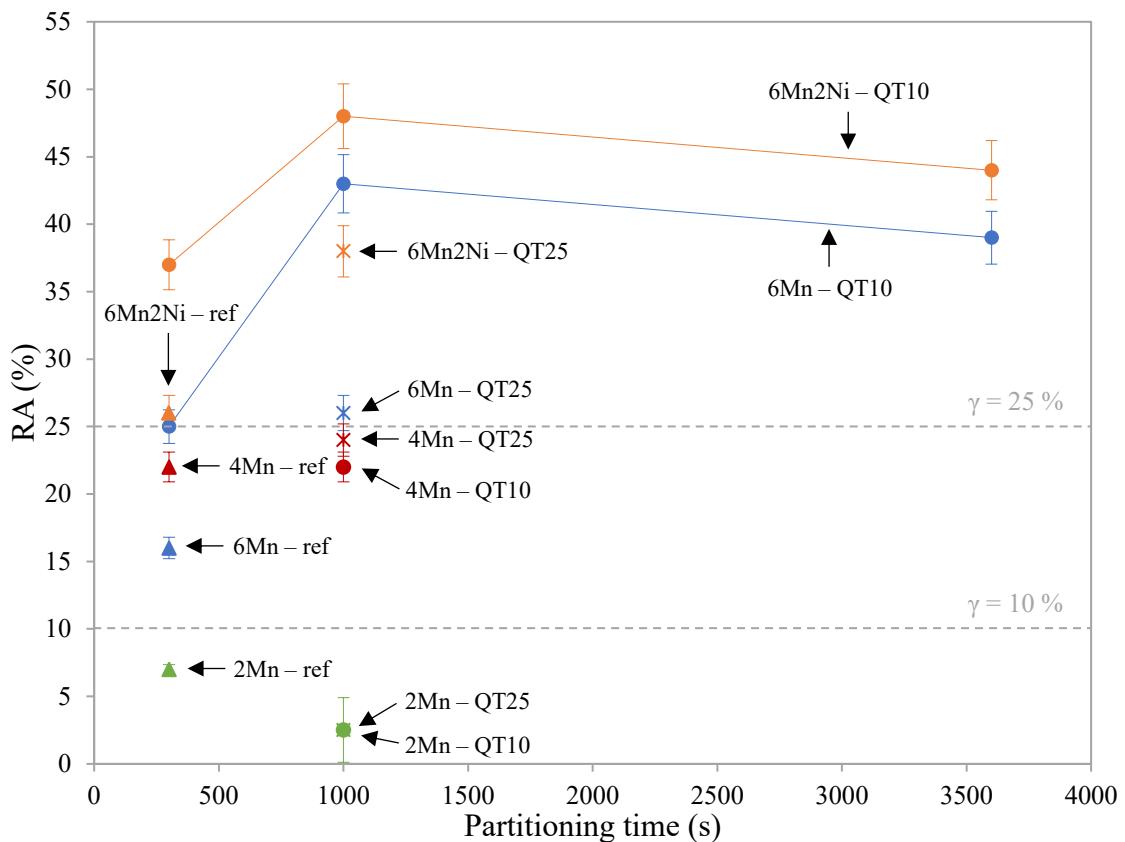


Figure 36. Retained austenite contents as a function of partitioning time measured after the application of all Q&P cycles.

The 6Mn and 6Mn2Ni steels after QT10-Pt1000 and QT25-Pt1000 conditions were selected for being observed in the FE-SEM due to the high retained austenite contents. Additionally, the microstructure after QT10-Pt3600 cycle was observed in the 6Mn2Ni steel to analyse the influence of partitioning time. The microstructure expected in these samples can be described as follows: After heating to obtain a fully austenitic microstructure, the Q&P steels were quenched to the predetermined QT in order to form a partially austenitic and partially martensitic microstructure. Then, heating to a partitioning temperature, which corresponded to the austenite reversion transformation start temperature, the pre-existing austenite was expected to grow and be enriched by Mn and C provided by the martensite [13,49]. In the 6Mn2Ni steel, Ni enrichment could also occur [211]. Thus, after final quenching, the austenite which contained enough C and Mn would become stable and be retained at room temperature [13,49], whereas the less enriched austenite would transform into secondary martensite (α'_{sec}). In this way, the expected final microstructure should consist of C and Mn depleted primary martensite (M1), RA laths and blocky RA, and martensite/austenite (MA) islands consisting of secondary martensite with fine RA. Carbide precipitation was also expected as a result of the tempering of martensite due to the high partitioning temperature employed.

In the FE-SEM micrographs obtained in the present work (Figure 37), bright thin films were observed in all micrographs, which were likely retained austenite. The dark phase was interpreted to be primary martensite (M1) containing a considerable amount of carbides. The carbides exhibited both acicular/plate and globular morphologies. Mn retards cementite dissolution, so observed carbides could include some cementite that did not dissolve in prior steps, along with cementite formed as a consequence of tempering of the martensite. The regions with dark-grey center and white edges are generally recognized as MA islands.

In the QT25-Pt1000 micrographs large areas of MA were evident. However, as shown later, the amount of secondary martensite determined from the dilatometry curves and XRD results was not significant. Therefore, the interpretation of these areas in the FE-SEM images was not entirely clear, but was presumably indicative of transformation during cooling near QT. In both steels, the microstructure observed after the QT25-Pt1000 cycle presented coarse and blocky constituents, whereas after the QT10-Pt1000 cycles the microstructure was thinner and exhibited a lath-type appearance. The microstructure features in the 6Mn2Ni steel after the QT10-Pt3600 cycle (Figure 37e) were thinner than after the QT25-Pt1000 cycle, but coarser than after the QT10-Pt1000 cycle.

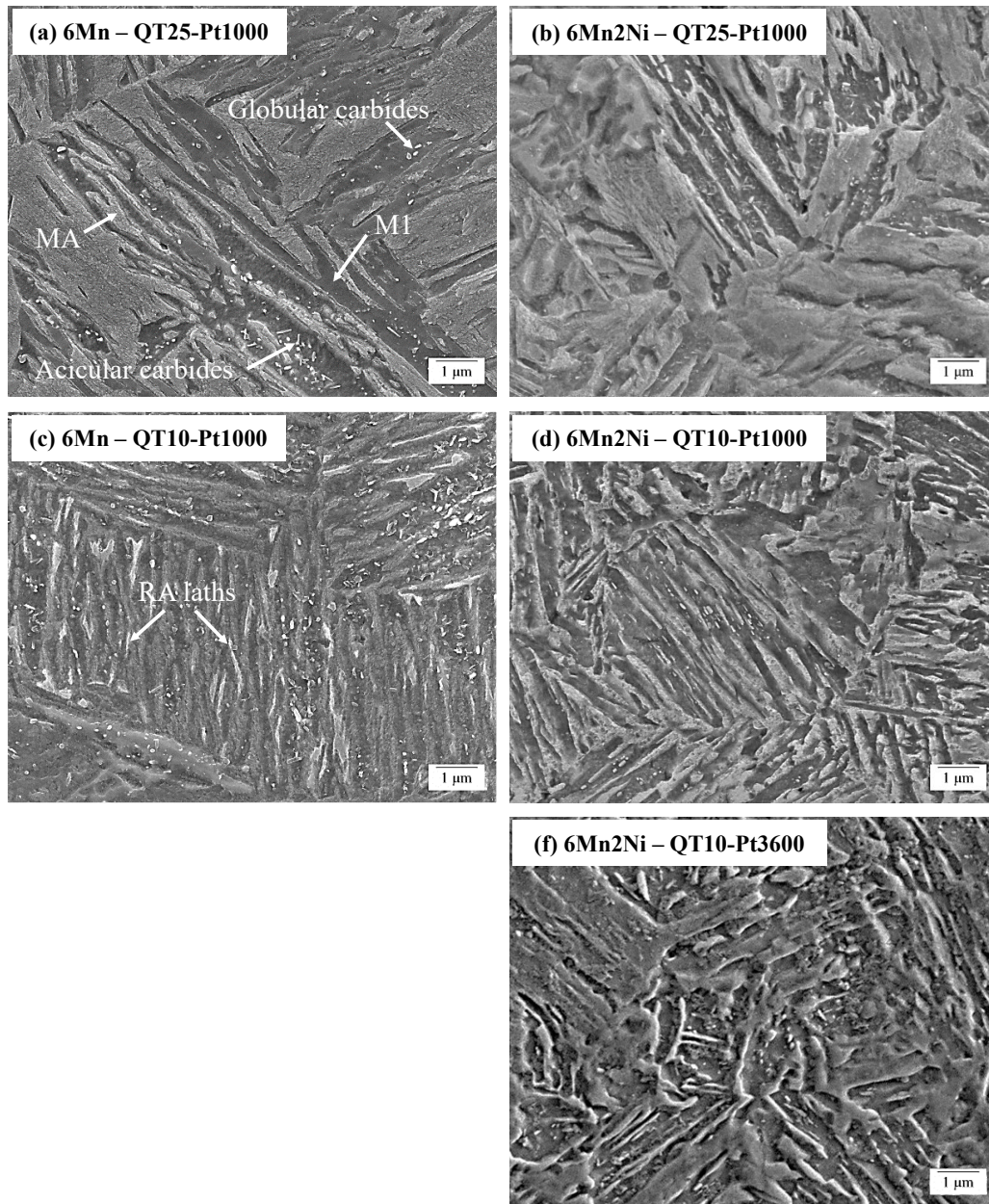


Figure 37. FE-SEM micrographs corresponding to the QT25-Pt1000 cycle for the 6Mn (a), and 6Mn2Ni (b) steels; the QT10-Pt1000 cycle for the 6Mn (c), and 6Mn2Ni (d) steels; and the QT10-Pt3600 cycle for the 6Mn2Ni steel (e).

EBSM phase maps were obtained for all the Pt1000 conditions of the 6Mn and 6Mn2Ni steels. EBSM phase maps are shown in Figure 38, where the red phase was identified as RA, green was martensite, and black indicates unidentified regions. From EBSM measurements, retained austenite content and size were obtained. In Table 15 a comparison between the RA content measured by XRD and EBSM is shown. The austenite content measured by EBSM was lower than that measured by XRD, which might be due to three reasons. First, the dark regions in the EBSM maps can be MA islands containing retained austenite. However, these regions are mostly recognized as unidentified regions. Second, detection of

nanometer sized film like retained austenite stabilized between the martensitic laths is difficult to identify with EBSD due to low resolution. Third, the area and depth of the measurements were different, playing an important role the step used in EBSD characterization. Most of the dark zones in the QT25 cycles (Figure 38a-b) likely corresponded to MA islands, whereas the thin dark zones between martensite areas in the QT10 condition (Figure 38c-d) likely included nanometer sized film-like retained austenite. In Table 15, average RA sizes estimated from EBSD measurements are also shown. In the 6Mn steel, the QT10-Pt1000 condition resulted in a coarser average austenite size in comparison with the QT25-Pt1000 condition. However, in the QT10-Pt1000 condition, the minimum austenite size was 110 nm and fine scale film-like retained austenite areas were mostly not detected in the measurement.

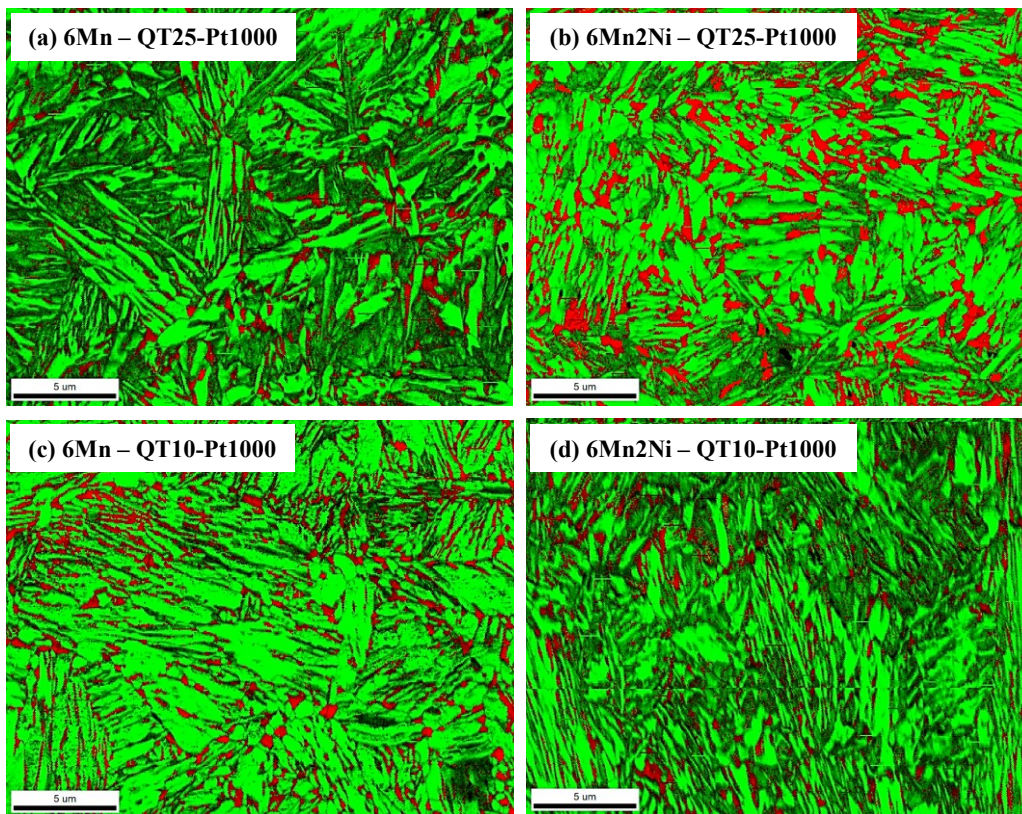


Figure 38. EBSD scans corresponding to the QT25-Pt1000 cycle for the 6Mn (a), and 6Mn2Ni (b) steels; and the QT10-Pt1000 cycle for the 6Mn (c), and 6Mn2Ni (d) steels.

Table 15. Comparison between retained austenite content (RA %) measured by XRD and EBSD. Average austenite grain size (RA nm) measured by EBSD.

Q&P cycle	6Mn			6Mn2Ni		
	XRD (RA %)	EBSD (RA %)	EBSD (RA nm)	XRD (RA %)	EBSD (RA %)	EBSD (RA nm)
QT25-Pt1000	26	17.4	168	38	25.2	220
QT10-Pt1000	43	20.4	237	48	17.6	161

In Figure 39, TEM characterization results are presented for the 6Mn2Ni steel. Figure 39a and Figure 39b show TEM micrographs after the application of the QT25-Pt1000 and QT10-Pt1000 cycles, respectively. In both cases, the microstructure consisted of lath-type constituents which were identified as martensite and austenite by means of Selected Area Diffraction (SAD). Carbides were also observed, and their characterization is described later. In general, the austenite and martensite laths appeared thinner in the QT10-Pt1000 condition. Moreover, a large number of laths were thinner than the detection limit employed in EBSD analysis (~ 100 nm). The laths identified as austenite in the QT25-Pt1000 condition had a width of 53 ± 5 nm, which would explain the lower RA contents measured by EBSD in comparison with XRD measurements.

With the aim of understanding the partitioning behaviour of Mn and Ni, TEM – Energy Dispersive Spectroscopy (EDS) analysis was performed and the compositional maps (Figure 39c-f) and concentration profiles (Figure 39g-h) were obtained for Mn and Ni alloying elements. The compositional maps revealed that the Mn concentration was not homogeneous, with austenite films enriched in this element. On the contrary, Ni concentration was more homogeneous. The concentration profiles obtained for the QT25-Pt1000 condition (Figure 39g), revealed high Mn enrichment in the region identified as austenite by SAD, obtaining a maximum concentration of 15 wt.%, and a lower Mn concentration in the laths identified as martensite. In the latter, Mn content was around the nominal value (grey laths) or above this value (white laths), and consequently, the laths were deduced to be primary and secondary martensite, respectively. Likely, initial austenite laths existing at QT25 were too large to be completely enriched in Mn and, as a consequence, a Mn gradient was observed from the boundary to the center of the initial austenite lath, existing a higher Mn concentration near the boundary. Hence, secondary martensite transformed from the interior of the austenite laths remaining from cooling to the QT, originating MA islands in the final microstructure [112,114].

On the contrary, in the QT10 condition (Figure 39h) a higher percentage of the lath was enriched in Mn and the concentration profile was more homogeneous. Furthermore, the Mn concentration in the enriched laths was significantly higher than in the QT25 condition. Therefore, it can be concluded that in the high partitioning temperature Q&P cycles applied in this work, Mn partitioning occurred and the lower QT condition was beneficial for the Mn enrichment of austenite laths, which likely contributed to austenite stabilization. Ni concentration profiles did not show such clear concentration differences between laths as

those of Mn, although in the QT10-Pt1000 cycle Ni concentration profile showed a trend similar to that shown by Mn. The effect of Ni is further discussed in section 4.1.6.

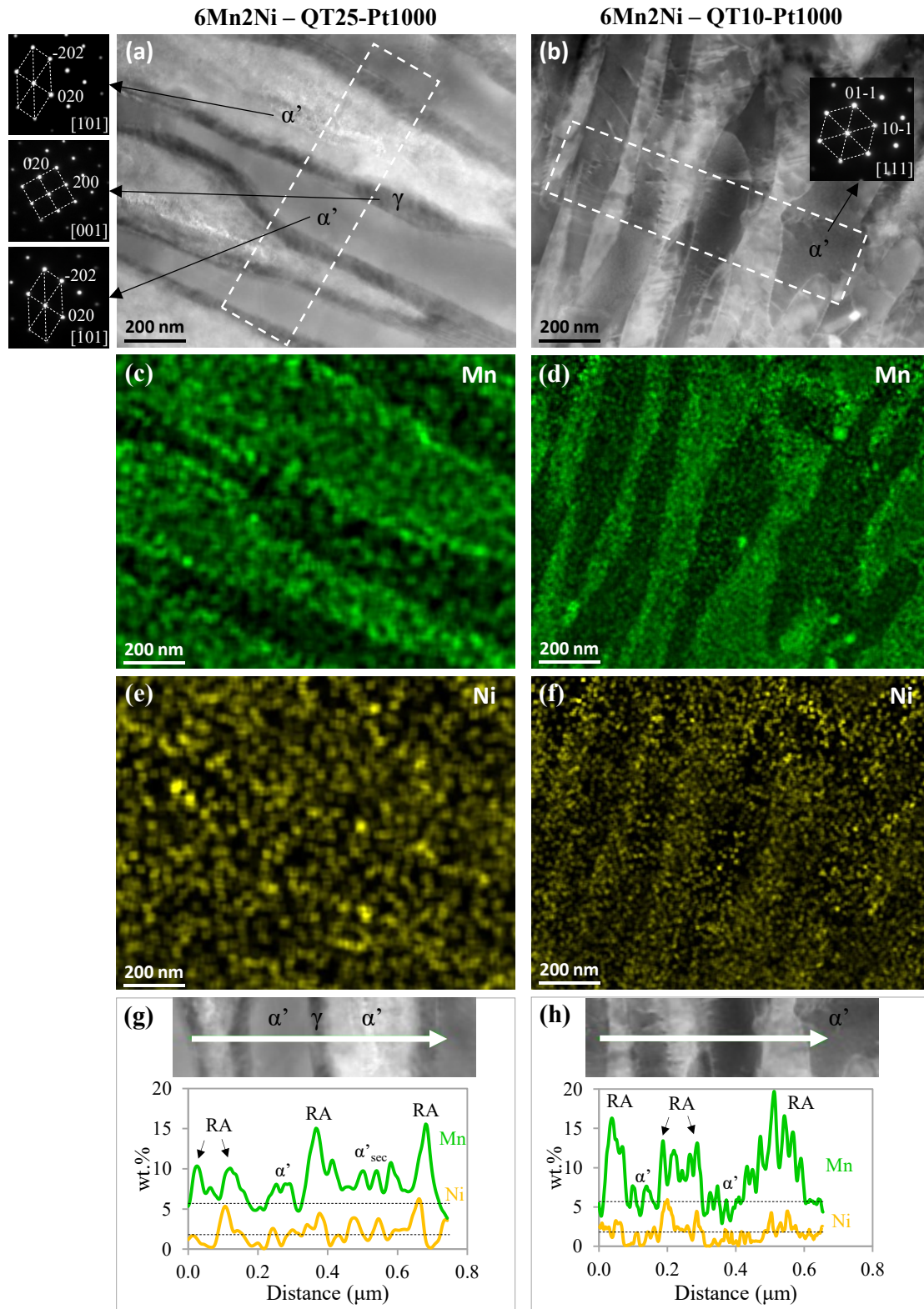


Figure 39. TEM analysis of 6Mn2Ni steel: Micrographs and SAD patterns for the QT25 (a) and the QT10 (b) conditions; EDS analysis representing the distribution of Mn concentration for the QT25 (c) and QT10 (d) conditions, and Ni concentration for the QT25 (e) and QT10 (f) conditions; concentration profiles of Mn and Ni line scans performed within the areas marked in (a) and (b) for the QT10 (g) and QT25 (h) conditions.

The microstructure characterization was finished by performing a TEM-EDS analysis of the carbides observed in the microstructure. As presented before, globular and acicular/plate carbides were present in the microstructure. The TEM-EDS analysis of the carbides revealed that the carbides contained Mn. As an example, the EDS spectrum of a globular carbide observed in the 6Mn steel after the QT10-Pt1000 cycle is shown in Figure 40b. Compositional mapping in an area examined in the 6Mn2Ni steel after the QT10-Pt1000 cycle, which contained both globular and acicular carbides, revealed the enrichment of both types of carbides with Mn (Figure 40d). In the 6Mn2Ni steel, the TEM-EDS analysis did not show the presence of Ni in the carbides. The formation of Mn enriched carbides resulted in less C and Mn available for austenite stabilization.

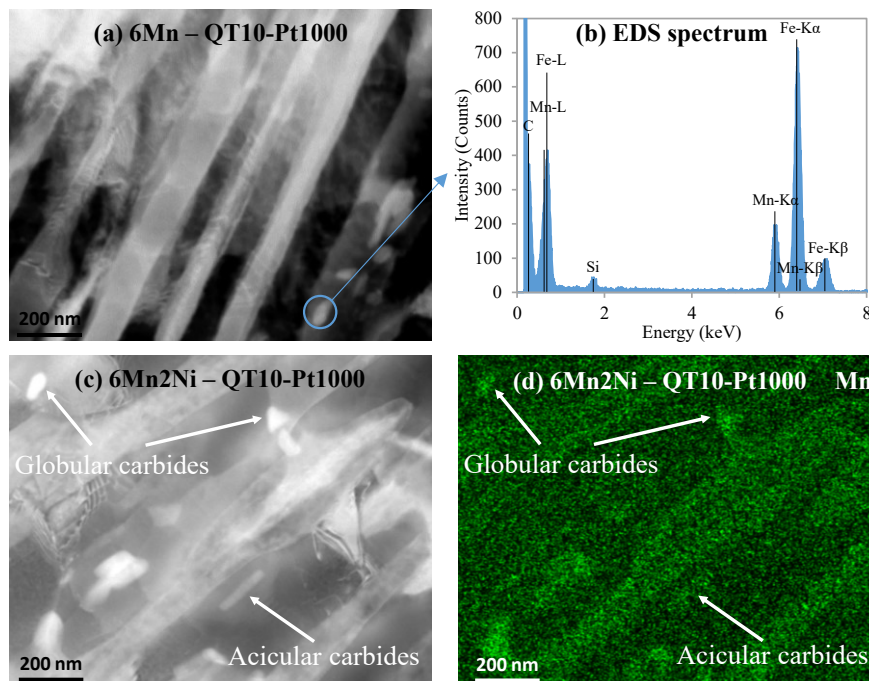


Figure 40. TEM micrographs of the 6Mn steel (a) and the 6Mn2Ni steel (c) after QT10-Pt1000 cycle, TEM-EDS spectrum of a globular carbide marked in (a) (b), and compositional mapping of the (c) micrograph (d). In the micrograph (c), acicular and globular carbides are visible; in the compositional map (d) a higher concentration of Mn is visible in the globular and acicular carbides.

4.1.3 Tensile properties

Figure 41, Figure 42, Figure 43 and Figure 44 show the stress-strain curves for all Q&P cycles of the 2Mn, 4Mn, 6Mn and 6Mn2Ni steels, respectively. All data obtained from the tensile tests are summarized in Table 16: Yield strength (YS), tensile strength (TS), YS/TS ratio, total elongation (TEL), and TS x TEL product. These data correspond to the average values obtained from two tests. In Appendix C the photographs of one fractured tensile specimen per steel and condition is shown. Tensile properties are related to the microstructure in section 4.1.8.

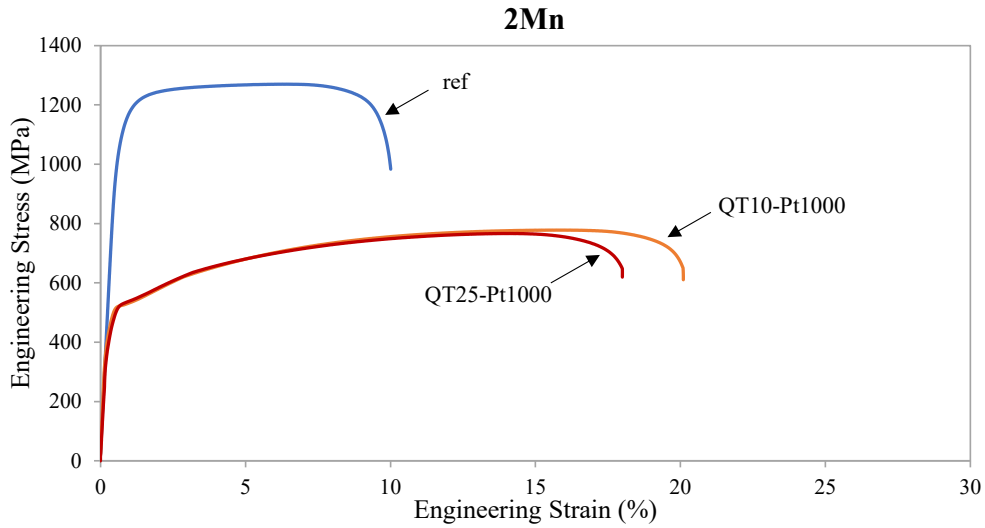


Figure 41. Engineering stress-strain curves obtained after Q&P treatments for the 2Mn steel.

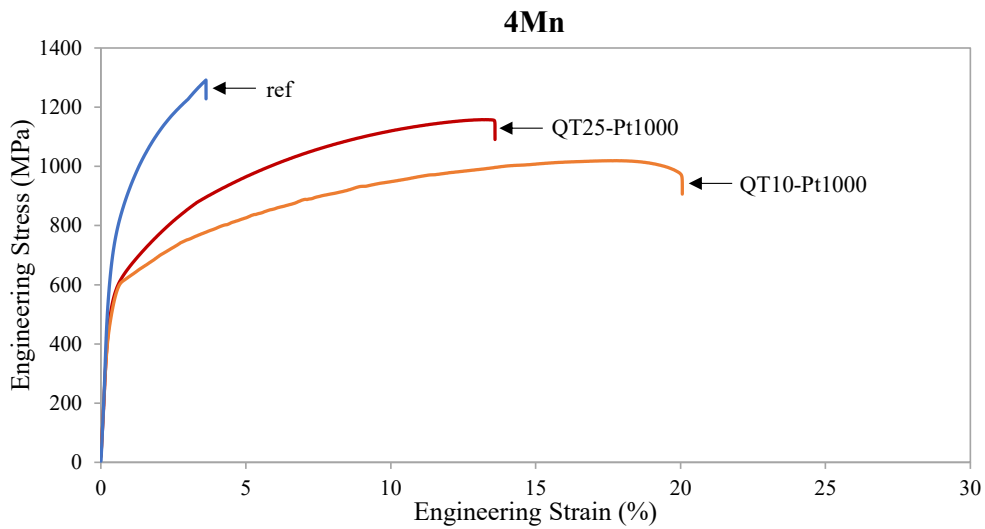


Figure 42. Engineering stress-strain curves obtained after Q&P treatments for the 4Mn steel.

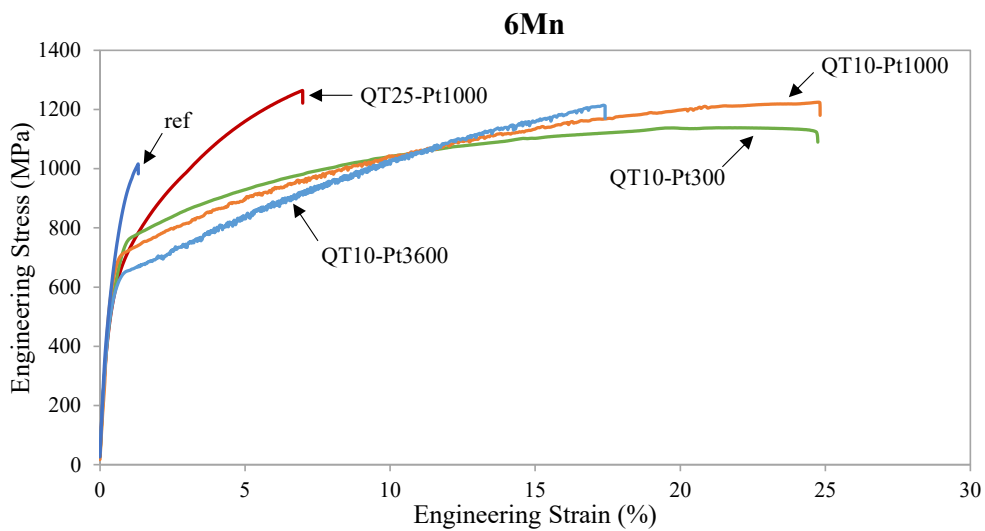


Figure 43. Engineering stress-strain curves obtained after Q&P treatments for the 6Mn steel.

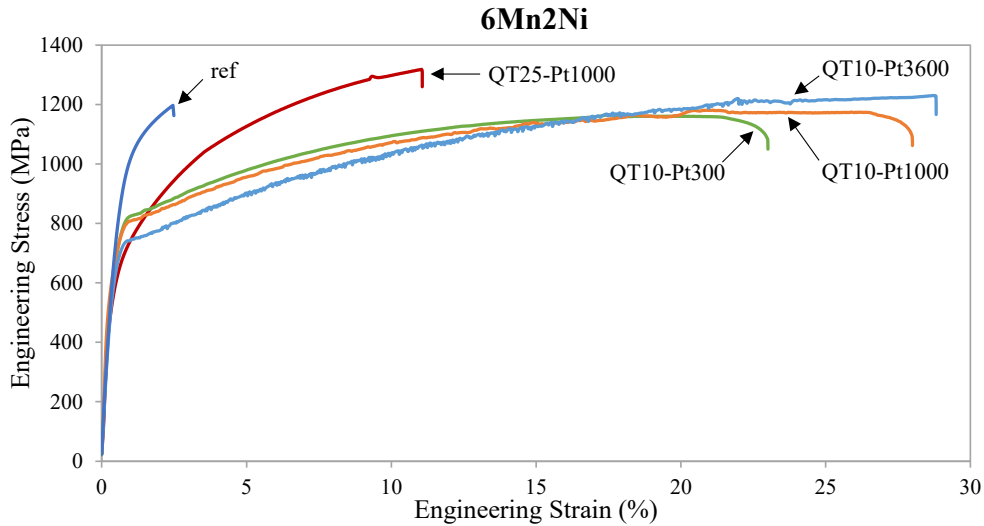


Figure 44. Engineering stress-strain curves obtained after Q&P treatments for the 6Mn2Ni steel.

Table 16. Summary of tensile properties for the 2Mn, 4Mn, 6Mn and 6Mn2Ni steels after each Q&P treatment.

Steel ref.	Q&P cycle	YS (0.2% offset) (MPa)	TS (MPa)	YS/TS ratio	TEL (%)	TS x TEL (GPa%)
2Mn	ref	974	1273	0.76	9.9	12.5
	QT25-Pt1000	512	767	0.67	18.3	14.0
	QT10-Pt1000	523	759	0.69	20.1	15.2
4Mn	ref	833	1259	0.66	3.7	4.7
	QT25-Pt1000	581	1182	0.49	13.6	16.1
	QT10-Pt1000	524	1064	0.49	20.3	21.5
6Mn	ref	735	993	0.74	0.6	0.5
	QT25-Pt1000	585	1251	0.47	6.9	8.6
	QT10-Pt300	644	1158	0.56	24.6	28.5
	QT10-Pt1000	651	1199	0.54	24.9	29.9
	QT10-Pt3600	584	1204	0.48	17.4	20.9
6Mn2Ni	ref	896	1170	0.77	1.6	1.9
	QT25-Pt1000	580	1329	0.44	11.1	14.7
	QT10-Pt300	727	1182	0.61	23.7	28.0
	QT10-Pt1000	694	1207	0.57	28.1	33.8
	QT10-Pt3600	705	1222	0.58	28.8	35.2

It can be seen that in the Q&P cycles with a partitioning temperature of 400 °C (ref cycle), the increase in Mn resulted in a noticeable decrease in elongation, and, also, in tensile strength. The further addition of Ni in 6Mn2Ni did not result in an improvement of tensile properties, obtaining, also in this case, a low elongation.

In comparison with the ref cycle, the higher PT cycles gave rise to a lower tensile strength and an improved elongation in the 2Mn and the 4Mn steels. In the high partitioning temperature cycles, the best tensile properties were obtained with the two steels containing 6 wt.% of Mn. In these steels, tensile properties obtained after high partitioning temperature cycles can be described as follows:

- In all cases TS values exceeded 1150 MPa. These values were higher for the QT25-Pt1000 cycles. In the QT10 cycles, a small rise in TS was shown by increasing Pt, as well as by the Ni content addition to the alloy. The influence of Ni on TS was more noticeable in the QT25 cycle.
- The YS was higher for the QT10 cycles, although, the YS/TS ratio was quite low in all cases.
- Stress-strain curves revealed good global formability (tensile ductility) in both steels, particularly for the QT10 cycles. However, post-uniform elongation was limited and, in the case of the QT25 cycles, fracture occurred before necking. In addition, discontinuous yielding was observed after the QT10 cycles with serrations present at long Pt-s (1000 s and 3600 s).
- When it comes to TEL, different levels were obtained depending on the Q&P cycle parameters. The influence of QT on tensile curves was clearly visible, resulting for the QT10 cycles in a notable increase of the TEL values in both steels. In the QT10 cycles, the influence of Pt on TEL depended on the steel: in the 6Mn steel, TEL reached its maximum value, 24.9%, with a partitioning time of 1000 s. In the 6Mn2Ni steel, TEL increased with partitioning time, achieving a total elongation of 28.8% in the cycle with a partitioning time of 3600 s. It was also observed that the addition of Ni was beneficial for increasing TEL.
- The product of tensile strength and total elongation (TS x TEL) was clearly different depending on the QT condition, resulting the QT25 cycles in significantly lower values. Outstanding values were obtained after QT10 cycles, particularly in the 6Mn2Ni steel with partitioning times of 1000 s and 3600 s, which resulted in 33.8 GPa% and 35.2 GPa%, respectively.

In Figure 45, TEL and TS data are represented for each steel and Q&P cycle, marking the regions corresponding to 10, 20 and 30 GPa% values of the product TS x TEL. It can be seen that the values obtained with the ref cycle were quite poor in the 4Mn, 6Mn and 6Mn2Ni steels, where values did not reach 10 GPa% due to the reduced elongation of the steels. On

the contrary, both 6Mn and 6Mn2Ni steels heat treated by QT10 cycles resulted in excellent results of the product of TS and TEL. In the case of 6Mn2Ni and QT10-Pt1000 and QT10-Pt3600, as said before, outstanding results were obtained.

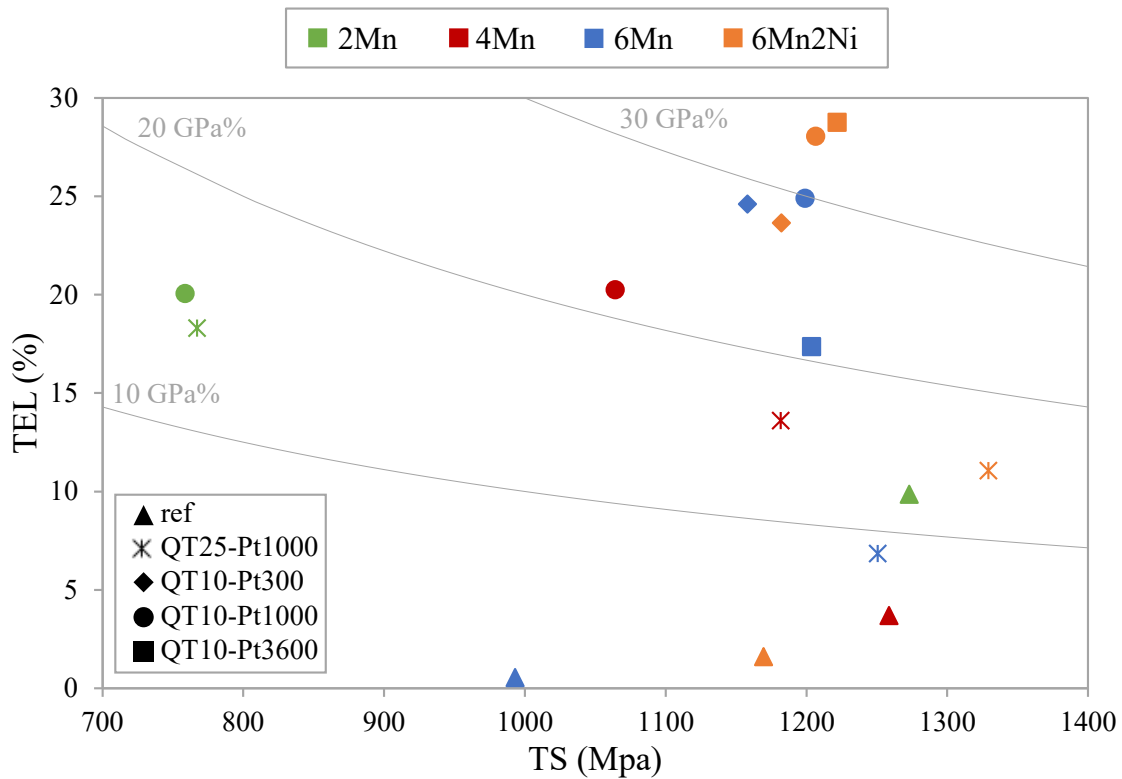


Figure 45. Relationship between total elongation (%) and tensile strength (MPa) obtained after Q&P cycles in 2Mn, 4Mn, 6Mn and 6Mn2Ni steels.

4.1.4 Interrupted tensile test results

Interrupted tensile tests were performed to study austenite transformation into martensite during the test and understand the influence of this transformation on the resulting tensile curve. The tests were performed considering QT10-Pt1000 cycle, due to the excellent tensile properties obtained in this condition, and, the 6Mn and 6Mn2Ni steels, to study the influence of Ni on austenite transformation. The results are shown in Figure 46. The figure provides the RA values obtained after different strain levels and the corresponding stress-strain curve.

The evolution of RA with strain was different in the 6Mn steel compared to the 6Mn2Ni steel. In the 6Mn steel, the RA slightly decreased from 43% to 38% after applying a strain of 5%, then, remained almost steady up to a strain of 10% and, afterward, considerably decreased down to 16% at an elongation of 15%. Finally, after final fracture, no austenite was measured. In the 6Mn2Ni steel, by contrast, a small near linear decrease of RA was observed up to 20% elongation, from 48% to 37%; then, a full transformation of remaining austenite occurred when the sample fractured at 28% elongation.

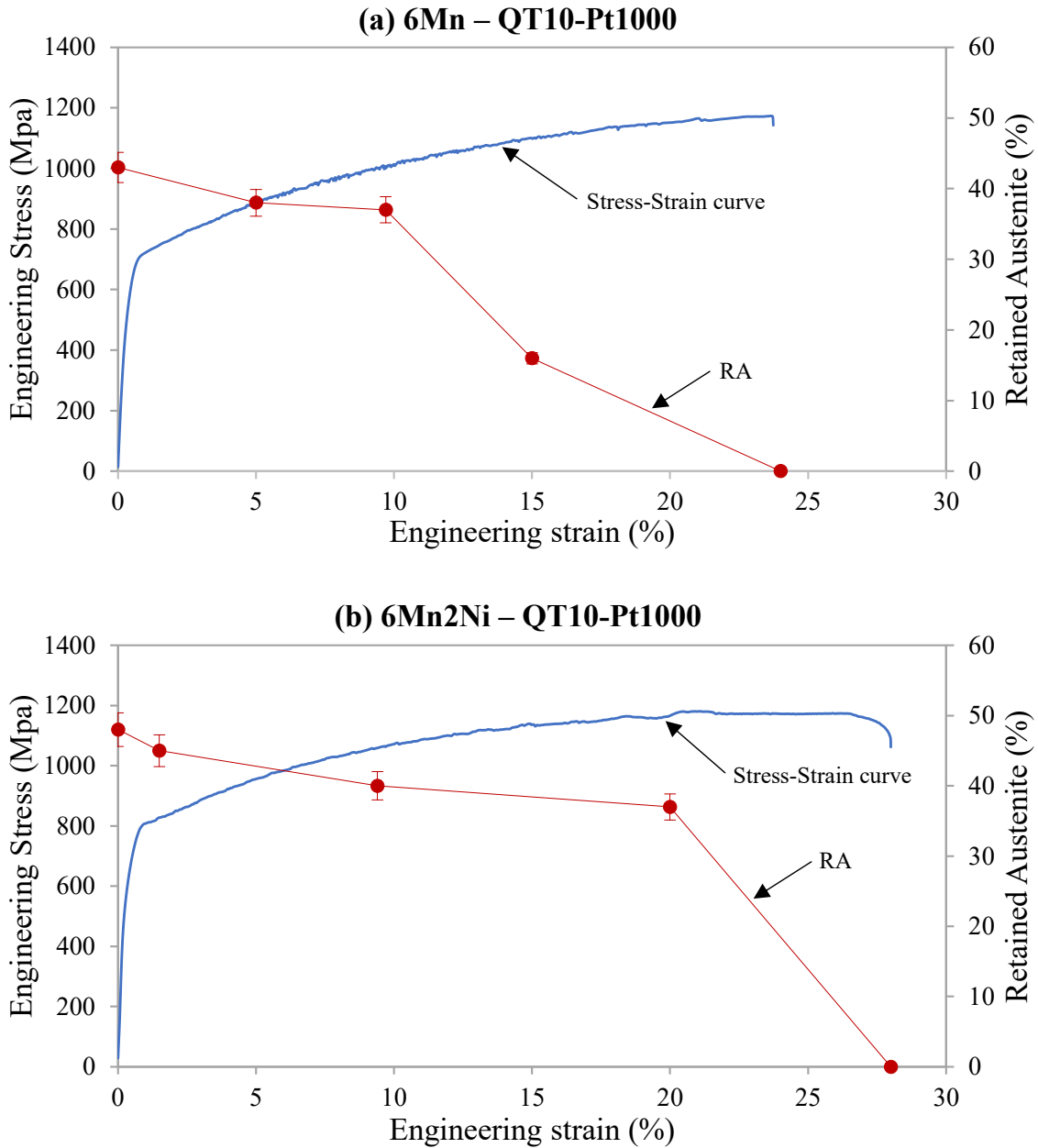


Figure 46. Engineering stress-strain curves obtained for the QT10-Pt1000 condition and RA measured at different strains for the 6Mn (a) and 6Mn2Ni (b) steels.

4.1.5 Analysis of the influence of the heat treatment parameters on microstructure and austenite stabilization

In the high partitioning temperature cycles applied in this work, a clear influence of quenching temperature and partitioning time on microstructure and degree of austenite stabilization was observed, which is analysed below.

4.1.5.1 Influence of quenching temperature

The lower QT applied, QT10, resulted in faster austenite formation kinetics in the partitioning stage (as denoted by the higher contraction observed in the partitioning stage, Figure 35),

less formation of secondary martensite during final cooling, and a final microstructure with a higher content of RA, which, at the same time, showed a lath-type microstructure with finer constituents. Therefore, preserving 10% of untransformed austenite in the quenching step (QT10 condition) was beneficial for austenite stabilization, as well as for enhancing microstructure refinement.

The faster kinetics observed for the QT10 condition were in agreement with the results reported in [112], where it was also reported that the amount of newly formed austenite increased while the amount of pre-existing austenite decreased. At lower quenching temperatures, it can be expected that the formation of fine martensite laths separates austenite into smaller sizes. Liu *et al.* [212] found that austenite lath size strongly decreased with decreased QT. Therefore, in the present work, it is likely that in the QT10 condition the initial martensite/austenite microstructure was finer and, consequently, more nucleation/growth sites were available for austenite formation accelerating the kinetics of the reaction, and the diffusion distances for substitutional solute redistribution were accordingly reduced.

As previously mentioned, the lower QT condition was beneficial for austenite stabilization. The Mn partitioning between martensite and austenite was expected to play a key role in the austenite stabilization. Many publications on intercritically annealed medium Mn steels, show that Mn partitioning occurs between ferrite and austenite contributing to stabilize high amounts of austenite [138,139]. Although long soaking times are commonly reported for this partitioning to occur [49,143,213], some investigations demonstrate that Mn partitioning occurs also in short annealing periods, similar to those employed in the present work [214]. De Moor *et al.* [215] suggested that the high density of dislocations and the grain boundaries should facilitate Mn diffusion. Therefore, some Mn partitioning was expected to occur in the partitioning time conditions applied in the present work, which, additionally, was likely facilitated by the small size of austenite grains in the QT10 condition due to the shorter diffusion paths. In the case of Ni, its partitioning behavior and contribution to stabilize austenite has been less investigated in the literature, however, some influence could also be expected [211].

In this work, Mn and Ni partitioning was characterized by means of TEM-EDS analysis in the 6Mn2Ni steel, observing that, particularly in the case of Mn, the extent of partitioning was different depending on the employed QT (Figure 39). Based on TEM results, thermal stability of austenite was analyzed for the QT10-Pt1000 and QT25-Pt1000 conditions. For this, the

local M_s was calculated by the Andrews equation (1) [195] for the laths where TEM-EDS line scans were performed in Figure 39 (two and three laths for the QT25 and QT10 conditions, respectively) and, then, the Koistinen–Marburger equation (2) [196] was applied to obtain the corresponding austenite volume fraction. Finally, the RA percent was calculated by integrating under the curve of local stable austenite fraction [216]. Values for Mn, Ni and Si were taken from TEM-EDS scan lines, while the equilibrium C content (0.003 wt.% for the martensite and 0.326 for the austenite) in the austenite was obtained by using Thermo-Calc. From these calculations it was shown that the QT10 condition led to a higher stability of austenite after partitioning. Specifically, an average of 82% of the austenite present at the end of partitioning was stabilized to room temperature in the QT10 condition. Thus, given that the measured RA in the final microstructure of this steel was 48%, the total amount of austenite at the end of partitioning would be estimated to be ~58% (considering that 82% of the austenite present at the end of partitioning was stabilized). Hence, the amount of secondary martensite formed during final cooling would be approximately 10%. In the case of the QT25 condition, only an average of 54% of the austenite existing at the end of partitioning was sufficiently stable to avoid transformation during final cooling. The austenite content in the final microstructure was 38%; thus, at the end of partitioning it would be 70%, indicating that the secondary martensite content in this steel would be around 32%, formed mainly inside the coarse austenite laths, where the Mn content was considerably lower than near the boundaries. A summary of the results is shown in Table 17.

Table 17. Summary of the austenite and secondary martensite values estimated and measured at the end of the partitioning and in the final microstructure.

QT condition	End of the partitioning		Final microstructure	
	Estimated % of γ stabilization	Estimated γ content (%)	Experimental RA (%)	Estimated α'_{sec} (%)
QT10	82	58	48	10
QT25	54	70	38	32

The estimated secondary martensite contents were higher than those expected from the dilatometry curves (Figure 33, and Figure 52, shown later), suggesting that other parameters, apart from composition could influence the thermal stability of the austenite. Arlazarov *et al.* [125] investigated the role that grain size plays in thermal stability of austenite in a Medium-Mn steel and they found that a grain size smaller than 0.5 μm clearly lowered the M_s , increasing austenite stability. In the previous calculations of M_s and final austenite amount, the effect of grain size was not considered, however, the microstructures present in

this work showed average grain sizes smaller than 0.5 μm , which likely implies that the thermal stability of the austenite was higher than the values presented above, especially in QT10 condition.

4.1.5.2 Influence of partitioning time

First, it must be highlighted that the partitioning times employed in the present work were significantly lower than those sometimes employed in the intercritical annealing of medium Mn steels (hours). However, the RA contents, particularly in the QT10 condition, were similar [143–145]. In [217] the authors studied austenite growth during intercritical annealing from as-quenched martensite containing interlath retained austenite. They found that apart from growing from the thin pre-existing films austenite also nucleated at martensite lath boundaries, packet boundaries, and within laths. In [112] authors obtained similar results, and they also concluded that the kinetics of austenite reversion take benefit from the fact that pre-existing austenite led to direct growth of austenite without the need of nucleating. Consequently, the time required to austenite reversion would be lowered and might explain the high austenite fractions obtained in the present work employing significantly lower partitioning times.

Second, in this work it was shown that the partitioning time influenced on the final austenite content (Figure 36). In both steels, RA content increased significantly by increasing the Pt from 300 s to 1000 s. However, a further increase to 3600 s resulted in a reduction of austenite. Austenite reversion kinetics are normally divided into three stages. In the first stage (negligible partitioning local equilibrium, NPLE), austenite fraction increases rapidly controlled by carbon diffusion. In the second stage (partitioning local equilibrium where the growth of austenite is controlled by the slow diffusion of substitutional elements in martensite, PLE-1), the growth of austenite is controlled by the slow diffusion of substitutional elements in martensite. Finally, in the third stage (partitioning local equilibrium where the austenite growth is controlled by the diffusion of substitutional elements in austenite, PLE-2), which is much slower than the previous stages, the austenite growth is controlled by the diffusion of substitutional elements in austenite. Ding *et al.* [112] found that these stages were not affected by the presence of pre-existing austenite. In addition, they observed that the transition from PLE-1 to PLE-2 occurred after 600 s approximately for a Fe-0.2C-8Mn-2Al steel. Wei *et al.* [217], instead, estimated that this transition occurred after almost 2000 s for a Fe-0.1C-3Mn-1.5Si steel. Thus, there is a possibility that this transition occurred not so far from 1000 s in the 6Mn and 6Mn2Ni steels. Therefore, with a partitioning time of 300 s,

austenite reversion kinetics would be in the PLE-1 stage. During this stage the austenite fraction was still growing, but the reverted austenite amount formed so far led to a relatively high amount of RA. By 1000 s of partitioning the growth of austenite was slowed and it is likely that the kinetics were at the end of the PLE-1 stage or the beginning of the PLE-2 stage. Reverted austenite was not far from its maximum and thus outstanding values of RA were obtained in this condition. Finally, at 3600 s of partitioning, the controlling kinetics would already be in the PLE-2 stage and no increase of austenite fraction occurred, leading to the slight decrease of RA measured by XRD.

From a chemical point of view, a large difference in austenite stability was not expected between the 1000 s and 3600 s partitioning time conditions. However, in FE-SEM microstructures (Figure 37d and Figure 37f) a coarsening of austenite laths was observed. This behavior was hypothesized to occur due to the coalescence of austenite grains during growth [218]. As mentioned above, grain size might influence the thermal stability of austenite [125], which can explain the slight decrease in RA measured after 3600 s partitioning time cycles in comparison with 1000 s cycles, where thinner austenite was observed.

4.1.6 Analysis of the influence of Ni on microstructure and austenite stabilization

The addition of Ni in the 6Mn2Ni steel was beneficial for increasing RA content in the final microstructure in all heat treatment conditions. The Ni addition did not seem to affect significantly the austenite formation kinetics (as denoted by the similar contraction observed in the partitioning stage, Figure 33 and Figure 35). However, Ni was effective in stabilizing a higher content of austenite. The latter could be related to an enrichment of austenite not only with Mn, but also with Ni. The behaviour of Ni partitioning was analyzed based on compositional maps and concentration profiles shown in Figure 39. In the QT10 condition, some redistribution of Ni can be appreciated in the compositional map (Figure 39f), although it was not as distinctive as in the Mn map. However, the concentration profile was very similar to that shown by Mn (Figure 39h), with areas enriched in Ni (apparently austenite) and areas depleted in Ni (identified as martensite), in the same positions as in the Mn profile. Thereby, the QT10 condition also seemed favourable for Ni partitioning. In the case of the QT25 condition, the Ni partitioning behaviour was less clear and would require further investigation.

On the other hand, as presented in section “4.1.2 Microstructure characterization”, the TEM-EDS analysis revealed that the carbides contained Mn. Besides, in the 6Mn2Ni steel, the analysis seemed to indicate that Ni was not present in the carbides. The composition of

carbides in Ni containing steels was studied in recent work. Pierce *et al.* [54] observed plate-like and globular carbides in TEM after partitioning at 450 °C for 300 s in a 0.2C-1.5Mn-1.3Si steel containing 1.5% Ni. Atom probe tomography (APT) revealed Mn enrichment of the carbides. They did not observe significant partitioning of Ni between carbide and matrix. Thus, both the morphology and chemical composition of the carbides observed in the present work were in agreement with that observed by Pierce *et al.* Similarly, Clarke *et al.* [219] reported no substantial partitioning of Ni between the matrix and the carbide in 4340 steel during tempering at 450 °C for 2 h. However, Clarke *et al.* showed via APT that significant rejection of Ni from carbides occurred during tempering at 575 °C for 2 h, with Ni enrichment persisting near the carbide/ferrite interface. With the aim of further investigating the possible Ni enrichment in the carbides, a line scan was performed in TEM across two globular carbides in the QT10-Pt1000 condition for 6Mn2Ni steel (Figure 47b). Both carbides contained a high amount of Mn, but no Ni enrichment was evident in the carbides or near the carbide/matrix interfaces.

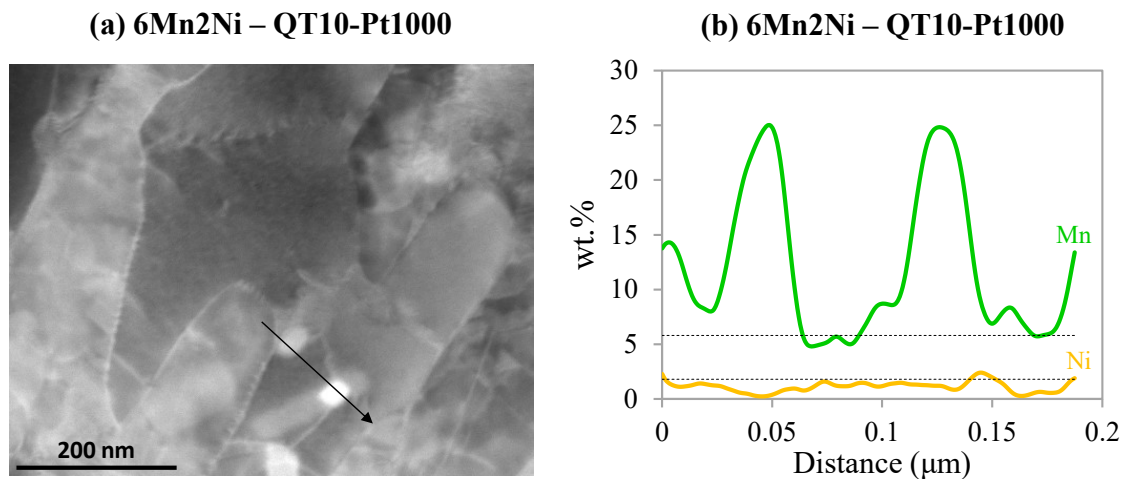


Figure 47. TEM micrograph of the 6Mn2Ni steel after the QT10-Pt1000 condition (a); and line scans of Mn and Ni weight concentration (b), corresponding to the line shown in (a).

4.1.7 Theoretical analysis of austenite stabilization using DICTRA

As shown earlier, the ART occurred in the high partitioning temperature stage and Mn partitioning from martensite into austenite was observed in TEM-EDS scans. The Mn concentration profiles were different depending on the QT condition. Furthermore, a substantial carbide fraction was observed, which contained a significant content of Mn. According to recent studies [220–223], austenite is likely to nucleate at carbide interfaces. Therefore, austenite formation could be the result of the growth of pre-existing austenite along with formation of new austenite at carbide interfaces. With the aim of better

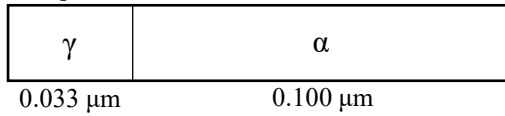
understanding these possible phenomena, DICTRA simulations were performed for the 6Mn2Ni steel considering the partitioning conditions employed in the present work. In the simulations two different set ups were considered. In the first one, the growth of pre-existing austenite in the austenite/martensite microstructures was simulated. In the second one, austenite nucleation at carbide interfaces was simulated. In both set ups, a single cell planar geometry was used [224]. Because of symmetry, only the half thickness was considered in the DICTRA calculation domain. Ferrite was considered instead of martensite, since martensite is not included in the thermodynamic and kinetic database. The results of these simulations were the Mn concentration profile in the considered systems and the growth of austenite for different partitioning times. The growth of austenite can be observed by the displacement of the interface.

In set up (1), 10 and 25 volume percent of austenite (QT10 and QT25 conditions, respectively) were considered in the initial austenite/martensite microstructure. The dimension of the martensite was set to 0.200 μm . It was based on the TEM observations of Krauss and colleagues, indicating that most martensitic lath widths range from approximately 0.150 to 0.200 μm [226,227], which seems consistent with the TEM analysis presented in this work. Corresponding austenite dimensions were obtained using the “constant ferrite width approach” [225]; i.e., the width of the austenite lath corresponded to a percentage of the total width (martensite + austenite) equal to the volume percent of austenite fixed in the QT. Thus, austenite initial lath widths equal to 0.22 or 0.66 μm were fixed. In the case of the QT10 condition, different Pt-s were considered. A schematic illustration of these initial conditions is shown in Figure 48a, and the results for the simulation comparing different QT and Pt conditions are shown in Figure 48b and Figure 48d, and Figure 48c and Figure 48e, respectively.

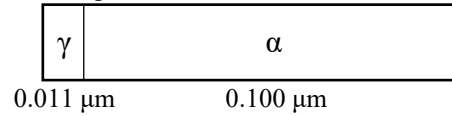
In set up (2), the average carbide size and Mn composition measured from TEM analysis were considered, 0.020 μm and 24.6 wt.%, respectively. The partitioning dimension in martensite was set to 0.200 μm , as in set up (1). The initial composition of α phase was considered from the equilibrium composition for the 6Mn2Ni steel at 640 °C obtained by Thermo-Calc (i.e., 0.003 C wt.% and 1.998 Mn wt.%). In addition, in order to simplify the simulation, the nucleation process was ignored, adding a 0.001 μm length austenite phase, with the same composition as the martensite, between the cementite and martensite phases. The initial conditions for this set up are shown in Figure 49a and the obtained results are shown in Figure 49b.

(a) Initial conditions for set up (1)

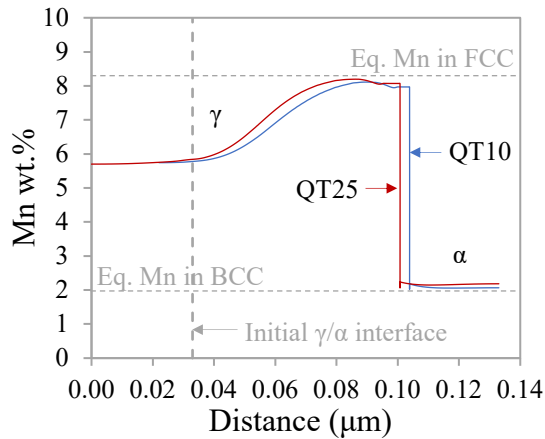
set up for the QT25 condition



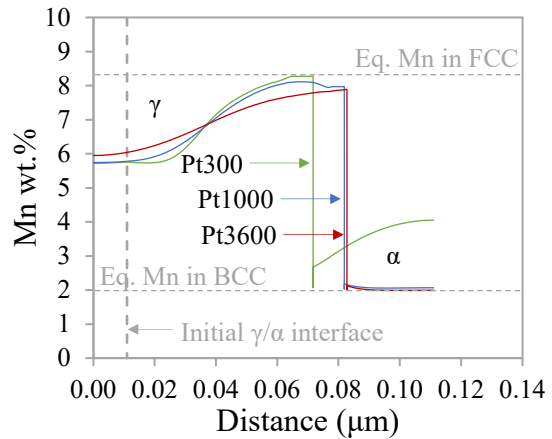
set up for the QT10 condition



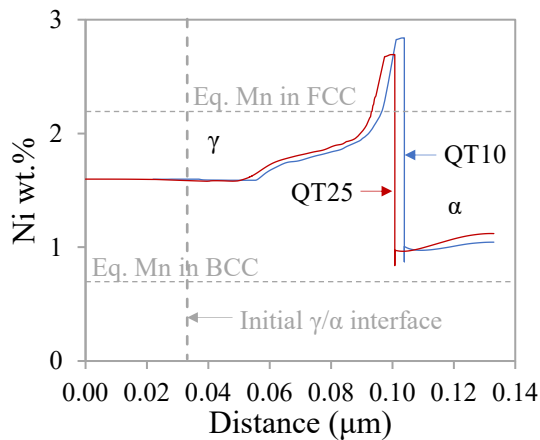
(b) 6Mn2Ni, set up (1), Pt1000 conditions



(c) 6Mn2Ni, set up (1), QT10 conditions



(d) 6Mn2Ni, set up (1), Pt1000 conditions



(e) 6Mn2Ni, set up (1), QT10 conditions

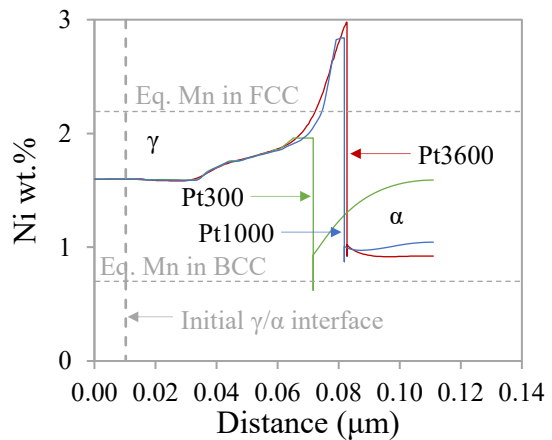


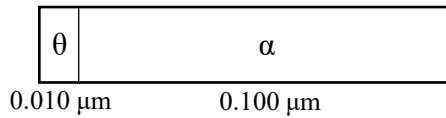
Figure 48. DICTRA simulations for 6Mn2Ni steel at 640 °C: schematic of the initial conditions of the simulations for set up (1) (a); results for set up (1), showing a comparison between the growth of austenite in QT10 and QT25 with Pt1000 and diffusion of Mn (b) and Ni (d) (the initial interface was set in the same position for QT10 and QT25), and showing the comparison between the growth of austenite with Pt300, Pt1000, and Pt3600 in QT10 and diffusion of Mn (c) and Ni (e).

In set up (1), austenite grew into the initial martensite lath and was enriched considerably in Mn, while the martensite was considerably depleted, almost reaching the equilibrium value (Figure 48b). With regard to Ni, it can be seen that, even the austenite was partially enriched, and the martensite was partially depleted, a 1000 s partitioning was not enough time to reach the equilibrium composition. Furthermore, the distribution of the Ni in the austenite lath was

quite heterogeneous (Figure 48d). Regarding the influence of QT, the DICTRA calculations appear to be in good agreement with the dilatometry results, where it was seen that the QT10 condition led to a greater amount of austenite formation (Figure 35). Thus, according to Figure 48b and Figure 48d, after 1000 s at the PT, the austenite lath size grew more in the QT10 condition, obtaining a final length 7.5 times the initial one, whereas for the QT25 condition the size was only 3.0 times the initial. With regards to Mn and Ni diffusion distance, the enriched width was quite similar for both QT conditions. However, the percentage of the lath size enriched in Mn was greater for the QT10 than the QT25 condition, specifically 78% and 60% austenite was enriched in the QT10 and the QT25, respectively. These percentages are somewhat lower regarding Ni diffusion distance, specifically 61% and 50% in the QT10 and the QT25, respectively. These observations were consistent with TEM-EDS line scans (Figure 39g and Figure 39h), and would imply that the quantity of secondary martensite formed in the QT25 condition during final cooling would be higher.

Calculations for different Pt-s, employing QT10, are shown in Figure 48c and Figure 48e. As expected, the growth of the austenite was greater with increased partitioning time, as the interface was moved to longer distances. The growth increment difference with increasing partitioning time from 300 to 1000 s was substantially larger than increasing it from 1000 s to 3600 s, although in these DICTRA simulations the aforementioned coalescence phenomenon was not considered. At Pt300, there was a clear distinction between the lath region enriched in Mn and the non-enriched region, which might lead to some secondary martensite formation. In addition, the martensite lath was not completely Mn depleted. At Pt1000, Mn was more homogeneously distributed across the lath, but there was still a small not enriched length, while at Pt3600 all the length was somewhat enriched, although a compositional difference within the lath was still visible and, thereby, the less enriched part of the lath would potentially transform into secondary martensite. Regarding Ni diffusion, the austenite length without enrichment was the same for the three Pt conditions. However, the Ni distribution within the lath was different. At Pt300, the Ni enrichment/depletion in the austenite and martensite, respectively, was poor and very localized nearby the interface. At Pt1000, the Ni enrichment in the austenite continued being located near the interface, but the maximum peak was over the equilibrium composition. The Ni depletion in the martensite led to a homogeneous distribution, although the content was still over the equilibrium value. Finally, at Pt3600, the behavior was like at Pt1000, obtaining a slightly higher Ni enrichment in the austenite near the interface.

(a) Initial conditions for set up (2)



(b) 6Mn2Ni, set up (2), γ nucleated at θ/α interface

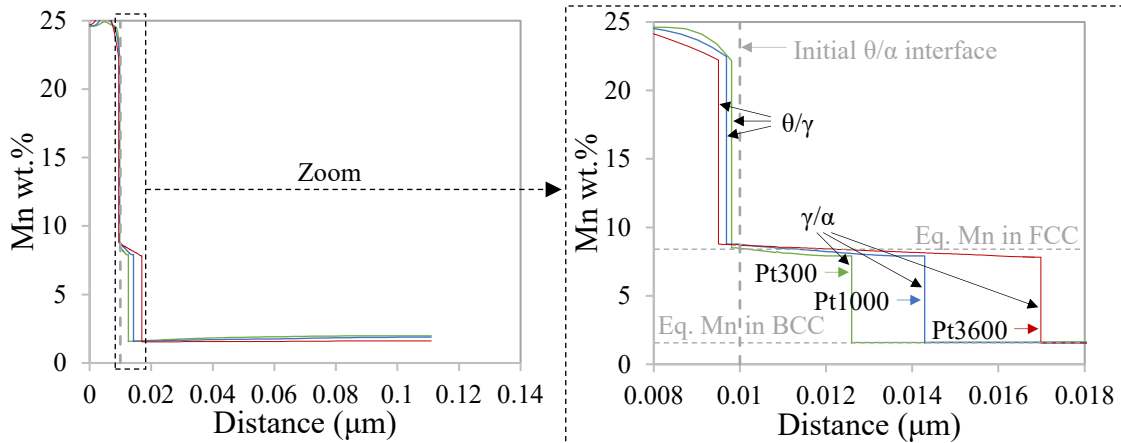


Figure 49. DICTRA simulations for 6Mn2Ni steel at 640 °C: schematic of the initial conditions of the simulations for set up (2) (a), and results for set up (2) configuration, where austenite nucleated at θ/α interface (b).

In set up (2), different austenite sizes and Mn profiles were obtained when comparing with set up (1). First, the Mn content across the austenite lath was almost constant and very close to the equilibrium content (8.4 wt.%). Second, the austenite lath size was significantly smaller than the size obtained in set up (1), specifically, the total size of the lath after 3600 s of partitioning did not reach 0.008 μm , with even lower values after 1000 and 300 s, 0.005 and 0.003 μm , respectively. In addition, according to DICTRA calculations, the austenite grew into the martensite rather than dissolving the cementite. Yan *et al.* [228] also observed that the lath size of austenite was much smaller when it nucleated at the interface between cementite and martensite than when it nucleated at the boundary of the martensite. However, comparing with the set up (1) on this work, they did not have pre-existing austenite in their simulations and, comparing with the set up (2). they found that carbides were totally dissolved after holding for 2000 s at the intercritical temperature. Additionally, Luo *et al.* [229] suggested that the dissolution of cementite was the main reason for the high enrichment of austenite with Mn, and the limited diffusion distance of Mn resulted in a refined austenite.

In general, Mn contents measured experimentally in austenite (Figure 39g-h) were significantly higher than those obtained by DICTRA. Furthermore, in DICTRA simulations, the austenite width enriched in Mn was less than observed by TEM-EDS scans. The regions

not enriched in Mn (or less enriched) would lead to a quite higher extent of secondary martensite transformation than that observed by dilatometry. This means that DICTRA calculations could underestimate Mn diffusion through the austenite. As said before, in the simulations ferrite was considered instead of martensite, since martensite is not included in the thermodynamic and kinetic database. The thermodynamic properties of martensite are very much the same as those of ferrite, however, the kinetic parameters may deviate between the two phases due to larger numbers of lattice defects, particularly dislocations, in martensite. Thus, mobilities of all alloying elements in martensite are increased compared to ferrite [124], which could explain the differences between the simulations and experimental data.

4.1.8 Relationship between microstructure and tensile properties

As presented in “4.1.3 Tensile properties” section, tensile properties strongly decreased by the addition of Mn in the ref cycle. The addition of Ni did not result in an improvement of these properties. Although the retained austenite content measured by XRD increased by the addition of Mn and Ni, in the present case, this increase did not result in better tensile properties. By rising the partitioning temperature to the start of ART temperature, it was shown that tensile strength decreased, and elongation increased in the 2Mn and 4Mn steels, which was mainly related to the tempering of the martensite phase.

From now on, the relationship between microstructure and tensile properties is analyzed for the 6Mn and 6Mn2Ni steels heat treated by high partitioning temperature cycles. First, with the aim of better analyzing the effect of the Q&P cycle conditions and the addition of Ni on the tensile properties, the tensile results are shown as a function of partitioning time in Figure 50. In general, the better tensile properties were obtained with the 6Mn2Ni steel in the QT10 conditions, except for TS, which was higher after the application of QT25-Pt1000 cycle. For the 6Mn2Ni steel, the properties did not deteriorate with the increase of the Pt, whereas in the 6Mn steel YS and TEL decreased for the Pt of 3600 s.

The product of tensile strength and total elongation is a parameter often applied to evaluate and compare steels for the automotive sector. In Figure 51, TS x TEL is represented as a function of RA. Except for QT10-Pt300 condition in the 6Mn steel, it can be said that the product TS x TEL increased with the austenite content. Thus, the presence of a higher content of RA in Ni containing steel and after the QT10 condition, likely contributed to the outstanding TS x TEL values obtained in this case. Moreover, the finer austenite laths for the

QT10 condition likely played an important role in improving the TS x TEL product [230,231]. On the contrary, the greater amount of secondary martensite reduced the ductility for the QT25 condition.

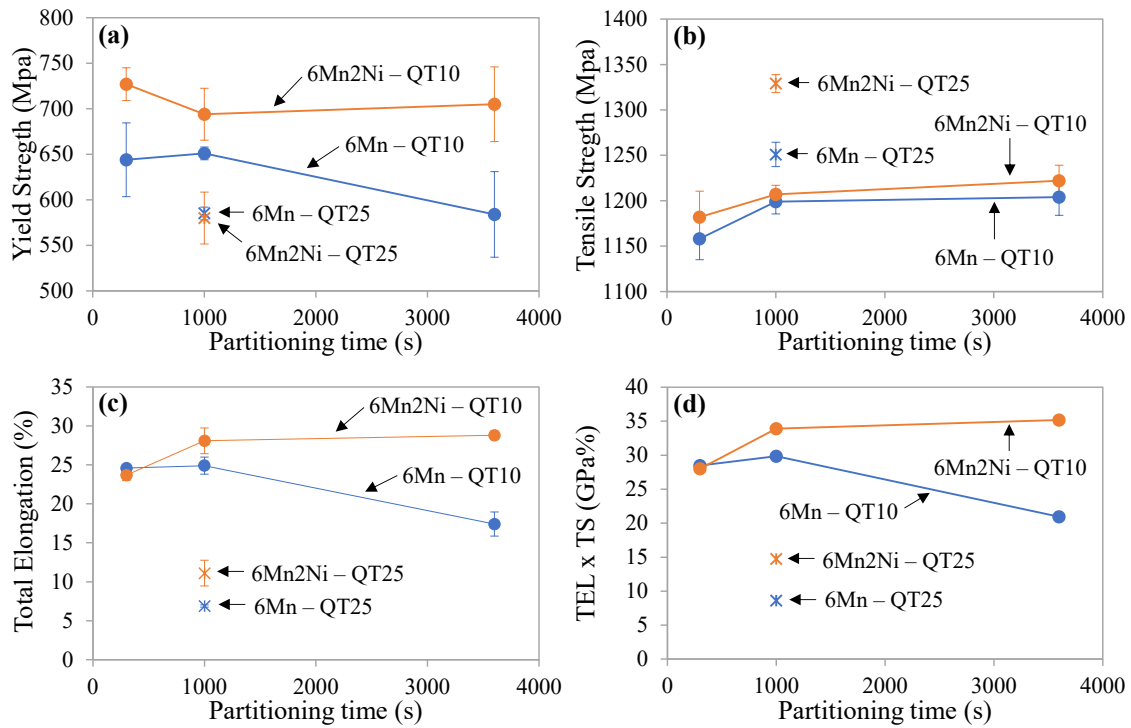


Figure 50. Tensile properties of the Q&P treated samples: yield strength (a); tensile strength (b); total elongation (c); and TEL x TS product (d).

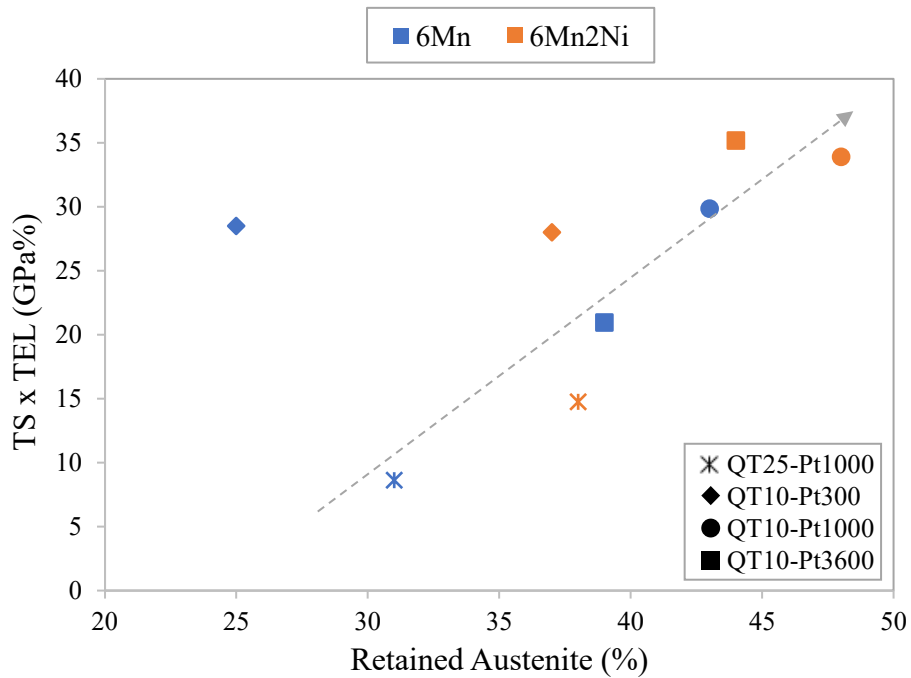


Figure 51. Graphical representation of the relationship between the product of tensile strength and total elongation and RA for each Q&P cycle of the 6Mn and 6Mn2Ni steels.

The presence of secondary martensite can be considered further, as it can be critical for the deterioration of tensile properties [112]. Even though secondary martensite transformation was difficult to detect by dilatometry for some of the conditions, a deeper analysis allows an approximation of the amount of each constituent in the final microstructure. Thus, the volume fraction of the phases existing in the final microstructure after heat treatments was estimated employing RA measurements (XRD) and dilatometry curves (Figure 52). Secondary martensite was obtained by comparing the change in length at the final cooling with the change in length given by the martensite transformation curve on the directly quenched sample, and primary martensite was calculated by balance [37]. From the graph, it can be confirmed that the greatest content of secondary martensite was obtained after the QT25-Pt1000 cycle, particularly in the 6Mn steel. The presence of a hard and brittle secondary martensite in this condition can explain the lower total elongation and higher tensile strength obtained after the QT25-Pt1000 cycle (Figure 50).

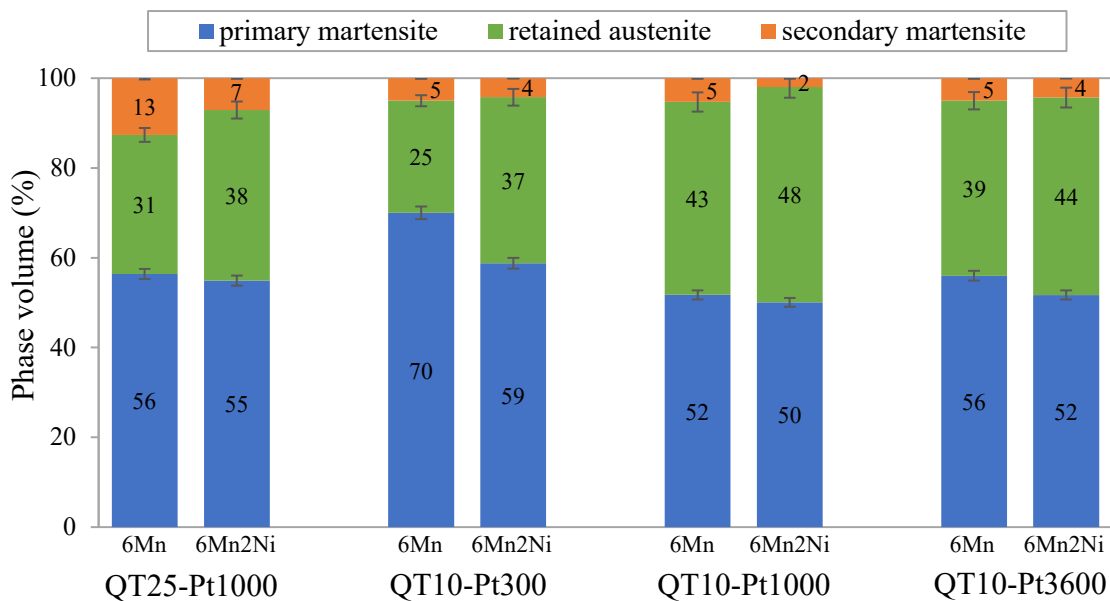


Figure 52. Volume percent of each phase in the 6Mn and 6Mn2Ni steels after the application of Q&P cycles calculated based on dilatometry curves and RA measured by XRD.

On the other hand, it is widely accepted that the transformation of austenite into martensite induced by deformation is also a critical factor that determines tensile properties. From the results obtained in the interrupted tensile tests, the evolution of normalized RA with strain in QT10-Pt1000 cycles for the 6Mn and 6Mn2Ni steels was represented (Figure 53). In both steels, little austenite transformation occurred up to 10% strain, where only about 15% of the austenite had transformed. Afterwards, the behavior was rather different in each steel. In the 6Mn steel the austenite content gradually decreased with strain, whereas in the 6Mn2Ni steel

the entirety of the remaining RA at 20% strain (77% of the initial RA) transformed close to the uniform strain, likely resulting in a high fraction of very hard martensite and thus provoking early fracture and the absence of post-uniform elongation. Although the 6Mn steel showed a more gradual decrease in the austenite fraction, it is likely that the amount of martensite transformed at strains close to the uniform elongation was still high and also provoked the absence of post-uniform elongation.

From the evolution of RA with strain, it can be deduced that adding Ni increased the mechanical stability of retained austenite and retarded the kinetics of the strain-induced martensite transformation. It can be explained by considering the effect of Ni on the strength of martensite. First, according to Hidalgo *et al.* [92] the strength of martensite can affect the mechanical stability of austenite. They concluded that austenite surrounded by a stronger martensitic matrix was mechanically more stable than that surrounded by a weaker martensite. Second, in the present work, Ni decreased the M_s temperature, so the martensite formed during the first cooling to QT should contain more dislocations and, thus, it was likely harder and contributed to the higher mechanical stability of austenite in this steel.

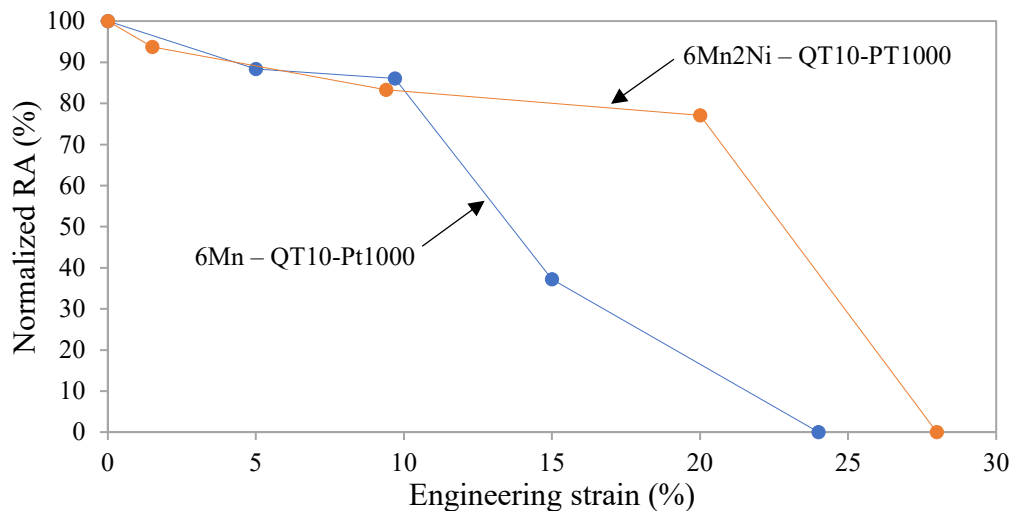


Figure 53. Evolution of normalized RA during tensile tests stopped at different strains for 6Mn and 6Mn2Ni steels after QT10-Pt1000 cycle.

Stress-strain curves in Figure 43 and Figure 44 indicated discontinuous yielding in QT10-Pt1000 and Pt3600 cycles, but not so in the shorter-time Pt300 condition. Raabe *et al.* [231] recently reviewed different mechanisms contributing to the occurrence of discontinuous yielding. They observed that ultra-refining the grain sizes, materials which normally exhibit continuous yielding, such as pure Al, austenitic steels and interstitial-free (IF) steels, yield discontinuously. In the present work, a very fine martensite/austenite microstructure was observed by TEM characterization after the QT10-Pt1000 cycle in the 6Mn and 6Mn2Ni

steels, as well as a large amount of retained austenite, as in medium Mn steels (Figure 39), which might help explain this discontinuous yielding [158,232]. In the case of the Pt300 cycle, a shorter partition time lead to less tempered martensite and, therefore, a higher population of mobile dislocations, resulting in the continuous yielding observed in the stress-strain curves of the QT10-Pt300 condition. In the case of the QT25, the presence of higher secondary martensite amount might explain the continuous yielding in the same way.

4.2 Q&P applied to medium and high C steels

4.2.1 Dilatometry study to select the steels and Q&P cycle to further study

As mentioned in the previous chapter, in a first stage three steel (1.2990, 1.2344 and 300M) were Q&P treated considering two cycles, referred to as PT400 and PT300. The Q&P treatments were applied in a dilatometer and then, samples were characterized in order to obtain their hardness and retained austenite content. The dilatometry curves as well as the hardness and RA values obtained for each Q&P cycle and steel are shown in Figure 54.

The objective of the Q&P cycles was to retain the maximum amount of austenite in the final microstructure, avoiding undesirable phase transformations like secondary martensite transformation. The hardness values obtained in the three steels were somewhat higher in the PT300 condition, while austenite was more satisfactorily retained in the PT400 cycle. In addition, in the PT300 condition of the 1.2990 steel, the dilatation curve in the final cooling deviated from linear contraction (Figure 54a), which denoted secondary martensite transformation. In all cycles a slight volume expansion was observed during the partitioning stage, which may be related to either carbon partitioning or bainite formation [108,209]. Possibly the values of austenite below 20%, established in the QT, were related to this second phenomenon, together with a slight formation of secondary martensite during the final cooling, undetectable by dilatometry (<5%), or with small inaccuracies regarding QT.

Since in Q&P steels hardness is not the only factor that affects wear properties, but retained austenite plays a fundamental role [186], it was decided to proceed to the second stage (application of Q&P treatments by means of laboratory furnace and salt baths) with the 1.2990 and 300M steels and the PT400 condition, in which the hardness obtained were yet relatively high (51-52 HRC) and it was possible to stabilize all the austenite existing at the QT in the case of the 1.2990 steel and a large amount of it in the 300M steel.

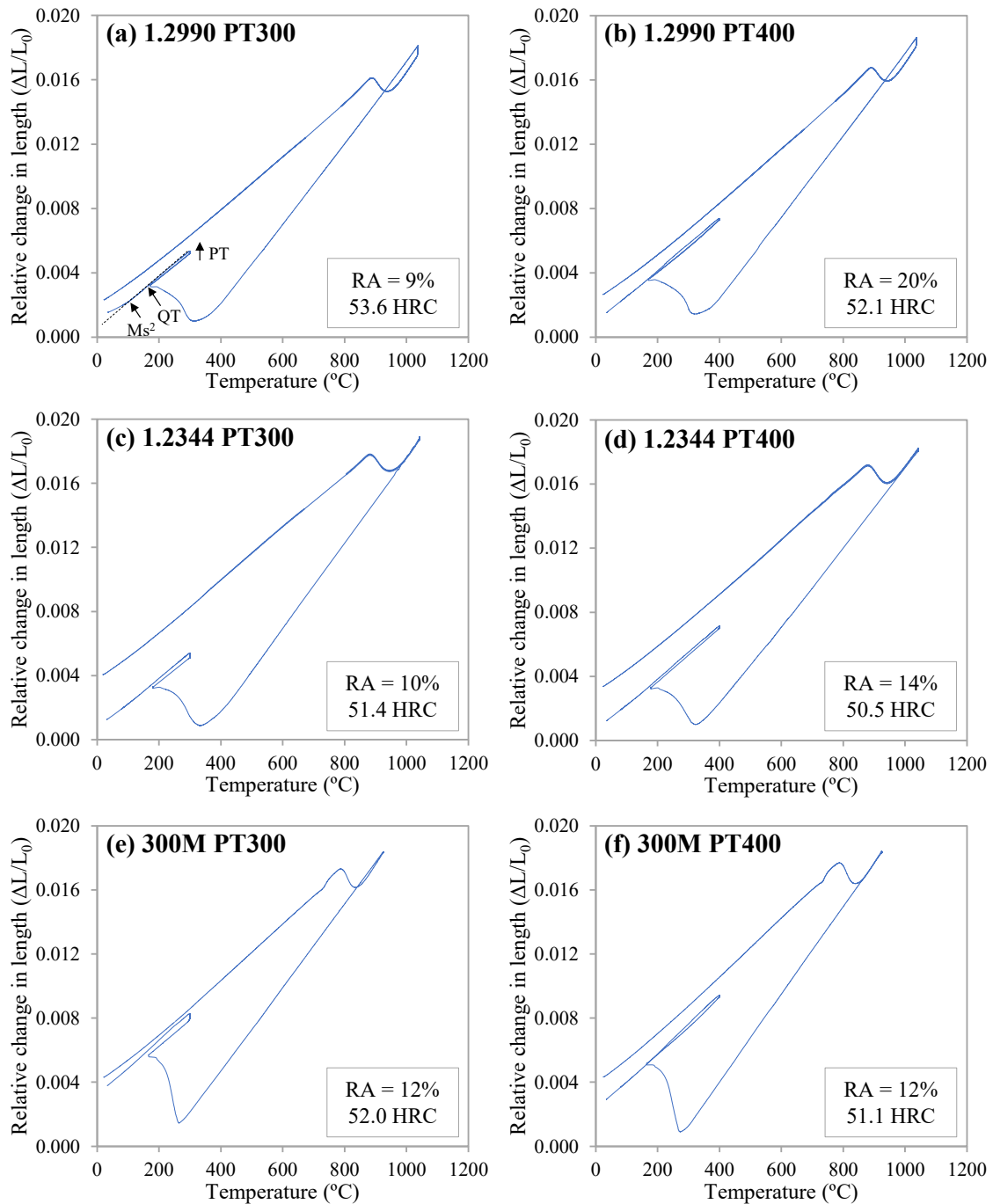


Figure 54. Dilatometry curves, hardness and RA content for the 1.2990 steel after the PT300 (a) PT400 (b) cycles; for the 1.2344 steel after the PT300 (c) and PT400 (d) cycles; and for the 300M steel after the PT300 (e) and PT400 (f) cycles.

4.2.2 Dilatometry curves of the Q&P cycle applied in furnaces and salt baths

The selected PT400 cycle was applied by means of a furnace and salt baths considering samples with disk geometry, as described in section 3, and the selected 1.2990 and 300M steels. No thermal gradients were observed between the inner and surface thermocouples, meaning that microstructural heterogeneities within the treated disks were likely avoided.

Afterward, the monitored thermal cycles were reproduced in the dilatometer to study the expansions and contractions occurred during heat treatments. In the case of 1.2990 steel, the temperature cycle monitored during the application of the Q&P cycle was quite similar to that simulated previously in the dilatometer. Therefore, it was decided not to repeat the dilatometry simulations and analyze the previously obtained curve (Figure 54b). In the case of the 300M steel, the real QT obtained in the preliminary dilatometry was somewhat lower than the selected one and, therefore, a repetition of the thermal cycle simulation was carried out in the dilatometer employing the real cycle parameters achieved in the salt baths.

In Figure 55 the dilatometry curves for the complete cycle of the 1.2990 and 300M steels are shown, whereas in Figure 56 the relative change in length obtained during the partitioning stage is represented as a function of the partitioning time. In both steels an expansion was observed during the partitioning stage, which was likely related with carbon partitioning from the martensite into the austenite [108,209]. This expansion was bigger in the 1.2990 steel, as well as it was the nominal carbon content. It is therefore to be expected that, for the end of the partitioning, more carbon had migrated from martensite into austenite in this steel. On the other hand, dilatometry curves during the final cooling were analyzed to study the possible formation of secondary martensite. In both steels, the curve was linear and volume change was not observed, which means that the formation of secondary martensite was not significant and, therefore, most of the austenite available at the end of the partitioning was retained in the final microstructure.

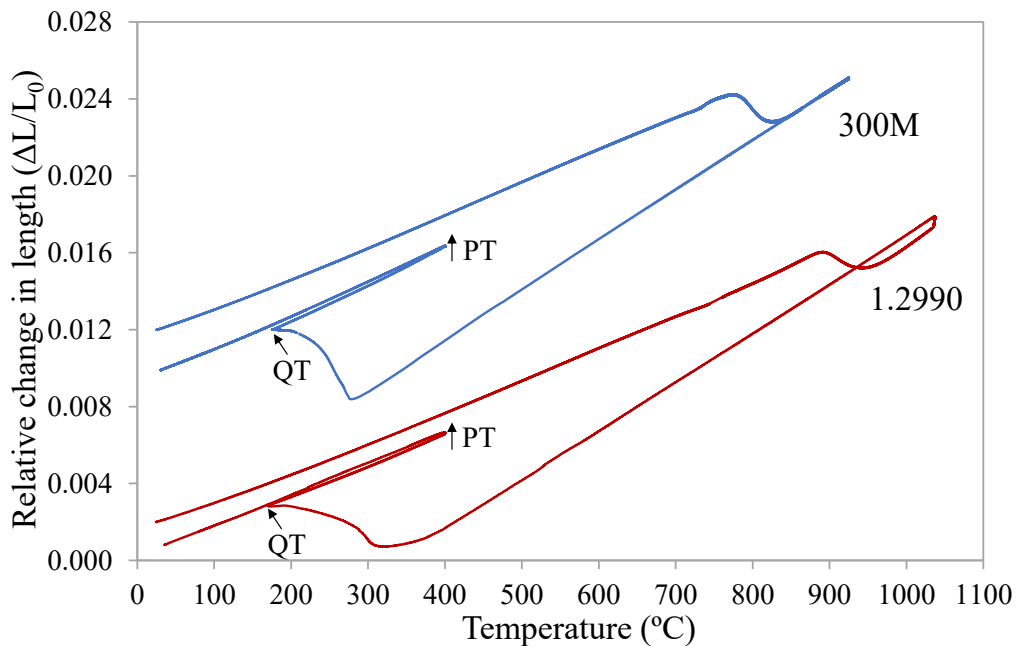


Figure 55. Dilatometry curves of the thermal Q&P cycle applied in the furnaces and salt baths for the 1.2990 and 300M steels.

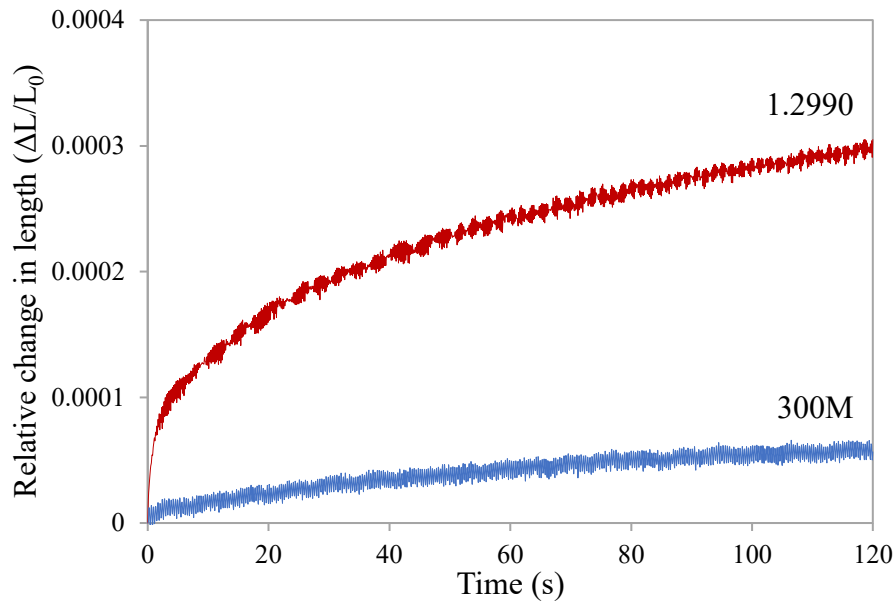


Figure 56. Relative change in length measured during the partitioning stage for the Q&P cycle applied to the 1.2990 and 300M steels.

4.2.3 Microstructure after Q&P treatment

The Q&P treated disks surfaces were characterized in a SEM. Figure 57 shows a SEM micrograph of the 300M steel, where the typical Q&P microstructure can be observed. It is mainly composed by bright areas, which are supposed to be blocky RA and RA laths, and grey areas, supposed to be tempered martensite (M1), with some little and fine carbide precipitation inside [13]. The austenite content measured by X-Ray diffraction after the application of the Q&P treatment in the salt baths was 20%, which means that the Q&P cycle was suitable to stabilize all the austenite existing at QT. This value was higher than that measured in the dilatometry sample (12%). However, as mentioned earlier, the real QT in the dilatometry was lower than the target QT, which means that less austenite was available to be stabilized.

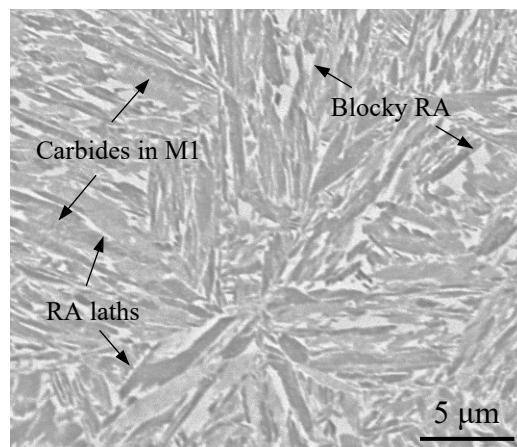


Figure 57. SEM micrograph of the 300M steel after the Q&P treatment.

In the case of 1.2990 steel, the microstructure after Q&P treatment (Figure 58a-b) showed distinctive features. Although tempered martensite and austenite laths can be also found, here the presence of carbides was more notable. Furthermore, carbides showed different size, morphology, and chemical composition. On the one hand, fine carbides with globular morphology (point x2 in Figure 58a) and containing V and Cr were observed and analyzed in Figure 58d. On the other hand, very coarse phases with irregular shape were also observed (points x3 and x4 in Figure 58b), which based on the EDS analysis (Figure 58e-f) were also supposed to be carbides. The coarse phases also contained Cr and V, but the appearance of these elements was notably more intense in these carbides than in the globular ones.

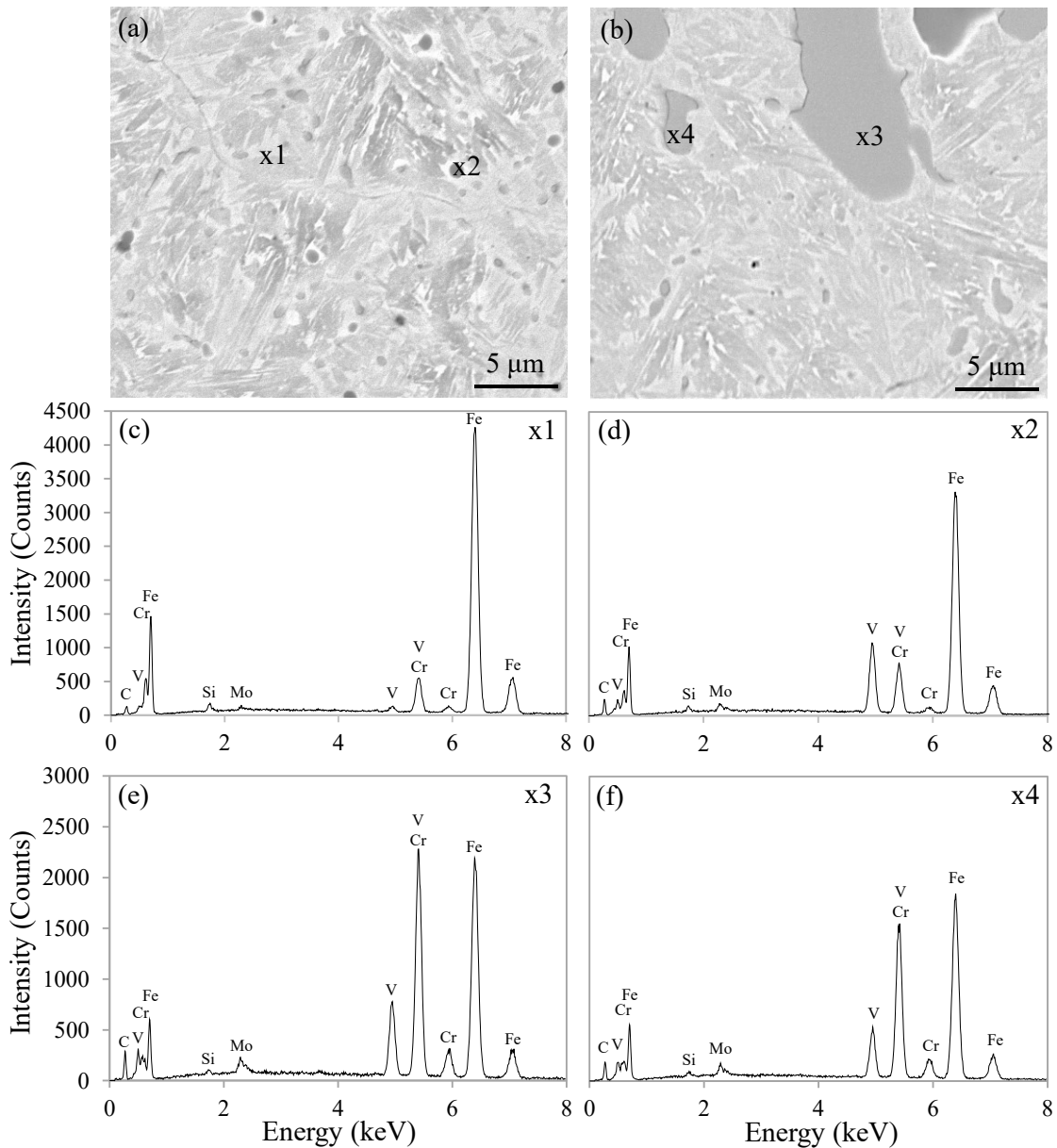


Figure 58. SEM micrographs (a) and (b), and EDS analysis of the matrix (c), globular carbide (d), and coarse carbides (e) and (f) of the 1.2990 steel after the Q&P treatment.

The retained austenite measured by XRD in 1.2990 steel after the Q&P treatment was $22 \pm 1.1\%$, which means that the thermal cycle was appropriate to stabilize all the austenite. The austenite content at the QT temperature was supposed to be 20%. The slight increase in the measured final RA could be due to two possible reasons: (1) The austenite content at the QT might have been higher. The cooling rate somewhat affect the martensite transformation curve [233], and the employed in the dilatometer and the achieved in the salt baths was not exactly the same. (2) In steels with high C content treated by Q&P, a displacement of the interface towards martensite has been reported, thus achieving values of retained austenite higher than those of the QT [23].

Thermo-Calc calculations were performed to better understand the phases present in both steels. The results are shown in Figure 59.

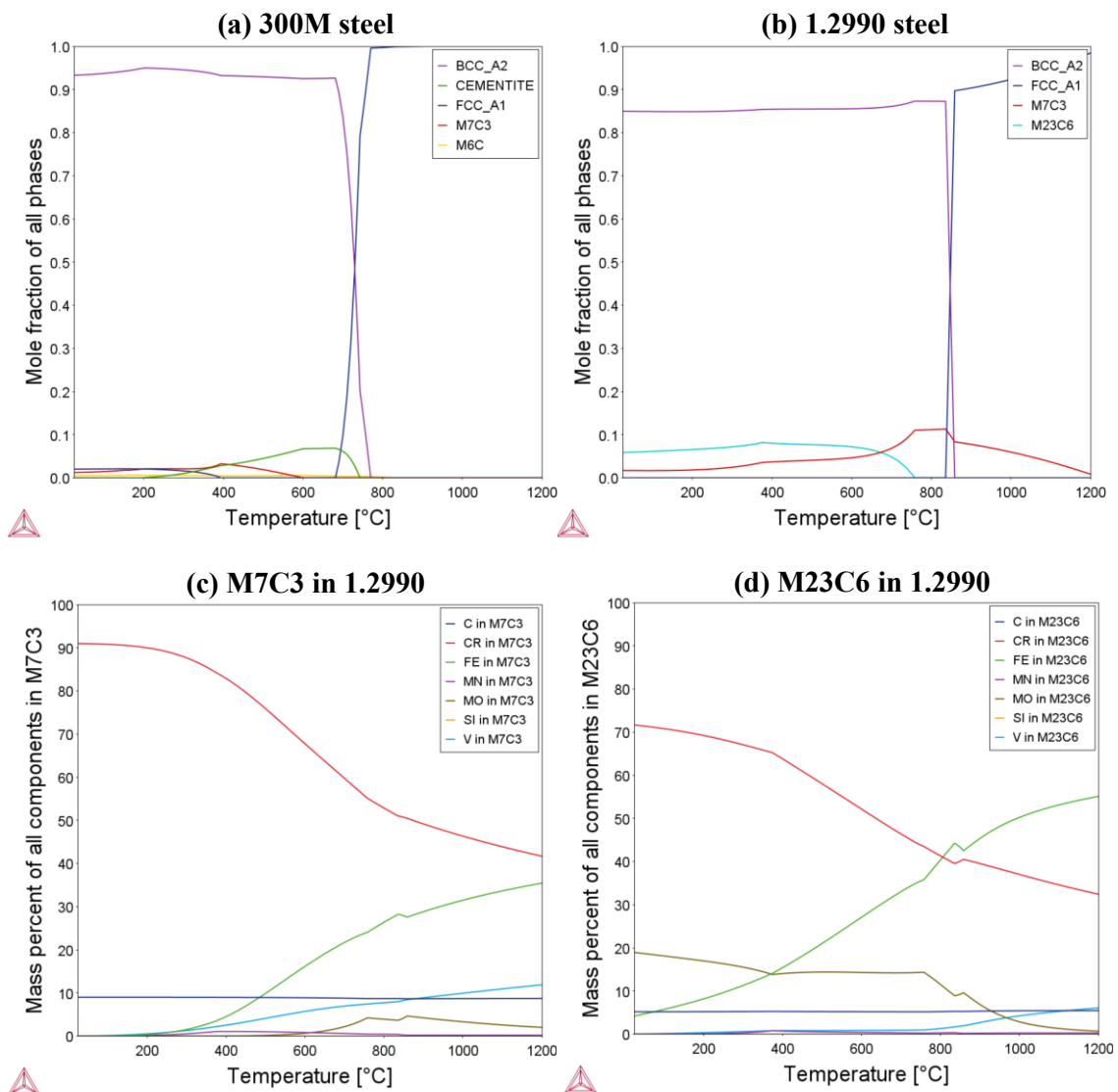


Figure 59. Phase fraction as a function of temperature of (a) 1.2990 and (b) 300M steels, and composition of 1.2990 steel (c) M7C3 and (d) M23C6 phases obtained by Thermo-Calc calculations.

As it can be seen in Figure 59a, the main precipitated phase in 300M steel was cementite, therefore, the carbides observed inside the tempered martensite in Figure 57 were likely this phase. In the 1.2990 steel up to around 10% of M7C3 and M23C6 phases can be expected in the microstructure (Figure 59b) according to Thermo-Calc, being M = Fe, Cr, V or Mo. The composition of each phase as a function of temperature is shown in Figure 59c-d. Both phases contain a high content of Cr, but only M7C3 phase contain a relatively high V content. Besides, M23C6 phase shows a considerable Mo content, which was barely detected by EDS analysis. Therefore, it can be said that the phases analyzed in Figure 58a-b (points x2, x3 and x4) might be M7C3, although a further research would be needed to better determine the type of carbide. According to Thermo-Calc, the dissolution temperature of M7C3 phase (~1220 °C) is significantly higher than the austenization temperature employed in the Q&P treatments (1037 °C), which means that likely these carbides were eutectic carbides present in the initial microstructure or precipitated during austenization and were not significantly affected by the heat treatment [234,235]. In cast irons with elevated contents of Cr, eutectic M7C3 carbides tend to transform into M23C6 carbides. However, when Cr content was below 10-25 wt.% M7C3 carbides do not appear to undergo any structural changes [235]. On the other hand, the austenization and subsequent quenching might led to a formation of secondary spheroid M7C3 particles (point x2 in Figure 58a) within the primary austenitic phase [236].

4.2.4 Hardness

Hardness measurements were performed in the Q&T and Q&P treated samples in both steels. The average values obtained after five indentations are shown in Figure 60 and the values obtained after each indentation are shown in Appendix D. The Q&P treatment resulted in a considerably lower hardness, especially in the 1.2990 steel. The 1.2990 steel contains relatively high contents of carbides forming elements like Cr (7.9%), V (1.5 wt.%) and Mo (1 wt.%). Thus, in the tempering, apart from eliminating the stresses generated during the martensitic transformation and soften the structure restoring the toughness of the material, secondary precipitation hardening can be achieved [10,98,99]. As it was seen in Figure 58, Cr, Mo and V containing carbides were visible in the microstructure of the Q&P treated 1.2990 steel. However, the total amount of carbides was likely lower than in the Q&T steel. Furthermore, the Q&P steel contained carbon-enriched retained austenite which likely lowered the overall hardness value [237].

In 300M steel, Q&P treatment resulted in lower hardness as well, although the decrease was less significant in comparison with the 1.2990 steel. Unlike in the 1.2990 steel, precipitation hardening does not occur in this steel, only little cementite precipitation inside the tempered martensite was observed (Figure 57). Thus, tempering treatment is only employed to eliminate residual stresses produced during the quenching and restore the toughness [8,238]. As in the 1.2990 steel, the presence of carbon-enriched austenite left less carbon available for the tempered martensite, thus decreasing the overall hardness of the Q&P steel.

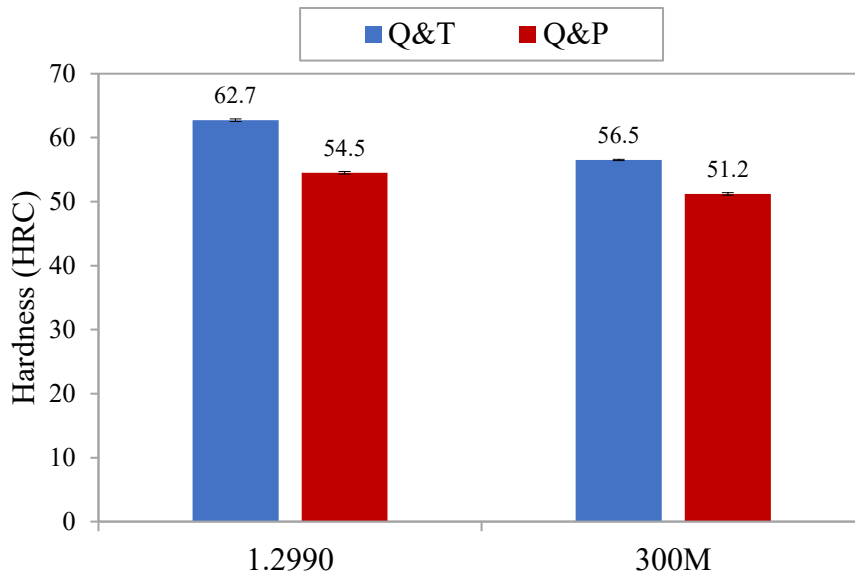


Figure 60. Hardness values measured in the 1.2990 and 300M steels after the application of Q&T or Q&P heat treatments.

4.2.5 Wear behavior

Wear rates were calculated from the pin-on-disk tests for both steels and both Q&P and Q&T treatments. Figure 61 shows comparisons between the values obtained with each steel and heat treatment. When comparing the influence of the heat treatment (Figure 61a-b), the difference in the wear rate was insignificant both in the 1.2990 and the 300M steels. However, it was shown before that the difference in hardness between the Q&P and Q&T treated steels was considerably high, especially in the 1.2990 steel. Thus, Q&P treated samples showed a significantly lower hardness but the same wear resistance than Q&T samples. This behavior demonstrates that hardness was not the only parameter affecting the wear resistance and that the retained austenite may play a key role [186].

On the other hand, when comparing the Q&P treated steels at the same linear velocity conditions (Figure 61c), as expected, the 1.2990 steel clearly showed a better wear resistance. Both steels had a similar RA content, hence, in this case, the hardness and the

composition of the steel were decisive when determining the wear response of each steel. The 1.2990 steel has a higher C content and hardness and additionally, it is very likely that the carbides observed in the microstructure of this steel were M7C3 and M23C6, as predicted by Thermo-Calc Figure 59a), which resulted beneficial for wear resistance [239].

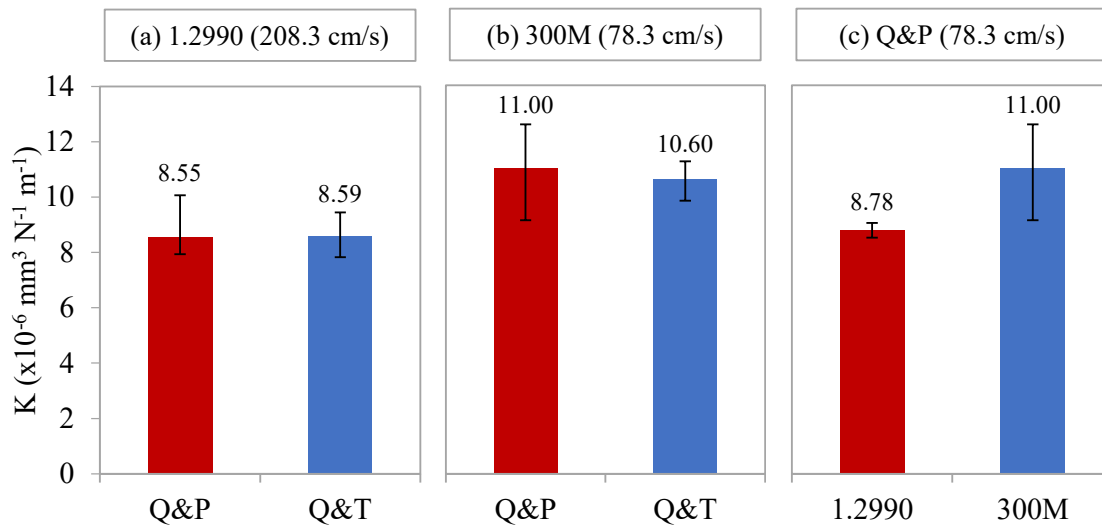


Figure 61. Wear rate (mm³/N.m) calculated from the PoD tests. Comparison between Q&P and Q&T treated 1.2990 (a) and 300M (b) steels; and comparison between Q&P treated 1.2990 and 300M steels tested with the same linear velocity (c).

It is difficult to compare the results obtained in this work with those reported in the literature. On the one hand, there is very little literature studying the wear resistance applied to Q&P steels, and even less studying the wear behavior through unidirectional sliding tests. On the other hand, the results obtained from PoD tests strongly depend on the testing conditions, therefore, the obtained wear rate results are specific for the employed conditions. However, most of the results reported in the literature show an improvement in the wear resistance by the application of Q&P heat treatments. Wasiak *et al.* [187], for example, observed that, after being Q&P treated, the 35CrSiMn5-5-4 steel exhibited twice better wear resistance under the dry sliding friction than after being Q&T treated. Wang *et al.* [240] found that by applying a Q&P treatment to a ductile cast iron wear resistance was improved and that the employed partitioning time affected the obtained wear rate, first increasing with the increase of the partitioning time and then decreasing with a further time increasing. In [192], the authors concluded that compared with Q&T treatment, wear resistance of a high C steel was improved by applying a series of Q&PT (quenching & partitioning-tempering) treatments, which was associated with the formation of film-like and blocky austenite during partitioning stage, but an increase in the partitioning temperature from 250 °C to 400 °C was found to be disadvantageous due to an increase in cementite carbide precipitation.

In the present work, wear resistance was not improved by the substitution of the Q&T by Q&P treatment. However, only one Q&P condition was studied, and it is possible that the optimization of the Q&P cycle parameters could result in an improvement. Nevertheless, the results showed similar wear rates after both treatments with significantly lower hardness after Q&P, which might be advantageous for other properties typically required in this type of steels, such as toughness.

4.2.6 Retained austenite stability

The austenite transformation into martensite it is thought to be responsible for enhancing the wear behavior in Q&P steels [186]. Therefore, austenite stability was studied measuring the RA content in the wear track of the PoD tested disk in order to examine the transformation given during the tests. In Figure 62, the RA contents measured by XRD in the wear track are shown for both steels and different linear velocity conditions employed (the latter only for 1.2990 steel) and these values are compared with RA contents measured before in the surface of the disks.

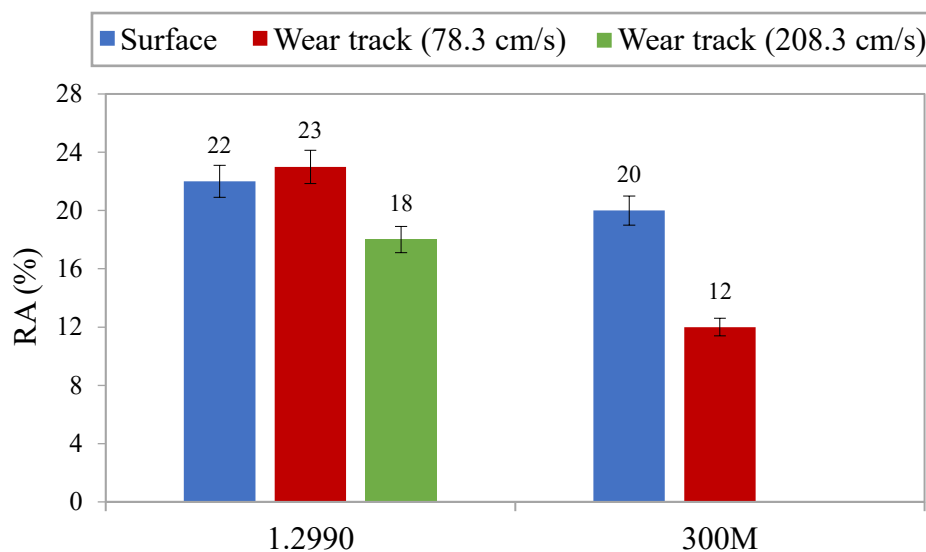


Figure 62. RA measured in the surface and wear tracks formed during PoD characterization of the 1.2990 and 300M steels.

In the 1.2990 steel and the lower linear velocity condition, austenite transformation was not observed, therefore, material did not benefit from transformation hardening. The higher linear velocity condition resulted in the transformation of less than 20% of the initial RA content. Therefore, it can be said that the mechanical stability of austenite against transformation in this steel, and, in the test conditions employed in this work, was too high. It is known that the C content is the main factor affecting RA stability [129,241,242]. In the 1.2990 steel the C

content was high (0.92%), and it is likely that, in spite of the high fraction of carbides present in the microstructure, the C content in the RA after the Q&P treatment was too high to allow martensite transformation. Possibly, with a higher load or linear velocity the improvement through the application of Q&P with respect to Q&T would be clearer, although further study is required.

In the 300M steel, due to material limitations, only the test with lower linear velocity was performed. In this case, a higher amount of the austenite transformed during the tests, specifically 40% of the initial RA. This steel contains a lower C content (0.41%), which might result in a lower C content in RA after Q&P treatment and consequently in a higher transformation into austenite. However, this transformation seemed to be still low to be beneficial for wear resistance. Same as in the 1.2990 steel, it is likely that employing a higher load or lineal velocity conditions the results would show a clearer improvement after the application of the Q&P treatment.

Apart from the C content, it is known that other factors can affect the stability of austenite. It has been reported that film RA can be mechanically more stable in martensitic microstructures than blocky RA, suggesting that this stability may be due to surrounding martensite laths suppressing the transformation of film RA [129,243,244]. In the SEM image of the 300M steel (Figure 57) some areas with blocky austenite were observed, whereas in the 1.2990 steel (Figure 58) austenite laths predominated. Furthermore, in the case of the 1.2990 steel, a stronger matrix could lead to an increase in the mechanical stability of RA and sometimes this makes the transformation of RA to martensite not to occur even under the actions of stress or strain [191]. In this work, only a preliminary study of the wear behavior of Q&P steels was performed, and future tests and characterization would be needed to better elucidate the factors determining the stability of austenite in both steels and the influence of the microstructure in wear behavior.

4.2.7 Toughness

As described before, 1.2990 steel showed important hardness differences between the Q&P and Q&T treated samples whereas the wear rates were similar. The lower hardness values measured in Q&P samples were expected to result in a better toughness [191–193], which would be a clear advantage, as those applications requiring wear resistance generally also require toughness. Thus, Charpy V-notch impact test were performed in both the Q&P and Q&T samples employing subsize standard specimens.

The toughness values obtained are summarized in Table 18 and the photographs of each specimen are shown in Appendix E. As it can be seen, the obtained values were too low to make an accurate comparison between the Q&P and Q&T treated steels. Particularly, the toughness of the Q&P steel was quite lower than expected based on literature results. Lai *et al.* [192,193] reported impact toughness values in the range of 17-22 J/cm² for a steel containing 1.2 wt.% C and RA and hardness values similar to those obtained in this work, 18% RA and 600 HV (~54,5 HRC), respectively. In addition, Liu *et al.* [191] measured an impact toughness of 19.4 J/cm² in a 0.95 wt.% C steel with 20% of RA and an approximate hardness of 600 HV, although the steel had a bainitic matrix rather than martensitic.

An explanation for the low toughness can be related with the machining operation of the Charpy specimens. Due to the complexity of machining the dimensions of the V-notch, it was done by wire cutting. There is no way to prove that through this cutting operation the austenite around the notch did not transform into martensite, which could be a possible reason for obtaining such low values in the impact tests, although further investigations would be required.

Table 18. Toughness values (J/cm²) obtained in Charpy V-notch impact test of the Q&P and Q&T treated 1.2990 steel.

Toughness (J/cm²)	Test 1	Test 2	Test 3	Average
Q&T	5.7	4.9	3.8	4.8
Q&P	4.5	3.7	3.7	4.0

Chapter 5

Conclusions

Chapter 5

Conclusions

In this thesis four medium Mn and Ni steel, and three medium and high C steels treated by different Q&P treatments were investigated. In this chapter the conclusions drawn from all the obtained results are presented.

5.1 Q&P applied to medium Mn and Ni steels

Conventional Q&P cycles and high partitioning temperature Q&P cycles in which the austenite reverse transformation phenomenon occurred, were investigated in four medium Mn steel with different Mn and Ni amounts. The following conclusions were drawn:

1. The addition of 2 wt.% Mn was not sufficient to stabilize high amounts of austenite. In the ref cycle competing reactions occurred during partitioning, likely decomposition of austenite into bainite. In high partitioning temperature cycles secondary martensite transformation occurred during final cooling, resulting in a final microstructure with less than 5 wt.% of RA.
2. In the steels with four or more wt.% of Mn, both austenite content and tensile properties were improved with the application of the high partitioning temperature cycles, independently of the QT and Pt conditions of the cycle.
3. In the 6Mn and 6Mn2Ni steels, treated with high PT cycles, large amounts of retained austenite were obtained in the final microstructure, which were comparable to those obtained after intercritical annealing of medium Mn steels. The addition of Ni further increased the content of retained austenite. The presence of pre-existing austenite (due to interrupted quenching) before the partitioning stage considerably reduced the partitioning time needed for austenite stabilization in comparison with some conventional intercritical annealing heat treatments of medium Mn steel.
4. In the 6Mn and 6Mn2Ni steels, a lower quenching temperature resulted in faster austenite formation kinetics in the high temperature partitioning stage, less formation of secondary martensite in the final cooling, and a final microstructure with a higher content of RA, which showed a lath-type microstructure with finer constituents.

5. After the high partitioning temperature cycles, Mn and Ni enriched austenite laths were observed in the 6Mn2Ni steel. The enrichment of Mn was different depending on the QT condition. In the lower QT condition, the partitioning of substitutional elements was more homogeneous due to the thinner austenite laths. In the higher QT condition, Mn was concentrated near the martensite/austenite interface.
6. Carbides with globular and acicular/plate-like morphologies and containing Mn were formed in the high partitioning temperature cycles, which left less C and Mn available for partitioning.
7. In the 6Mn2Ni steel, outstanding values of the product of tensile strength and total elongation, over 30 Gpa%, were obtained after the high temperature cycles employing the lower QT condition, It was related to the high amount of RA, thin microstructure with Mn and Ni enriched lath type austenite, strain induced transformation of retained austenite and absence of secondary martensite.
8. The mechanical stability of the austenite formed after high partitioning temperature cycles and the lower QT condition was enhanced by the addition of Ni. Thus, in the 6Mn2Ni steel, austenite transformation was very modest up to 20% strain. However, very abrupt austenite transformation occurred above this strain level, resulting in high fraction of strain-induced martensite. In the 6Mn steel, austenite transformed more gradually, but still resulting in an important quantity of strain-induced martensite at high strain levels. Therefore, the tensile curves of both steels showed very small or inexistent post-uniform elongation.

5.2 Q&P applied to medium and high C steels

The feasibility of employing the Q&P treatment to develop steels with improved wear resistance compared to steels treated with Q&T steels was studied. The study was initiated with three high and medium C commercial steels, deciding to continue the research with only two of them: one high C steel (the 1.2990 steel) and one medium C steel (the 300M steel). The conclusions drawn were the following:

1. Q&P treatments were effective in stabilizing the austenite content existing at QT, giving rise to a final microstructure containing tempered martensite and around 20% RA in both steels. Precipitation of Cr, V and Mo carbides was also observed in Q&P treated 1.2990 samples.
2. After the application of the Q&P treatment the wear rate values obtained in both steels were comparable to those obtained after the conventional Q&T treatment. However, the

hardness values of the Q&P treated samples were considerably lower than those of the Q&T treated samples, which means that hardness was not the only parameter influencing the wear resistance.

3. It was shown that the austenite content transformed into martensite during the wear tests was low in 1.2990 steel, which revealed a high mechanical stability of austenite phase in the applied wear test conditions. Therefore, austenite transformation phenomenon did not contribute to the attained wear resistance. In 300M steel, a higher content of austenite transformed during the test, although this transformation seemed to be not enough to provide an improved wear resistance in comparison with Q&T samples. The role of austenite in wear resistance would need to be further studied.
4. The higher mechanical stability of austenite in 1.2990 steel could be related with its higher C content, although other factors, such as austenite morphology and matrix strength, could also affect.

Chapter 6

Future work

Chapter 6

Future work

6.1 Q&P applied to medium Mn and Ni steels

In this work, the improvement of tensile properties of medium Mn steels by increasing the partitioning temperature into the intercritical range with respect to conventional Q&P treatment was demonstrated. The addition of Ni was also shown beneficial for such improvement. After carrying out a relatively in-depth microstructural study and analysis of both the influence of composition (Mn and Ni contents) and Q&P cycle conditions on tensile properties, the future work to be done would be the following:

- Optimization of process conditions (QT, PT and Pt) for the 6Mn and 6Mn2Ni steels to obtain a further improvement of tensile properties.
- In this work, only uniaxial tensile tests were carried out. The complexity of the microstructure of Q&P steels makes a more extensive study of the formability of the most promising steels mandatory. Thus, tests such as bending and hole expansion should be accomplished. In addition, a cold formability test to measure post-forming properties and measuring springback behavior (characteristic in cold stamping operations of AHSS steels) should be also performed.
- The industrial implementation of the high partitioning temperature treated Q&P steels should be evaluated, from the steelmaking stage to the application of the thermal treatment. Its viability should be evaluated both from cost and environmental impact point of view.
- The microstructure of the Q&P steels would change during welding operations. The intensive localized heat associated with some welding processes, for example, causes a significant change in the local microstructure, and hence affect properties. Therefore, weldability of the selected steels should be assessed.

6.2 Q&P applied to medium and high C steels

In this thesis, only a preliminary study of the benefits of Q&P treatment for wear resistance requiring applications was performed. There is still a lot of background work to be done in the study of Q&P steels in relation to wear applications and toughness.

- The influence of different microstructures on the wear performance of the steels should be studied. Particularly, the effect that the amount of each phase as retained austenite, secondary martensite or bainite has in wear resistance should be tested.
- Besides austenite amount, how its carbon content and morphology influence on its stability against wear tests must be study. For that purpose, microstructures with different RA contents, carbon in RA and morphology should be created and studied through wear tests employing different conditions.
- Once the effect of the microstructure is understood, an optimization of Q&P cycle parameters is necessary to achieve the desired microstructures.
- In this work only pin-on-disk test were carried out. The behavior of Q&P steels in other types of wear tests, such as abrasive test, could be studied.
- Regarding toughness, in this work an improvement after the application of the Q&P treatment was not verified, despite the lower hardness. There is uncertainty as to whether the retained austenite transformed during notch machining, therefore Charpy tests could be performed on unnotched specimens to check whether an improvement in toughness is indeed seen after application of the Q&P cycle.
- Since thermal gradients between the surface and the center of the disks were not observed during the heat treatments, the feasibility of applying the heat treatment into thicker specimens without obtaining heterogeneities in the microstructure could be studied.
- A study about energetical and economic advantages of replacing the conventional Q&T treatment by the Q&P treatment should be performed.
- In this part of the work, high partitioning temperature Q&P cycles were not applied, as further study is still required to better understand the influence of low partitioning temperature treatments on wear and toughness behavior. The application of high partitioning temperatures could also be interesting as part of future work.

Chapter 7

Bibliography

Chapter 7

Bibliography

- [1] T. Nanda, V. Singh, V. Singh, A. Chakraborty, S. Sharma, Third generation of advanced high-strength steels: Processing routes and properties, *Proceedings of the Institution of Mechanical Engineers, Part L: Journal of Materials: Design and Applications*. 233 (2019) 209–238. doi:10.1177/1464420716664198.
- [2] WorldAutoSteel, *Advanced High-Strength Steels Guidelines Version 7.0*, WorldAutoSteel. (2021). <https://www.worldautosteel.org/steel-basics/automotive-advanced-high-strength-steel-ahss-definitions/>.
- [3] E. De Moor, P.J. Gibbs, J.G. Speer, D.K. Matlock, J.G. Schroth, Strategies for third-generation advanced high-strength steel development, *Iron and Steel Technology*. 7 (2010) 133–144.
- [4] J. Zhao, Z. Jiang, Thermomechanical processing of advanced high strength steels, *Progress in Materials Science*. 94 (2018) 174–242. doi:10.1016/j.pmatsci.2018.01.006.
- [5] E. De Moor, *Advanced High-Strength Sheet Steels for Automotive Applications BT - High-Performance Ferrous Alloys*, in: R. Rana (Ed.), Springer International Publishing, Cham, 2021: pp. 113–151. doi:10.1007/978-3-030-53825-5_4.
- [6] J. Speer, D.K. Matlock, B.C. De Cooman, J.G. Schroth, Carbon partitioning into austenite after martensite transformation, *Acta Materialia*. 51 (2003) 2611–2622. doi:10.1016/S1359-6454(03)00059-4.
- [7] A.M. Streicher, J.G. Speer, D.K. Matlock, B.C. De Cooman, Quenching and partitioning response of a Si-added TRIP sheet steel, *International Conference on Advanced High Strength Sheet Steels for Automotive Applications - Proceedings*. (2004) 51–62.
- [8] N. Fonstein, *Advanced High Strength Sheet Steels*, 2015. doi:10.1007/978-3-319-19165-2.
- [9] S.C. Hong, Mechanical properties of high-Si plate steel produced by the quenching and partitioning process, *Metals and Materials International*. 13 (2007) 439–445. doi:10.3365/mmi.2007.12.439.
- [10] S. Zhou, K. Zhang, N. Chen, J. Gu, Y. Rong, Investigation on High Strength Hot-rolled Plates by Quenching-partitioning-tempering Process Suitable for Engineering, *ISIJ International*. 51 (2011) 1688–1695. doi:10.2355/isijinternational.51.1688.
- [11] M.C. Somani, L.P. Karjalainen, D.A. Porter, D.K. Misra, Evaluation of the behaviour and properties of a high-Si steel processed using direct quenching and partitioning, *Materials Science Forum*. 706–709 (2012) 2824–2829. doi:10.4028/www.scientific.net/MSF.706-709.2824.
- [12] J.G. Speer, F.C. Rizzo Assunção, D.K. Matlock, D. V. Edmonds, The “quenching and partitioning” process: Background and recent progress, *Materials Research*. 8 (2005) 417–423. doi:10.1590/S1516-14392005000400010.
- [13] D. V. Edmonds, K. He, F.C. Rizzo, B.C. De Cooman, D.K. Matlock, J.G. Speer, Quenching and partitioning martensite—A novel steel heat treatment, *Materials Science and Engineering: A*. 438–440 (2006) 25–34. doi:10.1016/J.MSEA.2006.02.133.
- [14] S.G. Sarikaya M, Thomas G, Steeds JW, Barnard SJ, Solute element partitioning and austenite stabilization in steels, *Proceedings of an International Conference on Solid to Solid Phase Transformations*. (1982) 1421–1425.

- [15] Y. Toji, G. Miyamoto, D. Raabe, Carbon partitioning during quenching and partitioning heat treatment accompanied by carbide precipitation, *Acta Materialia*. 86 (2015) 137–147. doi:10.1016/J.ACTAMAT.2014.11.049.
- [16] H.S. Yang, D.W. Suh, H.K.D.H. Bhadeshia, More complete theory for the calculation of the martensite-start temperature in steels, *ISIJ International*. 52 (2012) 164–166. doi:10.2355/isijinternational.52.164.
- [17] J.G. Speer, E. De Moor, A.J. Clarke, Critical assessment 7: Quenching and partitioning, *Materials Science and Technology (United Kingdom)*. 31 (2015) 3–9. doi:10.1179/1743284714Y.0000000628.
- [18] H.K.D.H. Bhadeshia, Carbon in cubic and tetragonal ferrite, *Philosophical Magazine*. 93 (2013) 3714–3725. doi:10.1080/14786435.2013.775518.
- [19] J.H. Jang, H.K.D.H. Bhadeshia, D.W. Suh, Solubility of carbon in tetragonal ferrite in equilibrium with austenite, *Scripta Materialia*. 68 (2013) 195–198. doi:10.1016/j.scriptamat.2012.10.017.
- [20] J.G. Speer, R.E. Hackenberg, B.C. DeCooman, D.K. Matlock, Influence of interface migration during annealing of martensite/austenite mixtures, *Philosophical Magazine Letters*. 87 (2007) 379–382. doi:10.1080/09500830701194173.
- [21] G.A. Thomas, J.G. Speer, Interface migration during partitioning of Q&P Steel, *Materials Science and Technology (United Kingdom)*. 30 (2014) 998–1007. doi:10.1179/1743284714Y.0000000546.
- [22] X. Zhanga, G. Shenb, C. Lic, J. Gud, Analysis of interface migration and isothermal martensite formation for quenching and partitioning process in a low-carbon steel by phase-field modelling, *Modelling and Simulation in Materials Science and Engineering*. 27 (2019) 075011. doi:https://doi.org/10.1088/1361-651X/ab3608.
- [23] N. Zhong, X. Wang, Y. Rong, L. Wang, Interface migration between martensite and austenite during quenching and partitioning (Q&P) process, *Journal of Materials Science and Technology*. 22 (2006) 751–754.
- [24] H.C. Lee, G. Krauss, Intralath carbide transitions in martensitic medium- carbon steels tempered between 200 and 300C, in: *Fundamentals of Aging and Tempering in Bainitic and Martensitic Steel Products*, 1992: pp. 39–43.
- [25] G. Krauss, Tempering and structural change in ferrous martensitic structures, in: *International Conference on Phase Transformations in Ferrous Alloys*, 1984: pp. 101–123.
- [26] D.C.B. Streicher AM, Speer JG, Matlock DK, Quenching and partitioning response of a Si-added TRIP sheet steel, in: *Proceedings of the International Conference on Advanced High-Strength Sheet Steels for Automotive Applications*, 2004: pp. 51–62.
- [27] G. Speer, J.; Streicher, A.; Matlock, D.; Rizzo, F.; Krauss, Quenching and partitioning: a fundamentally new process to create high strength TRIP sheet microstructures, in: *Austenite Formation and Decomposition*, 2003: pp. 505–522.
- [28] L. Barbé, K. Conlon, B.C. De Cooman, Characterization of the metastable austenite in low-alloy FeCMnSi TRIP-aided steel by neutron diffraction, *Zeitschrift Fuer Metallkunde/Materials Research and Advanced Techniques*. 93 (2002) 1217–1225. doi:10.3139/146.021217.
- [29] M. Hillert, J. Ågren, On the definitions of paraequilibrium and orthoequilibrium, *Scripta Materialia*. 50 (2004) 697–699. doi:10.1016/J.SCRIPTAMAT.2003.11.020.
- [30] J.G. Speer, D.K. Matlock, B.C. DeCooman, J.G. Schroth, Comments on “On the definitions of paraequilibrium and orthoequilibrium” by M. Hillert and J. Ågren, *Scripta Materialia*, 50, 697–9 (2004), *Scripta Materialia*. 52 (2005) 83–85. doi:10.1016/J.SCRIPTAMAT.2004.08.029.
- [31] M. Hillert, J. Ågren, Reply to comments on “On the definition of paraequilibrium and orthoequilibrium,” *Scripta Materialia*. 52 (2005) 87–88. doi:10.1016/J.SCRIPTAMAT.2004.08.026.

- [32] A.S. Nishikawa, M.J. Santofimia, J. Sietsma, H. Goldenstein, Influence of bainite reaction on the kinetics of carbon redistribution during the Quenching and Partitioning process, *Acta Materialia*. 142 (2018) 142–151. doi:10.1016/j.actamat.2017.09.048.
- [33] H. Kawata, K. Hayashi, N. Sugiura, N. Yoshinaga, M. Takahashi, Effect of martensite in initial structure on bainite transformation, *Materials Science Forum*. 638–642 (2010) 3307–3312. doi:10.4028/www.scientific.net/MSF.638-642.3307.
- [34] K. Seto, H. Matsuda, Application of nanoengineering to research and development and production of high strength steel sheets, *Materials Science and Technology (United Kingdom)*. 29 (2013) 1158–1165. doi:10.1179/1743284713Y.0000000226.
- [35] J. Mahieu, J. Maki, B.C. De Cooman, S. Claessens, Phase Transformation and Mechanical Properties of Si-Free CMnAl Transformation-Induced Plasticity-Aided Steel, *Metallurgical and Materials Transactions A*. 33A (2002) 2573–2580.
- [36] J. Sun, H. Yu, S. Wang, Y. Fan, Study of microstructural evolution, microstructure-mechanical properties correlation and collaborative deformation-transformation behavior of quenching and partitioning (Q&P) steel, *Materials Science and Engineering: A*. 596 (2014) 89–97. doi:10.1016/J.MSEA.2013.12.054.
- [37] M. Arribas, T. Gutiérrez, E. Del Molino, A. Arlazarov, I. De Diego-Calderón, D. Martin, D. De Caro, S. Ayenampudi, M.J. Santofimia, Austenite Reverse Transformation in a Q&P Route of Mn and Ni Added Steels, *Metals*. 10 (2020) 862. doi:10.3390/met10070862.
- [38] J. Hidalgo, C. Celada-Casero, M.J. Santofimia, Fracture mechanisms and microstructure in a medium Mn quenching and partitioning steel exhibiting macrosegregation, *Materials Science and Engineering: A*. 754 (2019) 766–777. doi:10.1016/J.MSEA.2019.03.055.
- [39] S. Ayenampudi, C. Celada-Casero, J. Sietsma, M.J. Santofimia, Microstructure evolution during high-temperature partitioning of a medium-Mn Quenching and Partitioning steel, *Materialia*. (2019). doi:10.1016/j.mtla.2019.100492.
- [40] F. HajyAkbar, J. Sietsma, G. Miyamoto, T. Furuhashi, M.J. Santofimia, Interaction of carbon partitioning, carbide precipitation and bainite formation during the Q&P process in a low C steel, *Acta Materialia*. 104 (2016) 72–83. doi:10.1016/J.ACTAMAT.2015.11.032.
- [41] D.V. Edmonds, K. He, M.K. Miller, F.C. Rizzo, A. Clarke, D.K. Matlock, J.G. Speer, Microstructural Features of “Quenching and Partitioning”: A New Martensitic Steel Heat Treatment, *Materials Science Forum*. 539–543 (2007) 4819–4825. doi:10.4028/www.scientific.net/msf.539-543.4819.
- [42] F. HajyAkbar, M.J. Santofimia, J. Sietsma, Optimizing mechanical properties of a 0.3C-1.5Si-3.5Mn Quenched and partitioned steel, *Advanced Materials Research*. 829 (2014) 100–104. doi:10.4028/www.scientific.net/AMR.829.100.
- [43] M.J. Santofimia, L. Zhao, J. Sietsma, Overview of mechanisms involved during the quenching and partitioning process in steels, *Metallurgical and Materials Transactions A: Physical Metallurgy and Materials Science*. 42 (2011) 3620–3626. doi:10.1007/s11661-011-0706-z.
- [44] H.K.D.H. Bhadeshia, S.R. Honeycombe, The Effects of Alloying Elements on Iron-Carbon Alloys, *Steels*. (2006) 71–93. doi:10.1016/B978-075068084-4/50006-6.
- [45] D. De Knijf, E.P. Da Silva, C. Föjer, R. Petrov, Study of heat treatment parameters and kinetics of quenching and partitioning cycles, *Materials Science and Technology (United Kingdom)*. 31 (2015) 817–828. doi:10.1179/1743284714Y.0000000710.
- [46] A. Arlazarov, O. Bouaziz, J.P. Masse, F. Kegel, Characterization and modeling of mechanical behavior of quenching and partitioning steels, *Materials Science and Engineering A*. 620 (2014) 293–300. doi:10.1016/j.msea.2014.10.034.
- [47] I. De Diego-Calderón, D. De Knijf, J.M. Molina-Aldareguia, I. Sabirov, C. Föjer, R. Petrov, Effect of Q&P parameters on microstructure development and mechanical behaviour of Q&P steels, *Revista de Metalurgia*. 51 (2015). doi:10.3989/revmetalm.035.
- [48] M.J. Santofimia, T. Nguyen-Minh, L. Zhao, R. Petrov, I. Sabirov, J. Sietsma, New low

- carbon Q&P steels containing film-like intercritical ferrite, *Materials Science and Engineering: A*. 527 (2010) 6429–6439. doi:10.1016/J.MSEA.2010.06.083.
- [49] E. De Moor, J.G. Speer, D.K. Matlock, J.H. Kwak, S.B. Lee, Effect of carbon and manganese on the quenching and partitioning response of CMnSi steels, *ISIJ International*. 51 (2011) 137–144. doi:10.2355/isijinternational.51.137.
- [50] K. Ren, Y. Kang, S. Zhu, Effect of partitioning time on the microstructure and mechanical properties of Q&P steels, *Materials Science Forum*. 749 (2013) 303–307. doi:10.4028/www.scientific.net/MSF.749.303.
- [51] I. De Diego-Calderón, M.J. Santofimia, J.M. Molina-Aldareguia, M.A. Monclús, I. Sabirov, Deformation behavior of a high strength multiphase steel at macro- and micro-scales, *Materials Science and Engineering: A*. 611 (2014) 201–211. doi:10.1016/J.MSEA.2014.05.068.
- [52] S. Ayenampudi, Z. Arechabaleta, M. Arribas, Microstructural Impact of Si and Ni During High Temperature Quenching and Partitioning Process in Medium-Mn Steels, *Metallurgical and Materials Transactions A*. 52 (2021) 5–11. doi:10.1007/s11661-021-06144-5.
- [53] K. Kim, S.J. Lee, Effect of Ni addition on the mechanical behavior of quenching and partitioning (Q&P) steel, *Materials Science and Engineering A*. 698 (2017) 183–190. doi:10.1016/j.msea.2017.05.030.
- [54] D.T. Pierce, D.R. Coughlin, K.D. Clarke, E. De Moor, J. Poplawsky, D.L. Williamson, B. Mazumder, J.G. Speer, A. Hood, A.J. Clarke, Microstructural evolution during quenching and partitioning of 0.2C-1.5Mn-1.3Si steels with Cr or Ni additions, *Acta Materialia*. 151 (2018) 454–469. doi:10.1016/j.actamat.2018.03.007.
- [55] E.J. Seo, L. Cho, B.C. De Cooman, Application of Quenching and Partitioning Processing to Medium Mn Steel, *Metallurgical and Materials Transactions A: Physical Metallurgy and Materials Science*. 46 (2015) 27–31. doi:10.1007/s11661-014-2657-7.
- [56] E.J. Seo, L. Cho, B.C. De Cooman, Application of Quenching and Partitioning (Q&P) Processing to Press Hardening Steel, *Metallurgical and Materials Transactions A*. 45A (2014) 4022–4037. doi:10.1007/s11661-014-2316-z.
- [57] X. Tan, Y. Xu, X. Yang, D. Wu, Microstructure–properties relationship in a one-step quenched and partitioned steel, *Materials Science and Engineering: A*. 589 (2014) 101–111. doi:10.1016/J.MSEA.2013.09.063.
- [58] H. Jirková, L. Kučerová, B. Mašek, The Effect of Chromium on Microstructure Development During Q-P Process, *Materials Today: Proceedings*. 2 (2015) S627–S630. doi:10.1016/J.MATPR.2015.07.362.
- [59] F.C. Rizzo, A.R. Martins, J.G. Speer, D.K. Matlock, A. Clarke, B.C. De Cooman, Quenching and Partitioning of Ni-Added High Strength Steels, *Materials Science Forum*. 539–543 (2007) 4476–4481. doi:10.4028/www.scientific.net/msf.539-543.4476.
- [60] G.T. Zhang, N.Q. Zhu, B.W. Sun, Z.Z. Zhao, Z.W. Zheng, D. Tang, L. Li, Effect of v addition on microstructure and mechanical properties in c–mn–si steels after quenching and partitioning processes, *Metals*. 11 (2021). doi:10.3390/met11081306.
- [61] X.D. Tan, X.L. Yang, Y.B. Xu, Z.P. Hu, F. Peng, H. Zhang, Y.M. Yu, D. Wu, Effect of ferrite status on mechanical properties of hot-rolled directly quenched and partitioned steel, *Materials Science Forum*. 816 (2015) 736–742. doi:10.4028/www.scientific.net/MSF.816.736.
- [62] J. Tobata, K.L. Ngo-Huynh, N. Nakada, T. Tsuchiyama, S. Takaki, Role of silicon in quenching and partitioning treatment of lowcarbon martensitic stainless steel, *ISIJ International*. 52 (2012) 1377–1382. doi:10.2355/isijinternational.52.1377.
- [63] G. Krauss, *Steels - Processing, Structure, and Performance*, 2nd ed., ASM International, 2012.
- [64] J.N.T.M. S. Morito, Dislocation Density within Lath Martensite in Fe–C and Fe–Ni Alloys, *ISIJ International*. 43 (2003) 1475–1477.

- [65] M. Cheng, H.W. Song, X. Li, S.H. Zhang, M. Cheng, T. Lin, Effects of quenching and partitioning process on mechanical properties of a hot-stamping steel, *Materials Science Forum*. 788 (2014) 340–345. doi:10.4028/www.scientific.net/MSF.788.340.
- [66] J.G. Speer, E. De Moor, K.O. Findley, D.K. Matlock, B.C. De Cooman, D. V Edmonds, Analysis of Microstructure Evolution in Quenching and Partitioning Automotive Sheet Steel, *Metallurgical and Materials Transactions A*. 42 (2011) 3591–3601. doi:10.1007/s11661-011-0869-7.
- [67] W.S. Owen, The Effect of Silicon on the Kinetics of Tempering, *Transactions of the ASM*. 46 (1954) 812–829.
- [68] S.S. Nayak, R. Anumolu, R.D.K. Misra, K.H. Kim, D.L. Lee, Microstructure–hardness relationship in quenched and partitioned medium-carbon and high-carbon steels containing silicon, *Materials Science and Engineering: A*. 498 (2008) 442–456. doi:10.1016/J.MSEA.2008.08.028.
- [69] T. Sourmail, F.G. Caballero, F. Moudian, D. De Castro, M. Benito, High hardness and retained austenite stability in Si-bearing hypereutectoid steel through new heat treatment design principles, *Materials & Design*. 142 (2018) 279–287. doi:10.1016/J.MATDES.2018.01.035.
- [70] C. Garcia-Mateo, F.G. Caballero, T. Sourmail, J. Cornide, V. Smanio, R. Elvira, Composition design of nanocrystalline bainitic steels by diffusionless solid reaction, *Metals and Materials International*. 20 (2014) 405–415. doi:10.1007/s12540-014-3002-9.
- [71] T. Sourmail, F.G. Caballero, C. Garcia-Mateo, V. Smanio, C. Ziegler, M. Kuntz, R. Elvira, A. Leiro, E. Vuorinen, T. Teeri, Evaluation of potential of high Si high C steel nanostructured bainite for wear and fatigue applications, *Materials Science and Technology (United Kingdom)*. 29 (2013) 1166–1173. doi:10.1179/1743284713Y.0000000242.
- [72] T. Sourmail, V. Smanio, Low temperature kinetics of bainite formation in high carbon steels, *Acta Materialia*. 61 (2013) 2639–2648. doi:10.1016/J.ACTAMAT.2013.01.044.
- [73] V. Ollilainen, W. Kasprzak, L. Holappa, The effect of silicon, vanadium and nitrogen on the microstructure and hardness of air cooled medium carbon low alloy steels, *Journal of Materials Processing Technology*. 134 (2003) 405–412. doi:10.1016/S0924-0136(02)01131-7.
- [74] W. Zhanshan, Z. Li, W. Lv, S. Zhenyao, The influence of the substitution of Si by Al on the properties of hot rolled C-MN-Si TRIP steel, *Materials Science Forum*. 896 MSF (2017) 198–201. doi:10.4028/www.scientific.net/MSF.896.198.
- [75] J. Mahieu, B.C. De Cooman, S. Claessens, Galvanizability of high-strength steels for automotive applications, *Metallurgical and Materials Transactions A: Physical Metallurgy and Materials Science*. 32 (2001) 2905–2908. doi:10.1007/s11661-001-1042-5.
- [76] and K.E.Y.W. D. Vanderschueren, M. De Meyer, B. C. De Cooman, The Influence of the Substitution of Si by Al on the Properties of Cold Rolled C-Mn-Si TRIP Steel, *ISIJ International*. 39 (1999) 813–822. doi:10.4028/www.scientific.net/MSF.896.198.
- [77] E. Girault, A. Mertens, P. Jacques, Y. Houbaert, B. Verlinden, J. Van Humbeeck, Comparison of the effects of silicon and aluminium on the tensile behaviour of multiphase TRIP-assisted steels, *Scripta Materialia*. 44 (2001) 885–892. doi:10.1016/S1359-6462(00)00697-7.
- [78] M.C. Somani, D.A. Porter, L.P. Karjalainen, P.P. Suikkanen, D.K. Misra, Innovation and processing of novel tough ductile ultra-high strength steels through TMR-DQP processing route, *Materials Science Forum*. 783–786 (2014) 1009–1014. doi:10.4028/www.scientific.net/msf.783-786.1009.
- [79] H.L. Yi, P. Chen, Z.Y. Hou, N. Hong, H.L. Cai, Y.B. Xu, D. Wu, G.D. Wang, A novel design: Partitioning achieved by quenching and tempering (Q–T & P) in an aluminium-added low-density steel, *Scripta Materialia*. 68 (2013) 370–374. doi:10.1016/J.SCRIPTAMAT.2012.10.018.
- [80] J. De Moor, E.; Speer, J. G.; Matlock, D. K.; Föjler, C.; Penning, Effect of Si, Al and Mo

- Alloying on Tensile Properties Obtained by Quenching and Partitioning, in: *Materials Science and Technology*, 2009: pp. 1554–1563.
- [81] C. Krishna Ande, M.H. Sluiter, First-Principles Calculations on Stabilization of Iron Carbides (Fe₃C, Fe₅C₂, and η-Fe₂C) in Steels by Common Alloying Elements, *Metallurgical and Materials Transactions A*. 43 (2012) 4436–4444. doi:10.1007/s11661-012-1229-y.
- [82] P.J. Jacques, E. Girault, A. Mertens, B. Verlinden, J. Van Humbeeck, F. Delannay, The developments of cold-rolled TRIP-assisted multiphase steels. Al-alloyed TRIP-assisted multiphase steels, *ISIJ International*. 41 (2001) 1068–1074. doi:10.2355/isijinternational.41.1068.
- [83] L. Samek, E. De Moor, J. Penning, B.C. De Cooman, Influence of Alloying Elements on the Kinetics of Strain-Induced Martensitic Nucleation in Low-Alloy, Multiphase High-Strength Steels, *Metallurgical and Materials Transactions A*. 37A (2006) 109–124.
- [84] S. Kim, C. Gil Lee, I. Choi, S. Lee, Effects of Heat Treatment and Alloying Elements on the Microstructures and Mechanical Properties of 0.15 Wt Pct C Transformation-Induced Plasticity-Aided Cold-Rolled Steel Sheets, *Metallurgical and Materials Transactions A*. 32A (2001) 505–514. doi:https://doi.org/10.1007/s11661-001-0067-0.
- [85] E. De Moor, J.G. Speer, D.K. Matlock, J.H. Kwak, S.B. Lee, Quenching and partitioning of CMnSi steels containing elevated manganese levels, *Steel Research International*. 83 (2012) 322–327. doi:10.1002/srin.201100318.
- [86] E. De Moor, J.G. Speer, Bainitic and quenching and partitioning steels, Elsevier Ltd, 2017. doi:10.1016/B978-0-08-100638-2.00010-9.
- [87] J. Wang, P.J. Van Der Wolk, S. Van Der Zwaag, On the influence of alloying elements on the bainite reaction in low alloy steels during continuous cooling, *Journal of Materials Science*. 35 (2000) 4393–4404.
- [88] S.J. Lee, D.K. Matlock, C.J. Van Tyne, An empirical model for carbon diffusion in austenite incorporating alloying element effects, *ISIJ International*. 51 (2011) 1903–1911. doi:10.2355/isijinternational.51.1903.
- [89] J.G.S. E. De Moor, C. Föjler, A.J. Clarke, J. Penning, Quench & partitioning response of a Mo-alloyed CMnSi steel, in: *Conf. New Dev. Metall. Appl. High Strength Steels, Minerals, Metals, & Materials*, 2008: pp. 721–729.
- [90] G. Kirchner, T. Nishizawa, B. Uhrenius, The distribution of chromium between ferrite and austenite and the thermodynamics of the α/γ equilibrium in the Fe-Cr and Fe-Mn Systems, *Metallurgical Transactions*. 4 (1973) 167–174. doi:10.1007/BF02649616.
- [91] A.K. Patra, C.N. Athreya, S. Mandal, K.C. Hari Kumar, V. Subramanya Sarma, High strength-high ductility medium Mn steel obtained through CALPHAD based alloy design and thermomechanical processing, *Materials Science and Engineering: A*. 810 (2021) 140756. doi:10.1016/J.MSEA.2021.140756.
- [92] J. Hidalgo, R.M. Huizenga, K.O. Findley, M.J. Santofimia, Interplay between metastable phases controls strength and ductility in steels, *Materials Science and Engineering: A*. 745 (2019) 185–194. doi:10.1016/J.MSEA.2018.12.096.
- [93] S. Mishra, R.P. Dalai, Effect of quenching and partitioning treatment on low carbon medium manganese alloyed steels-A short review, *Materials Today: Proceedings*. 43 (2021) 593–596. doi:10.1016/J.MATPR.2020.12.107.
- [94] P. Xu, C. Li, W. Li, M. Zhu, K. Zhang, Effect of microstructure on hydrogen embrittlement susceptibility in quenching-partitioning-tempering steel, *Materials Science and Engineering: A*. 831 (2022) 142046. doi:10.1016/J.MSEA.2021.142046.
- [95] P. hu Chen, Y. bo Li, R. qing Li, R. peng Jiang, S. sheng Zeng, X. qian Li, Microstructure, mechanical properties, and wear resistance of VCp-reinforced Fe-matrix composites treated by Q&P process, *International Journal of Minerals, Metallurgy and Materials*. 25 (2018) 1060–1069. doi:10.1007/s12613-018-1657-9.
- [96] Y. Xu, X. Tan, X. Yang, Z. Hu, F. Peng, D. Wu, G. Wang, Microstructure evolution and

- mechanical properties of a hot-rolled directly quenched and partitioned steel containing proeutectoid ferrite, *Materials Science and Engineering: A*. 607 (2014) 460–475. doi:10.1016/J.MSEA.2014.04.030.
- [97] N. Zhong, Y. Wang, K. Zhang, Y.H. Rong, Microstructural evolution of a Nb-microalloyed advanced high strength steel treated by quenching-partitioning-tempering process, *Steel Research International*. 82 (2011) 1332–1337. doi:10.1002/srin.201100125.
- [98] N. Zhong, X.D. Wang, L. Wang, Y.H. Rong, Enhancement of the mechanical properties of a Nb-microalloyed advanced high-strength steel treated by quenching–partitioning–tempering process, *Materials Science and Engineering: A*. 506 (2009) 111–116. doi:10.1016/J.MSEA.2008.11.014.
- [99] S. Zhou, K. Zhang, Y. Wang, J.F. Gu, Y.H. Rong, High strength-elongation product of Nb-microalloyed low-carbon steel by a novel quenching-partitioning-tempering process, *Materials Science and Engineering A*. 528 (2011) 8006–8012. doi:10.1016/j.msea.2011.07.008.
- [100] C. Kickingner, C. Suppan, T. Hebesberger, R. Schnitzer, C. Hofer, Microstructure and mechanical properties of partially ferritic Q&P steels, *Materials Science and Engineering: A*. 815 (2021) 141296. doi:10.1016/J.MSEA.2021.141296.
- [101] R. Ding, D. Tang, A. Zhao, R. Dong, J. Cheng, X. Zhang, A new type of quenching and partitioning processing developed from martensitic pre-microstructure, *Materials and Manufacturing Processes*. 29 (2014) 704–709. doi:10.1080/10426914.2014.912304.
- [102] R. Ding, D. Tang, A. Zhao, R. Dong, J. Cheng, X. Meng, Effect of intercritical temperature on quenching and partitioning steels originated from martensitic pre-microstructure, *Journal of Materials Research*. 29 (2014) 2525–2533. doi:10.1557/jmr.2014.285.
- [103] G. Liu, S. Zhang, J. Li, J. Wang, Q. Meng, Fast-heating for intercritical annealing of cold-rolled quenching and partitioning steel, *Materials Science and Engineering: A*. 669 (2016) 387–395. doi:10.1016/J.MSEA.2016.05.106.
- [104] D. De Knijf, A. Puype, C. Föjer, R. Petrov, The influence of ultra-fast annealing prior to quenching and partitioning on the microstructure and mechanical properties, *Materials Science and Engineering: A*. 627 (2015) 182–190. doi:10.1016/J.MSEA.2014.12.118.
- [105] M.J. Santofimia, L. Zhao, J. Sietsma, Model for the interaction between interface migration and carbon diffusion during annealing of martensite–austenite microstructures in steels, *Scripta Materialia*. 59 (2008) 159–162. doi:10.1016/J.SCRIPTAMAT.2008.02.045.
- [106] J. Sun, H. Yu, Microstructure development and mechanical properties of quenching and partitioning (Q&P) steel and an incorporation of hot-dipping galvanization during Q&P process, *Materials Science and Engineering: A*. 586 (2013) 100–107. doi:10.1016/J.MSEA.2013.08.021.
- [107] A.J. Clarke, J.G. Speer, M.K. Miller, R.E. Hackenberg, D. V. Edmonds, D.K. Matlock, F.C. Rizzo, K.D. Clarke, E. De Moor, Carbon partitioning to austenite from martensite or bainite during the quench and partition (Q&P) process: A critical assessment, *Acta Materialia*. 56 (2008) 16–22. doi:10.1016/J.ACTAMAT.2007.08.051.
- [108] M.J. Santofimia, L. Zhao, R. Petrov, C. Kwakernaak, W.G. Sloof, J. Sietsma, Microstructural development during the quenching and partitioning process in a newly designed low-carbon steel, *Acta Materialia*. 59 (2011) 6059–6068. doi:10.1016/J.ACTAMAT.2011.06.014.
- [109] E.A. Ariza-Echeverri, M. Masoumi, A.S. Nishikawa, D.H. Mesa, A.E. Marquez-Rossy, A.P. Tschiptschin, Development of a new generation of quench and partitioning steels: Influence of processing parameters on texture, nanoindentation, and mechanical properties, *Materials & Design*. 186 (2019) 108329. doi:10.1016/J.MATDES.2019.108329.
- [110] M.J. Santofimia, L. Zhao, R. Petrov, J. Sietsma, Characterization of the microstructure obtained by the quenching and partitioning process in a low-carbon steel, *Materials Characterization*. 59 (2008) 1758–1764. doi:10.1016/J.MATCHAR.2008.04.004.
- [111] E.J. Seo, L. Cho, B.C. De Cooman, Kinetics of the partitioning of carbon and substitutional alloying elements during quenching and partitioning (Q&P) processing of medium Mn

- steel, *Acta Materialia*. 107 (2016) 354–365. doi:10.1016/j.actamat.2016.01.059.
- [112] R. Ding, Z. Dai, M. Huang, Z. Yang, C. Zhang, H. Chen, Effect of pre-existed austenite on austenite reversion and mechanical behavior of an Fe-0.2C-8Mn-2Al medium Mn steel, *Acta Materialia*. 147 (2018) 59–69. doi:10.1016/j.actamat.2018.01.009.
- [113] D.K. Matlock, V.E. Bräutigam, J.G. Speer, Application of the quenching and partitioning (Q&P) process to a medium-carbon, high-Si microalloyed bar steel, *Materials Science Forum*. 426–432 (2003) 1089–1094. doi:10.4028/www.scientific.net/msf.426-432.1089.
- [114] T. Tsuchiyama, T. Sakamoto, S. Tanaka, T. Masumura, Control of core-shell type second phase formed via interrupted quenching and intercritical annealing in a medium manganese steel, *ISIJ International*. 60 (2020) 2954–2962. doi:10.2355/isijinternational.ISIJINT-2020-164.
- [115] A.J. Clarke, J.G. Speer, D.K. Matlock, F.C. Rizzo, D. V. Edmonds, M.J. Santofimia, Influence of carbon partitioning kinetics on final austenite fraction during quenching and partitioning, *Scripta Materialia*. 61 (2009) 149–152. doi:10.1016/J.SCRIPTAMAT.2009.03.021.
- [116] Y. Li, S. Chen, C. Wang, D.S. Martín, W. Xu, Modeling retained austenite in Q&P steels accounting for the bainitic transformation and correction of its mismatch on optimal conditions, *Acta Materialia*. 188 (2020) 528–538. doi:10.1016/J.ACTAMAT.2020.02.033.
- [117] A. Arlazarov, M. Ollat, J.P. Masse, M. Bouzat, Influence of partitioning on mechanical behavior of Q&P steels, *Materials Science and Engineering: A*. 661 (2016) 79–86. doi:10.1016/J.MSEA.2016.02.071.
- [118] W. FengYing, Z. YueFeng, Z. HuiHua, J. BoZhi, W. Guan, SCIENCE CHINA A novel microstructural design and heat treatment technique based on gradient control of carbon partitioning between austenite and martensite for high strength steels, *Sci China Tech Sci*. 56 (2013) 1847–1857. doi:10.1007/s11431-013-5206-5.
- [119] T.Y. Hsu, Z.Y. Xu, Design of Structure, Composition and Heat Treatment Process for High Strength Steel, *Materials Science Forum*. 561–565 (2007) 2283–2286. doi:10.4028/www.scientific.net/msf.561-565.2283.
- [120] Z.R. Hou, T. Opitz, X.C. Xiong, X.M. Zhao, H.L. Yi, Bake-partitioning in a press-hardening steel, *Scripta Materialia*. 162 (2019) 492–496. doi:10.1016/J.SCRIPTAMAT.2018.10.053.
- [121] H.L. Cai, P. Chen, J.K. Oh, Y.R. Cho, D. Wu, H.L. Yi, Quenching and flash-partitioning enables austenite stabilization during press-hardening processing, *Scripta Materialia*. 178 (2020) 77–81. doi:10.1016/J.SCRIPTAMAT.2019.10.047.
- [122] H.K.D.H. Bhadeshia, D. V. Edmonds, The Bainite Transformation in a Silicon Steel, *Metallurgical Transactions A*. 10A (1979) 895–907.
- [123] H.Y. Li, X.W. Lu, W.J. Li, X.J. Jin, Microstructure and mechanical properties of an Ultrahigh-Strength 40SiMnNiCr steel during the one-step quenching and partitioning process, *Metallurgical and Materials Transactions A: Physical Metallurgy and Materials Science*. 41 (2010) 1284–1300. doi:10.1007/s11661-010-0184-8.
- [124] O. Dmitrieva, D. Ponge, G. Inden, J. Millán, P. Choi, J. Sietsma, D. Raabe, Chemical gradients across phase boundaries between martensite and austenite in steel studied by atom probe tomography and simulation, *Acta Materialia*. 59 (2011) 364–374. doi:10.1016/j.actamat.2010.09.042.
- [125] A. Arlazarov, M. Gouné, O. Bouaziz, A. Hazotte, Critical factors governing the thermal stability of austenite in an ultra-fined grained Medium-Mn steel, *Philosophical Magazine Letters*. 97 (2017) 125–131. doi:10.1080/09500839.2017.1290293.
- [126] P.J. Jacques, J. Ladrière, F. Delannay, On the Influence of Interactions between Phases on the Mechanical Stability of Retained Austenite in Transformation-Induced Plasticity Multiphase Steels, *Metallurgical and Materials Transactions A*. 32A (2001) 2759–2768.
- [127] J.H. Ryu, D.I. Kim, H.S. Kim, H.K.D.H. Bhadeshia, D.W. Suh, Strain partitioning and mechanical stability of retained austenite, *Scripta Materialia*. 63 (2010) 297–299. doi:10.1016/J.SCRIPTAMAT.2010.04.020.

- [128] H.S. Yang, H.K.D.H. Bhadeshia, Austenite grain size and the martensite-start temperature, *Scripta Materialia*. 60 (2009) 493–495. doi:10.1016/J.SCRIPTAMAT.2008.11.043.
- [129] X.C. Xiong, B. Chen, M.X. Huang, J.F. Wang, L. Wang, The effect of morphology on the stability of retained austenite in a quenched and partitioned steel, *Scripta Materialia*. 68 (2013) 321–324. doi:10.1016/J.SCRIPTAMAT.2012.11.003.
- [130] J. Chiang, B. Lawrence, J.D. Boyd, A.K. Pilkey, Effect of microstructure on retained austenite stability and work hardening of TRIP steels, *Materials Science and Engineering: A*. 528 (2011) 4516–4521. doi:10.1016/J.MSEA.2011.02.032.
- [131] D. De Knijf, R. Petrov, C. Föjer, L.A.I. Kestens, Effect of fresh martensite on the stability of retained austenite in quenching and partitioning steel, *Materials Science and Engineering: A*. 615 (2014) 107–115. doi:10.1016/j.msea.2014.07.054.
- [132] S. Yan, X. Liu, W.J. Liu, H. Lan, H. Wu, Comparison on mechanical properties and microstructure of a C-Mn-Si steel treated by quenching and partitioning (Q&P) and quenching and tempering (Q&T) processes, *Materials Science and Engineering A*. 620 (2014) 58–66. doi:10.1016/j.msea.2014.09.047.
- [133] J. Lu, H. Yu, P. Kang, X. Duan, C. Song, Study of microstructure, mechanical properties and impact-abrasive wear behavior of medium-carbon steel treated by quenching and partitioning (Q&P) process, *Wear*. 414–415 (2018) 21–30. doi:10.1016/J.WEAR.2018.07.026.
- [134] Z.Z. Zhao, J.H. Liang, A.M. Zhao, J.T. Liang, D. Tang, Y.P. Gao, Effects of the austenitizing temperature on the mechanical properties of cold-rolled medium-Mn steel system, *Journal of Alloys and Compounds*. 691 (2017) 51–59. doi:10.1016/j.jallcom.2016.08.093.
- [135] E.J. Seo, L. Cho, Y. Estrin, B.C. De Cooman, Microstructure-mechanical properties relationships for quenching and partitioning (Q&P) processed steel, *Acta Materialia*. 113 (2016) 124–139. doi:10.1016/j.actamat.2016.04.048.
- [136] MILLER RL, Ultrafine- grained microstructures and mechanical properties of alloy steels, *Metallurgical Transactions*. 3 (1972) 905–912. doi:10.1007/bf02647665.
- [137] M.J. Merwin, Low-Carbon Manganese TRIP Steels, *Materials Science Forum*. 539–543 (2007) 4327–4332. doi:10.4028/www.scientific.net/msf.539-543.4327.
- [138] R.L. Miller, Ultrafine-Grained Microstructures and Mechanical Properties of Alloy Steels, 1972.
- [139] T. Furukawa, Dependence of strength–ductility characteristics on thermal history in lowcarbon, 5 wt-%Mn steels, *Materials Science and Technology (United Kingdom)*. 5 (1989) 465–470. doi:10.1179/mst.1989.5.5.465.
- [140] D.E. Kim, Y.K. Park, O.Y. Lee, K.G. Jin, S.J. Kim, Formation of Retained Austenite and Mechanical Properties of 4~8%Mn Hot Rolled TRIP Steels, *Korean Journal of Materials Research*. 15 (2005) 115–120. doi:10.3740/mrsk.2005.15.2.115.
- [141] P.J. Gibbs, E. De Moor, M.J. Merwin, J.G. Speer, D.K. Matlock, Austenite Stability Effects on Tensile Behavior of Manganese-Enriched-Austenite Transformation-Induced Plasticity Steel, *Metallurgical and Materials Transactions A*. 42A (2011). doi:10.1007/s11661-011-0687-y.
- [142] A. Arlazarov, M. Gouné, O. Bouaziz, A. Hazotte, G. Petitgand, P. Barges, Evolution of microstructure and mechanical properties of medium Mn steels during double annealing, *Materials Science and Engineering A*. 542 (2012) 31–39. doi:10.1016/j.msea.2012.02.024.
- [143] J. Shi, X. Sun, M. Wang, W. Hui, H. Dong, W. Cao, Enhanced work-hardening behavior and mechanical properties in ultrafine-grained steels with large-fractioned metastable austenite, *Scripta Materialia*. 63 (2010) 815–818. doi:10.1016/J.SCRIPTAMAT.2010.06.023.
- [144] A. Bhattacharya, P.K. Bokinala, R. Mitra, D. Chakrabarti, Relative effect of C and Mn on

- strength-toughness of medium Mn steels, *Materials Science and Technology* (United Kingdom). 35 (2019) 55–67. doi:10.1080/02670836.2018.1537609.
- [145] P.J. Du, D.P. Yang, M.K. Bai, X.C. Xiong, D. Wu, G.D. Wang, H.L. Yi, Austenite stabilisation by two step partitioning of manganese and carbon in a Mn-TRIP steel, *Materials Science and Technology* (United Kingdom). 35 (2019) 2084–2091. doi:10.1080/02670836.2019.1572316.
- [146] Z. Dai, H. Chen, R. Ding, Q. Lu, C. Zhang, Z. Yang, S. van der Zwaag, Fundamentals and application of solid-state phase transformations for advanced high strength steels containing metastable retained austenite, *Materials Science and Engineering: R: Reports*. 143 (2021) 100590. doi:10.1016/J.MSER.2020.100590.
- [147] R. Rana, Special issue on 'Medium manganese steels,' *Materials Science and Technology* (United Kingdom). 35 (2019) 2039–2044. doi:10.1080/02670836.2019.1673971.
- [148] E. De Moor, P.J. Gibbs, J.G. Speer, D.K. Matlock, J.G. Schroth, Strategies for third-generation advanced high-strength steel development, *Iron and Steel Technology*. 7 (2010) 133–144.
- [149] H.K.D.H. Bhadeshia, S.R. Honeycombe, *The Iron-Carbon Equilibrium Diagram and Plain Carbon Steels*, *Steels*. (2006) 39–70. doi:10.1016/B978-075068084-4/50005-4.
- [150] H.K.D.H. Bhadeshia, The bainite transformation: unresolved issues, *Materials Science and Engineering: A*. 273–275 (1999) 58–66. doi:10.1016/S0921-5093(99)00289-0.
- [151] L. Wang, J.G. Speer, Quenching and Partitioning Steel Heat Treatment, *Metallography, Microstructure, and Analysis*. 2 (2013) 268–281. doi:10.1007/s13632-013-0082-8.
- [152] X. Chen, C. Niu, C. Lian, J. Lin, The Evaluation of Formability of the 3rd Generation Advanced High Strength Steels QP980 based on Digital Image Correlation Method, *Procedia Engineering*. 207 (2017) 556–561. doi:10.1016/J.PROENG.2017.10.1020.
- [153] H. Ghassemi-armaki, Q. Khan, S.A. Varanasi, On the Advantages of Fortiform® 980 Gi - a 3rd Generation AHSS Grade With Superior Weldability, Presented at 2019 Great Designs in Steel, Sponsored by American Iron and Steel Institute. (2019).
- [154] C.D. Horvath, G. Motors, C.C. Matt, G.M. Company, Opportunities and Challenges for 3rd Generation Advanced High-Strength Steels in Automotive Body Structures, *Great Designs in STEEL Seminar*. (2017).
- [155] L. Specker, Ford's hot new Bronco built with Alabama steel, *AL.Com*. (2020). <https://www.al.com/news/mobile/2020/11/fords-hot-new-bronco-built-with-alabama-steel.html>.
- [156] FCA, All-new 2021 Jeep® Grand Cherokee Breaks New Ground in the Full-size SUV Segment, (2021).
- [157] L. Wang, J. Bian, J. Wang, Y. Ye, Development and Application of New Generation AHSS Based on Q&P Process, in: *Materials in Car Body Engineering*, Bad Nauheim, Germany, 2019.
- [158] J. Galán, L. Samek, P. Verleysen, K. Verbeken, Y. Houbaert, Advanced high strength steels for automotive industry, *Revista de Metalurgia*. 48 (2012) 118–131. doi:10.3989/revmetalm.1158.
- [159] Z.W. Wang, M. Liu, H. Zhang, G.M. Xie, P. Xue, L.H. Wu, Z. Zhang, D.R. Ni, B.L. Xiao, Z.Y. Ma, Welding behavior of an ultrahigh-strength quenching and partitioning steel by fusion and solid-state welding methods, *Journal of Materials Research and Technology*. 17 (2022) 1289–1301. doi:10.1016/j.jmrt.2022.01.086.
- [160] J.H. Lee, S.H. Park, H.S. Kwon, G.S. Kim, C.S. Lee, Laser, tungsten inert gas, and metal active gas welding of DP780 steel: Comparison of hardness, tensile properties and fatigue resistance, *Materials & Design*. 64 (2014) 559–565. doi:10.1016/J.MATDES.2014.07.065.
- [161] R.S. Sharma, P. Molian, Yb:YAG laser welding of TRIP780 steel with dual phase and mild steels for use in tailor welded blanks, *Materials & Design*. 30 (2009) 4146–4155. doi:10.1016/J.MATDES.2009.04.033.

- [162] L. Lu, Z. Liang, J. Yang, Q. Sun, T. Zhu, X. Wang, Investigation on laser welding of a novel hot-stamped steel with 2000 MPa, *Journal of Materials Research and Technology*. 9 (2020) 13147–13152. doi:10.1016/J.JMRT.2020.09.044.
- [163] M. Pouranvari, S.P.H. Marashi, D.S. Safanama, Failure mode transition in AHSS resistance spot welds. Part II: Experimental investigation and model validation, *Materials Science and Engineering: A*. 528 (2011) 8344–8352. doi:10.1016/J.MSEA.2011.08.016.
- [164] O. Siar, S. Dancette, T. Dupuy, D. Fabrègue, Impact of liquid metal embrittlement inner cracks on the mechanical behavior of 3rd generation advanced high strength steel spot welds, *Journal of Materials Research and Technology*. 15 (2021) 6678–6689. doi:10.1016/J.JMRT.2021.11.100.
- [165] V.H. Baltazar Hernandez, M.L. Kuntz, M.I. Khan, Y. Zhou, Influence of microstructure and weld size on the mechanical behaviour of dissimilar AHSS resistance spot welds, *Science and Technology of Welding and Joining*. 13 (2008) 769–776. doi:10.1179/136217108X325470.
- [166] G.K. Ahiale, Y.J. Oh, Microstructure and fatigue performance of butt-welded joints in advanced high-strength steels, *Materials Science and Engineering: A*. 597 (2014) 342–348. doi:10.1016/J.MSEA.2014.01.007.
- [167] R. Ohashi, M. Fujimoto, S. Mironov, Y.S. Sato, H. Kokawa, Effect of contamination on microstructure in friction stir spot welded DP590 steel, *Science and Technology of Welding and Joining*. 14 (2009) 221–227. doi:10.1179/136217108X388642.
- [168] Z.W. Wang, G.N. Ma, B.H. Yu, P. Xue, G.M. Xie, H. Zhang, D.R. Ni, B.L. Xiao, Z.Y. Ma, Improving mechanical properties of friction-stir-spot-welded advanced ultra-high-strength steel with additional water cooling, *Science and Technology of Welding and Joining*. 25 (2020) 336–344. doi:10.1080/13621718.2019.1706259.
- [169] S. Mironov, Y.S. Sato, S. Yoneyama, H. Kokawa, H.T. Fujii, S. Hirano, Microstructure and tensile behavior of friction-stir welded TRIP steel, *Materials Science and Engineering: A*. 717 (2018) 26–33. doi:10.1016/J.MSEA.2018.01.053.
- [170] M. Matsushita, Y. Kitani, R. Ikeda, M. Ono, H. Fujii, Y.D. Chung, Development of friction stir welding of high strength steel sheet, *Science and Technology of Welding and Joining*. 16 (2011) 181–187. doi:10.1179/1362171810Y.0000000026.
- [171] G. Weber, H. Thommes, H. Gaul, O. Hahn, M. Rethmeier, Resistance spot welding and weldbonding of advanced high strength steels, *Materialwissenschaft Und Werkstofftechnik*. 41 (2010) 931–939. doi:10.1002/mawe.201000687.
- [172] W. Guo, Z. Wan, P. Peng, Q. Jia, G. Zou, Y. Peng, Microstructure and mechanical properties of fiber laser welded QP980 steel, *Journal of Materials Processing Technology*. 256 (2018) 229–238. doi:10.1016/J.JMATPROTEC.2018.02.015.
- [173] W. Li, L. Ma, P. Peng, Q. Jia, Z. Wan, Y. Zhu, W. Guo, Microstructural evolution and deformation behavior of fiber laser welded QP980 steel joint, *Materials Science and Engineering: A*. 717 (2018) 124–133. doi:10.1016/J.MSEA.2018.01.050.
- [174] J. Xue, P. Peng, W. Guo, M. Xia, C. Tan, Z. Wan, H. Zhang, Y. Li, HAZ Characterization and Mechanical Properties of QP980-DP980 Laser Welded Joints, *Chinese Journal of Mechanical Engineering*. 34 (2021) 80. doi:10.1186/s10033-021-00596-x.
- [175] H. Lin, H. Jiang, Y. Wang, S. Tian, Microstructure gradient characteristics and mechanical properties of friction stir welded high strength QP980 steel, *Materials Research Express*. 6 (2018) 126584. <https://iopscience.iop.org/article/10.1088/2053-1583/abe778>.
- [176] X. Wu, H. Lin, W. Luo, H. Jiang, Microstructure and microhardness evolution of thermal simulated HAZ of Q&P980 steel, *Journal of Materials Research and Technology*. 15 (2021) 6067–6078. doi:10.1016/J.JMRT.2021.11.059.
- [177] Z.W. Wang, H. Zhang, X.H. An, L.H. Wu, P. Xue, Q.C. Zhang, D.R. Ni, B.L. Xiao, Z.Y. Ma, Achieving equal strength joint to parent metal in a friction stir welded ultra-high strength quenching and partitioning steel, *Materials Science and Engineering: A*. 793 (2020) 139979. doi:10.1016/J.MSEA.2020.139979.

- [178] S. Memon, J. Tomków, H.A. Derazkola, E. Garcia, A. Murillo-Marrodán, H.A. Derazkola, materials Thermo-Mechanical Simulation of Underwater Friction Stir Welding of Low Carbon Steel, *Materials*. 14 (2021) 4953. doi:10.3390/ma14174953.
- [179] H.A. Derazkola, E. García, A. Eyvazian, M. Aberoumand, materials Effects of Rapid Cooling on Properties of Aluminum-Steel Friction Stir Welded Joint, *Materials*. 14 (2021) 908. doi:10.3390/ma14040908.
- [180] Z.W. Wang, J.F. Zhang, G.M. Xie, L.H. Wu, H. Zhang, P. Xue, D.R. Ni, B.L. Xiao, Z.Y. Ma, Evolution mechanisms of microstructure and mechanical properties in a friction stir welded ultrahigh-strength quenching and partitioning steel, *Journal of Materials Science & Technology*. 102 (2022) 213–223. doi:10.1016/J.JMST.2021.06.031.
- [181] O. Haiko, I. Miettunen, D. Porter, N. Ojala, V. Ratia, V. Heino, A. Kemppainen, Effect of Finish rolling and quench stop temperatures on impact-abrasive wear resistance of 0.35 % carbon direct-quenched steel, *Tribologia*. 35 (2017) 5–21.
- [182] M.J. Pérez, M.M. Cisneros, H.F. López, Wear resistance of Cu–Ni–Mo austempered ductile iron, *Wear*. 260 (2006) 879–885. doi:10.1016/J.WEAR.2005.04.001.
- [183] J.J. Coronado, A. Sinatora, Particle size effect on abrasion resistance of mottled cast iron with different retained austenite contents, *Wear*. 267 (2009) 2077–2082. doi:10.1016/J.WEAR.2009.08.011.
- [184] L.C. Cheng, T.B. Wu, C.T. Hu, The role of microstructural features in abrasive wear of a D-2 tool steel, 1988.
- [185] T. Jian-Min, Z. Yi-Zhong, S. Tian-Yi, D. Hai-Jin, The influence of retained austenite in high chromium cast iron on impact-abrasive wear, *Wear*. 135 (1990) 217–226. doi:10.1016/0043-1648(90)90026-7.
- [186] H.Y. Dong, K.M. Wu, X.L. Wang, T.P. Hou, R. Yan, A comparative study on the three-body abrasive wear performance of Q&P processing and low-temperature bainitic transformation for a medium-carbon dual-phase steel, *Wear*. 402–403 (2018) 21–29. doi:10.1016/J.WEAR.2018.01.009.
- [187] K. Wasiak, E. Skołek, W.A. Źwiątnicki, Analysis of the microstructure and wear resistance 35CrSiMn5-5-4 steel after quenching and partitioning, in: *METAL 2014 - 23rd International Conference on Metallurgy and Materials, Conference Proceedings*, 2014: pp. 790–793.
- [188] P. Wolfram, C. Hensley, R. Youngblood, R. Stewart, E. de Moor, J.G. Speer, Toward the Development of AHSS for Wear Resistant Applications, *Materials Science Forum*. 941 (2018) 568–573. doi:10.4028/www.scientific.net/msf.941.568.
- [189] O. Haiko, M. Somani, D. Porter, P. Kantanen, J. Kömi, N. Ojala, V. Heino, Comparison of impact-abrasive wear characteristics and performance of direct quenched (DQ) and direct quenched and partitioned (DQ&P) steels, *Wear*. 400–401 (2018) 21–30. doi:10.1016/J.WEAR.2017.12.016.
- [190] R.A. Stewart, J.G. Speer, B.G. Thomas, E. De Moor, A.J. Clarke, Quenching and Partitioning of Plate Steels: Partitioning Design Methodology, *Metallurgical and Materials Transactions A*. 50 (2019) 4701–4713. doi:10.1007/s11661-019-05337-3.
- [191] B. Liu, W. Li, X. Lu, X. Jia, X. Jin, The effect of retained austenite stability on impact-abrasion wear resistance in carbide-free bainitic steels, *Wear*. 428–429 (2019) 127–136. doi:10.1016/j.wear.2019.02.032.
- [192] J. ping Lai, L. ping Zhang, W. Gong, X. Xu, C. an Xiao, Two-body abrasion resistance of high carbon steel treated by quenching-partitioning-tempering process, *Wear*. 440–441 (2019) 203096. doi:10.1016/J.WEAR.2019.203096.
- [193] J. ping Lai, J. xin Yu, J. Wang, Effect of quenching-partitioning treatment on the microstructure, mechanical and abrasive properties of high carbon steel, *International Journal of Minerals, Metallurgy and Materials*. (2020). doi:10.1007/s12613-020-2164-3.
- [194] F. Huang, J. Yang, Z. Guo, S. Chen, Y. Rong, N. Chen, Effect of Partitioning Treatment on the Mechanical Property of Fe-0.19C-1.47Mn-1.50Si Steel with Refined Martensitic Microstructure, *Metallurgical and Materials Transactions A: Physical Metallurgy and*

- Materials Science. 47 (2016) 1072–1082. doi:10.1007/s11661-015-3278-5.
- [195] K.W. Andrews, Empirical formulas for the calculation of some transformation temperatures, *Journal of the Iron and Steel Institute*. 203(7) (1965) 721–727.
- [196] D.P. Koistinen, R.E. Marburger, A general equation prescribing the extent of the austenite-martensite transformation in pure iron-carbon alloys and plain carbon steels, *Acta Metallurgica*. 7 (1959) 59–60. doi:10.1016/0001-6160(59)90170-1.
- [197] E. Atkins, *Elements of X-ray Diffraction*, 1978. doi:10.1088/0031-9112/29/12/034.
- [198] D. Brandon, W.D. Kaplan, Scanning electron microscopy, in: *Microstructural Characterization of Materials*, 2nd Editio, 2008: pp. 261–331. doi:10.1142/9789811207631_0044.
- [199] J. Jiang, A. Godfrey, W. Liu, Q. Liu, Microtexture evolution via deformation twinning and slip during compression of magnesium alloy AZ31, *Materials Science and Engineering: A*. 483–484 (2008) 576–579. doi:10.1016/J.MSEA.2006.07.175.
- [200] A. Bastos, S. Zaefferer, D. Raabe, C. Schuh, Characterization of the microstructure and texture of nanostructured electrodeposited NiCo using electron backscatter diffraction (EBSD), *Acta Materialia*. 54 (2006) 2451–2462. doi:10.1016/J.ACTAMAT.2006.01.033.
- [201] V. Randle, G.S. Rohrer, H.M. Miller, M. Coleman, G.T. Owen, Five-parameter grain boundary distribution of commercially grain boundary engineered nickel and copper, *Acta Materialia*. 56 (2008) 2363–2373. doi:10.1016/J.ACTAMAT.2008.01.039.
- [202] A.F. Gourgues-Lorenzon, Application of electron backscatter diffraction to the study of phase transformations: Present and possible future, *Journal of Microscopy*. 233 (2009) 460–473. doi:10.1111/j.1365-2818.2009.03130.x.
- [203] M.G. Perez, E.A. Kenik, M.J. O’Keefe, F.S. Miller, B. Johnson, Identification of phases in zinc alloy powders using electron backscatter diffraction, *Materials Science and Engineering: A*. 424 (2006) 239–250. doi:10.1016/J.MSEA.2006.03.015.
- [204] A.J. Wilkinson, G. Meaden, D.J. Dingley, High-resolution elastic strain measurement from electron backscatter diffraction patterns: New levels of sensitivity, *Ultramicroscopy*. 106 (2006) 307–313. doi:10.1016/J.ULTRAMIC.2005.10.001.
- [205] V. Randle, Electron backscatter diffraction: Strategies for reliable data acquisition and processing, *Materials Characterization*. 60 (2009) 913–922. doi:10.1016/J.MATCHAR.2009.05.011.
- [206] S.I. Wright, M.M. Nowell, EBSD image quality mapping, *Microscopy and Microanalysis*. 12 (2006) 72–84. doi:10.1017/S1431927606060090.
- [207] D. Stojakovic, Electron backscatter diffraction in materials characterization, *Processing and Application of Ceramics*. 6 (2012) 1–13. doi:10.2298/pac1201001s.
- [208] D. Brandon, W.D. Kaplan, Transmission Electron Microscopy - Microstructural Characterization of Materials, in: *Microstructural Characterization of Materials*, 2008: pp. 179–260.
- [209] M.J. Santofimia, L. Zhao, J. Sietsma, Volume change associated to carbon partitioning from martensite to austenite, in: *Materials Science Forum*, 2012. doi:10.4028/www.scientific.net/MSF.706-709.2290.
- [210] E. Del Molino, T. Gutierrez, M. Serna-Ruiz, M. Arribas, A. Arlazarov, Influence of Mn and Ni on Austenite Stabilization during a High Temperature Q&P Treatment, *Materials Science Forum*. 1016 (2021) 379–384.
- [211] N.G.S. and B.M. Mogutnov, Paraequilibria in the Fe–Cr(Ni,Mn)–C Systems and Their Effect on Phase Transformations, *Russian Metallurgy (Metally)*. 2007 (2007) 153–160. doi:10.1134/S0036029507020127.
- [212] L. Liu, B.B. He, G.J. Cheng, H.W. Yen, M.X. Huang, Optimum properties of quenching and partitioning steels achieved by balancing fraction and stability of retained austenite, *Scripta Materialia*. 150 (2018) 1–6. doi:10.1016/j.scriptamat.2018.02.035.

- [213] B.C. De Cooman, S. Lee, S.S. Kumar, Ultra-fine grained manganese TRIP steels, in: Proceedings of 2nd International Conference "Super-High Strength Steels", Italy, 2010: pp. 1–11.
- [214] S. Lee, B.C. De Cooman, On the Selection of the Optimal Intercritical Annealing Temperature for Medium Mn TRIP Steel, *Metallurgical and Materials Transactions A*. 44 (2013) 5018–5024. doi:10.1007/s11661-013-1860-2.
- [215] E. De Moor, S. Kang, J.G. Speer, D.K. Matlock, Manganese Diffusion in Third Generation Advanced High Strength Steels, Proceedings of the International Conference on Mining, Materials and Metallurgical Engineering. (2014) 1–7.
- [216] M.J. Santofimia, J.G. Speer, A.J. Clarke, L. Zhao, J. Sietsma, Influence of interface mobility on the evolution of austenite–martensite grain assemblies during annealing, *Acta Materialia*. 57 (2009) 4548–4557. doi:10.1016/J.ACTAMAT.2009.06.024.
- [217] R. Wei, M. Enomoto, R. Hadian, H.S. Zurob, G.R. Purdy, Growth of austenite from as-quenched martensite during intercritical annealing in an Fe–0.1C–3Mn–1.5Si alloy, *Acta Materialia*. 61 (2013) 697–707. doi:10.1016/j.actamat.2012.10.019.
- [218] T. Shinozaki, Y. Tomota, T. Fukino, T. Suzuki, Microstructure evolution during reverse transformation of austenite from tempered martensite in low alloy steel, *ISIJ International*. 57 (2017) 533–539. doi:10.2355/isijinternational.ISIJINT-2016-557.
- [219] A.J. Clarke, M.K. Miller, R.D. Field, D.R. Coughlin, P.J. Gibbs, K.D. Clarke, D.J. Alexander, K.A. Powers, P.A. Papin, G. Krauss, Atomic and nanoscale chemical and structural changes in quenched and tempered 4340 steel, *Acta Materialia*. 77 (2014) 17–27. doi:10.1016/J.ACTAMAT.2014.05.032.
- [220] Z.J. Xie, G. Han, Y.S. Yu, C.J. Shang, R.D.K. Misra, The determining role of intercritical annealing condition on retained austenite and mechanical properties of a low carbon steel: Experimental and theoretical analysis, *Materials Characterization*. 153 (2019) 208–214. doi:10.1016/j.matchar.2019.05.010.
- [221] J. Teixeira, M. Moreno, S.Y.P. Allain, C. Oberbillig, G. Geandier, F. Bonnet, Intercritical annealing of cold-rolled ferrite-pearlite steel: Microstructure evolutions and phase transformation kinetics, *Acta Materialia*. 212 (2021) 116920. doi:10.1016/J.ACTAMAT.2021.116920.
- [222] F. Huyan, J.Y. Yan, L. Höglund, J. Ågren, A. Borgenstam, Simulation of the Growth of Austenite from As-Quenched Martensite in Medium Mn Steels, *Metallurgical and Materials Transactions A: Physical Metallurgy and Materials Science*. 49 (2018) 1053–1060. doi:10.1007/s11661-018-4497-3.
- [223] J.J. Mueller, X. Hu, X. Sun, Y. Ren, K. Choi, E. Barker, J.G. Speer, D.K. Matlock, E. De Moor, Austenite formation and cementite dissolution during intercritical annealing of a medium-manganese steel from a martensitic condition, *Materials and Design*. 203 (2021). doi:10.1016/j.matdes.2021.109598.
- [224] A. Borgenstam, A. Engstro, L. Ho, J.A. Gren, DICTRA, a Tool for Simulation of Diffusional Transformations in Alloys, *Journal of Phase Equilibria*. 21 (2000) 269–280.
- [225] A.J. Clarke, Carbon partitioning into austenite from martensite in a silicon-containing high strength sheet steel, Ph.D. Thesis, Colorado School of Mines, Golden, CO, 2006.
- [226] C.A. Apple, R.N. Caron, G. Krauss, Packet Microstructure in Fe-0.2 pct C Martensite, *Metallurgical Transactions*. 5 (1974) 593–599.
- [227] T. Swarr, G. Krauss, The Effect of Structure on the Deformation of As-Quenched and Tempered Martensite in an Fe-0.2 Pct C Alloy, *Metallurgical Transactions A*. 7 (1976) 41–48.
- [228] N. Yan, H. Di, R.D.K. Misra, H. Huang, Y. Li, Enhancing austenite stability in a new medium-Mn steel by combining deep cryogenic treatment and intercritical annealing: An experimental and theoretical study, *Materials Science and Engineering: A*. 753 (2019) 11–21. doi:10.1016/J.MSEA.2019.01.026.
- [229] H. Luo, J. Shi, C. Wang, W. Cao, X. Sun, H. Dong, Experimental and numerical analysis

- on formation of stable austenite during the intercritical annealing of 5Mn steel, *Acta Materialia*. 59 (2011) 4002–4014. doi:10.1016/J.ACTAMAT.2011.03.025.
- [230] P. Gao, W. Chen, F. Li, B. Ning, Z. Zhao, Quasi-Situ Characterization of Deformation in Low-Carbon Steel with Equiaxed and Lamellar Microstructure Treated by the Quenching and Partitioning Process, *Acta Metallurgica Sinica (English Letters)*. (2020). doi:10.1007/s40195-020-01135-8.
- [231] D. Raabe, B. Sun, A. Kwiatkowski Da Silva, B. Gault, H.-W. Yen, K. Sedighiani, P. Thoudeden Sukumar, I.R. Souza Filho, S. Katnagallu, E. Jäggle, P. Kürnstener, N. Kusampudi, L. Stephenson, M. Herbig, C.H. Liebscher, H. Springer, S. Zaefferer, V. Shah, S.-L. Wong, C. Baron, M. Diehl, F. Roters, D. Ponge, Current Challenges and Opportunities in Microstructure-Related Properties of Advanced High-Strength Steels, *Metallurgical and Materials Transactions A*. (2020). doi:10.1007/s11661-020-05947-2.
- [232] J. Zhao, Z. Jiang, C.S. Lee, Effects of tungsten addition and heat treatment conditions on microstructure and mechanical properties of microalloyed forging steels, *Materials Science and Engineering: A*. 562 (2013) 144–151. doi:10.1016/J.MSEA.2012.11.006.
- [233] S. Pang, G. Wu, W. Liu, M. Sun, Y. Zhang, Z. Liu, W. Ding, Effect of cooling rate on the microstructure and mechanical properties, *Materials Science & Engineering A*. 562 (2013) 152–160. doi:10.1016/j.msea.2012.11.016.
- [234] S.K. Hann, J.D. Gates, J. V Be, Transmission electron microscopy of a transformation toughened white cast iron, 1997.
- [235] A. Wiengmoon, T. Chairuangstri, A. Brown, R. Brydson, D. V. Edmonds, J.T.H. Pearce, Microstructural and crystallographical study of carbides in 30wt.%Cr cast irons, *Acta Materialia*. 53 (2005) 4143–4154. doi:10.1016/J.ACTAMAT.2005.05.019.
- [236] A.E. Karantzalis, A. Lekatou, H. Mavros, Microstructural Modifications of As-Cast High-Chromium White Iron by Heat Treatment, *Journal of Materials Engineering and Performance*. 18 (2008) 174–181. doi:10.1007/s11665-008-9285-6.
- [237] P.J. Jacques, Q. Furnémont, F. Lani, T. Pardoën, F. Delannay, Multiscale mechanics of TRIP-assisted multiphase steels: I. Characterization and mechanical testing, *Acta Materialia*. 55 (2007) 3681–3693. doi:10.1016/J.ACTAMAT.2007.02.029.
- [238] V.I. Zurnadzy, V.G. Efremenko, K.M. Wu, A.Y. Azarkhov, Y.G. Chabak, V.L. Greshta, O.B. Isayev, M.V. Pomazkov, Effects of stress relief tempering on microstructure and tensile/impact behavior of quenched and partitioned commercial spring steel, *Materials Science and Engineering: A*. 745 (2019) 307–318. doi:10.1016/J.MSEA.2018.12.106.
- [239] Ö.N. Doğan, J.A. Hawk, J.H. Tylczak, Wear of cast chromium steels with TiC reinforcement, *Wear*. 250 (2001) 462–469. doi:10.1016/S0043-1648(01)00635-4.
- [240] Z. Wang, B. Huang, H. Chen, C. Wang, J. Ma, X. Zhao, The Effect of Quenching and Partitioning Heat Treatment on the Wear Resistance of Ductile Cast Iron, *Journal of Materials Engineering and Performance*. 29 (2020) 4370–4378. doi:10.1007/s11665-020-04871-1.
- [241] A.M. Gola, M. Ghadamgahi, S.W. Ooi, Microstructure evolution of carbide-free bainitic steels under abrasive wear conditions, *Wear*. 376–377 (2017) 975–982. doi:10.1016/J.WEAR.2016.12.038.
- [242] S. Hernandez, A. Leiro, M.R. Ripoll, E. Vuorinen, K.G. Sundin, B. Prakash, High temperature three-body abrasive wear of 0.25C 1.42Si steel with carbide free bainitic (CFB) and martensitic microstructures, *Wear*. 360–361 (2016) 21–28. doi:10.1016/J.WEAR.2016.04.012.
- [243] F. Hu, K.M. Wu, T.P. Hou, A.A. Shirzadi, Tempering stability of retained austenite in nanostructured dual phase steels, *Materials Science and Technology (United Kingdom)*. 29 (2013) 947–953. doi:10.1179/1743284713Y.0000000227.
- [244] F. Hu, K.M. Wu, P.D. Hodgson, Effect of retained austenite on wear resistance of nanostructured dual phase steels, *Materials Science and Technology (United Kingdom)*. 32 (2016) 40–48. doi:10.1179/1743284715Y.0000000061.

Publications related to the doctoral thesis

Contributions to national and international conferences and workshops:

- **Oral presentation** in an external **workshop**, ASPPRC semi-annual workshop, Colorado School of Mines, Golden, United States of America (March 2021).
- Del Molino, E., Gutiérrez, T., Serna-Ruiz, M., Arribas, M., Arlazarov, A., **Oral presentation** in THERMEC 2021, Vienna, Austria (June 2021).
- Del Molino, E., Gutiérrez, T., Serna-Ruiz, M., Arribas, M., **Oral presentation** in MZT 2021, Bilbao, Spain (November 2021).

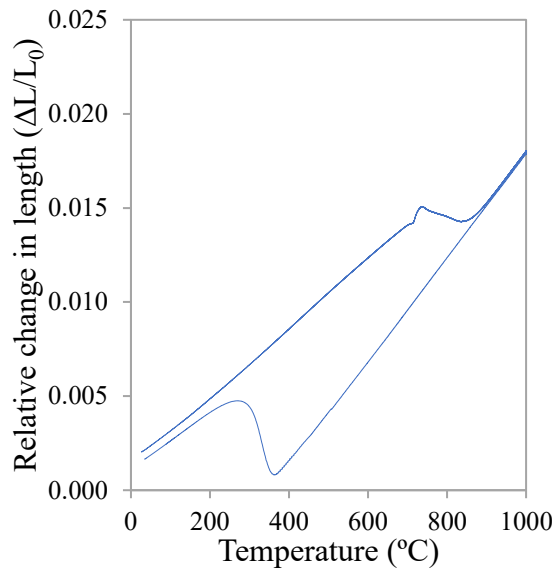
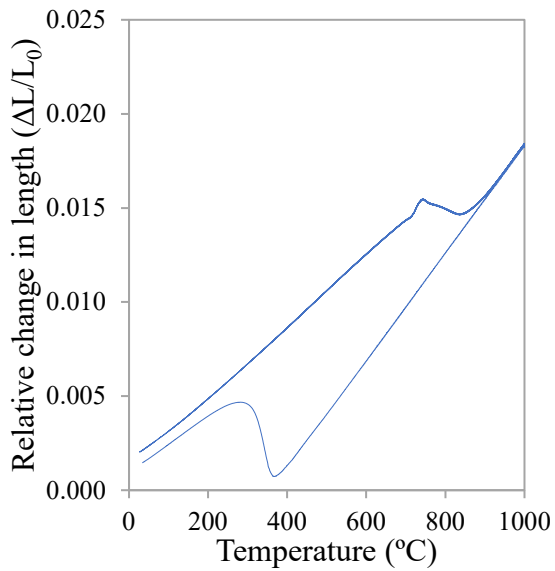
Published, submitted and under preparation articles:

- M. Arribas, T. Gutiérrez, E. Del Molino, A. Arlazarov, I. De Diego-Calderón, D. Martín, D. De Caro, S. Ayenampudi, M.J. Santofimia, *Austenite Reverse Transformation in a Q&P Route of Mn and Ni Added Steels*, *Metals*. 10 (2020) 862.
- E. Del Molino, T. Gutierrez, M. Serna-Ruiz, M. Arribas, A. Arlazarov, *Influence of Mn and Ni on Austenite Stabilization during a High Temperature Q&P Treatment*, *Materials Science Forum*. 1016 (2021) 379–384.
- M. Arribas, E. Del Molino, T. Gutiérrez, A. Arlazarov, D. Martín, D. De Caro, S. Ayenampudi, M.J. Santofimia, *Characterization of a Medium Mn-Ni Steel Q&P Treated by a High Partitioning Temperature Cycle*, *Metals*. 12 (2022) 483.
- E. Del Molino, M. Arribas, C. Gilliams, A. Arlazarov, J. J. González, E. De Moor, J. G. Speer, *Austenite stability in medium Mn steels heat treated by high partitioning temperature Quenching and Partitioning*, *Metallurgical and Materials Transactions A*, submitted.
- E. Del Molino, M. Arribas, J. J. González, F. Valdavidia, I. Pérez, *Microstructure and wear resistance in medium and high C steels treated by Quenching & Partitioning*, under preparation.

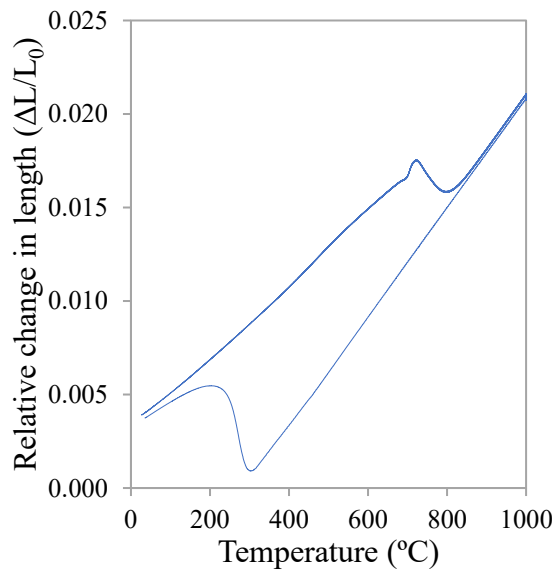
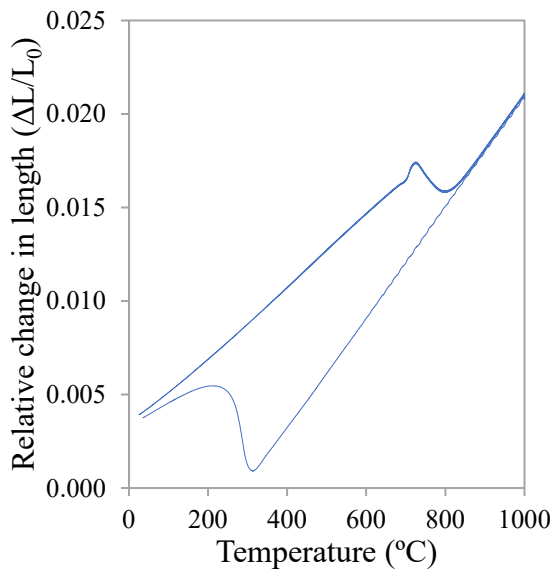
Appendix A: Dilatometry

Dilatometry curves to determine A_{c1} and A_{c3}

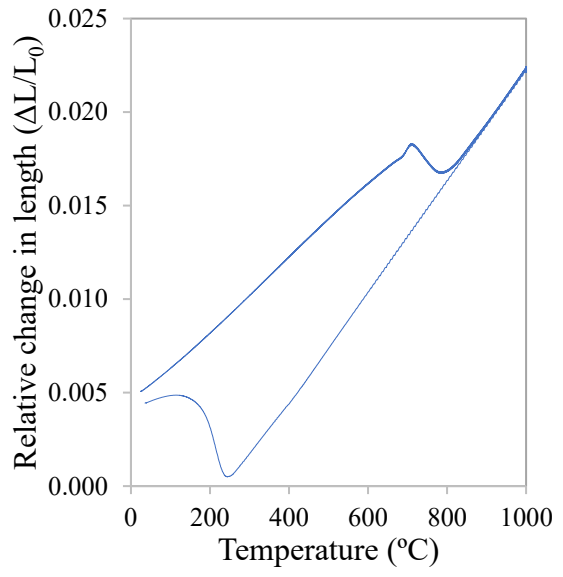
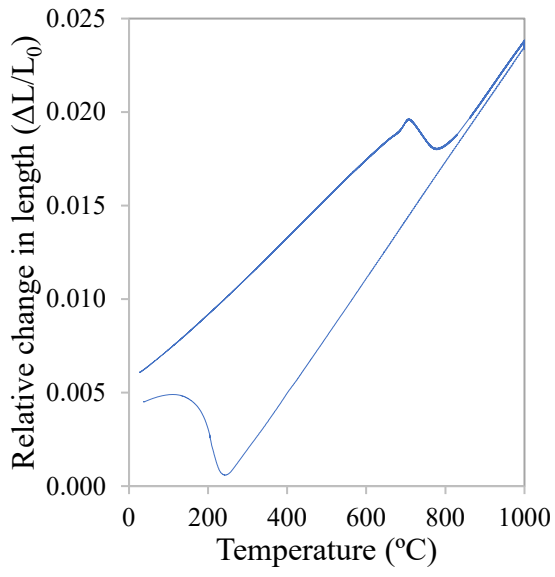
2Mn



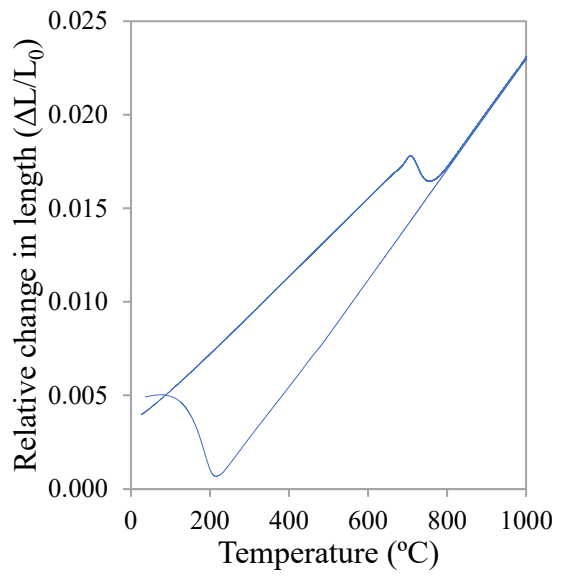
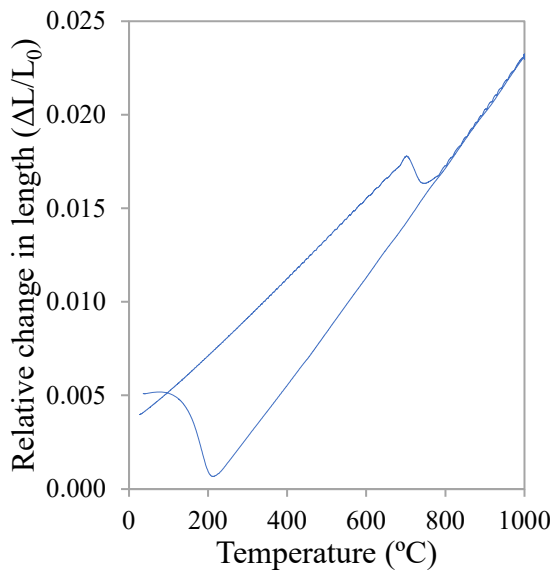
4Mn



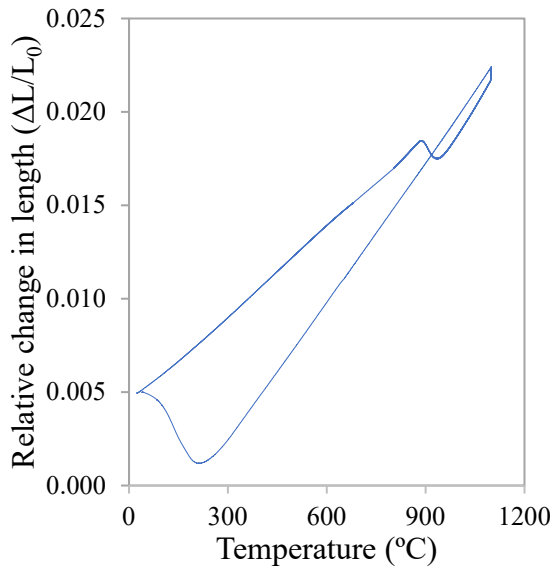
6Mn



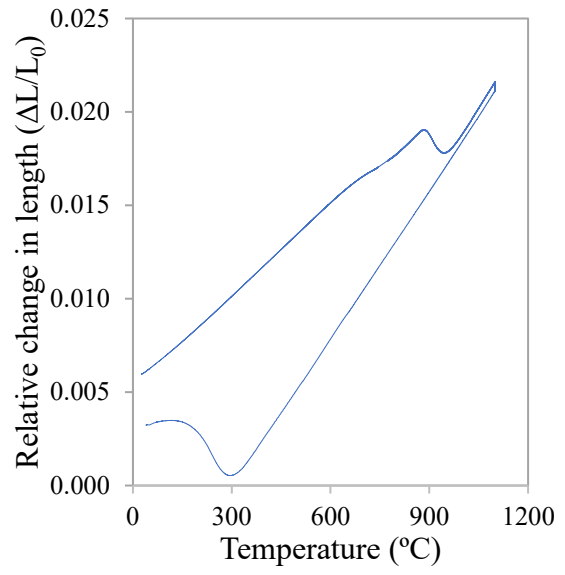
6Mn2Ni



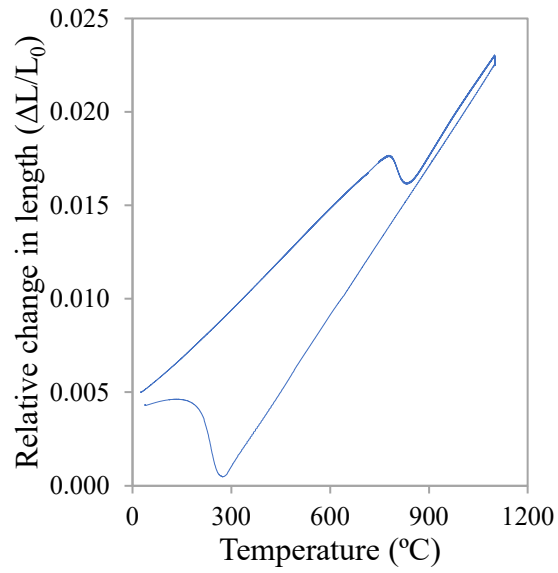
1.2990



1.2344

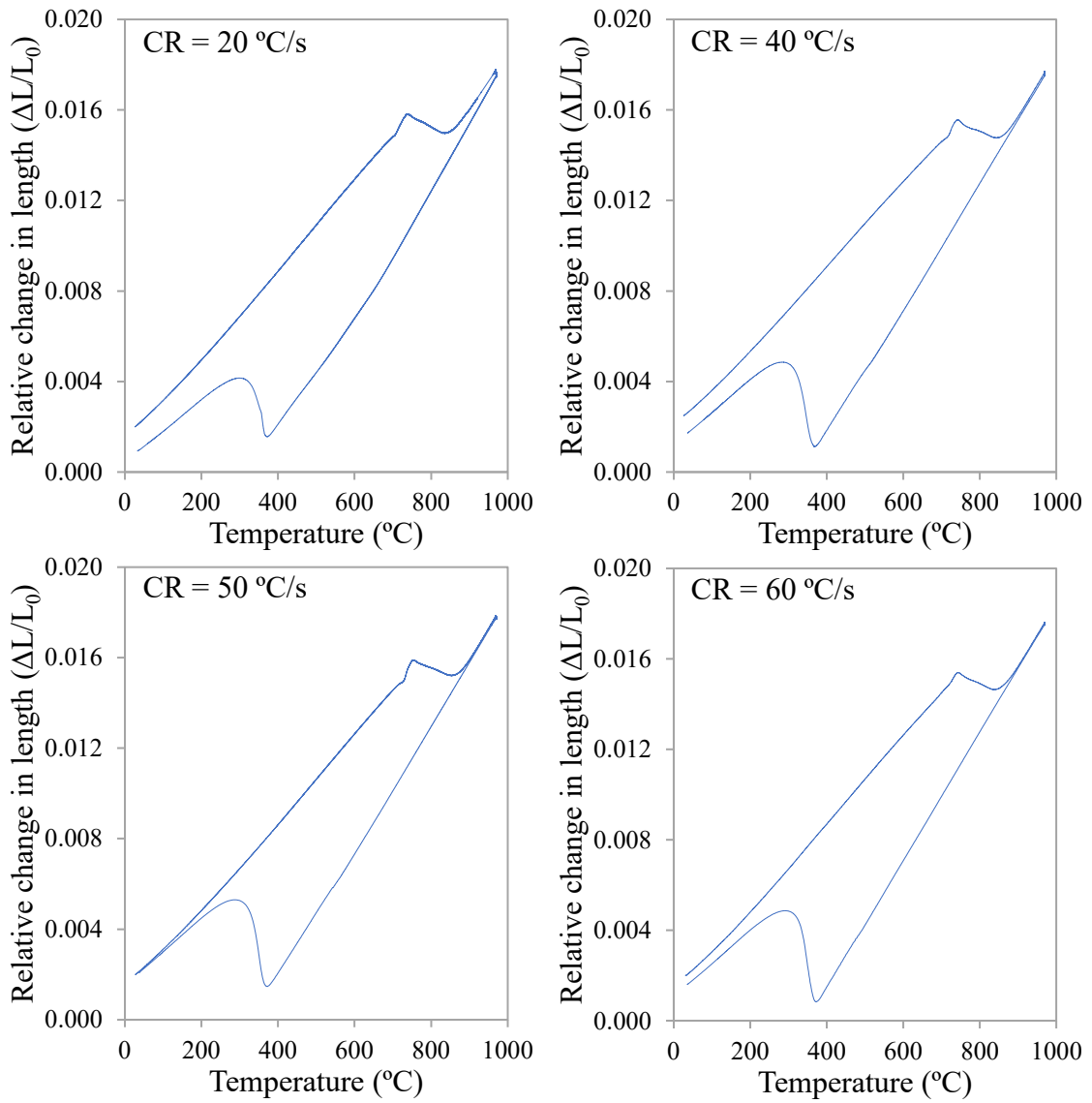


300M

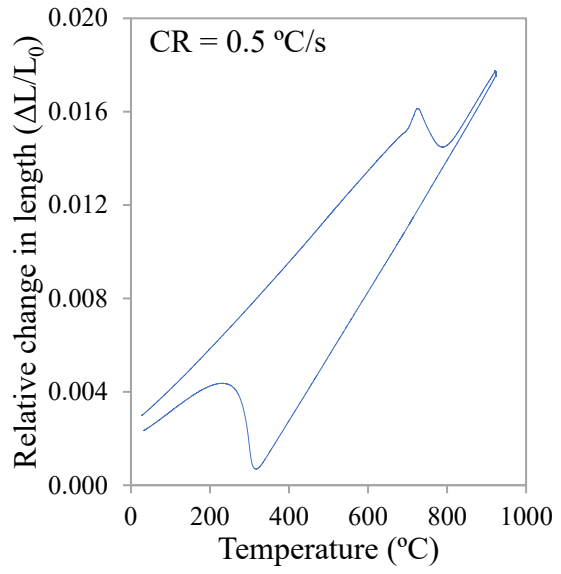
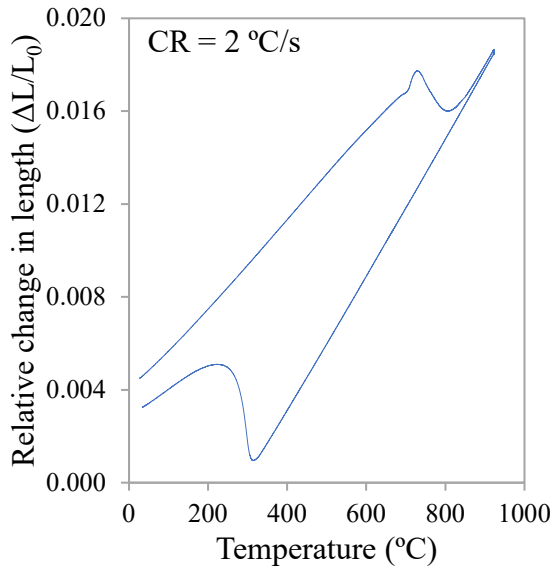


Dilatometry curves to determine CCR:

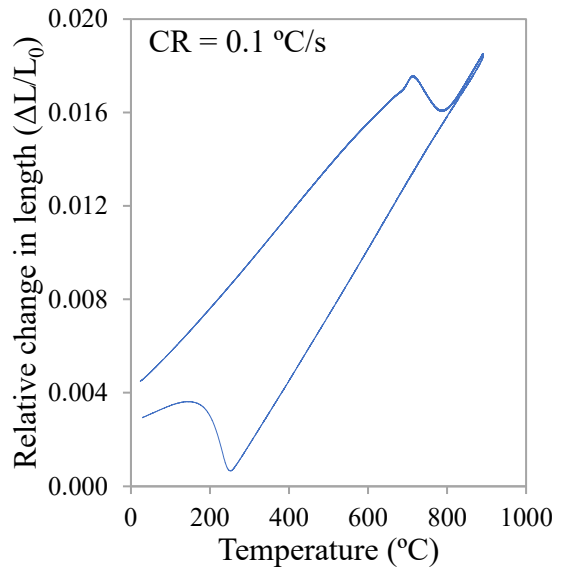
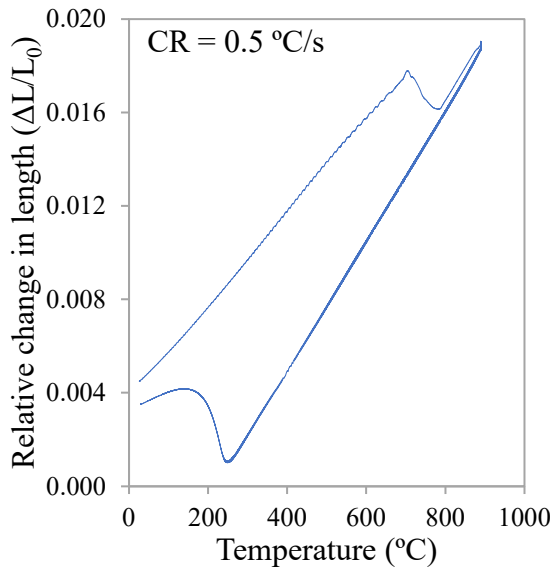
2Mn



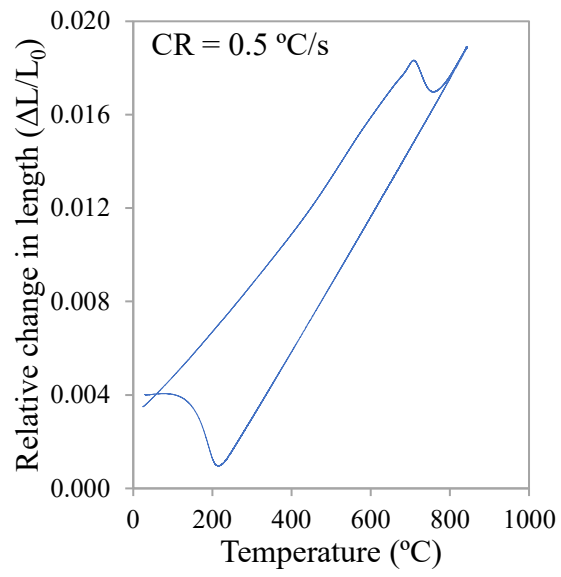
4Mn



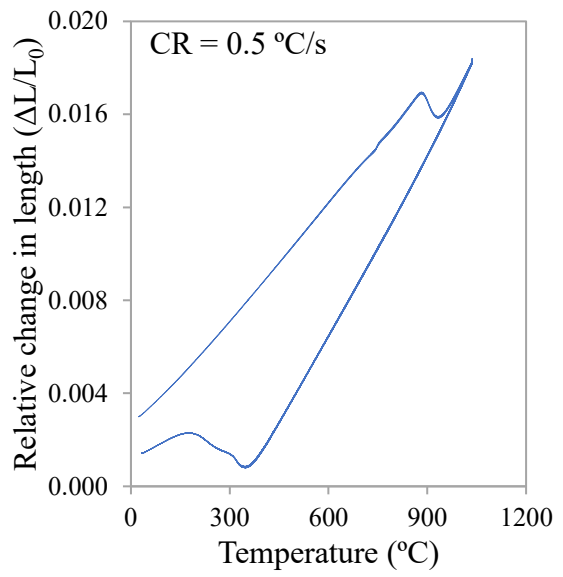
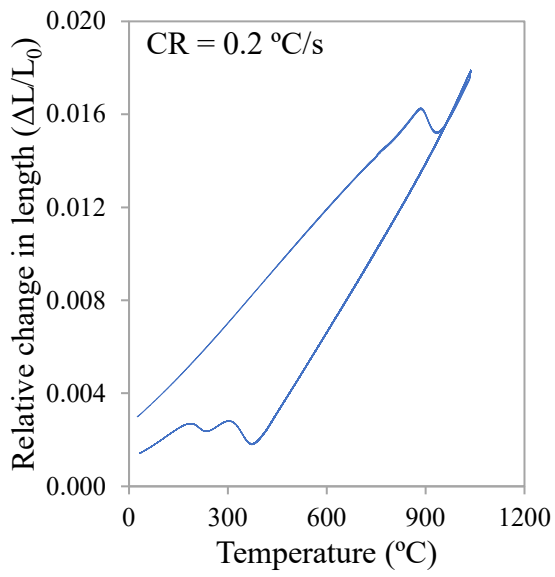
6Mn



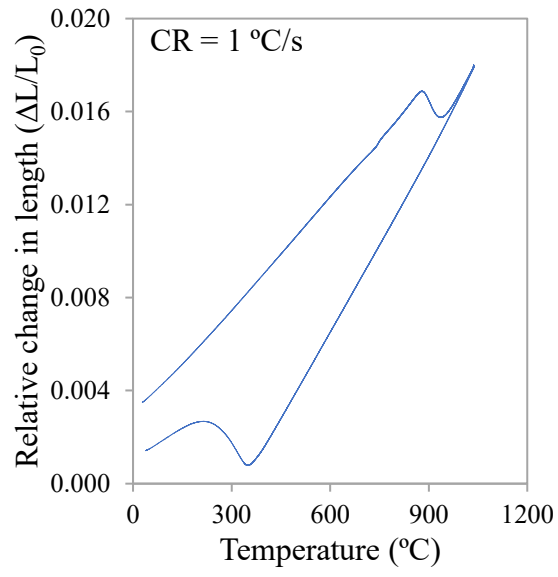
6Mn2Ni



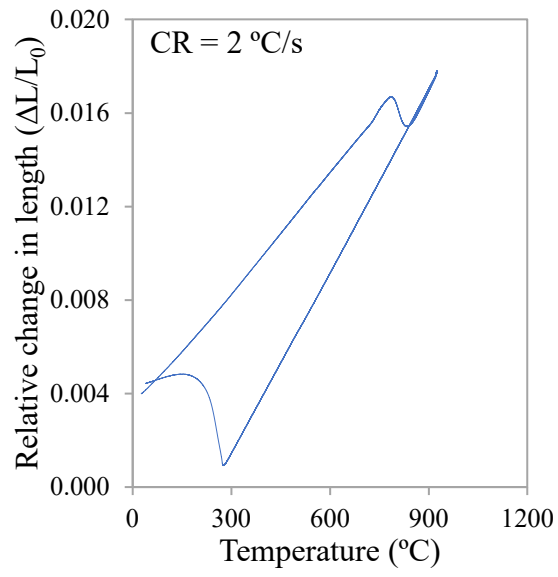
1.2990



1.2344



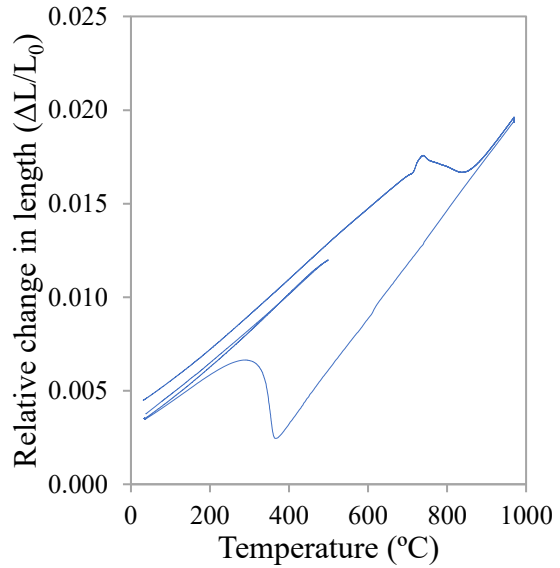
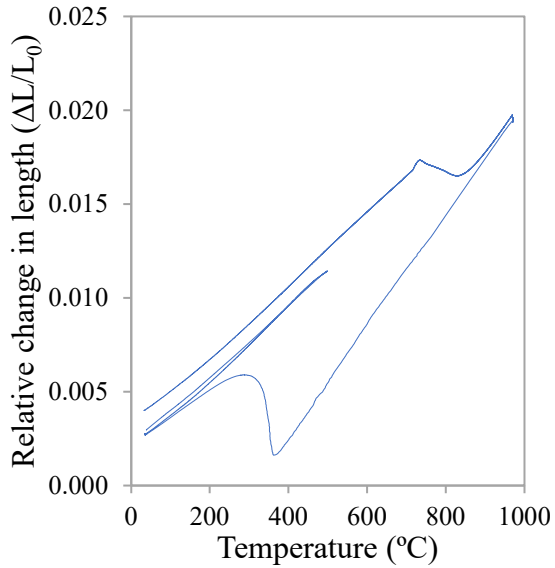
300M



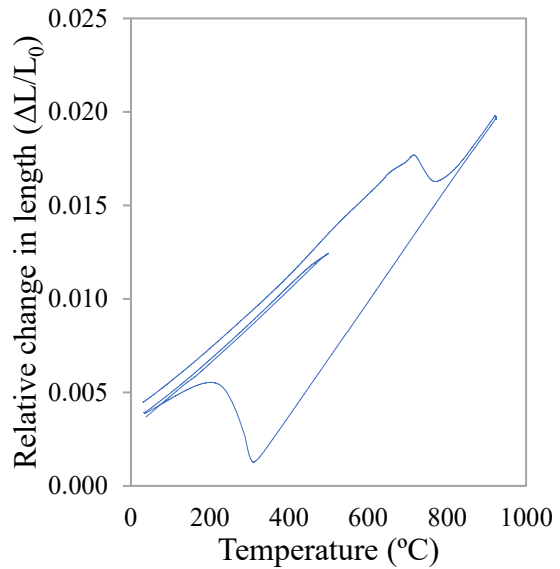
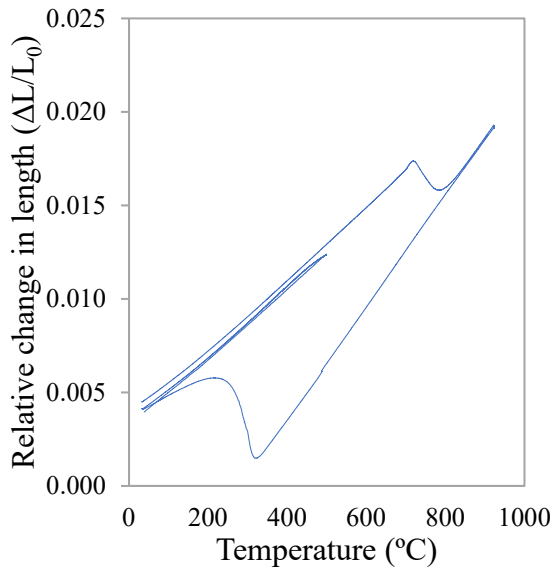
Dilatometry curves to determine M_s , M_f and martensitic transformation

curve:

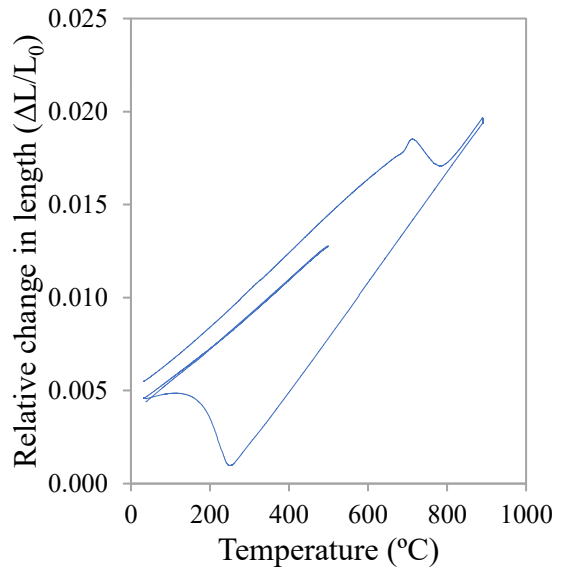
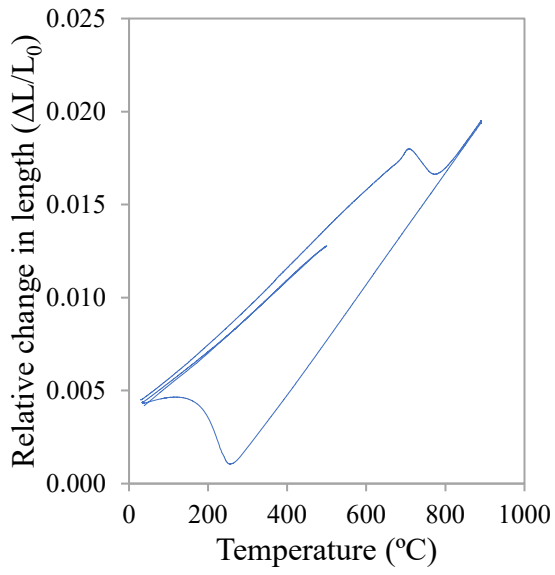
2Mn



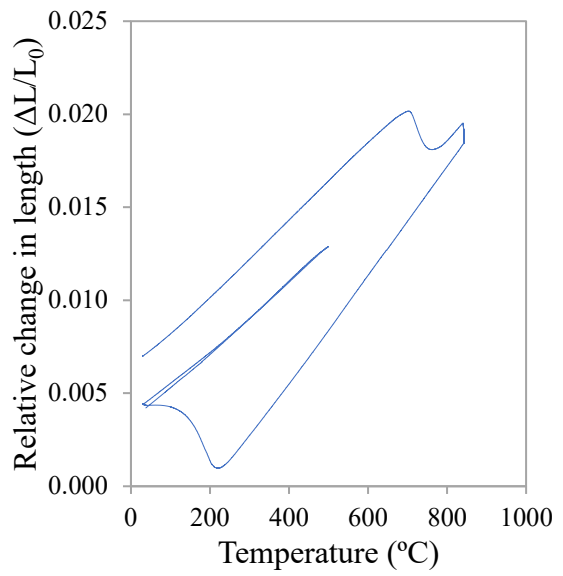
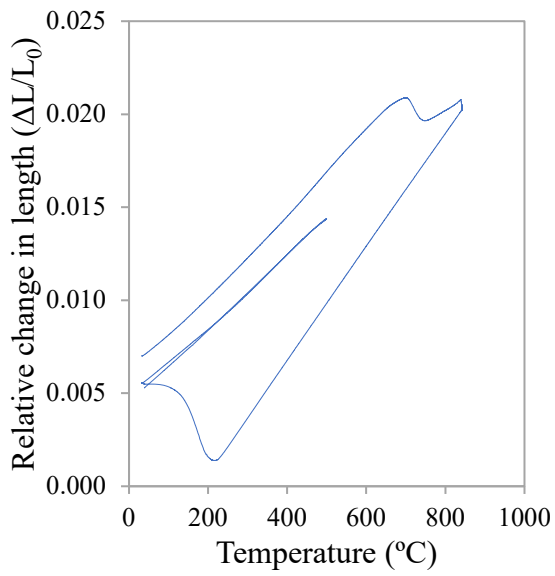
4Mn



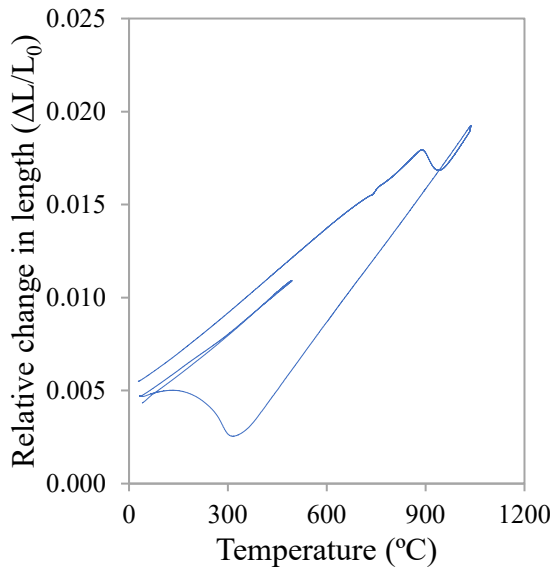
6Mn



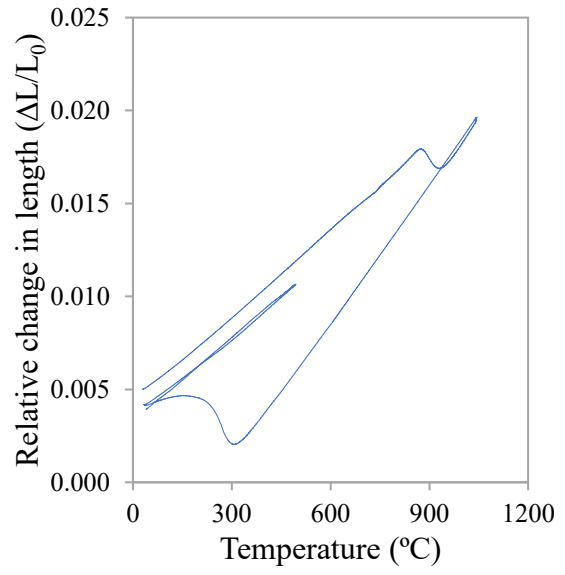
6Mn2Ni



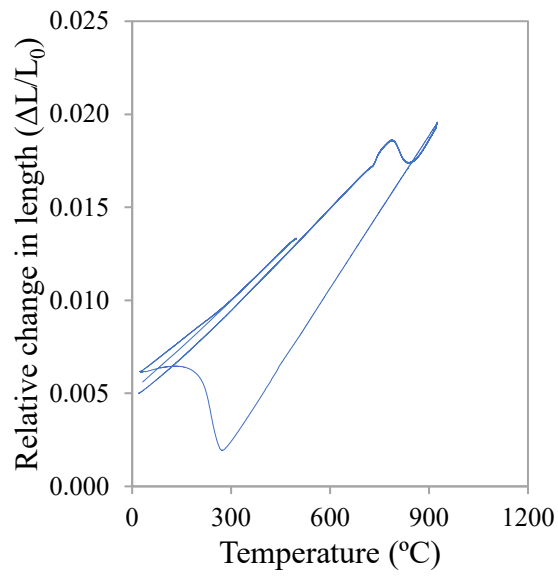
1.2990



1.2344

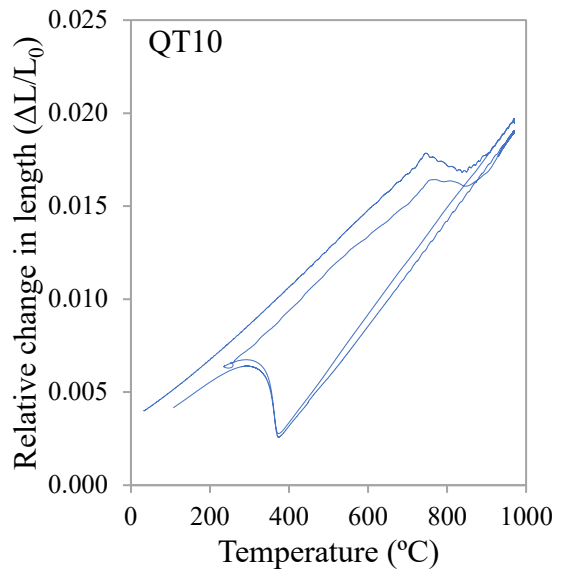
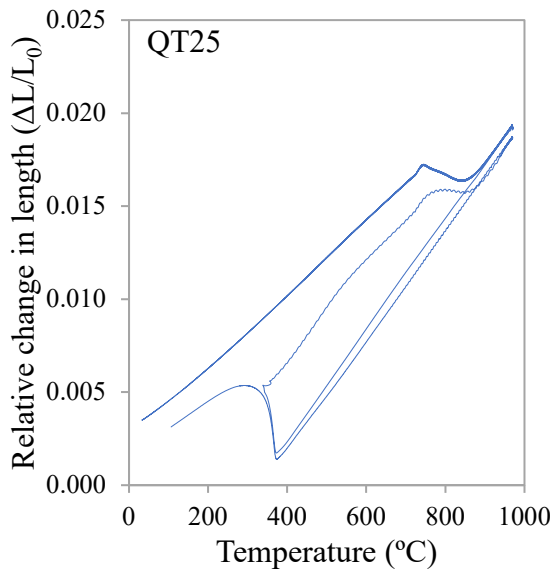


300M

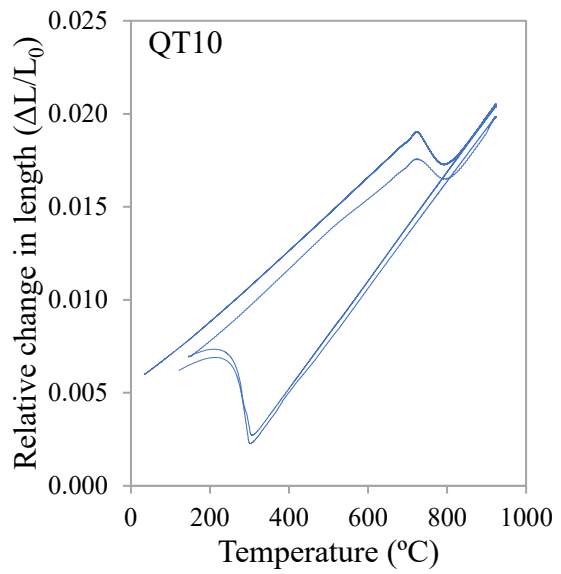
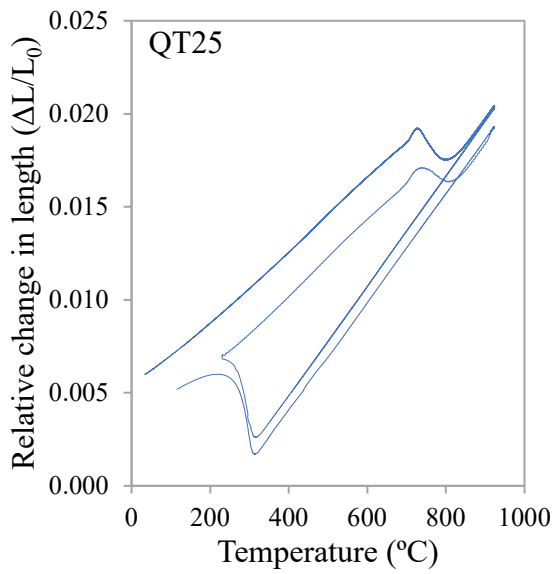


Dilatometry curves to determine T_{ART} :

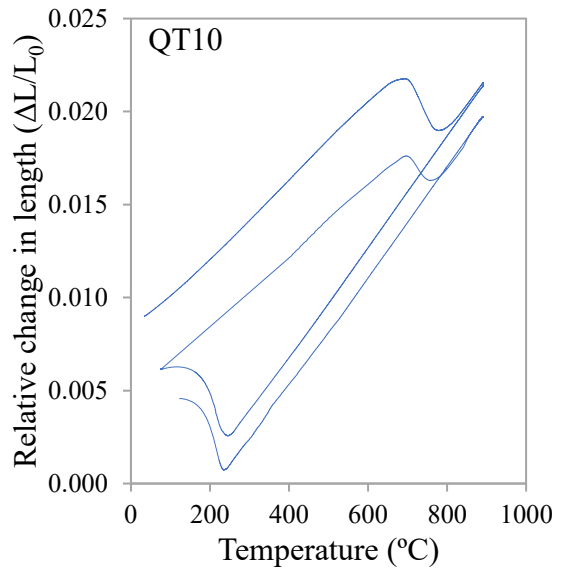
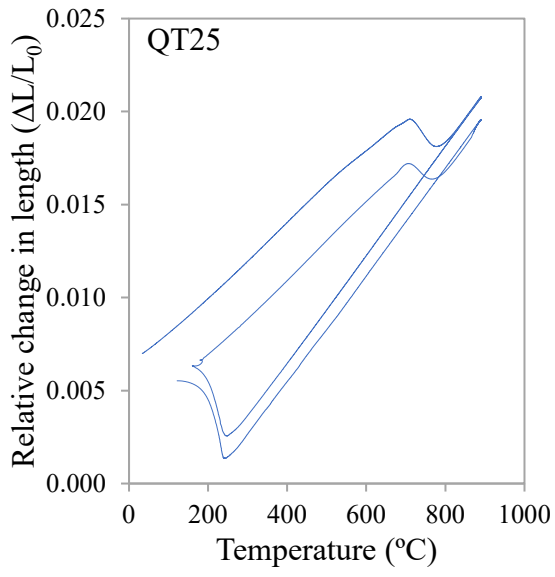
2Mn



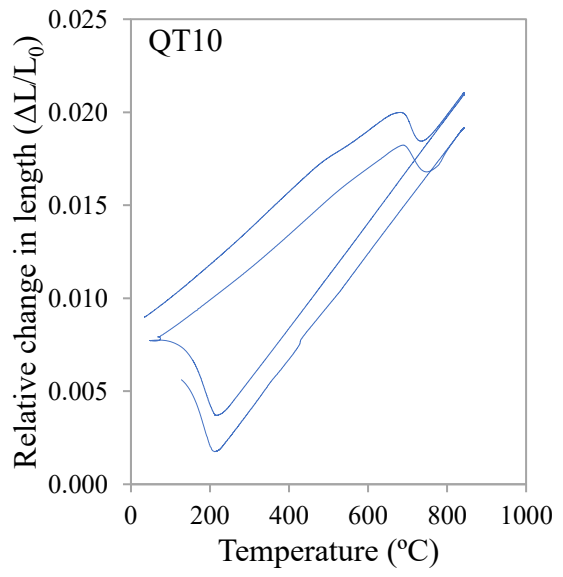
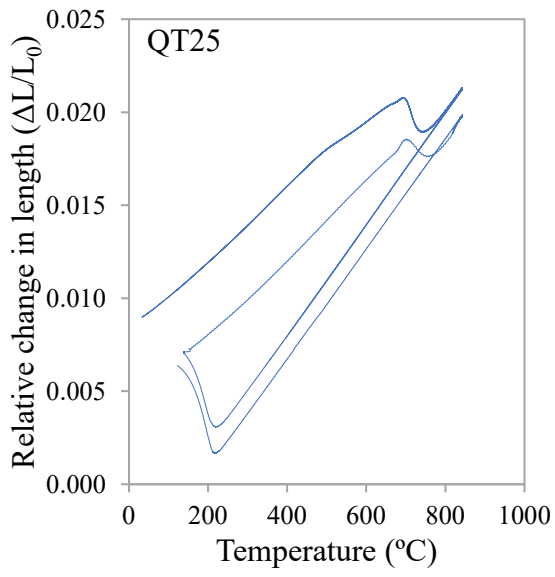
4Mn



6Mn



6Mn2Ni



Appendix B: Route followed in the furnaces and salt baths

Route followed for each steel and Q&P condition during the heat treatment in the furnaces and salt baths. F-1 and F-2 refer to furnace 1 and 2, and SB-1 and SB-2 refer to salt bath 1 and 2, respectively:

Steel ref.	Condition	F-1	SB-1	Air	SB-2	F-2	Water
Medium Mn steels							
2Mn	1	✓	✓	✗	✓	✗	✓
	2	✓	✓	✗	✗	✓	✓
	3	✓	✓	✗	✗	✓	✓
4Mn	1	✓	✓	✗	✓	✗	✓
	2	✓	✓	✗	✗	✓	✓
	3	✓	✗	✓	✗	✓	✓
6Mn	1	✓	✗	✓	✓	✗	✓
	2	✓	✗	✓	✗	✓	✓
	3	✓	✗	✓	✗	✓	✓
	4	✓	✗	✓	✗	✓	✓
	5	✓	✗	✓	✗	✓	✓
6Mn2Ni	1	✓	✗	✓	✓	✗	✓
	2	✓	✗	✓	✗	✓	✓
	3	✓	✗	✓	✗	✓	✓
	4	✓	✗	✓	✗	✓	✓
	5	✓	✗	✓	✗	✓	✓
Medium and high C steels							
1.2990	1	✓	✓	✓	✓	✗	✓
300M	1	✓	✓	✓	✓	✗	✓

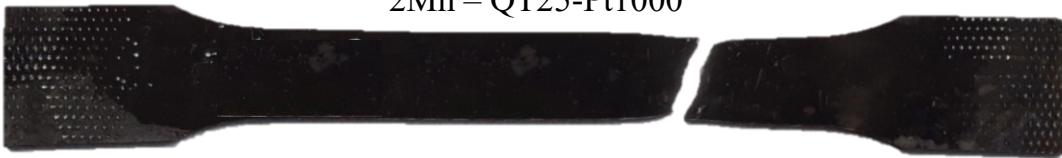
Appendix C: Tensile test specimens

Fractured tensile specimens of the 2Mn steel:

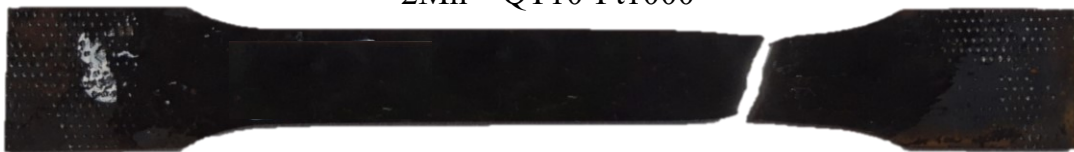
2Mn – ref



2Mn – QT25-Pt1000



2Mn – QT10-Pt1000



Fractured tensile specimens of the 4Mn steel:

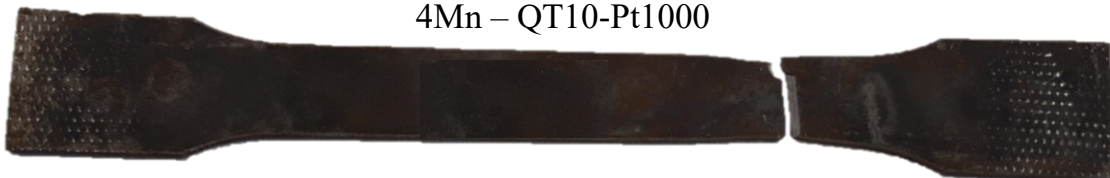
4Mn – ref



4Mn – QT25-Pt1000



4Mn – QT10-Pt1000

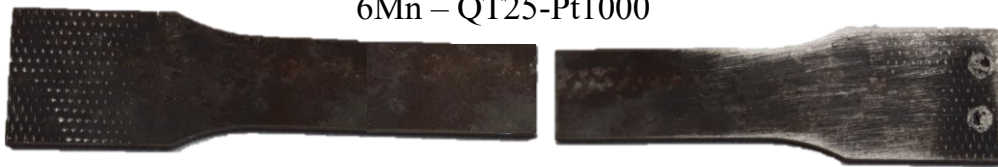


Fractured tensile specimens of the 6Mn steel:

6Mn – ref



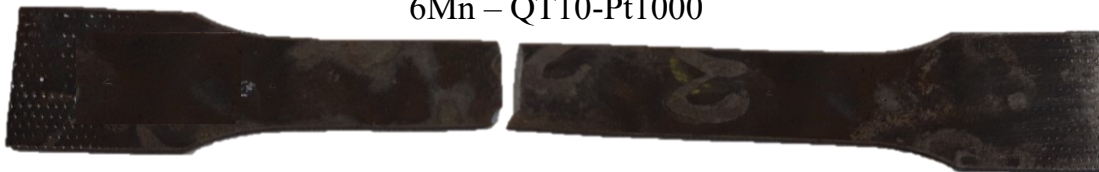
6Mn – QT25-Pt1000



6Mn – QT10-Pt300



6Mn – QT10-Pt1000



6Mn – QT10-Pt3600

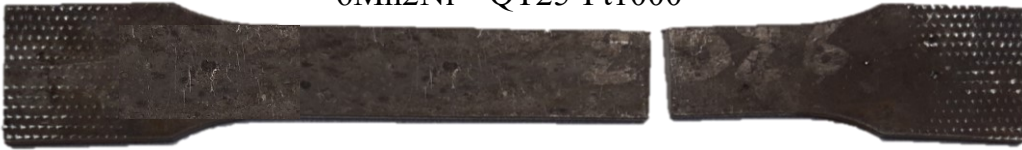


Fractured tensile specimens of the 6Mn2Ni steel:

6Mn2Ni – ref



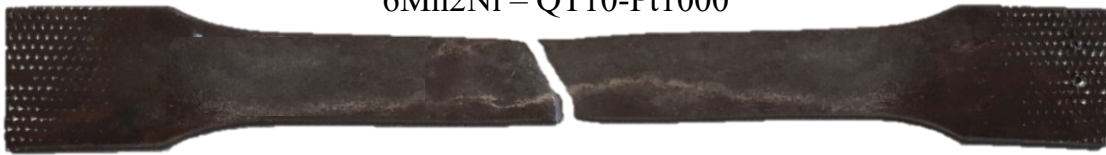
6Mn2Ni – QT25-Pt1000



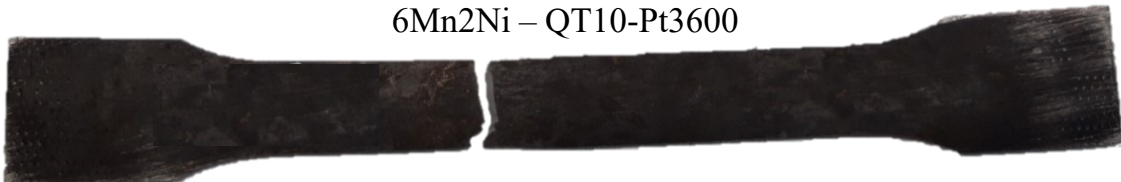
6Mn2Ni – QT10-Pt300



6Mn2Ni – QT10-Pt1000



6Mn2Ni – QT10-Pt3600



Appendix D: Hardness measurements

Hardness measurements of the dilatometry samples:

Hardness (HRC) of the directly quenched dilatometry samples:

Steel ref.	Test 1	Test 2	Test 3	Test 4	Test 5
1.2990	56.2	56.6	56.0	56.6	56.3
1.2344	53.3	53.1	52.9	54.2	54.2
300M	60.3	59.4	59.4	59.5	59.9

Hardness (HRC) of the samples after the application of the PT300 Q&P cycle:

Steel ref.	Test 1	Test 2	Test 3	Test 4	Test 5
1.2990	53.6	53.6	53.0	53.8	53.8
1.2344	51.6	50.8	51.0	52.4	51.4
300M	52.5	51.7	52.1	52.3	51.6

Hardness (HRC) of the samples after the application of the PT400 Q&P cycle:

Steel ref.	Test 1	Test 2	Test 3	Test 4	Test 5
1.2990	52.1	51.8	52.3	52.3	51.9
1.2344	50.9	49.8	50.4	50.5	51.0
300M	51.1	50.9	51.3	51.0	51.2

Hardness measurements of the disks treated in the salt baths:

Hardness (HRC) of the samples after the application of the PT400 Q&P cycle:

Steel ref.	Test 1	Test 2	Test 3	Test 4	Test 5
1.2990 disk1	54.5	53.6	53.5	54.6	54.9
1.2990 disk2	55.0	54.6	54.5	54.1	55.5
300M disk1	50.5	52.4	51.4	50.5	50.6
300M disk2	51.8	51.2	52.2	50.5	50.6

Hardness (HRC) of the samples after the application of the Q&T cycle:

Steel ref.	Test 1	Test 2	Test 3	Test 4	Test 5
1.2990 disk1	63.1	62.0	63.6	62.3	62.7
1.2990 disk2	62.1	62.4	62.1	62.7	63.7
300M disk1	56.9	56.6	56.1	56.4	56.9
300M disk2	55.8	56.6	56.8	56.1	57.1

Appendix E: Charpy specimens

